TECHNISCHE UNIVERSITÄT MÜNCHEN

Lehrstuhl für Erneuerbare und Nachhaltige Energiesysteme

A Power System Planning and Power Flow Simulation Framework for Generating and Evaluating Power Network Models

Investigating the Impact of Large-Scale Road Transportation Electrification on Urban Power Systems

David Ciechanowicz

Vollständiger Abdruck der von der Fakultät für Elektrotechnik und Informationstechnik der Technischen Universität München zur Erlangung des akademischen Grades eines

Doktor der Naturwissenschaften (Dr. rer. nat.)

genehmigten Dissertation.

Vorsitzender:		Prof. Dr.-Ing. Erwin Biebl
Prüfer der Dissertation:	1.	Prof. Dr. Thomas Hamacher
	2.	Prof. Dr.-Ing. Alois Chr. Knoll

Die Dissertation wurde am 09.05.2017 bei der Technischen Universität München eingereicht und durch die Fakultät für Elektrotechnik und Informationstechnik am 21.05.2018 angenommen.

Acknowledgements

This work concludes my employment as a Research Associate with TUMCREATE in Singapore and the Chair of Renewable and Sustainable Energy Systems of the Technische Universität München (TUM) in Munich, Germany. It has been submitted to the Department of Electrical and Computer Engineering of TUM in December 2016. Several people whom I would like to thank here supported me in my scientific endeavor making it never a lonely one.

First and foremost, I am deeply grateful to my doctoral advisor Prof. Dr. Thomas Hamacher who has always believed something great can emerge from interdisciplinary research, nourishing the field of electrical engineering with the power of structured information processing employed in computer science. I professionally and personally esteem him for his academic guidance and encouragement in exploring adjacent areas of research while also taking the liberty to make me focus when I was captive in the tempting world of knowledge discovery. I am indebted to Prof. Dr.-Ing. Alois Knoll for the opportunity to work at TUMCREATE and for taking on the task as my second advisor of this work. As such he passionately promoted marketing greatness and inspired me that any contribution has to be sound to have a significant impact; its advertisement, however, has to be outstanding. I also thank Prof. Dr. Martin Leucker for laying the foundation of my scientific career by providing me the opportunity to join TUMCREATE as a Research Associate in the first place.

I further owe my gratitude to my colleagues at TUMCREATE with whom I together worked on cutting-edge research topics, with whom I shared my life far away from home, and with whom I became friends. Of all my colleagues, Mr. Dominik Pelzer deserves a special mention. I particularly thank him for our fruitful collaboration and the many projects we started and finished together. He continuously challenged and enriched my ideas and with his maddening attention to detail sharpened my perception in many ways. I also thank him for his many valuable comments unblushingly exposing inconsistencies while proofreading this work. My special thanks goes to Mr. Daniel Zehe for his excellent technical guidance and support in many of my projects. I further thank Dr. Jordan Ivanchev, Dr.-Ing. Patrick Osswald, Mr. Reinhard Sellmair, and Dr.-Ing. Annette Trippe both professionally for their support during my research but even more personally for the great time we shared in Singapore. I am also glad I worked together with Mr. Benedikt Bartenschlager whose technical expertise enriched this work.

In the end, it is my pleasure to thank my family who encouraged me to venture out to Singapore, taking the journey of attaining a PhD, and leaving behind the overly tempting

alternative which was awaiting me. I express my particular gratitude to my parents who have always been an indispensable and inexhaustible source of support. With their love and dedication they fired up my motivation even at times when it was menaced to cease. I especially thank my brother for his guidance in every matter of my life. I have always appreciated the path he blazed for me. I also thank him for spending his time and effort proofreading this work thereby spicing up corrections with many amusing, exhilarant, and inspiring but most of all valuable comments. Finally, this work would not have been possible without the unwavering love, patience, encouragement, and support of my beloved wife who made our time in Singapore truly unforgettable. Thank you for turning our both lives into our life together.

Abstract

Plug-in electric vehicles (PEV) are energy-efficient, locally emission-free, and have the potential to diversify the energy sources applied in the transportation sector. Hence, governments worldwide accelerate the adoption of transportation electrification by providing different kinds of incentives. This fundamental change in transportation systems indisputably has an impact on power systems. It is only a question of quantifying this impact to accurately identify the effects down to a level of single electrical installations such as substations or power lines. Pinpointing those effects long before they occur in a real-world setting is essential. Otherwise, the initiated change in a transportation system may be disruptive to the corresponding power system due to its protracted investment decisions. Building up a fleet of PEVs and a network of charging stations can be done with comparably little effort considering the duration and costs of upgrading or newly building underground power lines, substations, or power stations. This is why simulations of the involved systems are necessary at an early stage to identify scenarios least affecting the power system infrastructure while at the same time not slowing down the expansion of transportation electrification-related operations.

It is the question of quantifying the impact of a large number of tempo-spatially distributed PEVs on urban power systems that motivates this work. A *power system simulation* framework is therefore presented that allows tackling multiple challenges on the way to answer this question. First, it allows generating and evaluating *power network models* (PNM) realistically emulating the actual power system infrastructure on both transmission and distribution level as detailed as single consumers, power lines, substations, and power stations. Generating those models is imperative as publicly available data on their real-world counterpart is typically rare. Second, the framework includes a power flow simulation computing the capacity utilization at every branch as well as the voltage at every bus. This allows conducting power flow studies on previously generated PNMs. Third, the price-responsive scheduling approach for battery energy storage prevents uncontrolled charging of PEVs by shifting charging into time periods being effective with respect to maintaining power grid stability. At the same time, an economically profitable operation for the battery owner is ensured. The developed framework is implemented in software as part of the distributed simulation platform termed *City Mobility Simulation* (CityMoS), additionally comprising an agent-based transportation system simulation as well as an interactive visualization. In this platform, the different, possibly *distributed simulations*, interoperate using the IEEE Standard 1516-2010 called *High Level Architecture*.

This work's research question of quantifying the impact of road transportation electrification is answered on the example of Singapore applying the CityMoS platform. At first, different PNMs of this region are specifically generated and evaluated with respect to available data allowing to identify the one best matching it. Subsequently, the trips of a PEV population corresponding to the actual vehicle population of Singapore are realistically simulated. Concurrently, power flows of the increased power demand due to charging are simulated on the previously generated PNM best matching Singapore. By investigating several electrification scenarios, the tempo-spatial impact of different parameters both on the generation capacities as well as on the utilization of substations and power lines is analyzed. For the simulated environment, the findings of the study allow drawing the conclusion that from the perspective of existing generation capacities no limitations apply; whereas 1 % of all power lines in the LV grid and 3 % of all substations in the MV grid are insufficiently designed. Transferring this conclusion one-to-one to the real power system of Singapore, however, fails due to limitations of the used models which are discussed in this work. They are mostly caused by insufficient data and therefore only allow an altered, qualitative conclusion. For Singapore, this implies that for individual electrical installations the impact of even a small number of PEVs is likely to be large enough to perturb the integration of the transportation and power system. A more realistic, quantitative conclusion for the real power system of Singapore requires either an improved methodology for generating PNMs from available limited data or authorities making the necessary data available.

Table of Contents

List of Figures

List of Tables

List of Listings

Nomenclature

ALSP	Aggregate Level Simulation Protocol
API	Application Programming Interface
B2G	Battery-to-Grid
CityMoS	City Mobility Simulation
CORBA	Common Object Request Broker Architecture
CRC	Central Runtime Component
CSV	Comma Separated Value
DBSCAN	Density-Based Spatial Clustering of Applications with Noise
DDS	Data Distribution Service
DIS	Distributed Interactive Simulation
DoD	Department of Defense
DT	Delaunay Triangulation
FMI	Functional Mock-up Interface
FOM	Federation Object Model
G2B	Grid-to-Battery
GIS	Geographical Information System
HLA	High Level Architecture
LRC	Local Runtime Component
LVC	Live, Virtual, and Constructive
M&S CO	Modeling and Simulation Coordination Office
MST	Minimum Spanning Tree
NYISO	New York Independent System Operator
OMG	Object Management Group
OMT	Object Model Template
PEV	Plug-in Electric Vehicle
PNM	Power Network Model
PSP	Power System Planning
PSS	Power System Simulation
RO	Receive Order
RTI	Runtime Infrastructure
SEMSim	Scalable Electric Mobility Simultion

SOC	State of Charge
SOM	Simulation Object Model
TCP	Transmission Control Protocol
TENA	Test and Training Enabling Architecture
TSO	Timestamp Order
TSP	Traveling Salesmen Problem
UDP	User Datagram Protocol
US	United States
USES	Universal Scheme for Modeling Energy Systems
V2G	Vehicle-to-Grid
XML	Extensible Markup Language
XSD	XML Schema Definition

1 | Introduction

Content

The rising share of plug-in electric vehicles may have an unpredictable impact on power systems. Simulations can help quantifying this impact.

1.1 Motivation

The complete global vehicle[1] fleet consists of approximately 1.2 billion vehicles [1]. In more than 99.9 %, vehicle propulsion is provided by the internal combustion of a fuel, typically petroleum derived, which is inefficient in regard to its primary energy content, noisy, and harmful to the environment in terms of CO_2 and other greenhouse gas emissions. *Plug-in electric vehicles* (PEV) including any kind of vehicle equipped with an electric power train and a possibility for external charging offer an energy-efficient, alternative drive concept which is locally emission-free. They reduce the dependency on fossil fuels and thereby allow for a diversification of energy sources applied in the transportation sector. Depending on the mixture of primary energy sources used to produce the required electricity[2], they overall may be even more environmental friendly. Cost effectiveness of using PEVs as a measure fighting climate change was, however, not created until recent advances in the field of battery electrochemistry [5] and renewable energy technologies [6]. It is therefore the goal of many governments to greatly increase the share of PEVs by providing incentives for consumers purchasing them [7]. Introducing PEVs on a large scale, meaning replacing the majority of vehicles with PEVs, however, requires an extensive charging infrastructure which yet has to be built. When getting charged, PEVs act as consumers of energy and therefore produce a load, each with an insignificantly low impact on the power system. A high share of PEVs forms a combined load with an impact that may be significantly high, especially during peak hours, to require for power system upgrades. The overall impact not only depends on the number of PEVs and the placement of *charging stations* (CS) including their connection power. More severely it also depends on the integration strategy, i.e., the application of *smart charging* and *demand response* strategies or the integration of the *battery-to-grid* (B2G) concept.

The electricity demand of a single PEV mostly depends on the driver's mobility and driving behavior but is also externally affected by environmental factors and the behavior of other drivers. All those factors are hardly predictable for single vehicles but may be very well approximated for groups of thousands of vehicles still leaving some degree of uncertainty. As the electricity demand and supply in a power system have to be kept at an equilibrium at all times, both the *spatial* and *temporal* component of the electricity consumption is essential. Consequently, analyses averaging the daily electricity consumption over time or space do not necessarily yield realistic results. The power system and its operation is designed to satisfy the current electricity demand of traditional consumers which is tempo-spatially highly predictable. Introducing a high share of PEVs may, however, increase either the temporal, the spatial, or both uncertainties in the forecast by a factor which is yet to be determined. Since investments in power system infrastructure are expensive and take rather long to be realized, their need has to be identified at an early stage to circumvent problems or disadvantages possibly arising from a too late investment. This work is therefore motivated by and will answer the following **research question**:

[1] Self-propelled wheeled vehicles that do not operate on rails.

[2] In 2015, the average non-electric vehicle in Germany produced 142.3 g/km of CO_2 [2] whereas, for instance, the BMW i3 with an energy consumption of 12.9 kWh/100 km [3] produces only 69 g/km of CO_2 assuming the current German energy mix with CO_2 emissions of 535 g/kWh [4].

Which impact does the power and energy demand induced by a large number of timely and spatially distributed PEVs have on urban power systems?

With the increasing electrification of the transportation system the dependency and influence on the power system grows stronger. Currently, PEVs exist only on a small scale resulting in a negligibly low dependency between both systems. But when applied on a large scale PEVs may become a disruptive technology turning the way how electricity is consumed, stored, and provided. Yet, the tempo-spatial impact of a large number of PEVs on a power system remains unknown. Although conceivable in the short- to medium-term future, a transportation system extensively interacting with a power system through CSs simply does not exist yet. It is therefore the following **problem statement** that impels this work to finally answer the previously posed research question:

How to study the electrification of the road transportation system in an environment of interdependent systems that does not yet exist?

1.2 Approach

In the realm of exploring the impact of road transportation electrification on urban power systems it is not enough to look at individual system components or systems in isolation. Both the transportation and the power system are intertwined showing tempo-spatial interdependence whose effects cannot properly be reflected in an isolated environment. Separating both systems therefore yields unrealistic results. An integrated approach as applied in this work is thus required in which the relevant parts of both systems including their environment are modeled together. The entire integrated system can then be analyzed with respect to the interaction and interdependence between the various subsystems or system components. Studying such an integrated system which does not yet exist in reality requires a simulation platform comprising all interacting entities, in this case at least a transportation and a power system simulation. For this purpose, such a platform is introduced in this work. Both system simulations use models on a *microscopic* scale [8] showing a level of detail allowing to explore the behavior of individual elements. Those elements are abstracted compared to their real-world counterparts to reduce complexity down to a level allowing to study the entire integrated system in real-time. For the transportation system, these elements conform to individual drivers and vehicles. In the field of *agent-based modeling* [9], each driver-vehicle pair is jointly modeled as an *agent* comprising a driver behavior and a vehicle component model. For the power system, individual elements include all types of electrical consumer load such as private households and commercial or industrial buildings, as well as electrical installations such as power plants, substations, and power lines. The focus of this work is on the power system part. The employed transportation system simulation was externally developed and is therefore only described to the extent necessary to understand its usage as part of the simulation platform.

From a modeling perspective a simulation in general comprises two different types of models: a *data* and a *computational* model. The former determines the structure of the data expressed in a modeling language. For purposes of specifically defining the data model of power systems, the *Universal Scheme for Modeling Energy Systems* (USES) has been self-developed and described in [10]. USES stands out by its concise yet formally fully specified syntax additionally offering an intuitive graphical representation. This work goes beyond the development of a data modeling notation by presenting a methodology for generating and evaluating specific data models in the context of power systems, termed *power network models* (PNM). The simulation platform introduced in this work implements the computational model capturing the behavior of both modeled systems, a transportation system interacting with a power system. The **proposed solution** to this work's problem statement can therefore be summarized as follows:

A simulation platform is developed allowing to microscopically evaluate the impact of road transportation electrification on power systems.

1.3 Contributions

To address the problem statement and thereby answer the posed research question, this work is framed into several chapters each providing its unique contribution. The conceptual framework is illustrated in Figure 1.1. In the following, the individual contributions of this work are outlined:

Power System Simulation Framework (Chapter 2) Simulation-based approaches can provide measures to investigate the impact of highly tempo-spatially variable demand on a power system and to support planners in making infrastructure development decisions. One crucial input for these simulations are PNMs comprising detailed information on a power system's electrical installations. This information may be confidentially accessible by planners or operators for the purpose of infrastructure development or maintenance. Publicly available data on these aspects as required, for instance, for academia is typically rare, thus impelling the development and application of a methodology to artificially generate PNMs that realistically emulate the actual infrastructure. In this chapter, a *power system simulation* (PSS) framework is presented that includes such a *power system planning* methodology for planning both the distribution and the transmission system. Its objective is to derive realistic PNMs from minimal input data, yet showing topological, electrical, and economic properties of real-world power systems. Those properties allow assessing the quality of the PNMs by contrasting values of different models to each other and to values of their real-world counterparts. Generated PNMs are thereby not limited to a cost-optimized satisfactory solution. In fact, the methodology provides high flexibility in tailoring PNMs to the requirements of individual use cases according to the available input data. Another part of the framework, the power flow simulation, allows conducting power flow studies on the PNMs. Especially in connection with the battery energy storage scheduling module, this enables realistically

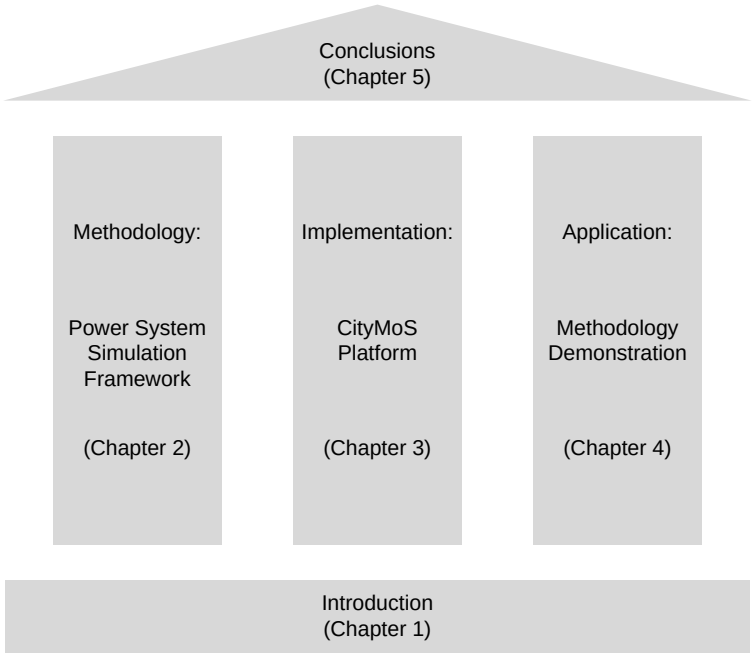

Figure 1.1: Conceptual framework of this work.

evaluating the impact of road transportation electrification on a power system. This chapter provides the methodological part of this work.

CityMoS Platform (Chapter 3) Besides the PSS framework introduced in Chapter 2, solving the problem statement at least requires yet another system simulation, specifically of the transportation system. In reality, both systems interact with each other in terms of charging/discharging events, so they have to do in a simulated environment. In the *City Mobility Simulation* (CityMoS) platform presented in this chapter, the individual entities interoperate using the IEEE Standard 1516-2010 called *High Level Architecture* (HLA). HLA describes an architecture to construct reusable and interoperable distributed system simulations. The platform comprises the following entities:

- A power system simulation based on the framework described in Chapter 2 allowing to generate and evaluate PNMs and subsequently conduct power flow studies on them.
- An agent-based transportation system simulation allowing to realistically simulate trips of a PEV population that correspond to the actual vehicle population of a city.
- An interactive visualization tool allowing participating in and controlling of simulations in a coupled environment using HLA.

This chapter provides the implementation part of this work.

Methodology Demonstration (Chapter 4) The simulation platform CityMoS presented in Chapter 3 is the proposed solution to the problem statement. This platform finally

enables conducting studies helping to find an answer to the posed research question on determining the impact of a large number of timely and spatially distributed PEVs on urban power systems. In this chapter, two case studies are therefore presented. In the first study, realistic PNMs showing topological and electrical properties of real-world power systems are generated and evaluated based on available data for Singapore. Thereby, the impact of different parameters and parameter uncertainty is investigated. The PNM best matching the data is then used in the second study to evaluate different road transportation electrification scenarios. By varying the PEV population size, the scheduling strategy, and other parameters, the sensitivity with respect to the generation capacities and the utilization of substations and power lines is analyzed to give a comprehensive answer to this work's research question. This chapter provides the application part of this work.

Conclusions (Chapter 5) This chapter summarizes the findings of this work's methodological, implementation, and application part. It further provides an outlook on domains requiring additional research in either part to improve the quality of the presented results. Concluding remarks on the applicability of the developed methodology geared to the target of answering the research question finalize this work.

2 | Power System Simulation Framework

Content

The proposed power system simulation framework facilitates generating and evaluating power network models abstracting real-world power systems. The integrated power flow simulation enables analyzing various road transportation electrification scenarios offering a profit-maximizing scheduling approach for battery energy storage.

2.1 Introduction

New types of consumers with tempo-spatially variable demand such as PEVs, intermittent renewable energy sources, and a trend towards a more distributed power infrastructure pose new challenges to power system operators. To ensure power grid stability and high power quality, these developments require more intelligent control of consumers and generators as well as extensions of the physical infrastructure. Simulation-based approaches can provide measures to investigate the impact of these developments on the power grid and to support power system planners in making infrastructure development decisions. This requires frameworks allowing tempo-spatially resolved simulations of the power flow on a system scale. One crucial input for these simulations is detailed information on the power network including the locations and capacities of generators, consumers, substations, and power lines. Publicly available data on these aspects is typically rare or, depending on the geographical market, may only be available for purchase, thus impeding the development and application of such simulation frameworks. Hence, there is a demand for a framework which generates *power network models* (PNM) that realistically emulate the actual infrastructure. Those models can facilitate the understanding of their mapped real-world power networks by allowing to simulate and analyze them and even predict processes taking place in them. They are, in fact, the only possibility to investigate what-if scenarios before they are implemented in a real-world setting.

PNMs that emulate the actual infrastructure can be generated by an approach referred to as *power system planning* (PSP) which includes the planning of both the distribution and transmission grid [11]. The objective of this approach is to derive realistic PNMs by applying general topological and electrical power system principles to the accessible data. The literature provides a number of PSP models addressing the PNM generation problem in different ways. They are discussed in Section 2.6.1. As one of the possibilities, holistic approaches are most promising when it comes to generating realistic large-scale PNMs spanning multiple voltage levels including geographical constraints. They use a combination of algorithms for different subproblems and apply iterative approaches to generate the final PNM.

In this chapter a *power system simulation* (PSS) framework is presented which uses such a holistic approach for its PSP process. Beyond the simple planning of PNMs it additionally allows evaluating as well as subsequently conducting power flow studies on them. It further includes a price-responsive scheduling approach for battery energy storage to realistically evaluate the impact of road transportation electrification on power systems. Offering this functionality within the same framework is currently unique among the investigated literature. Compared to existing approaches discussed in Section 2.6.1 the presented framework has the additional following advantages:

- Opposed to traditional approaches which are top-down methods, the presented framework is designed as a bottom-up process. It is therefore capable of generating PNMs based on locations and the active power demand of consumers. This allows a more realistic planning of the LV grid as tempo-spatially highly resolved data can be taken into account. This part of a power system is of particular interest as little redundancies make it vulnerable to load and supply perturbations. In addition, in cases in which only power demand data of individual consumers is available, a bottom-up approach is the only

possibility for generating a PNM. This is often the case as its strategic importance prevents authorities from revealing detailed information on the power system.

- The framework is not limited to planning a cost-minimal satisfactory solution, sometimes wrongly indicated as an optimal power grid. It, in fact, can be multi-purposely parametrized according to the available input data and can therefore generate PNMs with a large variety of different characteristics. By specifying available information on existing electrical installations the user can exert influence on the automatic planning process. Besides *greenfield planning* which conducts planning from scratch, existing PNMs can also be *expanded* to explore optimal transition paths to meet future requirements. This provides a high flexibility in tailoring the PNM to the requirements of each individual use case. *Monte Carlo* simulations and *ceteris paribus* sensitivity analyses can be conducted to identify the impact of parameter uncertainty.
- The planning scope is not limited to a certain number of electrical consumers or a specific number of different voltage levels. Due to the applied network decomposition approach, computational requirements grow linearly with the number of consumers. This allows planning a city-scale power system within minutes and conducting power flow studies on that PNM within seconds.
- To allow conducting power flow studies, the framework, besides the PSP module, offers the built-in possibility to simulate AC power flows on entire, possibly large-scale PNMs which none of the investigated frameworks is capable of. This way, users are able to plan a PNM and subsequently conduct power flow studies with the same framework without the need for exporting, modifying, and importing data to and from other tools. Those studies are not limited to a single time step but may cover arbitrary time horizons at any temporal resolution.
- The framework uniquely implements a module for scheduling charging/discharging of battery energy storage being effective to maintain power grid stability considering battery degradation and time-dependent electricity prices. It leads to a profit-maximizing solution being calculated sufficiently fast for real-time operation.
- The large variety of different topological, electrical, and economic properties being defined including reference values for real-world power systems allows evaluating and comparing PNMs. Investigated frameworks are limited to only a few of the mentioned properties while mostly neglecting real-world references.

The presented framework is capable of generating realistic PNMs from only little input data. It is thus mainly targeted to researchers and planners who want to conduct power flow studies on a large scale but for various reasons only have limited information on the actual power system. It further targets experts of adjacent areas who are not familiar with power systems but need to conduct interdisciplinary studies. While the resulting models are not an exact representation of the real-world environment, they are a powerful tool to investigate what-if scenarios to explore the large-scale impact of certain infrastructure measures on the overall system. In fact, PSP methodologies simplify power systems in many ways [11]. Power systems are abstracted by consuming (e.g., households), producing (e.g., power plants), and transmission facilities (e.g., substations, power lines) as their only components. The challenge of producing realistic results

although targeting for minimal input data is discussed in its various aspects in Section 2.6. In Chapter 4 the framework is applied to the case of Singapore by generating PNMs and further investigating the impact of large-scale road transportation electrification on those PNMs. Demonstrating the usefulness of such investigation using synthesized but close-to-reality data may further incentivize authorities to make more real-world data available to allow for more realistic analyses or to improve such simulation frameworks by employing them for their own planning purposes.

In addition to the discussion of the applicability and limitations of the presented PSS framework and the presentation of related work in Section 2.6 as well as the conclusions in Section 2.7, the remainder of this chapter is concerned with describing the individual components of the framework which are as follows:

Power System Planning (Section 2.2) The PSP approach is capable of generating PNMs with the characteristics of real-world power systems while using minimal input data. Section 2.2 outlines the individual steps of the process of generating PNMs. The description is extracted from [12] and slightly modified.

Power Flow Simulation (Section 2.3) The power flow simulation ensures PNMs generated by the approach presented in Section 2.2 to be able to reliably operate under the demand/supply-conditions defined by their input data. Section 2.3 outlines the applied power network model as well as the individual steps of simulating power flows on a previously generated PNM. The description is extracted from [12], slightly modified, and extended in respect to the applied power flow model.

Scheduling of Battery Energy Storage (Section 2.4) The integration of PEVs' mobile battery energy storage into the power system requires concepts such as *smart charging* or *battery-to-grid* (B2G). Those concepts in turn require appropriate scheduling approaches which have to be effective in respect to maintaining power grid stability and ensuring economically profitable operation for the battery owner. A price-responsive energy storage scheduling approach considering battery degradation and electricity price forecasts is explained in Section 2.4. The description is extracted from [13–15], slightly modified, and extended with regard to the description of the solution method.

Evaluating Power Network Models (Section 2.5) The PSP approach presented in Section 2.2 produces PNMs with a large variety of different characteristics. To allow analyzing and comparing them on an aggregated level, various topological, electrical, and economic properties are defined in Section 2.5. In addition, available data from real-world power systems is provided to be able to analyze how generated PNMs contrast to real-world power systems in respect to those properties.

2.2 Power System Planning

The goal of the presented PSP methodology is to create PNMs which connect the consumers of any given geographical *region* via power lines to substations of different voltage levels by fulfilling various technical and topological requirements. The planning process proceeds bottom-

up requiring data of consumers, each described by a distinct pair of spatial coordinates and its active power demand. Supplementary data, e.g., the reactive power demand or matching power factors, the number and technical specification of substations and power plants, total branch length and branch resistance/reactance values, as well as substation and branch capacity buffers may optionally be provided to further exert influence on the output. For the case of PNM expansion rather than greenfield planning, data of the initially existing PNM may also be used. Specific values of the input data are given in the demonstration of the PSP process on the example of Singapore in Section 4.2.1.

Throughout this work the graph theoretical term *node* refers to the electrical engineering term *bus*. It can either be a *load bus* (PQ), e.g., a consumer or a substation acting as a consumer, or a *generator bus* (PV), e.g., a power station or a substation acting as a producer. The same applies to an *edge* and a *branch* which both denote a power line. The planning process splits the region into one or multiple *areas*. An area is characterized by any non-zero number of PQ buses and exactly one PV bus. Each PQ bus has to be directly or indirectly connected to its area's PV bus via branches. For an area to be feasible, the criteria described in Section 2.2.1 have to be fulfilled. If not stated otherwise, i denotes a single node of the set N of all nodes of the cardinality n while j indicates a single power line of the set M of all m power lines. The set of all nodes can further be subdivided into the set N_{PQ} of all PQ buses and the set N_{PV} of all PV buses, the latter also distinguishing power plants in the set $N_{\mathrm{PV,PP}}$.

In reality, power lines are typically not laid in a beeline. For reasons of limited availability of data, economic, geographical, and environmental constraints are neglected when placing substations or laying power lines. To still emulate branched power lines and thereby realistically account for power losses, power lines are extended in length by a stretch factor. To allow for a different branching depth, this factor depends on the power line's voltage level. The specific stretch factors may be selected to produce a PNM with a total power line length similar to the target value. This way, realistic electrical and economic properties of the generated PNM can be maintained although the spatial composition of the installations may deviate in reality. Stretch factors are further discussed in Section 2.6.3.

The planning process, illustrated in Figure 2.1, starts at the lowest voltage level by clustering consumers into a certain number of spatial areas with a similar power demand (Step 1). A PV bus is then placed at the load center of each area (Step 2). A validation ensures areas to be technically feasible when directly connecting each consumer to the area's PV bus with a power line (Step 3). An optional step recombining the network to reduce the number of areas and thereby minimizing its costs may be conducted (Step 4) before applying the desired topology (Step 5). Step 3 to 5 include a validation of the feasibility criteria defined in Section 2.2.1. The regular greenfield planning Steps 1 to 5 are described in Sections 2.2.2 to 2.2.6. A voltage level may alternatively be planned non-regularly, either partly or entirely, as described in Section 2.2.7. After completing the planning for one voltage level, the process is iteratively executed for all higher voltage levels (Step 6). The output, each consisting of a model of a power system including areas, buses, and branches characterized by their attributes, is ultimately combined to form the entire PNM as described in Section 2.2.8.

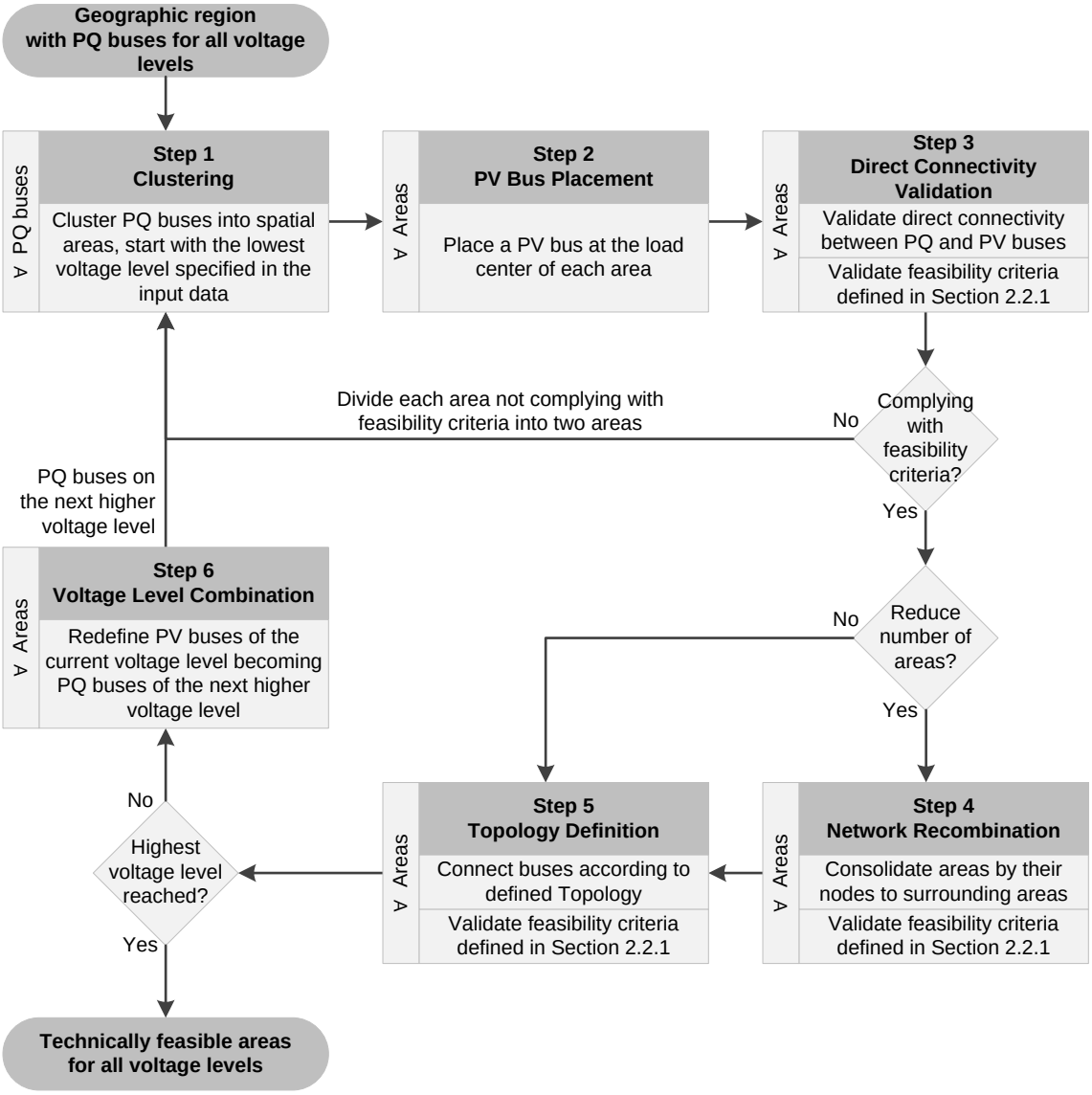

Figure 2.1: Regular power system planning process for a single voltage level.

2.2.1 Prerequisite: Feasibility Criteria

For an area α to be technically feasible, various conditions must be fulfilled. Most importantly, both *Kirchhoff's current* and *voltage law* [16] need to be satisfied which is ensured by the employed power flow model described in Section 2.3.1. Furthermore, the feasibility of an area's network is evaluated based on three additional conditions:

1. The aggregated power demand $P_{\mathrm{D},\alpha,i}$ of all n_α PQ buses i and the aggregated power losses $P_{\mathrm{L},\alpha,j}$ in all m_α branches j must not exceed the maximum power $P_{\mathrm{S},\alpha,\max}$ the

corresponding PV bus can supply:

$$P_{\mathrm{S,max},\alpha} \geq \sum_{i=1}^{n_\alpha} P_{\mathrm{D},\alpha,i} + \sum_{j=1}^{m_\alpha} P_{\mathrm{L},\alpha,j} \tag{2.1}$$

The apparent power $|S|$ can be calculated from P and Q as

$$|S| = \sqrt{P^2 + Q^2}$$

2. When current is flowing in a conductor, there is a voltage drop between its two ends. Therefore, the voltage of a PQ bus is not equal to the one at its connected PV bus. The voltage $V_{\alpha,i}$ at each PQ bus i must be within a predefined range:

$$V_{\min} \leq V_{\alpha,i} \leq V_{\max} \quad i = 1, 2, ..., n_\alpha \tag{2.2}$$

3. For each of the m_α branches j, a maximum length $L_{\max,\alpha,j}$ must not be exceeded. This length depends on the targeted minimum voltage $V_{\min}$, the branches' voltage level $U_{\alpha,j}$, its resistance $R_{\alpha,j}$ and reactance $X_{\alpha,j}$, the apparent power flow $|S_{\alpha,j}|$, and the power factor $\cos(\varphi_{\alpha,j}) = \frac{P}{|S_{\alpha,j}|}$ according to

$$L_{\max,\alpha,j} = \frac{(1 - V_{\min}) \cdot U_{\alpha,j}^2}{|S_{\alpha,j}| \cdot (R_{\alpha,j} \cdot \cos(\varphi_{\alpha,j}) + X_{\alpha,j} \cdot \sin(\varphi_{\alpha,j}))} \quad j = 1, 2, ..., m_\alpha \tag{2.3}$$

The same conditions have to be fulfilled for reactive power values Q. Validating those criteria is done by calculating power flow and voltage values for all branches and buses in α as described in the first step of the power flow simulation process in Section 2.3.2.1.

2.2.2 Step 1: Clustering

The first step of generating areas from a given geographical region is grouping all n_α PQ buses into K clusters with equal or similar power demand. This is achieved by employing a modified *k-means* [17] algorithm. The implementation found in [18] is extended by an option to produce clusters with equal or similar power demand. The functioning of equal-size k-means clustering is described in [19]. A cluster is considered the first stage of an area in which Constraint (2.1) is fulfilled. In a simple case, K equals the number of substations on one voltage level and may be provided by the input data. Alternatively, a minimum value can be determined from the aggregated peak power demand of all PQ buses and the operational power rating of the considered PV bus $P_{\mathrm{S,max}}$ by considering conversion losses η and an optional utilization rate μ. In this case, K is determined by

$$K = \left\lceil \frac{\sum_{i=1}^{n} P_{\mathrm{D},i}}{P_{\mathrm{S,max}} \cdot \eta \cdot \mu} \right\rceil \tag{2.4}$$

Depending on the available computational resources, the given area may first be divided into multiple non-overlapping subregions to reduce the number of nodes the k-means algorithm

has to process at once. This can, for instance, be achieved by iteratively bisecting the region and resulting subregions until each subregion holds a previously defined maximum number of nodes.

2.2.3 Step 2: PV Bus Placement

In the next step, a substation is placed at the location resulting in smallest power line transmission losses which is the load gravity center $\vec{r}_{\mathrm{c},\alpha}$ of each area α. According to [20], this location can be determined by weighting the geographical location $\vec{r}_{\alpha,i}$ of each PQ bus i within α with its power demand $P_{\mathrm{D},\alpha,i}$ so that

$$\vec{r}_{\mathrm{c},\alpha} = \frac{\sum_{i=1}^{n_\alpha} \left(P_{\mathrm{D},\alpha,i} \cdot \vec{r}_{\alpha,i} \right)}{\sum_{i=1}^{n_\alpha} P_{\mathrm{D},\alpha,i}} \tag{2.5}$$

2.2.4 Step 3: Direct Connectivity Validation

Before the buses in an area are connected according to the desired network topology, a basic feasibility test is conducted. The consumers of each area are tentatively directly connected to their area's PV bus via a power line. In case this setting already violates any of the feasibility criteria defined in Section 2.2.1, each infeasible area is further divided into two areas of equal or similar power demand according to Sections 2.2.2 and 2.2.3. Passing this test is a necessary yet not sufficient condition for an area's feasibility. Therefore, further feasibility checks are conducted at a later stage.

2.2.5 Step 4: Network Recombination

The preceding bisecting and a spatially inhomogeneous power demand may yield areas with a low number of PQ buses or a low utilization rate of the substation. This step therefore consolidates the number of areas. This can either be done with the objective to obtain a user-defined number of areas or to find a cost-optimized solution. An area is consolidated by trying to assign all its PQ buses to neighboring areas. If this can be achieved without violating the feasibility criteria in Section 2.2.1, the area which remains without any PQ buses is removed. Reconnecting a PQ bus to a neighboring area includes recalculating the location of this area's PV bus as described in Section 2.2.3 followed by a validation of the specified feasibility criteria. In case a cost-optimized solution is desired, the area is only consolidated if the total costs of all involved areas after reconnecting the buses are below the total initial costs. This procedure is performed for all areas in the order of their number of PQ buses, starting with the lowest. The network recombination procedure is iteratively repeated for the entire set of areas until the desired number of areas is reached or no more areas can be consolidated.

2.2.6 Step 5: Topology Definition

Depending on the voltage level, different topologies are commonly used in power grids. The kind of topology which should be applied to each voltage level can be specified in advance. The most common topologies in real-world power grids and the algorithmic process to generate them are described in the following:

- **Ring networks** are typically planned for LV and MV grids. The process of planning a ring is illustrated in Figure 2.2. To create such networks from the nodes of an area (Figure 2.2a), the implemented *density-based spatial clustering of applications with noise* (DBSCAN) [21] algorithm found in [22] generates clusters of nodes based on a maximum allowed distance between two nodes (Figure 2.2b). Only PQ buses are used for the clustering, the area's PV bus is excluded in this process. Each cluster serves as the basis for planning a ring. A ring with minimal total branch length is found by solving a *traveling salesmen problem* (TSP) [23] on all nodes of a cluster starting and ending with the area's PV bus using the implementation found in [24] (Figure 2.2c). In each planned ring Constraints (2.2) and (2.3) are validated for each branch and bus. In case any constraint is not satisfied, the ring is divided into two rings with an equal number of consumers (Figure 2.2d). For each of those rings the TSP is individually solved and the mentioned constraints are again validated.
- **Radial networks** may be used in LV and MV grids alternatively to ring networks. The process of planning a radial network is illustrated in Figure 2.2. The PQ buses of an area (Figure 2.2e) are clustered using the DBSCAN algorithm (Figure 2.2f) as described for generating a ring topology. A radial network is then created by constructing a *minimum spanning tree* (MST) using *Kruskal*'s [25] algorithm[1] which ensures a minimal total length of all branches (Figure 2.2g). In case any branch or consumer in the so-planned MST violates Constraints (2.2) or (2.3), the MST is divided into two MSTs with an equal number of buses (Figure 2.2h).
- **Meshed networks** show some degree of redundancy which makes this topology especially common for MV and HV grids. The process of planning a meshed network is illustrated in Figure 2.2. Starting from the PQ buses of an area (Figure 2.2i), this network type is generated by executing a *Delaunay triangulation* (DT) [26]. In a DT, triangles are built so that no node is inside the circumcircle of any triangle (Figure 2.2j), resulting in a partially connected meshed topology (Figure 2.2k). If the meshed network generated by the implemented algorithm found in [27] shows a higher redundancy than desired, branches are iteratively removed starting with the one connecting the two nodes with the highest node degree (Figure 2.2l). This removal is subject to the Constraints (2.2) and (2.3).

2.2.7 Alternative for Steps 1 to 5: Expansion Planning

Alternatively or in addition to the regular planning process described in Sections 2.2.2 to 2.2.6, a more customized planning can be performed compared to simply modifying parameter

[1] The algorithm was self-implemented based on the description given in [25].

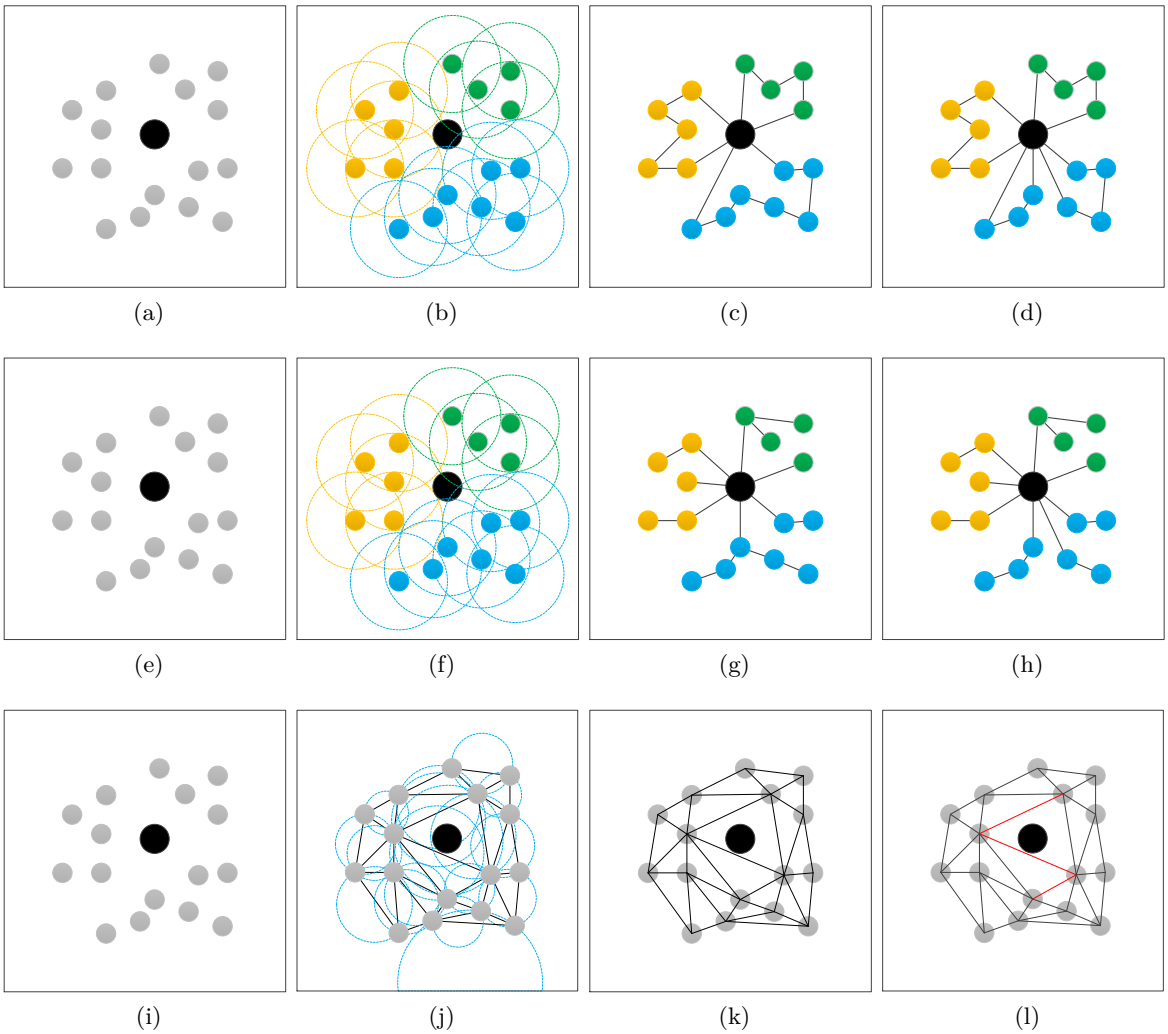

Figure 2.2: Process of planning (a - d) ring, (e - h) radial, and (i - l) meshed networks, each starting from the same initial situation applying different algorithms to come up with the final network topology after three steps.

settings. This includes the user-defined placement and specification of available buses and branches. The customized planning option is especially useful when detailed input data for parts of the power system to be planned is already available and should manifest in the resulting PNM. In case data for an entire voltage level is available, the regular planning process is omitted for this voltage level and both buses and branches are placed and specified as given by the data. If only parts of a voltage level should be planned this way, the regular planning process is executed considering the placement and specification of the given buses and branches. This way, available data on parts of the network can be directly integrated in the regular planning process to allow for expansion planning.

2.2.8 Step 6: Voltage Level Combination

After all areas in the lowest voltage layer have been planned, the algorithm continues at the next higher level. The set of PQ buses in this layer is given by the consumers directly connected to this voltage level and all substations from the lower layer acting as consumers on this level. The power demand of those substations equals their power supply to lower voltage consumer plus their internal conversion losses. For this and all higher layers, the entire planning procedure is repeated which finally leads to the PNM.

2.3 Power Flow Simulation

The power flow simulation computes the capacity utilization at every branch as well as the voltage at every bus. This is necessary for assessing the feasibility criteria defined in Section 2.2.1 during the PSP process. Most importantly the simulation can be applied for conducting simulation studies on an already planned PNM. This allows investigating the impact of changes of the tempo-spatial load distribution on an existing PNM. In a real-world setting, these changes may result from new load types (e.g., PEVs) or from changed power consumption behavior (e.g., increasing use of air-conditioners, use of smart loads, or deployment of demand response schemes). This step therefore does not aim at further modifying the PNM but at identifying times and locations of grid congestion and voltage drops. This is done by applying a user-defined discretization on an arbitrary period of time and independently executing the power flow model for each of the time steps.

Realistic *unit commitment* models found in [28] involve finding the least-cost dispatch schedule of available generation resources to meet the power demand. Since power plants are not able to arbitrarily ramp up or down their power output, the output at one point in time is to some degree dependent on its previous one. In the simple model implemented in this work the power supply of a power plant is set to a fixed percentage of its capacity while allowing only the slack bus to vary its output. This way, states are considered *memoryless*. This means that the state of the power system at one time step is independent of the state of preceding events and only depends on its input data.

In Section 2.3.1 the implemented power flow model is introduced followed by a description of the single steps of the simulation procedure for an entire PNM with multiple voltage levels in Section 2.3.2.

2.3.1 Power Flow Model

AC models realistically reproduce the power flow on power lines. Due to their non-linearity, finding a solution is, however, a computationally expensive task. This problem has been addressed by various programming techniques with the approximation of the AC power flow model by a computationally less expensive linear DC model being the most widespread solution [29]. DC models only consider active power flows but they fail to include reactive power, voltages, and power losses. Simplified assumptions include negligible power line resistances

as well as having a flat voltage profile [11]. Results of power flow studies comprising DC models are therefore inaccurate in respect to voltage stability and AC power flow feasibility. Different approaches have tried to assess this issue and extended the DC models by the missing factors [30]. Although results of those enhanced DC models are for some scenarios consistent with those produced by AC models, there is no general validation or maximum fault tolerance given. In this work, a standard AC power flow model is therefore taken which uses network decomposition to overcome possible performance issues when solving large-scale power flow problems. In this context, a power system is divided into independent parts which are then solved separately as described in Section 2.3.2 to reduce execution time.

The implemented power flow model *JPOWER* [31], exhaustively described in [32], uses the *Newton-Raphson* [33, pp. 222] algorithm for solving AC power flow problems. In distribution networks with a high ratio of resistance to reactance values, the Newton-Raphson algorithm may require a great number of iterations or might even not converge at all [34]. In case no convergence can be achieved after a predefined number of iterations, the power flow simulation for this part switches to the *Fast-Decoupled* algorithm [33, pp. 228] and, if still no solution can be found, to the *Gauss-Seidel* [33, pp. 212] algorithm, both of which are also implemented in JPOWER. Whichever algorithm is taken, the following simplifications compared to reality are assumed:

1. Balanced loading of all phases in a three-phase system
2. Steady-state operation
3. No transient power flow or voltage changes when power demand or supply changes
4. Constant system frequency

In an AC power flow problem buses, as shown in Table 2.1, are distinguished according to their known and unknown variables into PQ and PV buses. One of the PV buses serves as the slack bus balancing active and reactive power additionally arising from power losses [33, pp. 219]. In case the offered accuracy is not required or the applied network decomposition approach becomes infeasible due to an increasing desired redundancy within the investigated PNM, the AC model may optionally be approximated by a DC model also supported by JPOWER. This approximation is then subject to the above mentioned restraints.

Table 2.1: Known variables in an AC power flow problem for different bus types.

Bus type	Active power P	Reactive power Q	Voltage V
PQ	✓	✓	–
PV	✓	–	✓
PV (slack)	–	–	✓

When calculating power flows of a two-busbar system in which a power line directly connects a PV bus and a PQ bus, JPOWER usually does not find a solution with neither algorithm. Since two-busbar systems are in theory solvable by any of the algorithms, an implementation error is suspected. In each of these cases, a self-implementation of the iterative process described in [33, pp. 207] is applied which ensures finding a solution in case it exists.

By design, this solution obeys both of Kirchhoff's circuit laws. In the following, the key steps of the implemented process are outlined:

1. Initialize the voltage at the PV bus V_{PV} and at the PQ bus V_{PQ} both as

$$V_{\mathrm{PV}} = V_{\mathrm{PQ}} = 1.0\,\mathrm{pu} \tag{2.6}$$

2. Calculate the current I_j from the active power demand $P_{\mathrm{D,PQ}}$, the reactive power demand $Q_{\mathrm{D,PQ}}$, and the complex conjugated voltage V^*_{PQ} as

$$I_j = \frac{P_{\mathrm{D,PQ}} - j \cdot Q_{\mathrm{D,PQ}}}{V^*_{\mathrm{PQ}}} \tag{2.7}$$

3. Calculate the voltage of the PQ bus V_{PQ} from the voltage of the PV bus V_{PV}, the resistance R, the reactance X, and the current I_j as

$$V_{\mathrm{PQ}} = V_{\mathrm{PV}} - (R + jX) \cdot I_j \tag{2.8}$$

4. Repeat steps 2 and 3 until

$$|V^t_{\mathrm{PQ}} - V^{t-1}_{\mathrm{PQ}}| < \varepsilon \quad 0 < \varepsilon \ll 1 \tag{2.9}$$

5. Calculate the apparent power supply $|S_{\mathrm{S,PV}}|$ as

$$|S_{\mathrm{S,PV}}| = |P_{\mathrm{S,PV}} + j \cdot Q_{\mathrm{S,PV}}| = |V_{\mathrm{PV}} \cdot I^*_j| \tag{2.10}$$

and the minimum voltage V_{min} as

$$V_{\mathrm{min}} = \frac{\mathrm{Re}\,(V_{\mathrm{PQ}})}{\mathrm{Re}\,(V_{\mathrm{PV}})} \tag{2.11}$$

2.3.2 Simulation Process

In order to reduce computational requirements, power flow calculations are performed consecutively for independent parts of the network; the smallest being a ring, tree, or direct connection between a consumer and a substation, the largest being composed of multiple interconnected rings or trees spanning over multiple areas or even voltage levels. As a decomposition of a meshed network may go in hand with violating Kirchhoff's circuit laws, a meshed network is always treated as one single independent part. The upper boundary for the size of an independent part is only limited by the available computational resources. On an average work station, several thousand buses and branches can typically be processed at once in a time frame of a few minutes. To optimally use existing resources, either the size of an independent part can be adapted or calculating power flows for the independent parts can be done in parallel. In the following description of the simulation process an independent part is assumed to be an area as introduced in Section 2.2.

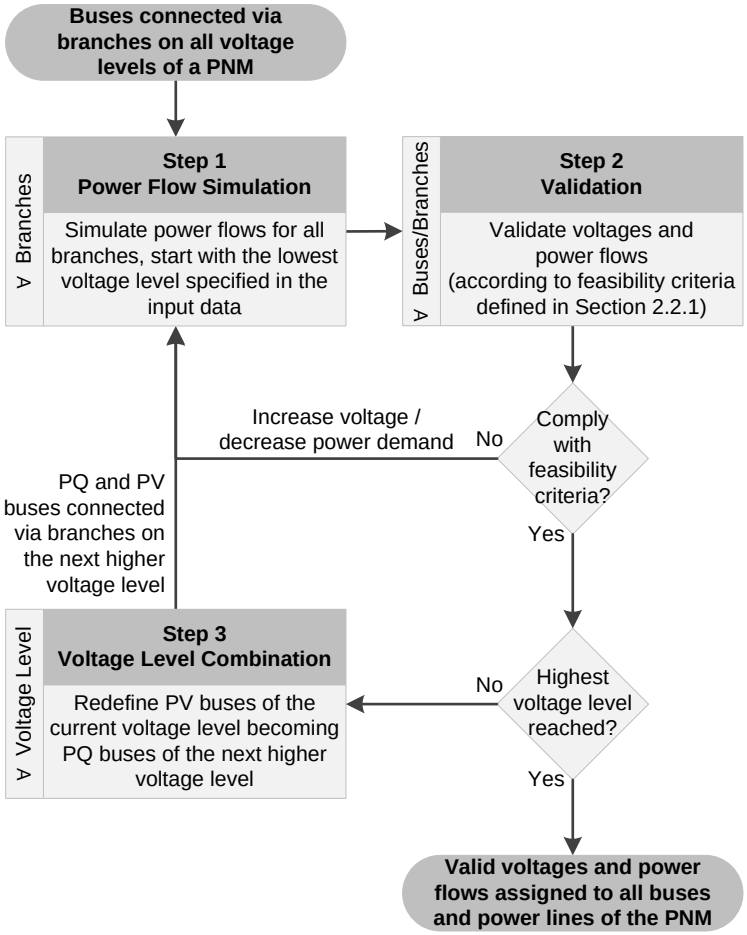

Figure 2.3: Regular power flow simulation process for an entire PNM with multiple voltage levels.

The process, illustrated in Figure 2.3, starts at the lowest voltage level by simulating power flows on every branch as described in Section 2.3.2.1 (Step 1). The results are then validated according to the feasibility criteria introduced in Section 2.2.1 as explained in Section 2.3.2.2 (Step 2). The outputs generated for a single voltage layer are then taken as inputs for the next level as described in Section 2.3.2.3 (Step 3). Voltage levels may alternatively be combined without installing voltage regulating devices as described in Section 2.3.2.4. The outcome of the entire simulation process consists of active and reactive power values on both ends of each branch and the power losses in every branch. Additionally, the voltage for each bus is determined.

2.3.2.1 Step 1: Power Flow Simulation

The simulation is initialized by defining all consumers or substations acting as consumers to be PQ buses, all power stations or substations acting as producers to be PV buses, and one of

the PV buses as the slack bus. PQ buses are initialized by their active and reactive power demand, $P_{\mathrm{D},i}$ and $Q_{\mathrm{D},i}$, respectively, PV buses by their active power supply $P_{\mathrm{S},i}$ and their voltage $V_i = 1.0\,\mathrm{pu}$, and the slack bus by its voltage $V_i = 1.0\,\mathrm{pu}$ according to Table 2.1.

The power flow simulation starts by determining the active and reactive power on both ends of each branch j and the voltage V_i at every bus i using the power flow model described in Section 2.3.1. The power difference between both ends of a branch is thus the active and reactive power loss, $P_{\mathrm{L},j}$ and $Q_{\mathrm{L},j}$. Applying Kirchhoff's current law, the power supply of each PV bus can be determined by the sum of power flows on all directly connected branches with outgoing power flows. The total active and reactive power the PV buses have to supply are then calculated as

$$P_{\mathrm{S},\alpha} = \sum_{i=1}^{n_\alpha} P_{\mathrm{D},\alpha,i} + \sum_{j=1}^{m_\alpha} P_{\mathrm{L},\alpha,j} \tag{2.12}$$

$$Q_{\mathrm{S},\alpha} = \sum_{i=1}^{n_\alpha} Q_{\mathrm{D},\alpha,i} + \sum_{j=1}^{m_\alpha} Q_{\mathrm{L},\alpha,j} \tag{2.13}$$

2.3.2.2 Step 2: Validation

Finding a feasible solution to the power flow problem is a necessary yet not sufficient condition for the validity of the power flows in the context of this simulation process. While a feasible solution guarantees adherence to Kirchoff's laws, Conditions (2.1) to (2.3) have additionally to be met. If at any PQ bus the voltage violates Condition (2.2), the initial voltage at the PV buses is increased using a binary search until either the condition is met or the maximum threshold for the value is reached. In the latter case or if at any bus Condition (2.1) or at any branch Condition (2.3) cannot be held, this particular part of the network is considered overloaded. This overload may only happen when the power demand at any PQ bus is higher than the one used to originally plan the PNM. This can occur in the presence of additional loads which were not considered for the planning of the PNM. In Section 4.3, an example for this case can be found where the impact of PEV charging is investigated for a PNM which was initially not designed to accommodate PEVs. In a real-world setting, this overload would require load reducing measures by the *power system operator* as, for instance, implemented through congestion pricing or more complex schemes such as demand response mechanisms. As a primary target, the framework identifies times and locations of grid congestion and voltage drops. The simulation therefore assumes that an appropriate load reducing measure is taken in an overloaded part of the grid by decreasing the power demand at the PQ buses. As a default setting which treats all consumers equally, the power demand for PQ buses is curtailed proportionally to their power demand compared to other PQ buses. Load curtailments are documented both temporally and spatially to allow analyzing them after conducting a power flow study. More sophisticated measures such as smart loads or distributed battery energy storage participating in demand response schemes or peak shaving may alternatively be implemented by the user.

2.3.2.3 Step 3: Voltage Level Combination

After calculating power flows in all branches within one voltage layer, the process continues at the next higher level. For this purpose, substations which on the lower voltage level are defined as PV buses are on the current level defined as PQ buses. The same substation therefore serves as a generator on a lower voltage level while it acts as a load on a higher level. P_{D} and Q_{D} at each of these PQ buses are set to the values of P_{S} and Q_{S} of its corresponding PV bus. This shifting of power between the two windings of a substation is done upwards for all voltage levels. It is assumed that voltage regulators, such as *on-load tap changers* or *series regulators*, are installed at each PV bus justifying initialization values of $V_i = 1.0\,\mathrm{pu}$ for each voltage level.

In case the power demand of any substation acting as a consumer has been decreased due to a violation of any of the Conditions (2.1) to (2.3), the demand of all PQ buses directly or indirectly affected by this decrease also has to be curtailed. This process is illustrated in Figure 2.4. This example includes 2 PV buses and 9 PQ buses which are connected in a ring topology over two voltage levels. For the sake of simplicity, power losses are neglected in this example. In the regular upward simulation process shown in Figure 2.4a, the power supply of substations acting as producers is determined by the power demand of connected consumers (blue: 200 kW each, green: 10 kW each). In the example, this results in Substation A supplying 60 kW and Substation B supplying 660 kW. As the demand exceeds the maximum rating of 600 kW of Substation B, this setting is considered infeasible. This network is therefore simulated again by setting the supply of Substation B to its maximum rating of 600 kW. The simulation proceeds downwards to determine the maximum possible power demand of the directly connected PQ buses as shown in Figure 2.4b. According to the description in Section 2.3.2.2 the demand of each blue colored consumer is reduced proportionally to its power demand compared to other PQ buses of the same independent part by around 9 % from 200 kW to 181.8 kW. At the same time the demand of Substation A is decreased by the same

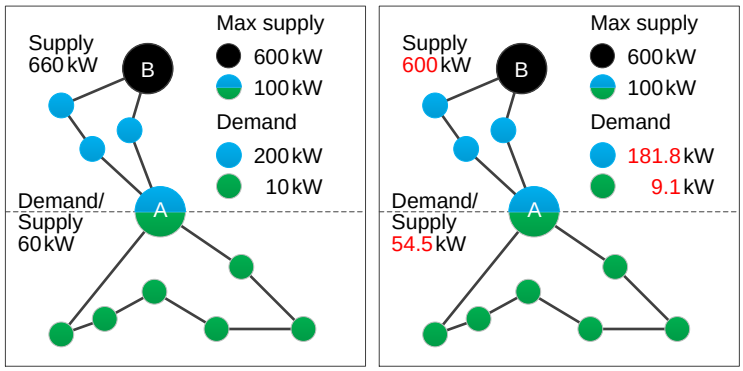

(a) (b)

Figure 2.4: Result of (a) the regular upward simulation process determining each PV bus' power supply and (b) its downward counterpart determining each PQ bus' maximum power demand in case of a PV bus' overload. The horizontal line divides the network into two different voltage levels.

percentage from 60 kW to 54.5 kW. As Substation A can now only consume 54.5 kW, all green consumers together are not allowed to consume more than this value. This requires curtailing the total power demand of each green colored PQ bus from 10 kW to 9.1 kW.

2.3.2.4 Alternative for Step 3: Voltage Level Combination without Regulating Devices

When the installation of voltage regulators at each substation of the PNM is not possible or desired for whatever reason, the voltage level combination step described in the previous Section 2.3.2.3 has to be changed to an iterative process to produce valid results. The first step, the upward simulation, remains identical. Since the installation of regulating devices is omitted, the initialization of each PV bus' voltage with $V_i = 1.0\,\text{pu}$ is only preliminary. The backward simulation process now becomes mandatory to determine the specific voltage at each bus for every voltage level. Additionally to the process described in Section 2.3.2.3, the voltage at each substation's lower voltage winding is set to the voltage of its higher voltage part. This way, the voltage at each consumer is determined only by the voltage drops on the branches being directly or indirectly connected to a power plant without the interference of any regulating device artificially increasing the voltage. If at any consumer at any voltage level Constraint (2.2) is violated, the initialization value of the connected PV bus' voltage is increased by either a fixed value, e.g., $V = 0.01\,\text{pu}$, or the value can be determined by a binary search. With the increased voltage initialization value another iteration of the process is started until Constraint (2.2) is valid for all consumers.

2.4 Scheduling of Battery Energy Storage

Distributed battery energy storage such as batteries of PEVs or small-scale home batteries can be employed to provide services to the power system. Through controlled charging or energy back-feeding, such *grid integrated batteries* could serve for shaving load peaks, filling load valleys, and balancing frequency fluctuations, thus facilitating the integration of renewable energies and mitigating possible grid congestion caused by uncontrolled PEV charging. In this section, a scheduling approach for battery energy storage is presented that can be equally used for demand-responsive charging and energy back-feeding. It includes a battery model appropriately considering the non-linear dependency of battery aging on the *state of charge* (SOC) and the *SOC swing* (alternatively denoted *depth of discharge*) ΔSOC as described in Section 2.4.1. At the same time, real-time electricity prices as well as price forecasts are exploited. This allows to effectively trade off revenues and degradation costs at each point in a battery's lifetime, thus leading to a profit-maximizing solution. Losses due to charging/discharging inefficiencies are also taken into account. In order to make the approach applicable to both stationary and mobile applications, charging needs for the purpose of driving are further considered through appropriate boundary conditions. The optimization procedure as described in Section 2.4.2 is based on a *dynamic programming* algorithm which computes a globally optimal solution sufficiently fast for real-time operation for a single PEV. It is thereby assumed that the charging/discharging power may take any value in a range specified by the maximum nominal C-rate and the used power connection. The optimization

process effectively exploits price information to increase attainable profits for the battery owner without explicitly targeting to maintain power grid stability. This can be achieved with electricity prices reflecting the state of a power system. Prices may be high in times of peak power demand and decrease during times of low power demand.

The presented scheduling approach was collaboratively developed and its basic principles as well as related work are outlined in [13–15]. In this work, the approach is described only to the extent necessary to understand its functioning in the context of the case study conducted in Section 4.3 investigating the power system impact of different road transportation electrification scenarios. Comprehensive information on the approach, its application in different electricity markets, and further details on the presented battery models is detailed in [35].

2.4.1 Models

The scheduling strategy presumes a price-taking battery agent with the objective to maximize its profit Π resulting from the difference between attainable revenues defined in Section 2.4.1.1 and incurring costs defined in Section 2.4.1.2. A large part of those costs is induced by battery aging which is why it has to be appropriately accounted for using the applied battery aging model described in Section 2.4.1.3. The decision variable is the power P, which determines the amount of energy being bought (*grid-to-battery*, G2B) or sold (*battery-to-grid*, B2G)[2]. The problem is time-discrete in the sense that the power P_i in a period i remains constant for the duration Δt.

2.4.1.1 Revenues

The revenue r_i in a period i is proportional to the compensation for providing G2B or B2G, $p_{\mathrm{G2B},i}$ or $p_{\mathrm{B2G},i}$, so that

$$r_{\mathrm{G2B},i} = p_{\mathrm{G2B},i} \cdot |P_i| \cdot \Delta t \tag{2.14}$$

$$r_{\mathrm{B2G},i} = p_{\mathrm{B2G},i} \cdot |P_i| \cdot \Delta t \tag{2.15}$$

The revenue R which can be attained in a sequence of n time intervals can then be written as

$$R = \sum_{i=0}^{n-1} [r_{\mathrm{G2B},i} \cdot \Theta(P_i) + r_{\mathrm{B2G},i} \cdot (1 - \Theta(P_i))] \cdot |P_i| \cdot \Delta t \tag{2.16}$$

In this equation, the indicator function defined as

$$\Theta(P) = \begin{cases} 1, & P \geq 0 \quad \text{(G2B)} \\ 0, & P < 0 \quad \text{(B2G)} \end{cases} \tag{2.17}$$

ensures that each time period generates revenues either from G2B or B2G only.

[2] In the remainder of this work the general idea of bidirectional power flow will be referred to as the *B2G concept*. The direction of power flows either from the grid to the battery or vice versa will simply be termed *G2B* or *B2G*, respectively.

2.4.1.2 Costs

For charging the battery, energy is purchased in period i at an electricity price $p_{\mathrm{E},i}$. A unit of energy further causes battery depreciation costs c_{D}. The power seen by the battery is smaller than the power P_i on the grid side, which is a consequence of energy losses in the system taken into account by the efficiency η. The G2B costs $c_{\mathrm{G2B},i}$ occurring in one period can thus be written as

$$c_{\mathrm{G2B},i} = (p_{\mathrm{E},i} + c_{\mathrm{D}} \cdot \eta_{\mathrm{G2B}}) \cdot |P_i| \cdot \Delta t \tag{2.18}$$

Equivalently, the costs $c_{\mathrm{B2G},i}$ for delivering a unit of energy to the grid are determined by the battery depreciation costs divided by the discharge efficiency η_{B2G} and are defined as

$$c_{\mathrm{B2G},i} = \left(\frac{c_{\mathrm{D}}}{\eta_{\mathrm{B2G}}}\right) \cdot |P_i| \cdot \Delta t \tag{2.19}$$

As the power P is measured from the grid side, charging/discharging energy losses according to η cause the power flow through the battery to be smaller/greater than P during charging/discharging. Therefore η appears in the numerator in Equation (2.18) and in the denominator in Equation (2.19).

Similarly to the revenues, total costs C occurring within n time periods can be written as

$$C = \sum_{i=0}^{n-1} [c_{\mathrm{G2B},i} \cdot \Theta(P_i) + c_{\mathrm{B2G},i} \cdot (1 - \Theta(P_i))] \cdot |P_i| \cdot \Delta t \tag{2.20}$$

2.4.1.3 Battery Aging

Battery degradation involves a decrease of capacity and a power fade, both of which result from calendar aging and cycling of energy. The related aging processes depend on various parameters including C-rate, current SOC, ΔSOC, temperature, humidity, and time. With regard to an optimal charging/discharging strategy, the capacity fade caused by cycle aging is the predominant process which is why the focus is put on this aspect neglecting calendar aging. A one-dimensional dependency on ΔSOC keeps the optimization problem rather simple but neglects the fact that degradation does not only depend on a cycle's depth but also on the SOC range this cycle occurs. A certain ΔSOC at a high or low SOC is generally more detrimental than the same ΔSOC at a moderate SOC. For this purpose, an empirical aging model is adapted from [36, 37] describing the capacity fade depending on ΔSOC and SOC at which the cycling takes place. At low C-rates in the range up to 2 C and constant temperature, these two parameters are the most important factors for G2B/B2G induced aging. The considered cell is a Li(NiMnCo)O_2-based 18650 lithium-ion battery with an initial capacity $CAP_{\mathrm{init}} = 2.15\,\mathrm{Ah}$.

According to this model, the normalized battery capacity $cap_{\mathrm{cyc}} = CAP(Q) \cdot CAP_{\mathrm{init}}^{-1}$ is scaled to $0 \leq cap_{\mathrm{cyc}} \leq 1$ and decreases as a function of the accumulated charge throughput Q according to the relation

$$cap_{\mathrm{cyc}}(Q) = 1 - \beta \cdot \sqrt{Q} \tag{2.21}$$

In this equation, β represents the cycle aging factor which was experimentally determined as

$$\beta = 7.348 \cdot 10^{-3} \cdot (\overline{U} - 3.667)^2 + 7.6 \cdot 10^{-4} + 4.081 \cdot 10^{-3} \cdot \Delta SOC \tag{2.22}$$

In this relation, $\overline{U}$ denotes the average voltage during a *half-cycle* between the start SOC, SOC_{start}, and the end SOC, SOC_{end}, at which the battery is cycled. This number can be retrieved from the *open-circuit voltage* curve by using the relation

$$\begin{aligned} \overline{U} &= \frac{1}{2} \cdot (U(SOC_{\text{start}}) + U(SOC_{\text{end}})) \\ &= \frac{1}{2} \cdot (U(SOC_{\text{start}}) + U(SOC_{\text{start}} + \Delta SOC)) \end{aligned} \tag{2.23}$$

This is a simplification since the voltage curves during charging and discharging are not exactly identical. In the given context the related error can, however, be neglected.

Using the convention that the cycle lifetime is reached once the capacity has decreased to a certain value cap_{EOL}, e.g., 0.8 for automotive applications or to even lower values for stationary or second-life applications, Equation (2.21) can be employed to calculate the battery depreciation costs. With $cap_{\text{EOL}} = 1 - \beta \cdot \sqrt{Q_{\text{EOL}}}$ according to Equation (2.21), the lifetime charge throughput Q_{EOL} of the considered reference battery resolves to $Q_{\text{EOL}} = (1 - cap_{\text{EOL}})^2 \cdot \beta^{-2}$. From a power system perspective, energy throughput in units of kWh is easier to handle than charge throughput given in Ah. This energy throughput associated with Q_{EOL} can be approximated using the average voltage $\overline{U}$ according to the relation $E_{\text{EOL}} = \overline{U} \cdot Q_{\text{EOL}}$. Dividing the cell's initial cost C_{Cell} by the amount of cyclable energy E_{EOL} yields the cell's depreciation costs $c_{\text{D,Cell}}$ per unit of energy at a particular cycling regime:

$$\begin{aligned} c_{\text{D,Cell}} &= \frac{C_{\text{Cell}}}{E_{\text{EOL}}} \\ &= \frac{C_{\text{Cell}}}{\overline{U} \cdot Q_{\text{EOL}}} \\ &= C_{\text{Cell}} \cdot \frac{\beta^2}{(1 - cap_{\text{EOL}})^2 \cdot \overline{U}} \end{aligned} \tag{2.24}$$

Through β and $\overline{U}$, this relation represents the variable battery aging costs depending on both SOC and ΔSOC. In general applications, every charge/discharge process occurs at a different SOC and ΔSOC so that each cycle is related to a distinct β. Consequently, E_{EOL} and $c_{\text{D,Cell}}$ are re-calculated whenever the cycling regime changes. The cell's depreciation costs can be scaled to a battery pack of arbitrary capacity CAP_{BP} as follows:

$$c_{\text{D,BP}} = c_{\text{D,Cell}} \cdot \frac{CAP_{\text{BP}}}{CAP} \tag{2.25}$$

The presented battery aging model produces costs as illustrated in Figure 2.5. Abstracting from any specific battery parameter, costs are depicted as a factor of the costs induced by an infinitesimal ΔSOC at the battery's optimal point of operation at $SOC = 0.44$. As a result,

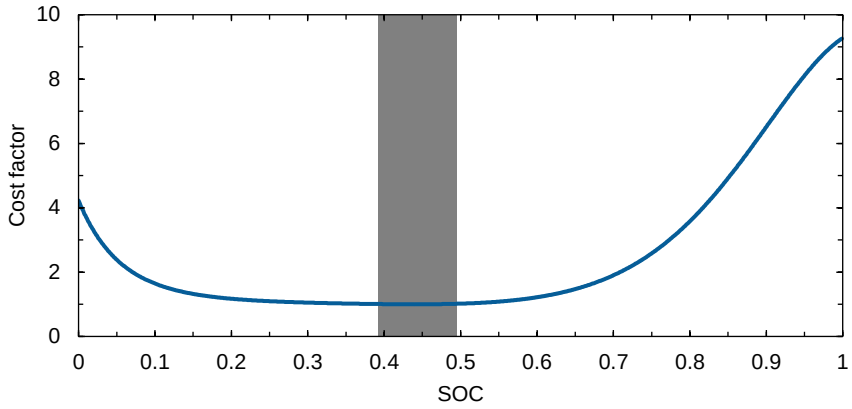

Figure 2.5: Cost factors of an infinitesimal ΔSOC in relation to the costs at the battery's optimal point of operation. The battery's ideal cycling range is illustrated in gray.

costs of a $\Delta SOC = 0.1$ are 2.5 times higher in the SOC range of 0 to 0.1 and even 8 times higher in the range of 0.9 to 1 than in the battery's ideal cycling range of 0.39 to 0.49. This relation is also reflected in the battery's cyclic lifetime of less than 2 000 cycles in the SOC range below 0.1 and less than 1 000 cycles in case of an SOC above 0.9 while exhibiting about 6 million cycles in its ideal cycling range assuming $cap_{\mathrm{EOL}} = 0.8$. This peripheral increase in costs and thus decrease in lifetime is expected to impede extreme SOC states only allowing them to occur when attainable revenues can compensate incurring costs.

2.4.2 Optimization Process

In this section, the cost and revenue model presented in the previous Section 2.4.1 is applied to an optimization process to derive a profit-maximizing charging/discharging schedule including optimal power values for each time period. Every power value thereby depends on current and future electricity prices, battery degradation costs, and possible SOC constraints which may have been imposed to provide a sufficient amount of energy for driving purposes. In Section 2.4.2.1 the optimization problem formulation including possible power and SOC constraints is presented. It is then described in Section 2.4.2.2 how this problem is solved using dynamic programming and a rolling horizon approach.

2.4.2.1 Problem Formulation

Considering battery capacity and C-rate constraints, maximum profits can be achieved by solving the following optimization problem:

$$\text{maximize} \quad \Pi = \sum_{i \in H} (r_i - c_i) \tag{2.26}$$

$$\text{subject to} \quad P_{\min} \leq P_i \leq P_{\max} \quad \forall i \tag{2.27}$$

$$\text{and} \quad 0 \leq SOC_i \leq 1 \quad \forall i \tag{2.28}$$

Both revenues r_i as defined in Equations (2.14) and (2.15) as well as costs c_i as defined in Equations (2.18) and (2.19) are functions of the charging/discharging power P_i. Unlike in *bang-bang control* approaches where P_i is restricted to $P_{\min}$, $P_{\max}$, and 0, P_i can assume any value in the interval ranging from $P_{\min}$ to $P_{\max}$. Given Constraint (2.27), the possible range of power values is determined by the specification of the power connection P^{C} or the battery pack P^{BP} with $\max\{P^{\mathrm{C}}_{\min}, P^{\mathrm{BP}}_{\min}\} \leq P_i \leq \min\{P^{\mathrm{C}}_{\max}, P^{\mathrm{BP}}_{\max}\}$. Equation (2.17) defines $P > 0$ in case the battery is being charged (G2B) and $P < 0$ otherwise (B2G). As described in Section 2.4.1.2, the power is measured from the perspective of the power grid such that a power P fed into the grid equals a power $P \cdot \eta^{-1}_{\mathrm{G2B}}$ drawn from the battery. Constraint (2.28) ensures that the battery's SOC remains between 0 and 1 avoiding deep discharges or overcharging. Solving the optimization problem from Equation (2.26) given Constraints (2.27) and (2.28) yields a maximum possible profit $\tilde{\Pi}$ and a profit-maximizing charging/discharging schedule $\vec{P} = (P_1, P_2, ..., P_{|H|})$ including optimal power values for each time period.

The sequence of charging/discharging power $\vec{P}$ leads to a time series of SOC states which is determined by

$$SOC_{i+1} = SOC_i + \Delta SOC_{\mathrm{G2B},i} \cdot \Theta(P_i) + \Delta SOC_{\mathrm{B2G},i} \cdot (1 - \Theta(P_i)) \tag{2.29}$$

Due to the energy dissipation discussed in Section 2.4.1.2, the charging/discharging efficiency needs to be considered for calculating SOC_{i+1} such that in case of G2B

$$\Delta SOC_{\mathrm{G2B},i} = \frac{P_i \cdot \Delta t}{CAP_{\mathrm{BP}}} \cdot \eta_{\mathrm{G2B}} \tag{2.30}$$

and in case of B2G

$$\Delta SOC_{\mathrm{B2G},i} = \frac{P_i \cdot \Delta t}{CAP_{\mathrm{BP}}} \cdot \frac{1}{\eta_{\mathrm{B2G}}} \tag{2.31}$$

Apart from the Constraints (2.27) and (2.28), additional boundary conditions may be imposed if the battery is not available for grid services. Unavailability from time period j to k leads to the simple constraint

$$P_i = 0 \qquad j \leq i \leq k \tag{2.32}$$

If the battery needs to provide energy during the unavailability time, e.g., for driving, a certain amount of energy $E_{\min}$ has to be stored before period j. At the end of period k, the quantity $E_{j,k}$ has then been drawn from the battery. The corresponding boundary conditions for the SOC before period j and the resulting SOC at the end of period k thus are

$$\begin{aligned} SOC_{j-1} &\geq \frac{E_{\min}}{E_{\mathrm{BP}}} \\ SOC_k &= SOC_{j-1} - \frac{E_{j,k}}{E_{\mathrm{BP}}} \end{aligned} \tag{2.33}$$

In case of a PEV, an expected travel distance $\tilde{d}_{j,k}$ and an estimated energy consumption per driving distance $\tilde{e}$ imply $E_{\min} = \tilde{e} \cdot \tilde{d}_{j,k}$. Upon trip completion, the actual mileage $d_{j,k}$ and energy consumption e are known such that the actual energy consumption is then given by $E_{j,k} = e \cdot d_{j,k}$.

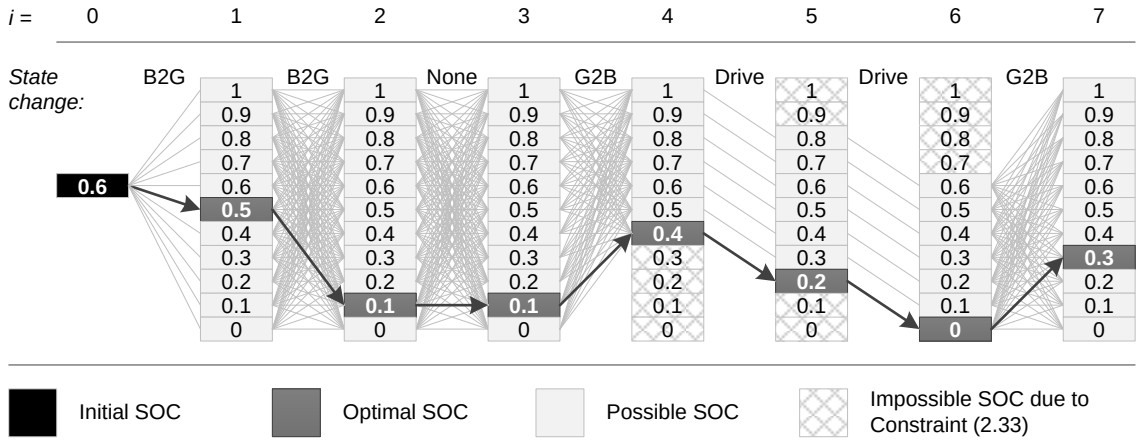

Figure 2.6: Example of a solution for a dynamic programming problem.

2.4.2.2 Solution Method

With a non-linear cost function, continuous variables P_i, and the indicator function introducing an integer, the naive problem formulation leads to a *mixed integer non-linear program*. The computational complexity of this approach is *NP*-hard and increases exponentially with the number of used price forecast periods, referred to as the *lookahead*. This way, computing power quickly becomes a limitation when solving problems with a realistic lookahead of a couple of hours. A more cost-effective approach can be realized by means of dynamic programming [38]. This method leverages on the fact that the optimization over a series of time periods can be decomposed into smaller subproblems which can be solved sequentially. This way, computational complexity is only linearly dependent on the lookahead and can thereby extensively be reduced. The resulting schedule can further be proven to be the global optimum presuming deterministic prices for the considered time periods [38].

The dynamic programming approach is illustrated with an example in Figure 2.6. Here, the evolution of the SOC over 7 time periods with $H = \{1, 2, ..., 7\}$ is shown. From one period to the next, the SOC may either increase when it is being charged (indicated by *G2B*), decrease when it is being discharged (*B2G* or *Drive*), or remain constant when it is neither charged nor discharged (*None*) neglecting calendar aging. Discharging the battery may either occur when energy is fed back to the power grid to provide *ancillary services* (B2G) or when it is used, e.g., for driving in case of a PEV (Drive). The battery's SOC may either remain constant when this is the optimal solution for this time period or in case of unavailability as indicated in Equation (2.32). At any period of time i the SOC can assume values between 0 and 1 being discretized into $\Delta SOC = 0.1$ resulting in a state space defined as

$$S_i = \{SOC_i \in \mathbb{R} \,|\, 0 \leq SOC_i \leq 1\} = \{0, 0.1, ...1\} \tag{2.34}$$

Discharging the battery for driving purposes (Drive) requires $\Delta SOC = 0.2$ for one time period and is assumed for the period 4 and 5. Equation (2.33) therefore requests $SOC_4 \geq 0.4$ and

$SOC_5 \geq 0.2$. The mentioned values are for illustrative purposes only and may individually be modified when applying the optimization algorithm to other cases. Computational requirements grow linearly with the number of time periods and possible SOC values at each period, therefore a reasonable trade-off between accuracy and computational efforts needs to be found in practice.

In the following, the different steps of computing an optimal charging/discharging schedule $\vec{P}$ are explained by applying a forward dynamic programming algorithm:

1. $i = 1$

   Starting with $SOC = 0.6$, the state spaces $S_0 = \{u \in \{0.6\}\}$ and $S_1 = \{v \in \{0, 0.1, ..., 1\}\}$ are in accordance with Equation (2.34). For each combination of u and v total profits $\Pi_1 = S_0 \times S_1$ are calculated according to Equation (2.26). In case a transition from any u to any v is impossible, e.g., due to power limitations, $\pi_{1,u\to v}$ is set to negative infinity for this combination.

2. $i = 2$ to 7

   In a second step, marginal profits are calculated for every transition from $S_1 = \{u \in \{0, 0.1, ..., 1\}\}$ to $S_2 = \{v \in \{0, 0.1, ..., 1\}\}$ resulting in $\pi_2 = S_1 \times S_2$ with $\pi_{2,u\to v} = -\infty$ for impossible transitions from u to v. Total profits are defined as $\Pi_2 = \Pi_1 + \pi_2$. This step is repeated for all remaining ordered pairs of neighboring state spaces $\{(S_2, S_3), (S_3, S_4), ..., (S_6, S_7)\}$.

3. $i = 7$

   In a last step, the maximum total profit $\Pi_{7,\max}$ indicates the final state v_7 of the optimal SOC schedule $\vec{S}$. Starting from this state, $\vec{S}$ is determined by traversing backward through the neighboring state spaces, for each pair picking the state with the maximum marginal profit previously calculated. For each transition between two neighboring SOC states in $\vec{S}$, the required power to allow for the transition can be calculated. The ordered set of those power values is the optimal charging/discharging schedule $\vec{P}$.

The time horizon H which is subject to optimization includes all time periods $i \in H$. In reality, price data will, however, only be available for a subset of those periods covering a time frame of several minutes up to multiple hours being continuously updated. The problem is therefore treated as a *rolling horizon* problem which is illustrated in Figure 2.7. In this example, $H = \{1, 2, ..., 5\}$. Price information available at each time period cover the current and as price forecasts also the next 4 periods. With an increasing size of the forecast horizon, price forecast uncertainties are also increasing which is why the number of time periods actually used in an optimization step, the lookahead, is limited to any number equal or smaller than the forecast horizon and is set to 2 in this example. The optimization process iteratively calculates the final profit-maximizing charging/discharging schedule $\vec{P}$ for all time periods $i \in H$ as follows:

1. $i = 1$

   Starting at $i = 1$, price information is available for the time periods 1 to 5. A subset including the periods 1 to 3 is taken to calculate an optimal but temporary charging/discharging schedule $\vec{P}_1 = (P_1, P_2, P_3)$ for those periods as described in Section 2.4.2.1.

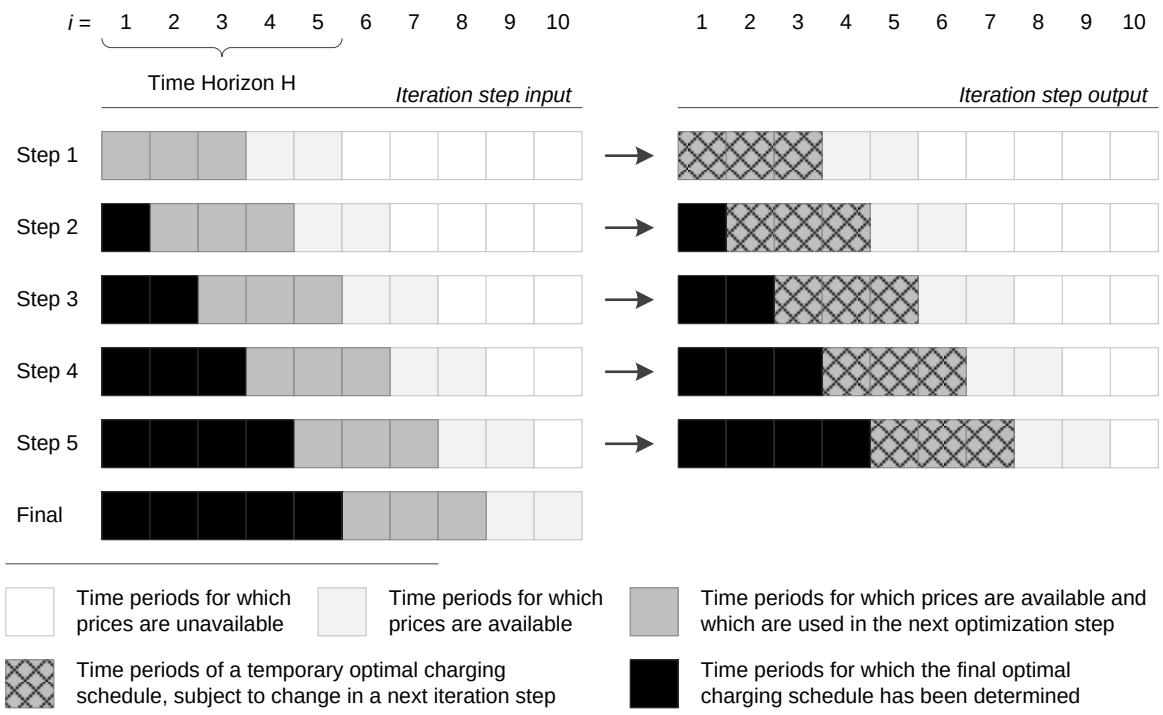

Figure 2.7: Example of a rolling horizon problem.

With respect to the following steps, P_1 is already in the past which is why it is considered immutable. It is thus added to the previously empty final schedule $\vec{P} = \vec{P} \cup \vec{P}_1(1)$.

2. $i = 2$

   In a second step, updated price information for the time periods 2 to 6 are available allowing to re-optimize time periods 2 and 3 while additionally considering period 4. This results in a temporary schedule $\vec{P}_2 = (P_2, P_3, P_4)$ from which again the first element is appended to the final schedule $\vec{P} = \vec{P} \cup \vec{P}_2(1)$.

3. $i = 3$ to 5

   In a last step, for each remaining $i \in (3, 4, 5)$ Step 2 is repeated allowing to add every temporary schedule's first element to the final schedule. This results in $\vec{P} = \left(\vec{P}_1(1), \vec{P}_2(1), \vec{P}_3(1), \vec{P}_4(1), \vec{P}_5(1)\right)$ being compacted to $\vec{P} = (P_1, P_2, P_3, P_4, P_5)$. The maximum possible profit $\tilde{\Pi}$ can be calculated from $\vec{P}$ according to Equations (2.16) and (2.20).

2.5 Evaluating Power Network Models

To conclude on the quality of the PNMs generated by the PSP process and to help differentiate between the various PNMs, emerging patterns need to be identified. As there is no one single pattern, various topological, electrical, and economic properties or metrics from *network*

science as well as from the fields of *electrical engineering* and *management accounting* are applied to allow for a broad evaluation. The PSP approach does not only enable planning customized PNMs of different flavor or for different use cases but instead those metrics also enable to easily compare them with each other on an aggregated level. This way, different PNMs can be analyzed in respect to how they contrast to each other. A comparison may be beneficial for evaluating the applicability of a generated PNM for a specific use case or for assessing the influence of different parameters on the resulting PNM.

The even more interesting usage of those metrics is the comparison with real-world power systems. Due to a limited availability of detailed large-scale power system data, a comprehensive comparison with a PNM is impractical. Instead, aggregated metrics are available for parts of real-world power systems in differing levels of granularity. Depending on the extent and the level of granularity of the available data, extrapolating those values from parts of a power system to an entire PNM may be feasible without jeopardizing the validity of the results.

This section builds the theoretical basis for comparing PNMs by introducing various power system metrics, also in relation to their real-world applicability. Starting with topological metrics in Section 2.5.1, electrical metrics are introduced in Section 2.5.2 followed by economic metrics in Section 2.5.3. Both comparisons of PNMs with each other and with real-world power systems based on the defined properties are conducted on the example of Singapore in Section 4.2.

2.5.1 Topological Properties

For the definition of topological properties a PNM is considered a *complex network* [39]. In principle, network science offers a wide variety of different metrics that could be taken to allow for comparing different PNMs with each other and with real-world power systems. Some of them are redundant because they are alike or have a similar expressiveness. Others may be unsuitable in the context of power systems. Yet others have a computational complexity equal or larger than $O\left(n^2\right)$ and are therefore impractical to determine for large-scale systems. In this section, the most meaningful topological properties for assessing PNMs are introduced and put into a real-world context. For some of the defined properties there is no real-world data available limiting their expressiveness to only comparing PNMs with each other. In Table 2.2, a value range for most of the presented topological metrics from real-world power systems is presented as found in literature. For some use cases the data may fit while for others it may not fit at all. For the LV/MV grid, this is due to the limited number of publicly available networks, all originating from the same source and having only hundreds of nodes. For the HV grid, the high standard deviation of the values, being the result of a large topological variety, limits the data's expressiveness. The given ranges therefore only allow for a rough evaluation of the quality of the generated PNMs in case no data for a specific investigated region or the power system under investigation is available. Applying the data to PNMs of different sizes than the original power systems may additionally distort results.

A PNM is considered a simple, undirected, weighted graph $G = (N, M)$ as defined in [59]. Each node $i \in N$ describes a single bus of the set N of all n buses while each edge $j \in M$ indicates a single branch of the set M of all m power lines. Buses and branches are defined as

Table 2.2: Topological metrics for the LV, MV, and HV part of real-world power systems.

Metric	LV grid [a]		MV grid [b]		HV grid [c]	
	$\bar{x}$	σ	$\bar{x}$	σ	$\bar{x}$	σ
Average path length l [d]	3.16	2.18	6.27	1.19	8.59	3.94
Betweenness b [d]	0.81	0.42	0.38	0.23	–	–
Clustering coefficient cc	0.0040	0.0049	0.0036	0.0043	0.0711	0.0826
Diameter, geodesic $\varnothing_{\mathrm{d}}$	–	–	–	–	49	26
Node degree, max. $deg_{\max}$	–	–	–	–	19.2	9.57
Node degree, mean deg	2.01	0.12	2.15	0.09	2.57	0.42
Node degree, $P(k) \sim \beta$	–	–	–	–	-0.65	0.2
Node degree, $P(k) \sim \gamma$ [e]	1.95	0.45	2.13	0.15	3.07	0.03
Pearson coefficient ρ	–	–	–	–	0.0254	0.1892

[a] All of the 11 networks only represent excerpts of LV networks, specifically from the northern part of the Netherlands. Data originates from [40–42]. The number of nodes n ranges from 14 to 188, the number of edges m from 14 to 191.

[b] All of the 12 networks only represent excerpts of MV networks, specifically from the northern part of the Netherlands. Data originates from [40–42]. The number of nodes n ranges from 191 to 884, the number of edges m from 204 to 1 059.

[c] All of the 48 networks represent full 380/400 kV networks, specifically from the US, Europe, China, and India. Data originates from [41, 43–58]. The number of nodes n ranges from 27 to 49 597, the number of edges m from 33 to 62 985.

[d] Given values are adapted to the definitions of the metrics in this section considering a power network a bidirectional instead of an unidirectional graph. Given values for the average path length are thus divided by 2 while betweenness values are multiplied by 2.

[e] Data about the power law degree distribution originates from [41] only.

in Section 2.2. For expanding the set of topological properties defined in this section, simple self-explanatory cardinalities can be calculated in a PNM such as the *number of nodes* n, *number of edges* m, *number of independent parts* p, as well as the *average number of nodes per independent part* $\bar{n}_p$ or the *total power line length* l. In addition to the mentioned cardinalities, the following supporting measures are defined:

- **Geodesic distance**

  The *geodesic distance* δ_{d} between two nodes i_1 and i_2 is the number of edges in their connecting shortest path σ_{i_1,i_2}. Pairs of nodes are considered to be unordered.

- **Geographical distance**

  The *geographical distance* δ_{g} between two nodes is their shortest path distance measured along the surface of the earth. A flat surface is legitimately assumed since geographical distances are short and power lines are laid underground close to the surface. The geographical shortest path may not be equal to the geodesic shortest path as the weight of each power line is its geographical length instead of its geodesic length being always 1. Pairs of nodes are considered to be unordered.

- **Neighborhood**

  The *neighborhood* H_i of a node i is the set of nodes directly connected to i via an edge.

Definitions of graph metrics can, for instance, be found in [59–62] or in the referenced work in Table 2.2. Depending on the source, the subjacent graph definition, and the employed scope of application, property terminologies and definitions may vary. For reasons of consistency with the previous definition of a PNM as a simple, undirected, and weighted graph and to allow comparing real-world values with those calculated by the PSS framework, properties are defined as follows:

- **Average distance**

  The *average distance* $\bar{\delta}$ of a graph is defined as the mean distance between any unordered pair of nodes i_1 and i_2 in a direct beeline connection as

$$\bar{\delta} = \frac{1}{2n\,(n-1)} \sum \delta\,\{i_1, i_2\} \quad \forall j_{i_1,i_2} \in M \tag{2.35}$$

  In this work, only the *average geographical distance* $\bar{\delta}_\mathrm{g}$ is considered since the geodesic counterpart is by definition always 1.

- **Average path length**

  The *average path length apl* of a graph is defined as the mean distance between any unordered pair of nodes i_1 and i_2 which are directly or indirectly connected as

$$apl = \frac{1}{2n\,(n-1)} \sum \delta\,\{i_1, i_2\} \quad \forall j_{i_1,\ldots}, \ldots, j_{\ldots,i_2} \in M \tag{2.36}$$

  In this work, both the geodesic and the geographical distances, δ_d and δ_g, are considered resulting in an *average geodesic path length* apl_d and an *average geographical path length* apl_g. The average path length is closely related to the average distance but differs in the way that the former calculates distances for pairs of nodes that are already directly or indirectly connected while the latter assumes direct connections between each pair of nodes.

- **Betweenness**

  The *betweenness* b of a graph is a measure for the frequency of nodes being on the shortest path between other nodes normalized to $0 \leq b \leq 1$ and is defined as

$$b = \frac{1}{\frac{1}{2}(n-1)(n-2)} \sum_{i_1 \neq i_2 \neq k} \Theta_{i_1,i_2}(k) \quad \forall i, k \in N \tag{2.37}$$

  In this equation, the indicator function is defined as

$$\Theta_{i_1,i_2}(k) = \begin{cases} 1, & k \in \sigma_{i_1,i_2} \\ 0, & k \notin \sigma_{i_1,i_2} \end{cases} \tag{2.38}$$

- **Clustering coefficient**

  The *clustering coefficient cc* correlates to the *redundancy r* but is scaled to $0 \leq cc \leq 1$. For a node i, the redundancy r_i is defined as the mean number of edges from a neighbor

of i to other neighbors of i. Its possible values are between 0 and $deg(i) - 1$. The clustering coefficient is the scaled mean of each node's redundancy and defined as

$$cc = \frac{1}{n} \sum_{i=1}^{n} \frac{r_i}{deg(i) - 1} \tag{2.39}$$

- **Density**

  The *density* d of a graph is defined as the ratio of the number of existing edges to the number of possible edges as

  $$d = \frac{m}{\frac{1}{2}n(n-1)} \tag{2.40}$$

  In a *dense* graph, the number of edges is close to the maximum number while a *sparse* graph exhibits only a small number of edges.

- **Diameter**

  The *diameter* $\varnothing$ of a graph is defined as the maximum distance between any unordered pair of nodes i_1 and i_2 which are directly or indirectly connected as

  $$\varnothing = \sup \{\delta \{i_1, i_2\}\} \quad \forall j_{i_1,\ldots}, \ldots, j_{\ldots,i_2} \in M \tag{2.41}$$

  In this work, both the geodesic and the geographical distance are considered resulting in a *geodesic diameter* $\varnothing_{\mathrm{d}}$ and a *geographical diameter* $\varnothing_{\mathrm{g}}$, respectively. The diameter is closely related to the average path length but differs in the way that the former calculates the maximum distance while the latter calculates the mean distance.

- **Node degree**

  The *mean node degree* deg of a graph is defined as the average number of edges incident on each node i or equally as the average cardinality of the neighborhood of i as

  $$deg = \frac{1}{n} \sum_{i=1}^{n} |H_i| = \frac{2m}{n} \tag{2.42}$$

  The *maximum node degree* $deg_{\max}$ of a graph is defined as the maximum of all node degrees

  $$deg_{\max} = \sup \{deg(i) | i \in N\} \tag{2.43}$$

- **Node degree probability distribution**

  The *node degree probability distribution* $P(k)$ of a graph is defined as the fraction of nodes having degree k or the probability that a randomly chosen node has degree k. $P(k)$ equals the underlying data of a histogram with a bin size of 1 showing the degree of all nodes in the graph. Real-world node degree probability distributions are *right-skewed* decaying either exponentially or as a power law as indicated in Table 2.2.

  An *exponential* distribution is characterized by the vast majority of nodes having a low degree while very few nodes show a relative high degree. In power systems, those node sets correspond to consumers and substations, respectively. Exponential distributions

show a fast decay in the probability of having nodes with a relative high degree. With its two parameters α and β it is defined as

$$P(k) = \alpha e^{\beta k} \tag{2.44}$$

A *power law* distribution is characterized by the majority of nodes having a small degree while few nodes show a relative high degree. Power law distributions are similar to exponential ones but in contrast they show a slower decay resulting in a higher probability of having nodes with a relative high degree. In a *log-log plot*, power law distributions appear as straight lines. With its two parameters α and γ it is defined as

$$P(k) = \alpha k^{-\gamma} \tag{2.45}$$

- **Pearson correlation coefficient**

  The *Pearson coefficient* ρ is a measure for the assortativity of a graph, describing the extent to which nodes tend to be connected to nodes having a similar degree. It is the *assortativity coefficient* which is normalized to $-1 \leq \rho \leq 1$ and defined as

$$\rho = \frac{m \sum_{i=1}^{n} deg\,(i_1) \cdot deg\,(i_2) - \sum_{i=1}^{n} deg\,(i_1) \sum_{i=1}^{n} deg\,(i_2)}{\sqrt{m \sum_{i=1}^{n} deg\,(i_1)^2 - \left(\sum_{i=1}^{n} deg\,(i_1)\right)^2} \sqrt{m \sum_{i=1}^{n} deg\,(i_2)^2 - \left(\sum_{i=1}^{n} deg\,(i_2)\right)^2}} \tag{2.46}$$

  A pair of nodes i_1 and i_2 is only used when there is a connecting branch j_{i_1,i_2}. Having a positive value, the graph is assortative meaning nodes tend to only be connected to nodes of the same or a similar degree. A negative value indicates a disassortative graph in which nodes tend to only be connected to nodes of a degree most different. With a value around 0 the graph does not show any assortativity resulting in nodes being connected to nodes of any other degree with a similar probability.

2.5.2 Electrical Properties

For the definition of electrical properties a PNM is considered a power system as described in Section 2.2. Other than topological metrics, electrical ones are time-dependent and in their magnitude only valid for a single period of time. In principle, the field of electrical engineering offers a wide variety of different metrics that could be used for comparing different PNMs with each other and with real-world power systems. As with the topological metrics, some of them are redundant or unsuitable. In the following, the most meaningful properties for PNM characterization and comparisons are therefore introduced:

- **Consumer voltage**

  The *average consumer voltage* $\bar{V}$ of a PNM is the average voltage at each consumer and is defined as

$$\bar{V} = \frac{1}{n_{\mathrm{PQ}}} \sum_{i=1}^{n_{\mathrm{PQ}}} V_i \tag{2.47}$$

- **Power line utilization**

  The *power line utilization* $\bar{u}_{\mathrm{PL}}$ of a PNM is the average ratio of the apparent power flow $|S_j|$ on each edge j and its maximum capacity $|S_{\mathrm{max},j}|$ according to Equation (2.3) and is defined as

$$\bar{u}_{\mathrm{PL}} = \frac{1}{m} \sum_{j=1}^{m} \frac{|S_j|}{|S_{\mathrm{max},j}|} \tag{2.48}$$

- **Substation utilization**

  The *substation utilization* $\bar{u}_{\mathrm{PV}}$ of a PNM is the average ratio of the apparent power supply $|S_{\mathrm{S},i}|$ at each substation i and its maximum power supply $|S_{\mathrm{S,max},i}|$ according to Equation (2.1) and is defined as

$$\bar{u}_{\mathrm{PV}} = \frac{1}{n_{\mathrm{PV}}} \sum_{i=1}^{n_{\mathrm{PV}}} \frac{|S_{\mathrm{S},i}|}{|S_{\mathrm{S,max},i}|} \tag{2.49}$$

- **Power demand**

  The total active *power demand* P_{D} of a PNM is the sum of the active power demand $P_{\mathrm{D},i}$ of each consumer i and is defined as

$$P_{\mathrm{D}} = \sum_{i=1}^{n_{\mathrm{PQ}}} P_{\mathrm{D},i} \tag{2.50}$$

  The power demand of a voltage level $P_{\mathrm{D,VL}}$ is accordingly defined as the sum of the active power demand $P_{\mathrm{D,VL},i}$ of each of the voltage level's PQ buses i. Instead of considering all consumers of this one and any lower voltage levels, PQ buses of only this one voltage level are taken into account in this metric. $P_{\mathrm{D,VL}}$ includes power losses which occurred in lower voltage levels and therefore represent the power demand to be satisfied by all PV buses in this voltage level.

- **Power supply**

  The total active *power supply* P_{S} of a PNM is the sum of the active power supply $P_{\mathrm{S},i}$ of each power plant i and is defined as

$$P_{\mathrm{S}} = \sum_{i=1}^{n_{\mathrm{PV,PP}}} P_{\mathrm{S},i} \tag{2.51}$$

  The power supply of a voltage level $P_{\mathrm{S,VL}}$ is accordingly defined as the sum of the active power supply $P_{\mathrm{S,VL},i}$ of each of the voltage level's PV bus i.

- **Power loss**

  The total active *power loss* P_{L} of a PNM is the ratio of the total active power demand and supply and is as percentage defined as

$$P_{\mathrm{L}} = \left(1 - \frac{P_{\mathrm{D}}}{P_{\mathrm{S}}}\right) \cdot 100 \tag{2.52}$$

2.5.3 Economic Properties

Although the focus in assessing a PNM in this work is put on topological and electrical properties, the economic side must not be neglected as it is probably of most interest in real-world applications. Costs may be calculated for installing and operating each single part in a power system. In the context of the PSP process presented in Section 2.2, only power lines and substations are considered resulting in costs C_{E} and C_{N}, respectively. Costs are individually linked to each planned part allowing for an economic assessment both during the execution of the planning process and in a comparative assessment of the final PNM. In the former case, planning additional power lines or laying those of better quality can, for instance, substitute the installation of a more costly substation. In the latter case, differently planned PNMs may not only be topologically or electrically compared but also economically, allowing for identifying unnecessarily expensive models. An economic assessment is especially important when it comes to reliability of and redundancy in a PNM. Here, costs for installing redundant parts have to be contrasted to those costs arising from outages. The cost assignment is an effective measure in case there are multiple, topologically or electrically, equivalent solutions. When planning a power system costs of an electrical part always refer to its *total cost of ownership* including fixed installation as well as variable operating costs over its lifetime.

2.6 Discussion and Related Work

The applied holistic approach is only one possibility on how to solve the problem of generating PNMs. Related approaches are provided in Section 2.6.1. PNMs generated by the framework show topological and electrical properties of real-world power systems. There are, however, several limitations when comparing those PNMs with real-world power systems or conducting power flow studies on them. Those limitations based on the presented methodology only are discussed in the following sections. Limitations on the applicability of PNMs, especially considering limited input data are separately addressed in the context of demonstrating the methodology on the specific example of Singapore in Section 4.2.4. In Section 2.6.2 challenges of reproducing the historic evolution of power systems are discussed. Taking up on this, the impact of neglecting constraints when placing buses or laying branches is described in Section 2.6.3. The various input data and parametrization options of the PSS process are presented in Section 2.6.4 right before the real-world applicability and comparison possibilities of the generated PNMs are discussed in Section 2.6.5. The drawback of limited redundancies when using the network decomposition approach to allow conducting power flow studies on possibly large-scale PNMs using realistic AC models is addressed in Section 2.6.6. Finally, effective restrictions of the presented scheduling approach of battery energy storage are discussed in Section 2.6.7.

2.6.1 Related Power System Planning Approaches

Holistic approaches divide the problem of generating PNMs into various subproblems and apply a particular algorithm to each one. Eventually, results are iteratively combined to

form the final PNM. The presented framework falls into this category of holistic approaches having the highest overlap with other approaches presented in [63–68]. The advantages of the presented framework compared to those approaches have already been outlined in Section 2.1.

From a mathematical point of view, PSP can be treated as a single complex mixed integer non-linear optimization problem [69]. Common approaches include numerical methods such as *mixed integer linear programming* [70–73], *non-linear programming* [74–77], or *dynamic programming* [78, 79]. Due to the *NP*-hardness of the problem, these methods, however, only show good performance for small-scale systems with a few hundred nodes and edges. Therefore, heuristics have been developed which address the problem on a larger scale. These mainly include *genetic algorithms* [80–84], *evolutionary algorithms* [85–89], *tabu search* [90–93], *particle swarm optimization* [94–101], and *simulated annealing* [102, 103].

Regardless of the mathematical approach, all of the investigated PSP models share the same generic problem statement of minimizing an economic cost function subject to technical and operational constraints. Thereby, the location and power rating of substations as well as the type and routing of power lines are considered the design variables. Power flow equality, substation and power line capacity limits, as well as bus angle and voltage limits are most commonly used as constraints. Mathematical approaches minimizing a cost function produce optimal results within their defined limits, thereby neglecting that real-world power systems are far away from being optimal due to their evolution as discussed in the following Section 2.6.2. Holistic approaches are differently motivated. Instead of requiring a fixed set of input data based on which an optimal PNM is generated, they can be parametrized to compensate missing data to some extent. Depending on the scope of application, one approach may be superior to the other. This framework is motivated by allowing researchers, planners, or experts of adjacent areas to use their various sets of incomplete input data to generate realistic PNMs tailored to their specific use case and subsequently conduct power flow studies on them as mentioned in Section 2.1.

PSP approaches can further be distinguished into their planning strategy: *greenfield planning* [64, 65, 87, 94, 95, 102], *expansion planning* [70–78, 81–83, 85, 86, 90, 92, 97–99, 103], or supporting both [66, 79, 80, 91]. The planning period may either be *static single-stage* [64–66, 72, 74, 75, 77, 79–81, 85–87, 90, 91, 94, 95, 102, 103] or *dynamic multi-stage* [70, 71, 73, 76, 78, 82, 83, 92, 97–99]. In the former, planning is conducted only based on the requirements of one single planning period, the latter spans the requirements over several planning periods temporally build on each other. PSP approaches also differ in the voltage level they are applied to: *LV* [64, 65, 80, 91], *MV* [70–73, 75–79, 81, 82, 85–87, 90, 92, 97–99, 102, 103], *HV* [104], or any combination of them [66, 74, 94, 95]. When supporting multiple voltage levels, planning and connecting them can be done *top-down* or *bottom-up*, depending on the kind of available data. The presented framework implements a holistic, bottom-up, static single-stage approach to plan PNM covering all voltage levels from scratch while also supporting expansion planning.

An excellent overview of the different approaches applied in the field of PSP, their design variables, constraints, planning strategies and periods, as well as voltage levels is provided in [69]. Not going into detail with respect to holistic approaches, current and future trends in this field are extensively analyzed and classified. Additionally, the shift from traditional single

objective PSP approaches being concerned with finding the most economic solution towards modern multi-objective PSP approaches including distributed generation technologies mainly being solved using heuristic algorithms is shown. Decomposition methods as applied in the presented framework are identified as a required trend in solving future PSP problems being decentralized, large-scale, multi-stage, and complex.

2.6.2 Evolution of Power Systems

The historic evolution of a power system does not necessarily follow an optimal development path as assumed by the greenfield planning. Using this approach, a power system which is able to satisfy the current power demand specified in the consumer input data is planned from scratch. This way, PNMs showing realistic aggregated topological, electrical, and economic properties of real-world power systems are indeed being generated. They may, however, significantly differ on a detailed level with respect to the geography and technical specification of the planned buses and branches. Using the same parametrization and input data for an entire voltage level without differentiating between planned electrical installations of this level fosters divergence from the represented real-world power system on a detailed level. This limitation of failing to reproduce the evolutionary development of real-world power systems partly falls by the implemented expansion planning.

Expansion planning describes the approach of modeling the evolution of the number of consumers and their power demand by extending an already planned PNM or parts of it with additional components, e.g., power lines, substations, consumers, etc. In [11, 105] the different aspects of expansion planning are further discussed. In reality, components may not always be newly built or *expanded* but instead existing ones get enhanced or *upgraded*. In contrast to expansion planning which extends a network by adding additional components, *upgrade planning* also considers the possibility of modifying existing parts of the network depending on certain topological, electrical, and especially economic conditions. In some cases it may, for instance, be economically more beneficial to upgrade a substation to increase its maximum power rating than planning an additional one. Although results would be more realistic, little efforts have yet been made in further investigating this approach in the context of PSP planning on a large scale. The already high complexity of the optimization problem would this way be increased by another dimension. Due to their modular composition, holistic approaches such as the presented framework are exceptionally suitable to be extended by an upgrade planning module in future.

With greenfield, expansion, and upgrade planning, the methodologies to realistically reproduce the evolution of real-world power systems exist. They, however, require an extensive amount of historic data which may be tough to acquire with regard to the rarity of even current detailed power system data. The presented framework therefore focuses on greenfield and expansion planning with the option to multi-purposely parametrize the planning process according to the available input data to generate PNMs with a large variety of different characteristics.

2.6.3 Placement Constraints

The presented PSP approach at its current stage does, for reasons of limited availability of data, not explicitly consider economic, geographical, or environmental constraints when placing buses or laying branches. Instead, buses are placed at the load gravity center of an area regardless of any constraint, e.g., regional subsidies, access to fuel and water, nature protection and pollution restrictions, etc. Power lines are laid as straight lines connecting two buses with the shortest beeline distance also neglecting physical routing constraints, e.g., obstacles or high-cost passages. If data is available, the locations of individual power plants and substations can be explicitly specified. For the focus of the PSP approach, generating PNMs which closely resemble provided metrics of corresponding real-world networks using minimal input data, considering placement constraints in the regular planning process is, however, not required. With regard to increasing the attractiveness of the approach to, for instance, power system planners, including a *geographical information system* (GIS) approach to account for the above-mentioned aspects would be a powerful extension. A possible implementation may be to divide the given region into tiles each associated with a cost value of placing a bus in or laying branches through it. In the former case, the part of the PSP process described in Section 2.2.3 is extended to select the cost-minimal tile closest to the load gravity center. In the latter case, the part described in Section 2.2.6 is extended by a cost-minimal routing option when connecting two buses with each other.

For generating PNMs with realistic properties, the power line length is, however, much more important than its exact path. Power line stretch factors virtually extend the length of power lines to account for non-beeline paths in reality without requiring to apply a data-intensive GIS approach. This way, electrical and economic properties such as power losses and investment costs are realistically considered. Choosing the correct stretch factors heavily depends on the available input data and is subject to individual tailoring. An indication for the magnitude of stretch factors may, for instance, be received assuming power lines are laid according to the road network of a region. In [66], the length of a power line in the LV (MV) grid has to be extended by a factor of approximately 1.2 (1.4). Those values can, however, only serve as a basis for further analyses individual to each use case, as perfect information on the input data is assumed and off-road power line branching within buildings is neglected. Although the spatial composition of installations may deviate in reality without applying a GIS approach, stretch factors allow employing incomplete input data while still being able to generate PNMs with realistic electrical and economic properties. If, for instance, the available set of consumers is incomplete and therefore less power lines are planned but the total power line length or power losses are known, generated PNMs may account for this lack of input data by an increased stretch factor.

2.6.4 Input Data and Parametrization

The PSP approach requires minimal input data including a number of consumers each specified by a distinct pair of spatial coordinates and its active power demand. Additional data may optionally be provided to further exert influence on the output. To realistically model power flows, the reactive power demand is additionally required. It may either be directly provided

or calculated from a power factor which can optionally be defined. If not stated otherwise, consumers are placed on the lowest available voltage level. In case of conducting power flow studies, power demand values for multiple time periods can be provided. Consumer power demand values may also be multiplied by a factor to investigate different scenarios both when planning a PNM or only when conducting power flow studies. The resulting PNM may largely differ in its dimension among different sets of input data as this data is elementary to the planning process. The PSP approach can furthermore be multi-purposely parametrized to accommodate different sets of input data and to generate PNMs with a large variety of different characteristics. Parametrization thereby takes place either generally on the level of single voltage layers in the regular PSP process or individually through expansion planning. The challenge is thus to find the parameter set most realistically reproducing the real-world power system under consideration. *Monte Carlo* simulations [106] and *ceteris paribus* sensitivity analyses [107] can both be conducted to identify the impact of the different parameters and parameter uncertainty. Providing parameter values is optional. In case a parameter is omitted, best practice values from different real-world power systems are applied. In Section 4.2.1.2 reference values for the Singapore power system are provided. The following parameters may be varied in the regular PSP process:

- **Voltage level**

  A real-world power system is divided into multiple voltage levels. As input, the number of specified voltage levels can be as fine-grained as the investigated power system. The PSP process is iteratively executed for all voltage levels starting with the lowest one.

- **Topology**

  The topology as described in Section 2.2.6 comprises ring, radial, and meshed networks and can be varied per voltage level.

- **Stretch factor**

  Power lines connect two buses with the shortest beeline distance. Stretch factors are introduced to realistically consider selected electrical and economic properties in the generated PNM by virtually extending the length of power lines to account for non-beeline paths in reality. More details on stretch factors can be found in Section 2.6.3.

- **Substation specification**

  Besides the target number of substations, their maximum power supply, efficiency, and costs as well as constraints regarding their minimum and maximum utilization may be specified per voltage level. Additionally, a bus voltage range can be optionally provided. The mentioned parameters have an immediate effect on the actual number and utilization of planned substations and therefore also on the number, utilization, and length of the laid power lines.

- **Power line specification**

  Power line parameters include the resistance and reactance of power lines, their costs, as well as constraints regarding their minimum and maximum utilization specified per voltage level. The mentioned parameters have an immediate effect on the number,

utilization, and length of the laid power lines and therefore also on the number and utilization of the planned substations.

- **Algorithmic parameters**

  Each applied algorithm can be parametrized resulting in a maximum number of nodes for each subregion for the bisecting (Section 2.2.2), the number of iterations for the k-means (Section 2.2.2), the maximum distance between two nodes for the DBSCAN (Section 2.2.6), as well as the target average mean degree for the DT (Section 2.2.6). The mentioned parameters have an effect on the specific outcome of each algorithm without altering their general functioning.

- **Customized planning**

  Besides greenfield planning, an already planned PNM or parts of it can be expanded using available data on existing electrical installations to exert influence on the planning process. Data which can be provided include the location plus the data specified under the list item *Substation specification* earlier in this section for both substations and power plants as well as data specified under the list item *Power line specification*. More details on customized planning can be found in Section 2.6.2.

- **Network recombination**

  The part of the PSP process described in Section 2.2.5 may be used to reduce the number of planned substations per voltage level to any value arriving down at the cost-optimized solution. Due to the large parameter space requiring a heuristic approach, the cost-optimized planning option cannot be expected to yield a global optimum. Results presented in Chapter 4, however, show that the presented network recombination heuristic is able to exploit the optimization potential to a large extent independently of the specific network. Reducing the target number of planned substations has an immediate effect on the actual number and utilization of planned substations and therefore also on the number, utilization, and length of the laid power lines.

2.6.5 Applicability of Network Properties

As discussed in Section 2.6.2, the historic evolution of a power system does not necessarily follow an optimal development path. Instead, real-world power systems gradually grow according to changing demands impeding their artificial reproduction. The question if there is one unifying underlying generative process for all or most of them has driven research to come up with different approaches of generating PNMs producing different results. Network science can help quantifying those differences by recognizing emerging pattern and defining properties to conclude on the quality of the generated PNMs. Topological, electrical, and economic properties defined in Section 2.5 cover a broad range of possibilities to quantitatively compare different PNMs with and analyze how they contrast to each other. Comparing the different PNMs with real-world power systems based on those properties allows evaluating the applicability of the generated PNMs for specific use cases.

Real-world power systems are quite similar in some of the presented metrics although not concurring in all of them. If only a few properties are taken when evaluating PNMs there is the risk of overfitting the PSP process to generate PNMs trying to match those characteristics while neglecting others. The more properties are included in the design of the PSP process and a later comparison, the better different PNMs can be distinguished but also the more likely it is to identify differences to the investigated real-world power system. The problem with those properties is that they conclude on an aggregated level while being unable to spot differences in a PNM's details. An explicit reproduction of real-world power systems requires large amounts of evolutionary data often being unavailable thus limiting conclusions on the quality of a PNM to a comparison of those aggregated metrics.

In the context of limited availability of real-world power system data it is important to define the parameters that match each individual's purpose. In case, for instance, the total branch length and therefore realistic power losses are of interest, power lines may either be laid connecting buses in a beeline and afterwards being extended by an average stretch factor or they may follow available data on how they are routed. The resulting PNMs for both variants are equal on an aggregated level regarding the defined metric but they may highly differ in their details. Developing a unifying process for generating realistic PNM showing all the characteristics of real-world power systems is data-intensive and, because those systems are multifarious, very challenging. The presented approach therefore addresses this problem with a modular multi-algorithm process which can be multi-purposely parametrized to tailor the generated PNMs to the specific use case. For this purpose, a set of different metrics is defined and augmented by reference values from real-world power systems to allow evaluating and comparing generated PNMs. Provided reference values can, however, only indicate the order but not the exact values which are biased due to the small number of available power grids.

2.6.6 Network Decomposition

Conducting power flow studies on large-scale PNMs within a reasonable amount of time using a realistic non-linear AC model requires decreasing the solution space. A network decomposition approach is therefore implemented which divides a PNM into independent parts allowing the power flow problem to be individually solved for each part. Alternatively, the AC model can be approximated by a linear DC one trading in accuracy for performance. Either way, computational requirements only grow linearly with the size of the PNM not limiting the number of electrical consumers or voltage levels to a certain number. Power flow studies on city-scale PNMs can thus be conducted within seconds.

The network decomposition approach is not applicable to PNMs showing high redundancies as it is based on dividing a PNM into independent parts. The larger the individual parts the higher the computational requirements. In the PSP process, radial and ring networks are currently planned without connections between different areas. Since both types of topologies are mainly used in LV and MV real-world power systems showing only limited redundancies if any at all, generated PNMs quite, although not absolutely, accurately reproduce reality in this regard. Meshed networks, mostly found in HV grids, by definition already show redundancies. Since HV grids typically only comprise a couple of hundreds or thousands

of buses and branches, computational requirements are manageable. Allowing to freely set the level of redundancy according to the available computational resources to realistically account for redundancies existing in real-world power systems would certainly increase the attractiveness of the approach.

2.6.7 Scheduling of Battery Energy Storage

The scheduling approach optimizes charging/discharging of mobile or stationary battery energy storage by means of dynamic programming. It builds on a battery model allowing to realistically quantify battery aging costs and utilizes present and forecasted electricity prices to determine a charging/discharging schedule which is globally optimal given deterministic prices. In practice, however, several limitations restrict optimality:

- **Battery aging model**

  The applied battery aging model defined in Section 2.4.1.3 is empirically derived for a specific cell type. Common to all empirically derived models is their limited expressiveness to precisely quantify battery aging costs for other cells of this type, much less for cells of other types. This is mainly due to deviations in the manufacturing process. Another reason are the many changes in the cycling regime of a PEV's battery that cannot be accurately reflected in synthetic cycling tests. Based on an empirical model, continuous re-calibration during operation time is required by employing a battery *state of health* online-monitoring technology [108]. This way, a sound cost estimation depending on the current battery state including calendar aging which is so far neglected in the current model can be achieved.

- **SOC operating range**

  Related to the applied battery aging model is the operating range of the SOC. The scheduling approach tends to keep the battery at SOC states around its optimal point of operation at 0.44 and moderate ΔSOCs. This way, extreme SOC states or deep cycling can be avoided both having a detrimental effect on the battery's lifetime. Imposed restrictions on the charging/discharging power thus only have a negligible effect on the resulting profits. Similarly, keeping a moderate SOC buffer reserved for driving purposes of almost up to the battery's optimal operation point only insignificantly reduce profits.

- **Price information**

  Available price information for real-time electricity markets often include a forecast horizon of several hours. Those forecasts, however, are subject to uncertainties, usually the larger the more ahead they predict the future. The optimization process implicitly deals with those price uncertainties by means of the rolling horizon approach without explicitly learning from historical data. The latter approach would be a powerful extension since imperfect price information may distort optimality of the process and narrow down profits. Given price information exhibiting high accuracy as they are usually available in electricity markets for a couple of hours, the lookahead can have a significant positive effect on profits when increased within a range of several hours while any further increase does not lead to notable improvements as shown in [15].

- **Dispatch probability**

  The optimization process assumes probabilities of 100 % on its determined power values neglecting possible power system constraints. For small-scale batteries as employed in PEVs or at home this assumption may be accurate in today's power systems in the G2B case. An uncontrolled energy supply in the B2G case may destabilize the power system. Energy dispatch therefore needs to be coordinated by a central instance resulting in probabilities of less than 100 %. Lacking dispatch probability data from any real-world power system, the influence of the made assumption remains an open question and needs to be further investigated.

2.7 Conclusions

In this chapter, a holistic modular PSS framework including a PSP and power flow simulation approach for generating and evaluating large-scale PNMs is presented. The methodology iteratively employs a combination of algorithms allowing to create PNMs with a great variety of different characteristics using minimal input data. The framework is able to generate PNMs bottom-up using consumer location and power demand data to particularly allow for a more realistic planning of the LV grid. With its versatility and ability to flexibly tailor the power grid to individual use cases, the framework overcomes the common problem of limited availability of information on real-world power systems. The analysis and comparison of different PNMs especially compared to real-world power systems is facilitated by defining various topological, electrical, and economic properties.

The PSS framework comprises an AC power flow simulation which is used to ensure that the generated PNMs are functional. Furthermore, it can be used to conduct studies simulating power flows under arbitrary tempo-spatial load profiles. The simulation calculates the capacity utilization at every bus and branch as well as the voltage at each consumer and substation which allows identifying times and locations of grid congestion and voltage drops. The price-responsive energy storage scheduling approach considers battery degradation and electricity price forecasts to shift charging/discharging into time periods being effective with respect to maintaining power grid stability. It also ensures an economically profitable operation for the battery owner while complying with given constraints. This becomes handy in case of a large-scale integration of battery energy storage into the investigated power system to avoid further peak load increase when charging those batteries.

On the level of topological and electrical properties, PNMs generated by the framework match real-world power systems. The framework, however, comprises several limitations which can be ascribed to a lack of available input data. It misses to emulate the evolution of real-world power systems and neglects placement constraints and inhomogeneities of electrical installations on the same voltage level. While for some purposes PNMs may not require a more detailed modeling, for others the value of those PNMs may be limited. In the context of applying the framework on the example of Singapore in Section 4.2, the effect of limited input data in general and the mentioned limitations in particular on the explanatory power of the generated PNMs is discussed.

3 | CityMoS Platform

Content

As a distributed simulation platform comprising a power and a transportation system simulation, CityMoS provides the infrastructure required for investigating the impact of different road transportation electrification scenarios on urban power systems.

3.1 Introduction

Answering this work's research question of quantifying the impact of large-scale road transportation electrification on urban power systems requires a simulation platform, as anticipated in the proposed solution statement. Such a platform has to comprise at least a power and a transportation system simulation interoperating with each other. A detailed investigation requires both simulations to be modeled at the microscopic level considering the behavior of individual elements. For the transportation system these elements are the single vehicles while for the power system individual consumers, substations, power stations, and power lines need to be modeled. This allows exploring the power system impact of a great variety of different electrification scenarios, scheduling strategies, *vehicle-to-grid* (V2G) implementations, charging behaviors, and CS distributions. Considering both systems at the same time further allows optimizing charging infrastructures and scheduling strategies with regard to optimal satisfaction of the power demand and minimal power system impact. Other possible application scenarios include the investigation of the impact of distributed energy sources or the transition towards more intelligent consumers participating in demand response schemes. Also, scenarios for expanding power networks in developing countries under fast changing conditions can be explored.

The *City Mobility Simulation* (CityMoS), previously termed the *Scalable Electric Mobility Simulation* (SEMSim), described in this work is such a simulation platform allowing different, possibly *distributed simulations* [109] to interact with each other. In CityMoS, the specific interacting simulations are not stipulated but instead they depend on the individual use case allowing them to be freely combined. CityMoS as used in the context of this work comprises an agent-based transportation system simulation interoperating with a power system simulation using an open standard while at the same time offering the possibility to interactively and visually influence the simulation which is currently unique, especially with the offered functionality of the different platform components. In the following, the individual components of CityMoS used in this work are presented:

High Level Architecture (Section 3.2) is a standard for constructing reusable and interoperable distributed system simulations enabling bidirectional communication among the different entities, even across heterogeneous hardware and software platforms. This section outlines the different components of the standard, discusses available implementations, and provides an overview on the general process involving multiple interacting simulations.

CityMoS Power (Section 3.3) is an implementation of the PSS framework described in Chapter 2. Its purpose is planning and evaluating PNMs which realistically emulate an actual infrastructure as well as subsequently conducting power flow studies with different road transportation electrification scenarios on those PNMs. This section focuses on the software implementation part of the PSS framework as part of the CityMoS platform.

CityMoS Traffic (Section 3.4) is an agent-based transportation system simulation able to realistically simulate trips of a PEV population corresponding to the real vehicle population of a city. In this section the different simulation components are described. CityMoS Traffic is the only part of the CityMoS platform which was not developed in

the context of this work but instead simply used as an externally prepared simulation component.

CityMoS Frontend (Section 3.5) is an interactive visualization tool allowing to participate in and controlling of distributed simulations using the High Level Architecture. The user is thereby enabled to simultaneously interact with multiple simulations and visually inspect their output at runtime. In addition to possible interactions occurring in the context of the CityMoS platform, its main functionality with respect to both visualizing data and providing user interactivity is described in this section.

The remainder of this chapter is concerned with explaining the platform's architecture, the specific requirements for each simulation to participate in a distributed simulation, and the exchanged interactions in Section 3.6. This description is followed by a discussion of alternative ways of constructing distributed system simulations, experiences with the implemented standard, as well as the CityMoS platform in general and alternatives to its power and transportation system simulation in Section 3.7. Section 3.8 concludes this chapter.

3.2 High Level Architecture

The *High Level Architecture* (HLA) is a standard describing an architecture to construct reusable and interoperable distributed system simulations. It was developed by the *Modeling and Simulation Coordination Office* (M&S CO) of the *United States Department of Defense* (US DoD). A first complete specification, HLA 1.3, became available in 1998 [110]. In 2000, a slightly revised version was merged into the superseded IEEE Standard 1516-2000 [111]. It later evolved into the active IEEE Standard 1516-2010 [112]. In HLA-compliant system simulations a participating entity is termed *federate*. This may either be a simulation, an interface to a human-controlled system, or a supporting utility, e.g., a visualization or data collection. The declaration of a set of distributed federates interacting with each other is termed *federation*. By instantiating a federation and therefore executing the system simulation a *federation execution* is created and their members become *joined federates*.

HLA is composed of three parts as shown in Figure 3.1. First, the *object model template* (OMT) provides a specification for the definition of data that is produced or required by a federate. A description is given in Section 3.2.1. Second, services are specified which allow federates to connect, exchange data, and coordinate activities during a federation execution. This *interface specification* is outlined in Section 3.2.2. Third, HLA provides a set of ten rules to ensure a proper interaction of federates within a federation. They are described in Section 3.2.3. As a standard, HLA itself provides no implementation of the specified services. Creating a federation execution therefore requires an additional software component that implements the interface specification called the *runtime infrastructure* (RTI). General information and an overview of the most common RTIs are presented in Section 3.2.4. For a better understanding of the federation execution process, necessary service calls shared by all joined federates are illustrated in Section 3.2.5.

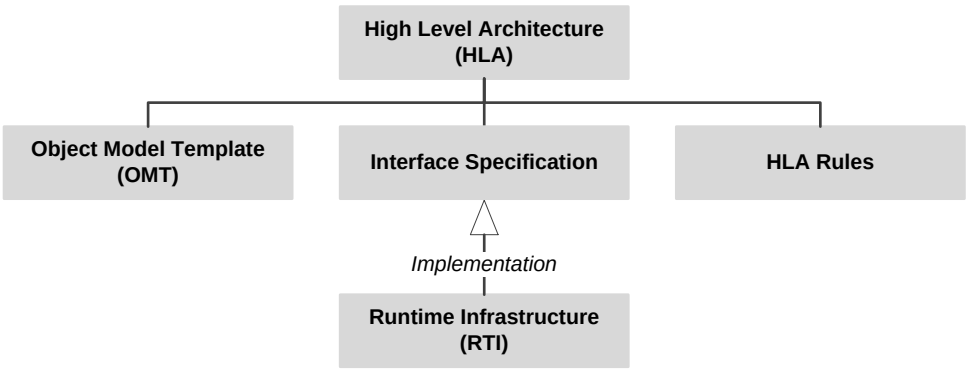

Figure 3.1: Components of HLA.

3.2.1 Object Model Template

The OMT specifies the format and syntax how object and interaction classes are defined and is described in full detail in the IEEE Standard 1516.2-2010 found in [113]. Its objective is to facilitate interoperability among simulations and reuse of simulation components. The relation between the different elements defined in the OMT is illustrated in Figure 3.2. Data being exchanged in a federation execution is either an *object instance* or an *interaction* characterized by *instance attributes* or *parameters*, respectively. Object instances are unique instantiations of *object classes* having their state defined by the values of their instance attributes. They are created or destroyed at will by their owning federates. An object class is a template described by a set of *class attributes*. No operations are defined in an object class but instead kept resident in the individual federates. Object instances do not directly interact but instead individual federates interact with each other via HLA services by updating instance attributes or by sending interactions. An interaction is regarded an event within the federation execution which is of a specific *interaction class* type and described by a set of parameters. In contrast to object instances, interactions are not persistent and no reference is kept after they have been delivered.

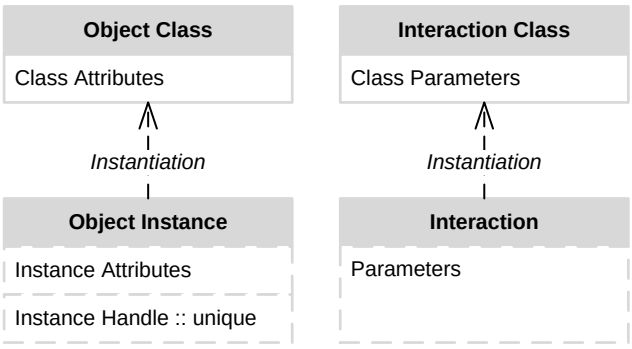

Figure 3.2: Elements defined in the OMT.

The OMT provides a standardized mechanism for describing the capabilities of an individual federate as well as for specifying data being exchanged between joined federates of a federation. Both mechanisms are described in the following:

- **Simulation object model (SOM)**

  The SOM describes the entire set of object and interaction classes along with their attributes and parameters that an *individual federate* is able to produce or request. It provides the required information to assess the appropriateness of a federate to participate in a federation. A SOM may be specified in one or multiple subsets called *modules*.

- **Federation object model (FOM)**

  The FOM describes the entire set of object and interaction classes along with their attributes and parameters that the *entirety of joined federates* within a federation is able to produce or request. It therefore specifies the data that is being exchanged between the joined federates. The intersecting set of all joined federates' SOM modules forms a FOM that comprises all possible object and interaction classes together with their attributes and parameters. Other FOMs being a subset of this FOM may alternatively be specified to limit the federation execution's functionality according to the applied use case. In any case, the FOM, like the SOM, may be specified in one or multiple modules.

FOMs and SOMs are described using the *Extensible Markup Language* (XML) [114], a simple yet very flexible markup language for encoding documents readable to both humans and machines. The XML specification defines two levels of correctness for XML documents being *well-formed* and *valid*. Documents following the syntax constraints of the XML specification are well-formed. An XML document is valid if it is well-formed and complies with an XML Schema which can be defined by applying a schema system like the *XML Schema Definition* (XSD) [115, 116]. An XSD file therefore provides a formal specification of an XML document's syntax. It can be used to easily check a referring XML file for compliance violations regarding required and optional elements and attributes, applying restrictions, as well as key, key reference, and uniqueness constraints. Semantic constraints cannot be expressed in an XSD. Instead, the ISO/IEC Standard 19757-3 *Schematron*, a rule-based validation language for XML files, described in [117], may be used.

In the IEEE Standard 1516.2-2010 two possible XML Schema definitions are provided which differ in being strict or relaxed regarding the required or optional usage of elements and attributes. The strict version defines most elements and attributes to be required. This version is targeted for the final object model definition. For development purposes or when an object model definition is split over multiple modules the usage of the more relaxed version is intended. With neither of the provided XML Schemas the entire IEEE Standard 1516.2-2010 can be expressed due to XSD inherent limitations. Conformance tests regarding attribute and parameter name duplication cannot be expressed in XSD but instead another language, e.g., Schematron, has to be used. All object models used within a federation execution should either fully conform to the complete definition of this XSD file or ideally to the rules and constraints stated in the IEEE Standard 1516.2-2010.

3.2.2 Interface Specification

The *interface specification* describes the interfaces for the available services between federates and the RTI. Those services can be initiated by either the federate or directly by the RTI. The first case describes the normal process of having a federate calling an RTI service. In the latter, services implemented by a federate are called by the RTI to forward data from other joined federates or for callback purposes on federate requests in the latter case. The interface specification explicitly describes the functionality of each service, i.e., interface name, description of service, passed argument and returned values, pre- and postconditions, exceptions, and related services. It thus specifies the interaction of HLA-compliant simulations and the RTI but does not itself provide the functional implementation. A detailed description of the interface specification is given in the IEEE Standard 1516.1-2010 found in [118]. Services specified are logically arranged into the following service groups:

- **Federation management**

  Services offered by the federation management control activities applying to the entire federation throughout the lifetime of a federation execution. Those services mainly include the creation and destruction of federation executions as well as federates joining and resigning from them. Additional services are related to the management of synchronization points and the federation's save and restore process.

- **Declaration management**

  Services offered by the declaration management are concerned with specifying the data a joined federate produces or requests. Publication and subscription services for object and interaction classes are provided.

- **Object management**

  It is the object management that is responsible for managing life cycle activities of object instances and interactions exchanged between joined federates within a federation execution. Services mainly include registering, discovering and deleting object instances, updating and reflecting instance attribute values, as well as sending and receiving interactions.

- **Ownership management**

  Each instance attribute among a federation execution is owned by at most one joined federate which is the only entity allowed to update its value. This way, data coherency across a federation execution is guaranteed. The ownership management provides services to request, divest, or acquire ownership for individual instance attributes.

- **Time management**

  HLA's time management service is designed to support both *discrete-event* and *time-stepped* simulations, the latter also including real-time and scaled real-time simulations. Time in a federation execution is defined as points along the HLA time axis being a distributed virtual clock. The internal time representation of a joined federate synchronized to this time axis is called *logical time*. Services offered by the time management are concerned with advancing all joined federates' individual logical times along the

HLA time axis in a controlled way. A regression in time is not allowed. Joined federates request to individually advance their time not necessarily in the same but also in a different or variable resolution. This may result in joined federates being at different logical times at any instant during the course of the federation execution.

Messages exchanged among joined federates may be either in *timestamp order* (TSO) or in *receive order* (RO) differing only in the order in which they can be received by other federates. By default messages are received as RO messages in an arbitrary order. Allowing joined federates to receive well-ordered TSO messages the following conditions have to be satisfied:

1. A timestamp is provided in the message
2. The sending federate is *time-regulating*
3. The receiving federate is *time-constrained*

In case only the first two conditions are satisfied, a TSO message is indeed being sent but converted to an RO message before being delivered to the receiving federate.

During the federation execution process joined federates may request to advance their logical time. Messages sent by joined federates are then received by subscribing federates. It is guaranteed though that all messages with a timestamp equal or less to the requested advancing time are delivered to the federate and that no messages with a timestamp equal or greater are to be sent by this federate before granting the time advancement.

- **Data distribution management**

  Services of the data distribution management extend those of the declaration management by specifying distribution conditions. Data transmission and reception may be limited on instance instead of class attribute level as well as on interaction level instead of interaction class level. Data irrelevant to individual federates may thus already be effectively filtered at the source without the need to transmit the data in the first place.

- **Support services**

  Upon creation, each federate, object class, object instance, instance attribute, interaction class, or parameter is allocated a name and a unique identifier. The support service group mainly provides services to resolve the name to its unique identifier and vice versa. An additional service includes setting advisory switches to permit or prohibit services on attribute relevance offered by the data distribution management.

3.2.3 HLA Rules

HLA provides a set of ten rules, five for federations and five for individual federates, to express design goals and constraints on federates and federations to be compliant with the standard. They are mainly concerned with requiring the OMT for defining FOMs/SOMs and the usage of HLA services described in the interface specification. The HLA rules are described in full detail in the IEEE Standard 1516-2010 found in [112]. In the following, the rules applying to federations are listed and briefly explained:

1. **Federations shall have an HLA FOM, documented in accordance with the HLA OMT**

   All data being exchanged using HLA services during a federation execution have to be specified in one or more FOM modules. Conditions on and restrictions for the data may optionally be provided. The specification has to be compliant with the OMT.

2. **In a federation, all simulation-associated object instance representation shall be in the federates, not in the RTI**

   It is one of the design principles of HLA to separate federate-specific functionality from general-purpose supporting infrastructure. It is only consequent to let object instance attributes be owned by federates and not by the RTI. Maintenance of the respective attribute values therefore also takes place in the federate.

3. **During a federation execution, all exchange of FOM data among joined federates shall occur via the RTI**

   Federates specify data they can provide or require in the FOM or SOM, respectively, while the RTI ensures that this data is delivered according to the federate's declared requirements, e.g., on the kind of data, the reliability of transport, and the event order. Direct data exchange between federates regarding data that has been specified in the FOM is not allowed. This way, coordination requirements of the federation are consistently fulfilled for all federates over the entire lifetime of the federation execution. The coherency in data exchange within the federation execution would be violated if any data exchange happened outside the RTI.

4. **During a federation execution, joined federates shall interact with the RTI in accordance with the HLA interface specification**

   Object instances do not directly interact but instead individual federates interact with each other via HLA services by updating instance attributes or by sending interactions.

5. **During a federation execution, an instance attribute shall be owned by, at most, one joined federate at any given time**

   To ensure data coherency across a federation execution the concept of ownership of instance attributes is introduced in HLA. Updating the value of an instance attribute is only allowed by the owning federate. Ownership may be transferred to other joined federates not only on object class or object instance level but on a level as granular as for each single instance attribute.

In the following, the rules applying to individual federates are listed and briefly explained:

6. **Federates shall have an HLA SOM, documented in accordance with the HLA OMT**

   All data a joined federate is able to produce or request within the federation execution has to be specified in one or more SOM modules. Conditions and restrictions on the data may optionally be provided. The specification has to be compliant with the OMT.

7. **Federates shall be able to update and/or reflect any instance attributes and send and/or receive interactions, as specified in their SOMs**

   The capabilities of the federate on producing or requesting data specified in its SOM have to be implemented. The federate therefore has the obligation to send updates for instance attributes or interactions accordingly.

8. **Federates shall be able to transfer and/or accept ownership of instance attributes dynamically during a federation execution, as specified in their SOMs**

   Data coherency across a federation execution is ensured by allowing each single instance attribute to be owned by at most one joined federate. This ownership can be transferred to other joined federates in accordance with their SOMs.

9. **Federates shall be able to vary the conditions (e.g., thresholds) under which they provide updates of instance attributes, as specified in their SOMs**

   A joined federate is committed to update instance attributes on certain conditions, e.g., the update rate or thresholds on attribute values, according to its SOM. These conditions can be changed during a federation execution.

10. **Federates shall be able to manage local time in a way that will allow them to coordinate data exchange with other members of a federation**

    HLA supports interoperability of federates having different internal concepts of time, e.g., time-stepped or event-driven. Those concepts are hidden from the RTI and kept to the individual federates. Therefore, the concept of distributed logical times synchronized to the HLA time axis is implemented among all joined federates. When exchanging data, joined federates have to adhere to the time management approach of the federation.

3.2.4 Runtime Infrastructure

The RTI is a software library that implements the HLA interface specification but is not itself part of the IEEE Standard 1516-2010. It manages the creation of federation executions and distribution of data while synchronizing time among federates. The full set of services the RTI provides is specified in [118] and briefly described in Section 3.2.2. While the RTI does not have to have knowledge of neither structure nor content of the data it distributes, the specific network details are hidden from the federates. This way, heterogeneous system simulations using different programming languages and operating systems can connect to and exchange data with each other. By not including a specific data encoding or network protocol in the IEEE Standard 1516-2010, different vendors may implement different encoding or protocols resulting in limited interoperability between those RTIs [119, 120]. Widely used protocols are *transmission control protocol* (TCP) and *user datagram protocol* (UDP) sending data either as *unicast*, *multicast*, or *broadcast*.

As the IEEE Standard 1516-2010 does not specify any implementation details, an RTI may be implemented *centralized* or *decentralized*. In a centralized architecture joined federates interact only with a central RTI server that forwards incoming messages to subscribing

federates. This type of architecture exhibits multiple performance bottlenecks and contradicts the principles of distributed simulations [109, 121]. This is why RTIs of the different vendors are exclusively implemented at least partially in a decentralized way in which each joined federate embeds a *local runtime component* (LRC). Each LRC is a full-fledged RTI directly forwarding messages only to those joined federates the messages are intended for. By adhering to the federation execution's FOM, message passing between joined federates and therefore data transmission is reduced. A *central runtime component* (CRC) may only be implemented to facilitate establishing a connection between joined federates, for status retrieval, or diagnostic purposes.

To guarantee implementation of the full specification and therefore ensure the behavior of an RTI to be compliant with the standard in all cases, an official certification procedure has been set up by the M&S CO [122]. A necessary condition for RTIs implemented in C++ or Java to comply with the standard is the mandatory usage of the interfaces explicitly given for those programming languages in the HLA interface specification. This explicit stating of interfaces for the two programming languages allows for an unproblematic federation execution-wide exchange of an RTI implemented in either of those languages with another implementation. RTIs implemented in other languages, e.g., C#, Python, or Matlab, may define and implement their own interfaces according to the body of the standard to still comply with it. In this case, the lack of an explicit stating of interfaces practically limits the widespread adoption of RTIs developed in other languages as they may certainly not be interchangeable. If, however, existing simulations implemented in different languages need to be coupled using HLA, a wrapper in the desired language may be implemented. RTI vendors offering multi-language *application programming interface*s (API) usually implement their RTI once and provide wrapper classes for other languages. This way, they can minimize development and maintenance effort at the cost of performance which, especially in high-throughput scenarios, may heavily drain for the wrapper implementation [123].

Other factors influencing the performance, measured in messages per second, is the context in which measurements take place. Besides the native programming language of the API, the number of joined federates, the message size, and the type of used services offered by the RTI are decisive criteria. The different context in which the performance values officially published by the various vendors are measured disallows comparing them with each other. They most likely also need to be replaced by own measurements for each individual context. A detailed explanation of factors influencing the performance can be found in [124] and [125].

Design Decision and Requirements

In the CityMoS context there are two requirements for an RTI to fulfill:

1. **Implementing the active IEEE Standard 1516-2010**

   The active IEEE Standard 1516-2010 reveals many advantages over its 10-years older and superseded predecessor. The most interesting ones are a standardized time representation, modularity and extensibility of FOMs/SOMs, and an increased update performance.

Table 3.1: Overview of RTIs implementing the IEEE Standard 1516-2010.

Name	Version	Standard			API [a]		License
		US DoD HLA 1.3	IEEE 1516-2000	IEEE 1516-2010	C++	Java	
CERTI	3.5.1	✓	(✓) [b]	(✓) [b]	**✓**	(✓) [c]	GPL v2
Open HLA	0.6.1	✓	✓	✓	–	**✓**	Apache v2
OpenRTI	0.7.1	✓	✓	✓	**✓**	–	LGPL
Pitch pRTI	5.1	✓	✓	(✓) [d]	✓	**✓**	Commercial
poRTIco	2.0.2	✓	✓	(✓) [b]	✓	**✓**	CDDL
VT MÄK RTI	4.4.1	✓	✓	✓	**✓**	✓	Commercial

[a] The RTI's native implementation is indicated with a bold ✓, APIs in other languages only wrap this implementation.
[b] Partial compliance only, no information available to the extent.
[c] Only available for US DoD HLA 1.3.
[d] IEEE Standard 1516-2010 compliance was not available until version 5.0 dated 14th February 2014 and therefore not at the time of deciding for an RTI.

2. **API with interfaces in Java and C++**

   As described in Section 3.3 and 3.4, the two main federates, CityMoS Power and CityMoS Traffic, are implemented in Java and C++, respectively. Because of the limited interoperability between RTIs from different vendors, an RTI suitable for the CityMoS platform has to exhibit interfaces in both languages.

Table 3.1 lists both commercial and open-source RTIs whose vendors claim to have the current IEEE Standard 1516-2010 implemented. At the time of deciding for an RTI, the two mentioned requirements were only fulfilled by poRTIco and VT MÄK RTI. Because of its open-source license, its good documentation, an active user community, and its widespread usage in research projects poRTIco was chosen at first. Various crucial bugs[1] and the not documented and therefore previously unknown limited compliance with the IEEE Standard 1516-2010 prevented a final usage. VT MÄK RTI did not show such bugs and therefore became the default RTI in the CityMoS platform.

3.2.5 Federation Execution Process

The HLA federation execution process consists of multiple steps shared by all joined federates. For each federate, they include joining and resigning from the federation execution, declaring produced and requested data, as well as updating them. The federation execution process can be either *regular* or *non-regular*. The regular case can be broken down into the phases

[1] The bug that ultimately disqualified poRTIco for further usage was the unsuccessful update of an object attribute value in an environment having one federate using the C++ API and one using the Java API while at the same time using time management services. Further bugs included a limitation regarding the number of object instances registered at the same time and the maximum size of an update message being sent (this bug was fixed in the lastest used version poRTIco 2.0.2).

Initialization, *Simulation*, and *Finalization* and is illustrated for an exemplified federate in Figure 3.3. The non-regular one uses the save and restore functionality of the federation management service. It is rather uncommon and therefore deliberately left out.

As starting point, the federate is connected to the RTI but no services have been invoked relative to the federation execution.

1. **Initialization**
   a) The first federate started spawns a new named federation execution. Any later attempt by the first or other federates to create another execution with the same name in the same network will fail. Federates, including the first one, may now join the federation execution by declaring its SOM.
   b) Per default a federate is considered non-time regulating and non-time constrained as described in Section 3.2.2. It may enable either time policy if necessary.
   c) A federate has to declare the data it produces or requests, either as object or interaction class. It does not necessarily have to make use of all four permutations but at least one is necessary to become sensible within the federation execution. This declaration has to be in accordance with the federation execution's FOM.
2. **Simulation**
   a) The actual simulation loop starts with the federate executing own initialization functions, if required.
   b) It then registers object instances as specified in its SOM. This does not include any instance attribute values but only registers a new object instance by reserving a unique identifier, the *instance handle*. In case no object classes were indicated for publishing by this federate this step is omitted. The federate may also delete already registered object instances.
   c) For each object instance, attribute values are being updated by its owning federate who registered it. Federates may, additionally, send interactions at this point in time.
   d) Afterwards, each federate has the opportunity to execute its own simulation functions.
   e) It then indicates its wish to advance its logical time.
   f) The instance handles of object instances registered and deleted by a federate are now forwarded to the other joined federates. Also, object instance updates and interactions are reflected and received, respectively, by subscribing federates.
   g) The RTI will advance time only after all joined federates indicated their wish to do so. For each federate the simulation loop may repeat with an individual step size until its own simulation exit condition, e.g., the simulation end time or an exception, is reached.

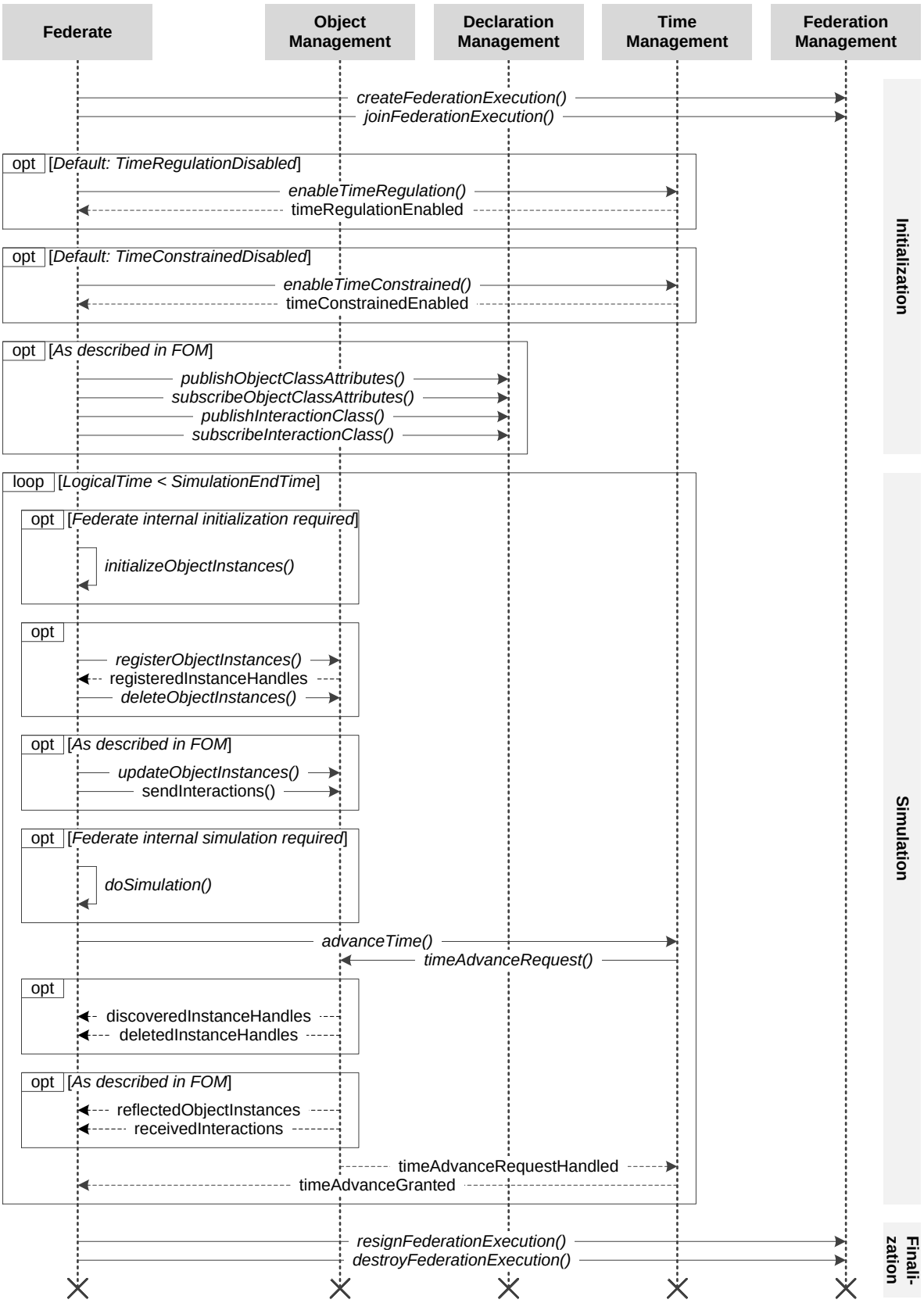

Figure 3.3: Regular federation execution process.

3. **Finalization**

   a) After finishing its simulation loop the federate resigns from the federation execution and tries to destroy it. The latter will only succeed in case the federate is the last one in the federation execution. Otherwise, the attempt will fail and the federation execution will continue to exist.

3.3 CityMoS Power

CityMoS Power is a power system simulation written in Java and was self-developed as part of this work. It comprises different modules for planning and evaluating PNMs as well as to subsequently conduct power flow studies on those PNMs including a battery energy storage scheduling approach to realistically evaluate the impact of road transportation electrification on power systems. Both the power flow simulation and the scheduling approach are time-stepped modeling the operation of the power system and the battery energy storage, respectively, as a discrete sequence of equal sized time slices at which system state updates can occur. CityMoS Power may either operate as a standalone simulation using static offline data or as a joined federate dynamically exchanging data with other participants of the same federation execution.

Its functionality is provided in the modules *power system planning*, *power flow simulation*, *scheduling of battery energy storage*, and *evaluating PNMs* which have been comprehensively motivated, described, and discussed in the respective sections of Chapter 2. This section focuses on the software implementation part of the framework. An architectural overview in which the sequence of interactions is explained is therefore provided in Section 3.3.1. The data format used for input and output data is discussed in Section 3.3.2.

3.3.1 Interactions

CityMoS Power provides its main functionality in two modules which can be used either solely for PSP purposes or combined also for conducting power flow studies. Both usage modes are illustrated in Figures 3.4 and 3.5, respectively. The interaction sequence in either case starts with the main class **MainPlanning** to which program arguments have already been passed by the user. Those arguments contain various parameters for the applied algorithms, values for the used electrical equipment, settings regarding the usage of CityMoS Power in a coupled environment using HLA, and other configuration parameters related to logging, input and output file handling, as well as the mode of usage. Possible input data is described in Section 2.6.4 and defined in the following Section 3.3.2.

Regardless of the usage mode, the interaction sequence in the PSP module shown in Figure 3.4 is the same and as follows:

1. A new **PowerSystemPlanning** object is created. Its purpose is to return an entire PNM.
2. To achieve this, the PNM can either be deserialized from an already previously planned PNM using the **SerializerDeserializer** class, or it can be newly planned.

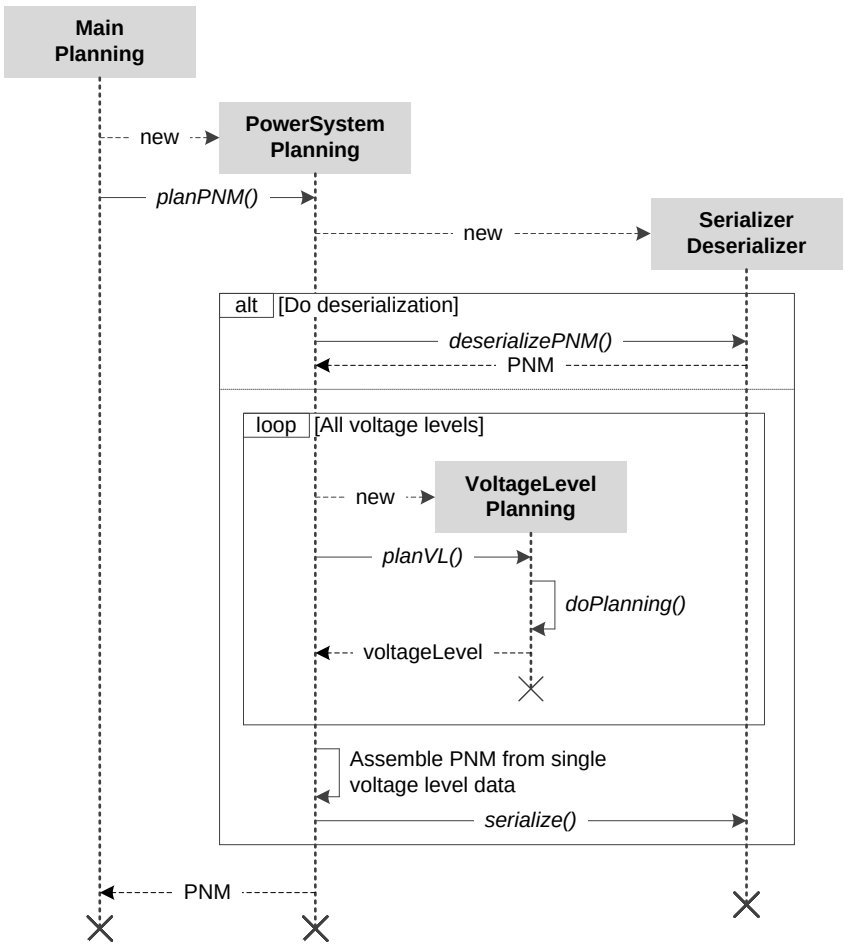

Figure 3.4: Interactions in the power system planning process.

3. Planning a new PNM involves planning all the different voltage levels bottom-up using the **VoltageLevelPlanning** class. At the end, the single newly planned voltage levels have to be assembled to form the entire PNM. Both the planning and assembling process is done as described in Section 2.2. The PNM is finally serialized.
4. The control flow is given back to the **MainPlanning** class.

If the mode of usage includes conducting power flow studies, the following steps as illustrated in Figure 3.5 are performed:

1. At first, a **PowerSystemPlanning** object is created. A PNM is then planned as previously described and shown in detail in Figure 3.4.
2. A newly created **PowerFlowSimulation** object simulates the power flows within the given PNM, either in a coupled environment using HLA or as a standalone simulation.
   a) In a coupled environment, the regular federation execution process described in Section 3.2.5 is applied with the *doSimulation()* method as explained in Section 2.3.

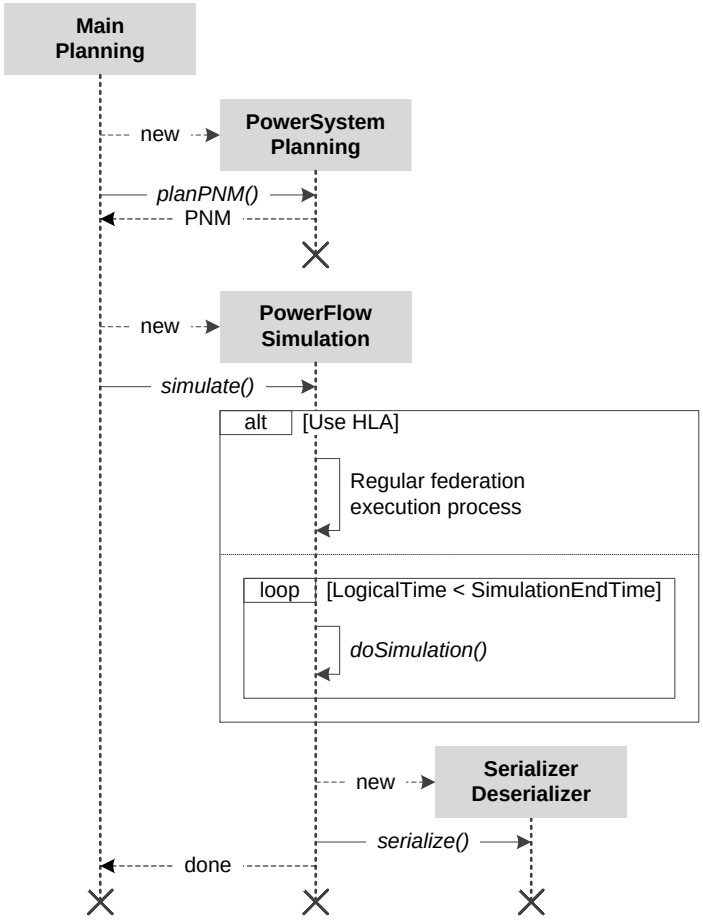

Figure 3.5: Interactions in the power flow simulation process.

b) In case CityMoS Power is used as a standalone simulation, only the *doSimulation()* method is repeatedly called. Its functionality equals the *doSimulation()* method from the previous step.

3. The power flow values are then serialized and the control flow is given back to the **MainPlanning** class.

3.3.2 Data Format

The default input and output data format for CityMoS Power is XML. This format applies to both the input data required when instantiating the main class **MainPlanning** as well as to the serialized and deserialized PNMs and power flow values. A definition of XML and XSD, a schema system for validating XML documents, is given in Section 3.2.1. In Section 3.3.2.1, an XSD file providing a formal specification of the XML documents' syntax is described. An example of an XML input file complying with the XSD and illustrating the implementation of its main concepts is shown and discussed in Section 3.3.2.2. Because of its broad spread and

in some cases clear advantages over XML, the *Comma Separated Value* (CSV) file format is additionally supported. Its usage is described in Section 3.3.2.3.

3.3.2.1 XSD

Input and output data for CityMoS Power is stated using XML. The XML documents' syntax is formally specified by an XSD file. Listing 3.1 provides an overview of such an XSD used for defining both input and output data required and generated by CityMoS Power. In the following, the main concepts of elements, attributes, restrictions, and constraints are introduced necessary to understand the XML file described in Section 3.3.2.2.

Listing 3.1 Overview of CityMoS Power's XSD.

```
1  <xs:schema
2
3    targetNamespace="http://rp5.info"
4    xmlns:sp="http://rp5.info"
5    xmlns:xs="http://www.w3.org/2001/XMLSchema"
6    elementFormDefault="qualified">
7
8    <xs:element name="PowerSystem">
9      <xs:complexType>
10       <xs:sequence>
11         <xs:element name="Node" type="sp:NodeType" minOccurs="2" maxOccurs="
               unbounded" />
12         <xs:element name="Edge" type="sp:EdgeType" minOccurs="0" maxOccurs="
               unbounded" />
13         <xs:element name="Area" type="sp:AreaType" minOccurs="0" maxOccurs="
               unbounded" />
14       </xs:sequence>
15       <xs:attribute name="Author"  type="xs:string" use="required" />
16       <xs:attribute name="Date"    type="xs:string" use="required" />
17       <xs:attribute name="Version" type="xs:string" use="required" />
18     </xs:complexType>
19
20     <!-- KEY, KEYREF, & UNIQUE CONSTRAINTS FOR NODE -->
21     <!-- ... -->
22     <!-- KEY, KEYREF, & UNIQUE CONSTRAINTS FOR EDGE -->
23     <!-- ... -->
24     <!-- KEY, KEYREF, & UNIQUE CONSTRAINTS FOR AREA -->
25     <!-- ... -->
26
27   </xs:element>
28
29   <!-- DEFINITION OF THE COMPLEX TYPE NODETYPE -->
30   <!-- ... -->
31   <!-- DEFINITION OF THE COMPLEX TYPE EDGETYPE -->
32   <!-- ... -->
33   <!-- DEFINITION OF THE COMPLEX TYPE AREATYPE -->
34   <!-- ... -->
35
36 </xs:schema>
```

The document starts with the definition of the namespaces sp (line 4) and xs (line 5) which include all elements, attributes, and datatypes defined by the given XML schema and in the language definition itself. It is further stated that elements used and declared in this XSD must

be namespace qualified (line 6) meaning their namespace must always be specified along with their name. The body of the file contains the definition of the main element PowerSystem (line 8). This element specifies possible subelements Node (line 11), Edge (line 12), and Area (line 13) as well as the additional attributes Author (line 15), Version (line 16), and Date (line 17). Primary key, key reference, as well as uniqueness constraints for all three subelements are also defined. To provide an easy overview some definitions are intentionally left out, indicated by <!-- ... -->. They are defined or discussed onward in the course of this section.

The data type of elements and attributes may be either simple, e.g., int, decimal, string, etc., or complex, e.g., PowerSystem, Node, Edge, or Area. Listing 3.2 shows the definition of a complex type on the example of NodeType, the data type for the subelement Node. The definition is logically split into four parts indicating time-dependent subelements (line 3) as well as static mandatory (line 9), optional (line 12), and additional attributes (line 15). An attribute is hereby defined by its name, its simple datatype, a required or optional flag, and in the optional case an additional default value. The anyAttribute definition (line 16) allows the XML document to be extended by additional attributes not explicitly specified in the XSD. The definition of EdgeType, the data type for the subelement Edge, is done accordingly.

Listing 3.2 Definition of the complex type NodeType.

```
1  <xs:complexType name="NodeType">
2
3    <!-- TIME-DEPENDENT SUBELEMENTS -->
4    <xs:sequence>
5      <xs:element name="Input"  type="sp:NodeInputType"  minOccurs="0" maxOccurs="
           unbounded" />
6      <xs:element name="Output" type="sp:NodeOutputType" minOccurs="0" maxOccurs="
           unbounded" />
7    </xs:sequence>
8
9    <!-- REQUIRED ATTRIBUTES -->
10   <xs:attribute name="IdNode" type="xs:int" use="required" />
11
12   <!-- OPTIONAL ATTRIBUTES -->
13   <!-- ... -->
14
15   <!-- ADDITIONAL ATTRIBUTES -->
16   <xs:anyAttribute processContents="lax" />
17
18 </xs:complexType>
```

Time-dependent complex types such as NodeInputType which is provided by Listing 3.3 or NodeOutputType are characterized by the mandatory attributes TimePeriod (line 4), PowerDemandActive (line 5), and PowerDemandReactive (line 6). Those attributes specify the active and reactive power demand of a Node at each unique time period. Depending on the specific complex type, additional required and optional attributes are also defined.

Simple data types as defined by the xs namespace may also be subtyped and amended by additional restrictions. Those restrictions are called *facets*. Listing 3.4 shows the definition of a facet on the example of the VoltageLevelType defined for the optional VoltageLevel attribute of NodeType. The voltage level is hereby restricted to the specifically mentioned values between 0.4 and 400 (line 3).

Listing 3.3 Definition of the complex type NodeInputType.

```
<xs:complexType name="NodeInputType">

  <!-- REQUIRED ATTRIBUTES -->
  <xs:attribute name="TimePeriod" type="xs:int" use="required" />
  <xs:attribute name="PowerDemandActive" type="xs:decimal" use="required" />
  <xs:attribute name="PowerDemandReactive" type="xs:decimal" use="required" />

  <!-- OPTIONAL ATTRIBUTES -->
  <!-- ... -->

  <!-- ADDITIONAL ATTRIBUTES -->
  <xs:anyAttribute processContents="lax" />

</xs:complexType>
```

Listing 3.4 Definition of a facet on the example of the simple type VoltageLevelType.

```
<xs:simpleType name="VoltageLevelType">
  <xs:restriction base="xs:decimal">
    <xs:pattern value="0.4|6.6|22|66|230|400" />
  </xs:restriction>
</xs:simpleType>
```

An XML schema cannot only include facets but also key, key reference, and uniqueness constraints indicated by the elements key, keyref, and unique. In Listing 3.5, a key constraint is defined for the attribute IdNode of the element Node.

Listing 3.5 Definition of a key constraint on the example of the element Node.

```
<xs:key name="Node_IdNode_Key">
  <xs:selector xpath="sp:Node" />
  <xs:field xpath="@IdNode" />
</xs:key>
```

The given key can be referenced by other attributes. Those referring attributes can then only take values of that key attribute. Listing 3.6 provides an exemplified definition of a key reference constraint in which the attributes IdNode1 and IdNode2 of the element Edge are referencing the previously defined key Node_IdNode_Key. This allows the element Edge to be valid only when referencing two existing Node elements.

Listing 3.6 Definition of a key reference constraint on the example of the element Edge.

```
<xs:keyref name="Edge_IdNode1_Ref" refer="sp:Node_IdNode_Key">
  <xs:selector xpath="sp:Edge" />
  <xs:field xpath="@IdNode1" />
</xs:keyref>
<xs:keyref name="Edge_IdNode2_Ref" refer="sp:Node_IdNode_Key">
  <xs:selector xpath="sp:Edge" />
  <xs:field xpath="@IdNode2" />
</xs:keyref>
```

In the context of CityMoS Power it is a necessary requirement that the location of each Node is unique for the entire planning process. In Listing 3.7 such a uniqueness definition is provided for the element Node based on the combination of its attributes Latitude and Longitude.

Listing 3.7 Definition of a uniqueness constraint on the example of the element Node.

```
1 <xs:unique name="Node_Location_Uni">
2   <xs:selector xpath="sp:Node" />
3   <xs:field xpath="@Latitude" />
4   <xs:field xpath="@Longitude" />
5 </xs:unique>
```

3.3.2.2 XML

Data for CityMoS Power is specified in XML files complying with the XSD described in the previous Section 3.3.2.1. Those files have to be valid and thus well-formed. Although there is only one XSD all XML files have to comply with, different XML files varying in structure and content are used to cover the various use cases of CityMoS Power. Investigated use cases are described in Chapter 4. In the following, a minimal implementation of the XML schema's elements for input data is exemplarily illustrated.

Each XML file consists of one PowerSystem element which is defined by a reference to the applied XML schema (line 3), a set of namespaces (lines 4 and 5), and the stipulated attributes Author, Date, and Version (line 6) as illustrated in Listing 3.8. The body of the file contains definitions for the elements Node (line 9) and Edge (line 10). Area elements do not appear in the input data but are only part of the output of the PSP process. Definitions indicated by <!-- ... --> are deliberately left out to improve readability and will be discussed onwards in the course of this section.

Listing 3.8 Simplified example of an input file for CityMoS Power.

```
1  <PowerSystem
2
3     xsi:schemaLocation="http://rp5.info CityMoS_Power.xsd"
4     xmlns="http://rp5.info"
5     xmlns:xsi="http://www.w3.org/2001/XMLSchema-instance"
6     Author="David_Ciechanowicz" Date="2016-01-01" Version="3.3">
7
8     <!-- NODE ELEMENTS -->
9     <!-- ... -->
10    <!-- EDGE ELEMENTS -->
11    <!-- ... -->
12
13 </PowerSystem>
```

Node elements may be differentiated into PQ and PV nodes, the latter distinguishing substations and power plants. An example of a minimal PQ node is illustrated in Listing 3.9. It is defined by its required attribute IdNode as well as the optional attributes Latitude and Longitude (line 1). With the key and uniqueness constraints defined in the XSD, this allows to uniquely identify and locate the PQ node. Default values apply to all other non-mentioned

optional attributes as defined in the XSD. Depending on the use case, these optional or other attributes may additionally be specified here.

To plan a power system or conduct power flow studies, the active and reactive power demand of all PQ nodes for any but the same period of time must be provided. The subelement Input therefore includes the attributes TimePeriod, PowerDemandActive, and PowerDemandReactive (lines 2 to 4). In case the reactive power demand is not specified, CityMoS Power will calculate this value from the given active power demand and a power factor. If not changed in the settings, a default value for the power factor is taken.

Listing 3.9 Exemplified definition for the input of a PQ node.

```
1 <Node IdNode="200001" Latitude="1.2998914" Longitude="103.6254562">
2   <Input TimePeriod="1" PowerDemandActive="66.14" PowerDemandReactive="32.03" />
3   <Input TimePeriod="2" PowerDemandActive="66.07" PowerDemandReactive="32.00" />
4   <Input TimePeriod="3" PowerDemandActive="66.01" PowerDemandReactive="31.97" />
5 </Node>
```

The regular PSP process may optionally be adjusted by additionally defining existing elements with specific properties. An example for a substation is shown in Listing 3.10. In addition to the attributes Name and Description, a substation is distinct from a PQ node by the attribute IdNodeType as well as its voltage level, specified by both the lower and upper winding attribute VoltageLevel and VoltageLevelUpper, respectively. No Input subelement should be provided as substations do not have a distinct time-dependent power demand.

Listing 3.10 Exemplified definition for the minimal input of a substation.

```
1 <Node IdNode="3477376" Description="Labrador substation" IdNodeType="2" Latitude="
      1.2705389" Longitude="103.7984964" Name="Labrador" VoltageLevel="230"
      VoltageLevelUpper="400" />
```

In the PSP process, power plants are specified as input as illustrated in Listing 3.11. They can be distinguished from substations by a different value for the attribute IdNodeType. Additionally, attributes indicating its minimum and maximum active and reactive power supply must be specified.

Listing 3.11 Exemplified definition for the input of a power plant.

```
1 <Node IdNode="3477385" Description="Tuas power plant" IdNodeType="3" Latitude="
      1.2871997" Longitude="103.6405873" Name="Tuas PowerGeneration"
      PowerSupplyActiveMax="2609000" PowerSupplyActiveMin="0" PowerSupplyReactiveMax
      ="1374000" PowerSupplyReactiveMin="-815000" VoltageLevel="400"
      VoltageLevelUpper="400" />
```

In case specific power lines for already defined Node elements are known in advance of the PSP process, they can be specified as shown in Listing 3.12. Besides the mandatory attributes IdEdge, IdNode1, and IdNode2, a Name as well as Reactance and Resistance values may optionally be provided.

Listing 3.12 Exemplified definition for the input of a power line.

```
<Edge IdEdge="2671151" IdNode1="3477385" IdNode2="3477376" Name="Tuas - Labrador"
    Reactance="0.0001093" Resistance="0.000009" />
```

3.3.2.3 CSV

XML files allow for an easy formal specification of their syntax with the help of XSD files. The structure of the data as well as restrictions and key, key reference, and uniqueness constraints can be specified. This advantage comes at the cost of a higher complexity when specifying data in this format. For simple tabular data or large data sets without the requirement for a formal syntax specification the CSV file format is favorable. CSV files have less overhead compared to their payload. Hence, they require less storage and can be processed much faster. When specifying hierarchical data, additional effort, however, has to be taken to avoid excessive redundancies in the data.

Alternatively to XML, CityMoS Power therefore supports input and output data in the CSV file format. Since this format does not allow representing multiple data sets with different attributes in one file, separate files for each of the XML schema's element and subelement types need to be created. Besides a header naming all the attributes required for its use case, a CSV file also contains a body with values in a comma separated format. Although the XSD file cannot be used to formally validate a CSV file's syntax, it is still informally used to describe allowed attributes. In Listing 3.13 and 3.14, an example for the input of a PQ node in the CSV file format matching the one for the XML format shown in Listing 3.9 is given. Since the input data is hierarchical, two separate CSV files have to be created to reduce redundancies in the output. The distributed data is linked by the node's unique attribute IdNode.

Listing 3.13 Exemplified definition for the static part of the input of a PQ node in the CSV file format.

```
IdNode,Latitude,Longitude
200001,1.2998914,103.6254562
```

Listing 3.14 Exemplified definition for the dynamic time-dependent part of the input of a PQ node in the CSV file format.

```
IdNode,TimePeriod,PowerDemandActive,PowerDemandRective
200001,1,66.14,32.03
200001,2,66.07,32.00
200001,3,66.01,31.97
```

Defining the time-dependent power demand per sector instead of per PQ node is only supported in the CSV file format. This option allows CityMoS Power to automatically assign a power demand value to each single PQ node in case it is only available on a by-sector basis. Hereby, given power demand values for a sector are by default equally distributed to all nodes associated with this sector by their IdSector attribute. A more fine-grained distribution can be achieved by additionally specifying the IdBuildingType which further distinguishes a sector.

3.4 CityMoS Traffic

CityMoS Traffic is an agent-based transportation system simulation written in C++. Its purpose is to realistically simulate trips of a PEV population that correspond to the actual vehicle population of a city. CityMoS Traffic is a *discrete-event simulation* [126] modeling the operation of the transportation system as a discrete sequence of events in time each marking a change of state in the system. The development of CityMoS Traffic was explicitly not part of this work. Instead, it is solely used as a joined federate in federation executions as part of the CityMoS platform to conduct studies investigated in Chapter 4. Details provided on CityMoS Traffic are therefore limited to an extent necessary to understand the way how traffic is generated and simulated and to understand its interactions with other joined federates. A comprehensive explanation of CityMoS Traffic can be found in [127, 128]; in the context of the literature still termed SEMSim Traffic. Its main components are described in Section 3.4.1 followed by an overview on the data format used for output data in Section 3.4.2.

To use CityMoS Traffic in a federation execution it has to implement an HLA module which is able to process data as described in Section 3.2.5. This functionality is currently not available in CityMoS Traffic. The development of an additional external HLA module that reads and processes the output data of CityMoS Traffic to forward it within the federation execution was therefore part of this work. This way, no changes to the source code of CityMoS Traffic are required while maintaining the usage of real simulation data in federation executions. At the same time, sparing re-running CityMoS Traffic for each federation execution drastically decreases execution time. Application scenarios are, however, limited to unidirectional data flow without the possibility to send messages to CityMoS Traffic. The entire package consisting of the transportation system simulation and the additional external HLA module is termed CityMoS Traffic in this work.

3.4.1 Components

CityMoS Traffic provides its functionality by means of interactions of different components. The following list gives a non-exhaustive overview on its main components. Further information can be found in [127, 128].

- **Driver-vehicle unit**

  The transportation system is modeled as a collection of autonomously acting entities perceiving their environment, individually assessing their situation, and making decisions based on a set of rules. Those entities are called *agents* in the field of *agent-based modeling* [9]. This field is used to capture emergent phenomena resulting from interactions of individual entities and therefore to explore the dynamics of a system. In CityMoS Traffic an agent is represented by a *driver-vehicle unit* containing both *driver behavior* and *vehicle component* models. Implemented behavioral models include car-following, lane-changing, acceleration/deceleration, overtaking, intersection, and charging models. Depending on an agent's status and the environment dynamic re-routing may be triggered by the agent. Component models are differentiated into PEV and infrastructure component models. The first category comprises battery, drive train, and air conditioning models to assess

the energy consumption of the various vehicle components while the second one includes traffic light and parking space models. Modeling agents as driver-vehicle units each with an individual driver behavior and vehicle component model allows a population of agents to be flexibly arranged combining various driver and vehicle types.

- **Road network and routing**

  The road network used in CityMoS Traffic was commercially obtained from Navteq [129]. It is a directed graph comprising edges, being *lanes*, and nodes, longitude and latitude of the start and end point of a lane, including various properties, e.g., road type or speed limits. Lanes having the same start and end point are allocated to a *link*. Routing on the road network is done based on either shortest path or shortest travel time obeying effective speed limits using *Dijkstra*'s algorithm [130]. The movement of an agent is represented by a change in its coordinates restricted to those belonging to existing lanes. At approximately 200 intersections traffic lights are placed operating either statically with fixed timings or dynamically based on link occupancy.

- **Trip generation**

  A trip is characterized by a pair of coordinates, an origin and a destination, and a starting time. Origins and destinations are restricted to any of Singapore's unique 6-digit postal code available for each building. At the start of a trip an agent is spawned at a random lane next to the origin postal code. It is removed when the agent reaches any lane next to the destination postal code. At its first trip, each agent is assigned an initial *SOC* at random. Trip data for the entire vehicle population over a specific time interval, e.g., one day, is not available for Singapore. Even data on the average daily mileage is conflicting and ranges between 23 km [131] and 48 km [132]. In CityMoS Traffic, trip generation is based on data collected via the *household interview travel survey* [131], a survey on individual travel patterns conducted in 10 500 representative households in 2012. This data is temporally and spatially extrapolated to produce trips that cover all postal codes and the entire vehicle population of Singapore. Temporally, the starting time of each trip is uniformly delayed by up to 30 minutes. Spatially, only the first two digits of each trip's origin and destination postal code are taken while the remaining four digits are randomly selected ensuring a valid postal code is generated. An agent can have multiple trips per day called its *itinerary*. To account for uncertainty in the originating trip data, different daily mileages are applied and investigated in the context of the case study conducted in Section 4.3.

3.4.2 Data Format

CityMoS Traffic exhibits different output formats, each related to a specific use case. Since the development of CityMoS Traffic is not part of this work, only the output data format as used in the case study presented in Section 4.3 is introduced in this section. A description of other formats and the required input data can be found in [127]. CityMoS Traffic supports two different types of output: *aggregated* and *disaggregated*. Especially in the disaggregated type, the XML format's large overhead-to-payload ratio results in storage requirements in the

region of tens to hundreds of GB when simulating traffic of an entire city over the course of a day. This format therefore rapidly becomes unhandy. Instead, the CSV file format is thus used for both output types.

In Listing 3.15, aggregated information on the agent's itineraries is shown. For each trip of every agent their start and end time and location as well as their required energy and covered distance are provided. This data is used, for instance, when investigating charging events as done in Section 4.3 without requiring temporally resolved information on an agent's location.

Listing 3.15 Exemplified definition for the aggregated output of each agent's itinerary.

```
1  IdAgent,IdTrip,TripStart[min],TripEnd[min],EnergyUsed[kWh],Distance[km],
       PostalCodeStart,PostalCodeEnd
2  1686,0,366,372,0.79,5.25,648368,629144
3  1686,1,1145,1149,0.45,3.11,629144,640961
4  1686,2,1212,1216,0.48,3.27,640961,648368
5  1223,0,457,472,2.01,15.21,680252,638899
6  1223,1,1058,1074,1.99,15.21,638899,680252
```

In Listings 3.16, an example for the disaggregated output of an agent is provided. An agent is characterized by a unique identifier as well as its tempo-spatial location and *SOC* status. This data is used, for instance, by CityMoS Frontend when visualizing the microscopic behavior of CityMoS Traffic and thereby the location of each agent temporally resolved over the course of the entire simulation.

Listing 3.16 Exemplified definition for the disaggregated output of an agent.

```
1  IdAgent,TimePeriod,Latitude,Longitude,Soc
2  1,1,1.299891677,103.6254565,0.95
3  1,2,1.299891824,103.6254832,0.95
4  1,3,1.299891973,103.6254982,0.94
```

For the sake of completeness, Listing 3.17 shows an example for the definition of a link. A link is defined by a unique identifier and two pairs of spatial coordinates describing its start and end point. It is immutably used as input data to initialize the road network of CityMoS Traffic.

Listing 3.17 Exemplified definition for the input of a link.

```
1  IdLink,Latitude1,Longitude1,Latitude2,Longitude2
2  1,1.299891677,103.6254565,1.299891824,103.6254832
```

3.5 CityMoS Frontend

CityMoS Frontend is a software which was self-implemented as part of this work. It is an interactive visualization tool that allows participating in and controlling of federation executions in a coupled environment using HLA. It may either be used as a standalone

visualization of static offline data or as a live interactive visualization of dynamically exchanged data between joined federates by participating in a federation execution. The design goal of CityMoS Frontend evolved, first being merely a supporting tool for visually inspecting data used as input for or generated as output by CityMoS Power in 2D. It later emerged as a 3D visualization of complex moving scenes and was ultimately extended by supporting HLA not only passively consuming data to be visualized but also actively producing data. From a simulation perspective the contribution of CityMoS Frontend may be low. This tool, however, facilitates work with the CityMoS platform by allowing to visualize and influence the interactions between CityMoS Traffic and CityMoS Power and thereby provide insights into federation executions at runtime. This is especially important to attract new users which in principal enables a rapid adaption of the entire CityMoS platform.

CityMoS Frontend is implemented in Processing, an open source programming language and *integrated development environment* [133]. Processing was developed as a cross-platform environment for programming within the context of visual design and visual arts at the MIT Media Lab in 2001. Processing is based on Java and is, besides its new graphics and utility API, fully compatible with it. It supports both 2D and 3D visualization and uses the *open graphics library* [134] to interact with the system's *graphics processing unit* to achieve hardware accelerated rendering.

The various functionality provided by CityMoS Frontend supports simple and complex visualization of graph-related data and allows for user interactions with either the standalone visualization or the joined federates in a federation execution. Its main functionality is described in Section 3.5.1 followed by an architectural overview in which the sequence of interactions is explained in Section 3.5.2. The data format used for input and output data is discussed in Section 3.5.3. Examples for the visual output generated by CityMoS Frontend are provided in the context of applying the platform to the case of Singapore in Chapter 4.

3.5.1 Main Functionality

CityMoS Frontend comprises various functionality for visualizing data, especially graph-related data, and supporting the user in visually interacting with simulations coupled via HLA at runtime. The following list provides an overview on CityMoS Frontend's main functionality:

- **Execution mode**

  CityMoS Frontend implements HLA functionality which allows it to join federation executions and act as a regular federate. As such it can register, delete, update, and reflect object instances as well as send and receive interactions. It therefore acts not only as a sink visualizing received data but also as a source being able to influence the federation execution by sending data. A standalone execution mode only visualizing offline data from a file system without joining any federation execution is also available.

- **Visualization**

  Graph-based data, in this context nodes and edges, can be visualized both in 2D and 3D allowing to switch the way of presentation at runtime. Data is thereby drawn on multiple layers whose visibility can be toggled to visualize only parts of the data being of

interest to the user. Currently, layers for power system, road and railway transportation system, and general purpose graph-based data as well as layers for showing a background and general visualization parameters are supported. The layer for power system data is further distinguished into the different voltage levels, the layer for road and railway transportation system as well as general data is split up each into a layer for nodes and edges. The visualization is not restricted to the screen resolution. Instead, the resolution can be arbitrarily changed. It is only limited by the used graphics and processing hardware. This is especially important when reducing the resolution to improve performance or increasing the resolution for rendering images or videos in a higher than the native resolution. Rendered images may not only be directly visualized but also saved to the file system for later processing.

- **User interactivity**

  CityMoS Frontend implements user interaction possibilities for both execution modes visualizing offline and online data coming from the file system or from other joined federates, respectively. Direct interactions with the visualized data set is restricted to inserting and deleting nodes or edges as well as selecting them and showing or modifying their attributes. Modifications to the initial data set coming from the user or other joined federates can be saved to the file system. Visualization parameters, e.g., resolution, layer visibility and their elevation when drawing in 3D, as well as color and size of drawn nodes and edges can be modified at runtime over the main *graphical user interface*. With simple mouse movements the user may also change the camera view settings by moving along the two or three axes in 2D or 3D mode, respectively. This includes zooming in and out functionality. The user may also pixel-based compare two rendered images to conclude on the degree of equality of the underlying data sets. This especially comes in handy when spotting the differences of two different scenes that are not obviously visible at first glance.

3.5.2 Interactions

In Figure 3.6, the interaction sequence is shown for the execution mode in which CityMoS Frontend acts as a joined federate in a federation execution. The sequence is as follows:

1. At the beginning, the user passes program arguments to the main class **MainFrontend**. Those arguments contain various parameters for rendering images, illustrating nodes and edges, composing the different layers, settings regarding the usage of CityMoS Frontend in a coupled environment using HLA, and other configuration parameters related to logging as well as input and output file handling.
2. Within **MainFrontend** a new **Visualization** object is created. Its purpose is to visualize data, handle user interactions, and manage interactions within the federation execution.
3. For interactions with other joined federates, an **RTI** object is created serving as an interface for calling functions offered by and providing callback functions from the RTI. Available services are defined in the interface specification of HLA as described

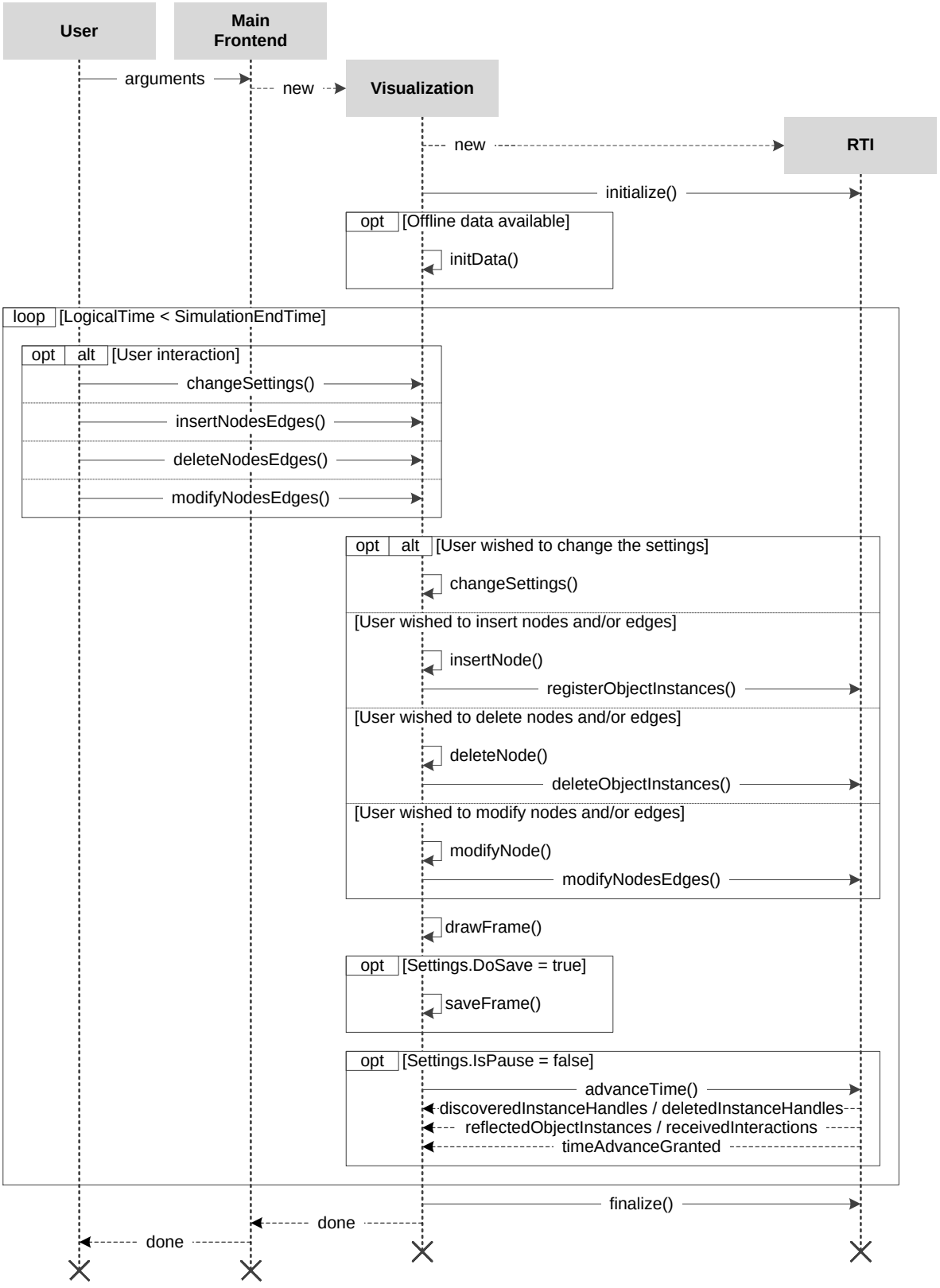

Figure 3.6: Interactions in CityMoS Frontend.

in Section 3.2.2. In case of the standalone execution mode the **RTI** object does neither forward any calls to nor receive any messages from the RTI.

4. The **RTI** object is initialized as described in the *Initialization* phase in Section 3.2.5.
5. In case there is offline data available it is initialized and registered to the federation execution.
6. A continuous loop is running until the simulation exit condition, e.g., the simulation end time or an exception, is reached. The loop consists of the followings steps:
   a) The user may interact with the **Visualization** object at the beginning of each time step. Possible interactions are described in Section 3.5.1 and include modifications to program settings and to the visualized data such as inserting, deleting, or updating nodes or edges.
   b) The **Visualization** object executes the desired user interaction and, in case of a modification of the visualized data, additionally delegates it to the **RTI** object to inform other joined federates of the modification.
   c) The actual visualization is performed by calling the *drawFrame()* method of the **Visualization** object. If the user indicated to save the rendered images the *saveFrame()* method is additionally being called.
   d) In case the federate is paused the time advancing functionality is disabled resulting in rendering the exact same frame at the next iteration of the loop. This allows the user to interact multiple times with the federate at the same time period. In the usual case where the federate is not paused the time advances and data modified by other joined federates is being reflected as described in Section 3.2.5.
7. The **RTI** object is finalized as described in the *Finalization* phase in Section 3.2.5 and the control flow is first given back to the **MainFrontend** class and then to the user.

3.5.3 Data Format

As a tool interacting with and visualizing data of other federates, CityMoS Frontend does not define its own data format. Instead, the XML and CSV format used by each individual federate is supported. CityMoS Frontend as a live interactive visualization tool allows the user to interact with the input data, either being offline or dynamically exchanged between joined federates. Regardless of the execution model, visualized data can be output to the file system including any modifications applied by the users of other joined federates. The data format equals the one used by the respective federate. Output files comply with their matching XSD, if existing, and are therefore valid. Semantic constraints are not validated but assumed to already have been checked by each particular federate.

3.6 Architecture and Interactions

Within the CityMoS platform different entities interact with each other over HLA. The architecture of a federation execution is shown in Figure 3.7. Illustrated are the federates of CityMoS: *CityMoS Power*, *CityMoS Traffic*, and *CityMoS Frontend*. Each federate consists of the packages *Local Runtime Component* and *Custom Code*. The former is the LRC as described in Section 3.2.4 and is embedded as an external library. It offers the set of HLA services available to the respective federate and accepts messages from other joined federates as described in Section 3.2.2, thereby complying with the federation execution's FOM. The latter contains code specific to each federate, like **PowerFlowSimulation** to CityMoS Power, **TransportationSystemSimulation** to CityMoS Traffic, and **Visualization** to CityMoS Frontend. The peculiarities of each of the CityMoS platform's federates are described in Sections 3.3 to 3.5. For a federate to be able to send and receive messages to and from other joined federates over HLA it has to implement additional functionality:

- For CityMoS Power and CityMoS Frontend the **PowerFlowSimulation** and the **Visualization** class, respectively, were extended to directly interact with the LRC. Besides the federate's individual **PowerSOM** and **FrontendSOM** class, the *HLA Bridge* package comprises the **PowerAmbassador** and the **FrontendAmbassador** class, respectively, which both extend the **Ambassador** class of the LRC resulting in FOM-compliant message receiving. Received messages are directly processed allowing the federate to respond thus resulting in a bidirectional communication.

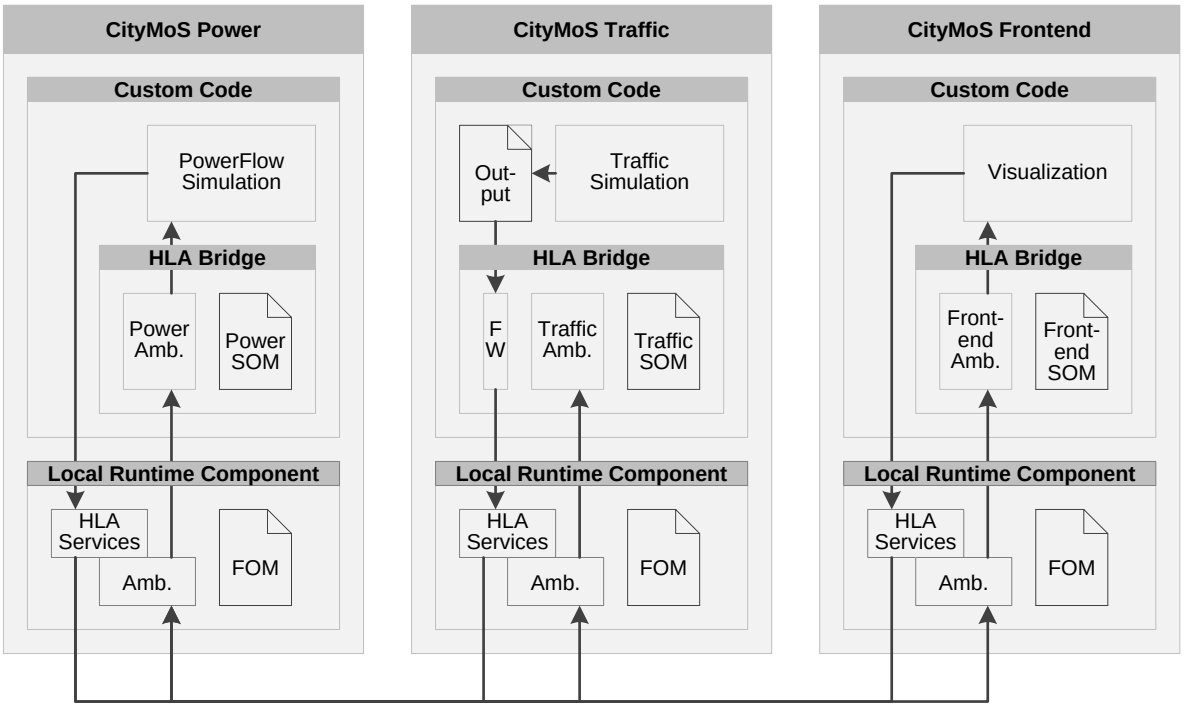

Figure 3.7: Architecture of a CityMoS federation execution.

Table 3.2: Interactivity in the regular federation execution process of the CityMoS platform.

	CityMoS Traffic	**CityMoS Power**	**CityMoS Frontend**
Publish/ update	Agent (dynamic)	Node, Edge (dynamic)	Link, Node, Edge (static)
Subscribe/ reflect	Link, Node (static)	Node, Edge (static)	Agent, Node, Edge (dynamic)
Send	ChargingAgent Requested	ChargingAgent Performed	–
Receive	ChargingAgent Performed	ChargingAgent Requested	ChargingAgent Requested

- For CityMoS Traffic modifications of the **TransportationSystemSimulation** class to directly interact with the LRC are excluded for reasons explained in Section 3.4. The generated **Output** file comprising the location and *SOC* of each agent at every point in time is therefore processed and forwarded to the LRC by the **FW** class according to the **TrafficSOM**. The *HLA Bridge* package comprises the **TrafficAmbassador** class extending the **Ambassador** class of the LRC resulting in FOM-compliant message receiving. Received messages cannot be forwarded to the **TransportationSystemSimulation** class since only unidirectional communication is possible as described in Section 3.4.

To allow an arbitrary simulation to act as a federate, either of the above options have additionally to be implemented. By doing so further simulations, e.g., a *railway transportation system* simulation can in principal be included in the CityMoS platform.

The architectural illustration in Figure 3.7 indicates interactions between each federate's LRC. The regular federation execution process of the CityMoS platform focuses on basic interactions regarding the charging of PEVs (**Agent**) from CityMoS Traffic at CSs (**Node**) from CityMoS Power. User interactions with CityMoS Frontend, in the regular process being reduced to a data consuming visualization federate only, can additionally be included as described in Section 3.5.2. Published and subscribed object instances as well as interactions sent and received by the federates are defined in Table 3.2. The attributes of an object instance are logically separated into *static*, non-time dependent attributes which are published/updated only once at the time of their registration and *dynamic* ones which are published/updated at each time period they are modified by their owning federate. The following observations can be made:

- CityMoS Frontend, being the federate interacting with the user, publishes/updates all static attributes of **Link**, **Node**, and **Edge** object instances. It further subscribes/reflects all dynamic attributes of **Agent**, **Node**, and **Edge** object instances.
- CityMoS Power subscribes/reflects the static attributes of **Node** and **Edge** object instances while it publishes/updates their dynamic ones.
- CityMoS Traffic subscribes/reflects the static attributes of **Link** and **Node** object instances while it publishes/updates the dynamic attributes of **Agent** object instances.

- The **ChargingAgentRequested** event is sent by CityMoS Traffic whenever a PEV checks in at a CS. This event is received by CityMoS Power to calculate the PEV's charging schedule and by CityMoS Frontend to temporarily exclude this PEV from the visualization.
- The **ChargingAgentPerformed** event is sent by CityMoS Power whenever a PEV checks out from a CS. This event is received by CityMoS Traffic to continue simulating traffic including this PEV. CityMoS Frontend does not subscribe to this event as it anyhow reflects **Agent** object instance updates.
- To reduce the number of messages only CityMoS Power is aware of a PEV's current *SOC* during charging.
- A premature checkout of a PEV from a CS is not anticipated and would require including an additional event.

Based on the description of the regular federation execution process for a single federate in Section 3.2.5 and the interactions defined in Table 3.2, the regular federation execution process for the CityMoS platform is illustrated in Figure 3.8. Just as in Section 3.2.5, the process is separated into the phases *Initialization*, *Simulation*, and *Finalization*. Since the first and last phase are in both cases content-wise equal, only the *Simulation* phase is shown in this case. The LRC of the **CityMoS Power**, **CityMoS Traffic**, and **CityMoS Frontend** class are for clarity reasons not separately mentioned but instead combined to the **RTI** class. Furthermore, there is no distinction made between the different HLA classes offering services to the federate and the **Ambassador** class being concerned with callbacks as this information can be extracted from Section 3.2.5. In addition to the name of each service or callback function, the specific related object instance or interaction is provided, abbreviated by its capital letters, e.g., **A** for **Agent** or **CAR** for **ChargingAgentRequested**.

In the following, the regular federation execution process of the CityMoS platform is described. As starting point, each federate is connected to its LRC but no services have been invoked relative to the federation execution:

1. **Initialization**

   Each federate has to join the federation execution previously spawned by either federate, optionally declare itself time-regulating and time-constrained, and indicate the data it produces and requests as described in Section 3.2.5.

2. **Simulation**

   a) $t = 0$

      i. **CityMoS Frontend** serves as an interface to the user and therefore registers and updates all object instances which form the static simulation environment (**Link**, **Node**, **Edge**).

      ii. Each federate then indicates its wish to advance its logical time.

      iii. **CityMoS Power** discovers registered object instances that it has subscribed to (**Node**, **Edge**) and reflects their updates, so does **CityMoS Traffic** (**Link**).

      iv. Time is advanced by **RTI**.

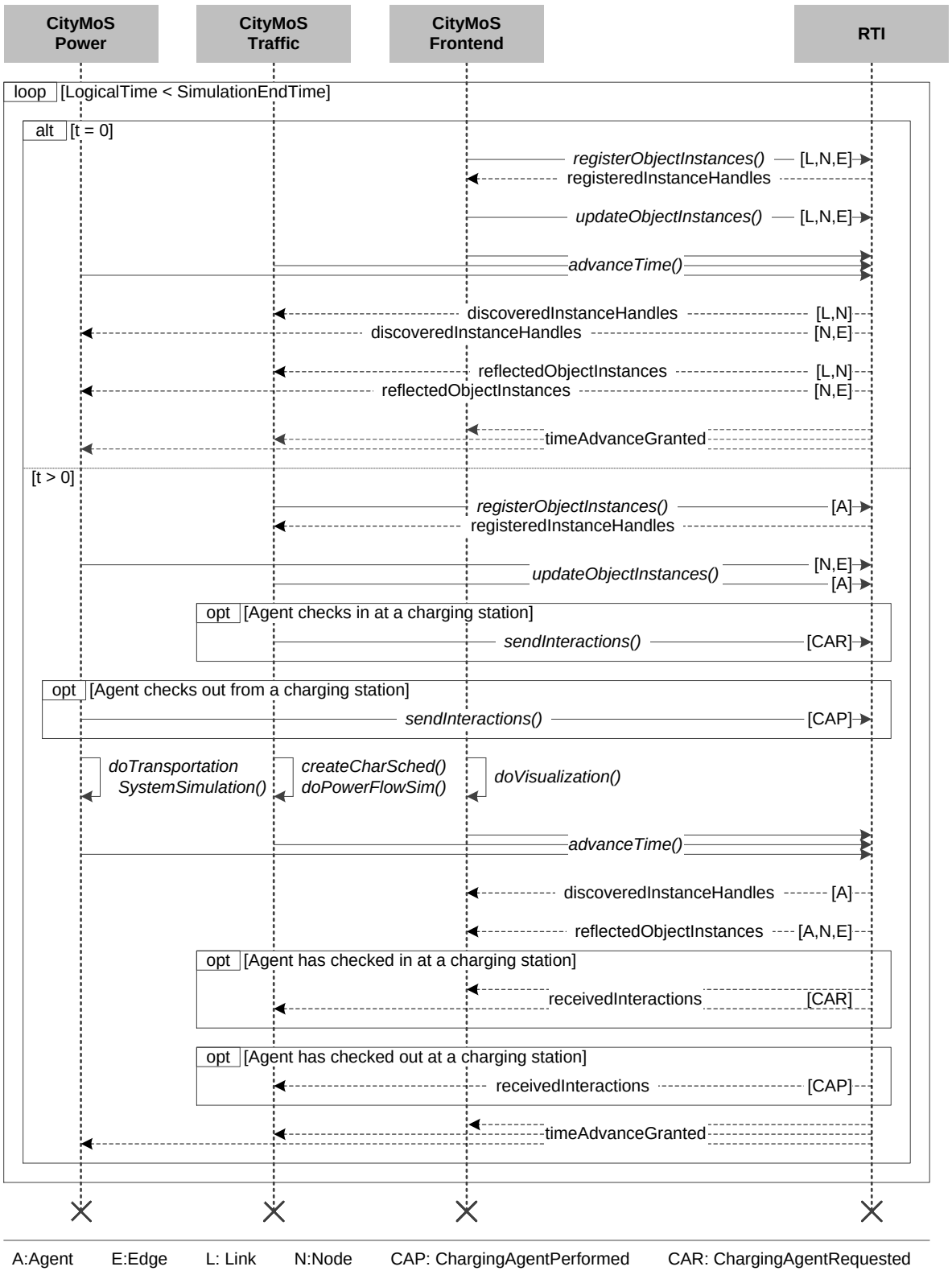

Figure 3.8: Simulation phase of the regular federation execution process of CityMoS.

b) $t > 0$

i. **CityMoS Traffic** registers and updates object instances (**Agent**) based on the previously reflected ones (**Link**), so does **CityMoS Power** (**Node**, **Edge**).

ii. In case a PEV checks in at a CS, a **ChargingAgentRequest** interaction is sent by **CityMoS Traffic**. In case a PEV checks out from a CS, **CityMoS Power** sends a **ChargingAgentPerformed** interaction.

iii. After CS-related interactions are sent, each federate has the opportunity to execute its own simulation functions. For **CityMoS Power** it is the creation of a charging schedule for each agent of a received **ChargingAgentRequest** interaction and the power flow simulation. For **CityMoS Traffic** it is the transportation system simulation and for **CityMoS Frontend** the visualization.

iv. The federates then indicate their wish to advance their logical time.

v. **CityMoS Frontend** discovers registered object instances that it has subscribed to (**Agent**) and reflects all previously published updates (**Agent**, **Node**, **Edge**).

vi. If a **ChargingAgentRequest** or **ChargingAgentPerformed** interaction is sent, it is forwarded to **CityMoS Frontend**, in the former case additionally to **CityMoS Power**.

vii. Time is advanced by **RTI**.

3. **Finalization**

After finishing its simulation loop, each federate resigns from the federation execution and tries to destroy it as described in Section 3.2.5.

To illustrate the regular federation execution process, Figure 3.9 provides a small-scale scenario in which a PEV interacts with both a transportation and a power system over a horizon of 42 time periods. The transportation system consists of two **Link** objects while the power system is composed of one **Edge** and two **Node** objects. The power system's **Node** marked *SS* represents a substation acting as a PV bus whereas the **Node** marked *CS* stands for a charging station acting as a PQ bus.

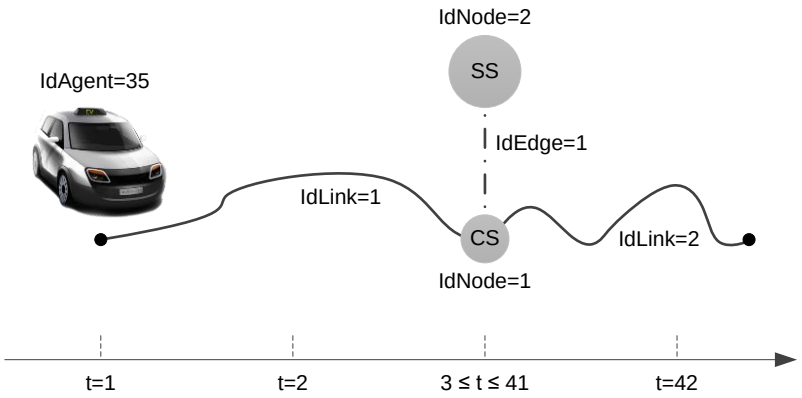

Figure 3.9: Example of a PEV interacting with both a transportation and a power system.

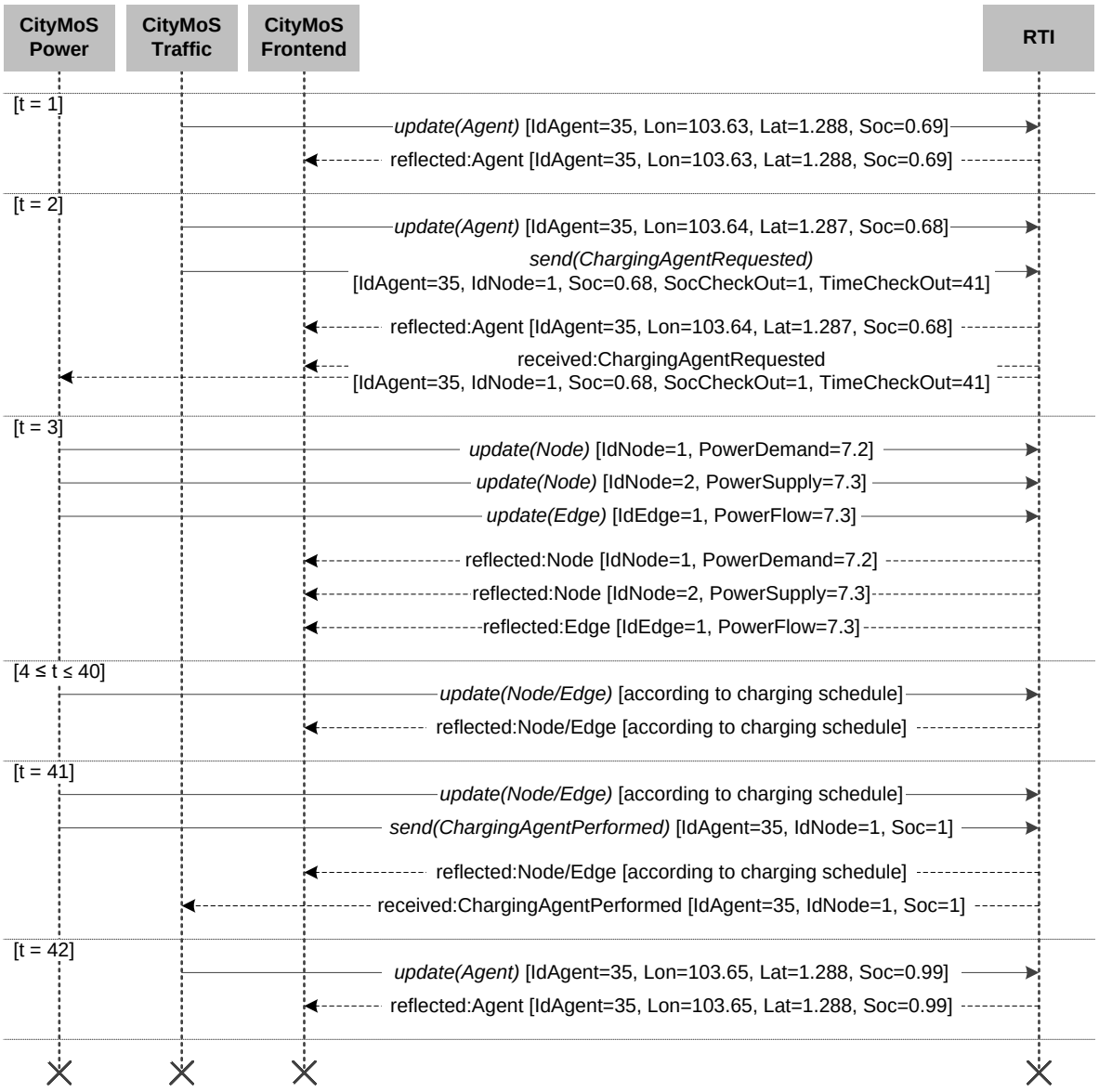

Figure 3.10: Example of the data exchange in the simulation phase of the regular federation execution process of CityMoS.

Within the time horizon, the PEV moves along the first **Link**, stops at the CS to fully charge its battery, and continues its trip on the second **Link**. In accordance with the interactivity definitions of Table 3.2, published and subscribed object instances as well as interactions sent and received by the involved federates are illustrated in Figure 3.10. Each message only contains the object's unique identifier and the most essential attributes which are updated at the respective time period. It is assumed that the PEV starts with an SOC of 0.7 and consumes energy equivalent to an SOC decrease of 0.01 per time period of driving. In the following, the data exchange at each time period is described leaving the specific values of

each attribute and every parameter at Figure 3.10. As a starting point, object instances are already registered, discovered, and reflected by all federates as previously described for $t = 0$ in Step 2a) of Figure 3.8:

1. $t = 1$

   The PEV moves forward on the first **Link**. **CityMoS Traffic** therefore updates its Longitude, Latitude, and Soc. This update is reflected by **CityMoS Frontend** visualizing the PEV at its new location.

2. $t = 2$

   The PEV moves forward on the first **Link** and checks in at the CS. **CityMoS Traffic** therefore updates its Longitude, Latitude, and Soc and additionally sends a **ChargingAgentRequest** interaction including the IdNode of the CS as well as information on the PEV's current and targeted SOC and on the targeted check out time TimeCheckOut. The update is reflected by **CityMoS Frontend** visualizing the PEV at its new location. The interaction is received by both **CityMoS Power**, calculating a charging schedule, and **CityMoS Frontend**, visualizing the charging process.

3. $t = 3$ to 41

   Based on the PEV's charging schedule, **CityMoS Power** conducts a power flow simulation at each time period and updates PowerDemand, PowerSupply, and PowerFlow of the involved **Node** and **Edge** objects. Differences between PowerSupply and PowerDemand are considered power losses which are occurring when transmitting power over the **Edge** object. The updated values may be different for each time period depending on the calculated charging schedule. Updates are reflected by **CityMoS Frontend** visualizing the new status of the power system at each time period. At its targeted check out time $t = 41$, **CityMoS Power** additionally sends a **ChargingAgentPerformed** interaction indicating the PEV's current SOC. This interaction is received by **CityMoS Traffic** updating the SOC of its internal PEV's representation.

4. $t = 42$

   The PEV leaves the CS and moves forward on the second **Link**. **CityMoS Traffic** therefore updates its Longitude, Latitude, and Soc. This update is reflected by **CityMoS Frontend** visualizing the PEV at its new location.

3.7 Discussion and Related Work

Although the functionality offered by the ensemble of the CityMoS platform's components is currently unique among the investigated literature, single components may be replaced by an alternative. In Section 3.7.1, alternative standards for constructing reusable and interoperable distributed system simulations are introduced. Reasons for and experiences obtained using HLA as the interoperability standard in CityMoS are then discussed in Section 3.7.2. Alternatives to the platform's power and transportation system simulation are presented in Section 3.7.3.

3.7.1 Distributed System Simulation Standards

Besides HLA there are multiple other standards for describing an architecture to construct reusable and interoperable distributed system simulations. System simulations are not restricted to computer simulations but instead they form a class of its own called *live, virtual, and constructive* (LVC) systems [135]. Live systems involve real people operating real systems, virtual systems refer to simulated systems operated by real people while in constructive systems both the systems and operating people are simulated. Different standards support all or only parts of those LVC systems. A historical review on the reasoning for the development of those standards which is centered around HLA is described in [136]. In case communication between systems implementing different standards has to be enabled, interposing gateways, e.g., VT MÄK VR-Exchange [137] can be used which in turn increases the complexity of those systems. For comprehensibility reasons, the terminology which has already been introduced in the context of HLA is used when the most important standards are presented in the following:

- **Aggregate Level Simulation Protocol (ALSP)**

  ALSP, consisting of both protocols and software, was developed on behalf of the US DoD in the early 1990s with the purpose to establish standardized inter-model communication. Interacting simulations can freely join or leave a federation execution, they can be geographically distributed and interact by exchanging message thereby retaining their autonomy in controlling their own resources. ALSP further offers time and data management. It is not actively developed as it was quickly superseded by HLA and is therefore not further described in this context. Additional information can be found in [138].

- **Common Object Request Broker Architecture (CORBA)**

  CORBA is an active standard to provide interoperability among distributed objects defined by the *Object Management Group* (OMG) [139–141] and has also been released as ISO/IEC Standard 19500 [142–144]. It was first published in 1991 and has evolved every since. CORBA enables the exchange of information between systems independent of their hardware platforms, programming languages, and operating systems. In systems implementing CORBA, there is a strict separation of the implementation and public interfaces. The system can be implemented in any programming language while the interfaces are defined in the OMG's standard *interface definition language* [145]. This separation enables a client system to call a method or access properties on a proxy of a distributed object for which only the interface specification is known. This call is forwarded to the host object by the *object request broker* which runs on both the client and server system and which returns all responses back to the caller. Communication between both brokers happens over the standardized *internet inter-object request broker protocol* enabling full compatibility between different vendors of CORBA systems as opposed to HLA. The standardized definition of the data, operations, and the communication protocol thereby provide consistency between multiple systems in heterogeneous environments. CORBA also perfectly complements HLA when used together as described in [146]. Further information on CORBA can be found in [147].

- **Data Distribution Service (DDS)**

  DDS is an active standard defined by the OMG [148] which was first defined in 2003 and has evolved every since. As a middleware between an application and operating system, it facilitates the efficient distribution of data in a federation execution by introducing a virtual *global data space* individual federates can read from and write to. Using a publisher/subscriber pattern, data objects are addressed and filtered based on topics and keys without the requirement for a central instance managing communication or handling data. Instead, DDS proposes a decentralized architecture with a dynamic discovery service for joining federates. It automatically establishes connections between joined federates at runtime without the requirement for predefining data sharing within a federation execution at design or compile time. With 22 different policies, DDS offers an extensive set of *quality of service* characteristics including reliability and bandwidth restrictions, delivery deadlines, and resource limits. APIs are provided in multiple programming languages allowing federates to interoperate across different operating systems and programming languages. Interoperability between federates using DDS implementations of different vendors was demonstrated in [149]. Opposed to HLA, DDS does not offer federation or time management besides simple time stamping. A comprehensive comparison and mapping of the different functionality between DDS and HLA is provided in [150, 151]. Creating real-time simulations jointly using both DDS and HLA is described in [152].

- **Distributed Interactive Simulation (DIS)**

  In 1993, DIS was defined in the active IEEE Standard 1278 which is subdivided into the parts *Application Protocols* [153], *Communication Services and Profiles* [154], *Exercise Management & Feedback* [155], as well as *Verification, Validation, and Accreditation* [156]. Although the standard is superseded by HLA it is for legacy purposes still actively being developed. Without any central server managing communication within a federation execution, termed *exercise* in the context of DIS, federates communicate with each other by broadcasting *protocol data units* over UDP whenever there is a significant change in a federate's state and at certain intervals to indicate the federate is still alive. A unit's format is strictly specified in the DIS standard and may individually be extended by arbitrary data only since the most recent version of the standard. Federates may join and leave a federation execution at any time. Without offering time management services, federation executions are limited to real-time applications.

- **Functional Mock-up Interface (FMI)**

  The FMI is a tool-independent, standardized interface to support model-based development of systems and thereby facilitate interoperability, exchange, and reuse of systems initiated by Daimler AG in 2010 [157, 158]. In its active version 2.0 from 2014, the FMI supports the exchange of simulation models generated in different languages using different tools not being restricted to any application domain. A component implementing the FMI is called *functional mock-up unit*. It consists of variable definitions and general information about the model, the model description itself represented by a set of functions in either source or binary form, and resource files which may be required to

run the model. Exporting a model as a functional mock-up unit allows for its usage as a shared component among various systems in a standardized way. The FMI is notably different from other mentioned standards in a way that only a standardized interface to simulation components is specified. The architecture to support federation executions is not part of the standard. A way of jointly using both FMI and HLA to run federation executions and thereby taking advantage of both standards by wrapping functional mock-up units to act as HLA federates is described in [159, 160].

- **Test and Training Enabling Architecture (TENA)**

  TENA is an architecture developed at the behest of the US DoD to enable interoperability, provide composability, and foster reuse of distributed LVC testing and training systems requiring real-time interactions [161, 162]. Its development was motivated by the inadequate support of HLA to provide low-latency, high-performance services in real-time applications integrating live assets. Although designed for military range systems, TENA is agnostic to the particular user domain. As opposed to competing standards, TENA supports and is designed for live, real-time systems in which the flow of time is only constrained by reality thus lacking any time management mechanisms. Using TENA, federates can be servers who publish objects, called *servants*, or clients who subscribe to objects, called *proxies*, or both at the same time for different objects. Only the publisher can modify a servant, the proxy is a read-only copy of it. Ownership management as supported, for instance, by HLA is thus not offered. Both servants and proxies include properties, local methods, and a remote interface. Local methods are executed in the context of the server or client, respectively, while the remote interface forwards calls from a client to the servant's server in whose context they are executed. Similarly to the OMT of HLA, TENA defines a meta-model, *logical range object model*, for specifying servants. TENA is actively maintained by the TENA *software development activity* [163] and free to use but neither open source nor an official standard.

When coupling LVC systems, the presented standards are most commonly and actively used by a broad international audience. Some of them are receding, e.g., ALSP and DIS, offering similar functionality, e.g., DDS and TENA, or are complementing HLA, e.g., CORBA and FMI. LVC systems can implement only a single standard or they can be enhanced by an additional, complementing standard compensating for a standard's design decisions not matching the individual requirements. Interposing gateways allow for federation executions consisting of systems implementing different standards. In the context of CityMoS, HLA is chosen as the only standard for reasons discussed in the following Section 3.7.2.

3.7.2 Simulation Interoperability with the High Level Architecture

The different federates of CityMoS communicate with each other over HLA which abstracts data formatting and transmission. Objects and interactions are defined by a FOM and transmitted according to this definition using the RTI, a software library implementing the HLA interface specification. Although any of the standards presented in Section 3.7.1 could have been implemented, CityMoS uses HLA for two reasons. First, HLA already implements rich time management services to globally consistently synchronize simulation time among all

interacting federates thereby allowing each federate to maintain its own logical time. Second, HLA is broadly used in related scientific literature resulting in a large user community featuring many different implementations.

Instead of loosely coupling the different federates using a standardized architecture, a proprietary data exchange between the individual federates of CityMoS could alternatively have been implemented. This, however, would have been opposed to the design goal of CityMoS offering a flexible platform for different, at design time possibly unknown or already existing simulation components. Those components should be flexibly arranged while guaranteeing their interoperability and reusability. Besides, advantages of HLA like offering rich time management services or an automatic data type conversion between different operating systems and programming languages would have been disregarded.

In contrast to the advantages of HLA as a standard compared to other solutions, shortcomings in its implementation became evident in the course of this work. In CityMoS, various bugs mentioned in Section 3.2.4 prevented the usage of the previously preferred RTI poRTIco and required switching to VT MÄK RTI. Although functionally working as expected, VT MÄK RTI showed several performance issues in the used version. Registering or updating a large number of object instances results in a lower performance of 25 000 instead of 120 000 object instances per seconds as advertised in [125]. Those issues are related to bugs[2], the execution context, and C++ being the native programming language of the API slowing down the Java version as described in Section 3.2.4. Although no general conclusion about the degree of interoperability between RTIs of different vendors can be drawn, switching from poRTIco to VT MÄK RTI involves source code modifications limited to linking to a different library. This convenient option of switching RTIs of different vendors allows circumventing problems potentially occurring with a vendor in a specific individual context.

Concluding from the experience of using HLA in form of poRTIco and VT MÄK RTI in CityMoS, both RTIs in their current implementation do not seem to be foolproof ready for an application in all scenarios. Especially in heterogeneous environments including different operating systems and programming languages exchanging tens to hundreds of thousands of messages as they accrue in large-scale microscopic distributed simulations, interoperability and performance issues can occur. This might require additional implementation efforts on the user side or the adoption of other distributed system simulation standards especially designed for high-performance applications, e.g., TENA. In case the environment is more homogeneous or the investigated scenario more elementary, HLA with its rich time management services is a simple, yet powerful way of coupling multiple simulations. It is easy to use and to integrate with any federate implemented in a programming language for which the used RTI offers an API.

3.7.3 CityMoS Platform

The functionality offered by the CityMoS platform as described in this chapter is currently unique among the investigated literature. CityMoS provides the architecture to compose

[2] Several bugs reducing the performance have been found and acknowledged by the vendor resulting in a yet unpublished interim version 4.4.1i.

interoperable distributed system simulations and is thereby not limited to neither the described power and transportation system simulations nor the presented interactive visualization. In principle, any simulation implementing an HLA Bridge package as specified in Section 3.6 can be included. This also allows replacing any of the provided federates by other simulations in case their functionality better matches the individual use case. Competing tools focus on either the transportation or the power system side. Achieving interoperability among multiple simulations has never been the design goal of any of those tools. As argued in [164], extensive source code modifications are therefore required to allow studying bidirectional dependencies instead of simply implementing an HLA Bridge package into a new federate of the CityMoS platform as described in Section 3.6. Albeit, in the following, alternatives for both CityMoS Power and CityMoS Traffic are outlined:

- **CityMoS Power**

  The functionality of CityMoS Power which is provided in four different modules can currently not be replaced by a single tool as argued in Section 2.1. Related approaches providing a functionality approximating the one of the first two modules, planning and evaluating PNMs, were already presented and discussed in Section 2.6.1. Software tools implementing any of those approaches are publicly not available. Alternatives to the third module, scheduling of battery energy storage, are described in [13–15]. Again, a software implementation of any of the approaches is publicly not available. With the fourth module offering the possibility for conducting power flow simulations, the situation is different. There are multiple different algorithms and tools available allowing for computing the capacity utilization at every branch as well as the voltage at every bus. A total of 40 commercial and 25 non-commercial power system simulation software packages are provided in [165, 166], each being equivalently able of replacing JPOWER as the applied power flow model.

- **CityMoS Traffic**

  Transportation system simulations can be distinguished according to their level of detail representing the traffic flow into *macro-, meso-, micro-*, and *nanoscopic* simulations [167]. Only at a micro- and nanoscopic level of detail individual agents are simulated. This level is assumed necessary for this work's investigation. On a more coarse-grained level, individual driving pattern or driver behavior is not modeled thus providing results which tempo-spatially do not have the level of detail required in the context of this work. An excellent primer into agent-based transportation system modeling and simulation can be found in [168, 169].

  In Table 3.3, a list of the most relevant transportation system simulations distinguished by their license type is provided. A detailed comparison of many of them can, for instance, be found in [164, 168–170]. With regard to the current limitation of CityMoS Traffic lacking a proper bidirectional HLA module as described in Section 3.4, any of the presented simulations may alternatively be used, assuming a proper implementation. This is due to the usage of the same well-known driver behavior and vehicle component models as well as similar routing algorithms. Applying the same trip data as input, the

Table 3.3: Overview of transportation system simulation tools.

	Acronym	Name	Literature
Open source	JAAMSIM	Java Animation Modelling and Simulation	[173, 174]
	MAINSIM	Multimodal Innercity Simulation	[175]
	MATSim	Multi-Agent Transport Simulation	[176]
	MITSIMLab	Microscopic Traffic Simulator Laboratory	[177]
	MovSim	Multi-model Open-source Vehicular-traffic Simulator	[178]
	REPAST	Recursive Porous Agent Simulation Toolkit	[179, 180]
	SUMO	Simulation of Urban Mobility	[181, 182]
	TRANSIMS	Transportation Analysis and Simulation System	[183, 184]
	Veins	Vehicles in Network Simulation	[185, 186]
Commercial	AIMSUN	Advanced Interactive Microscopic Simulator for Urban and Non-Urban Networks	[187]
	CORSIM	Corridor Simulation	[188]
	ITSUMO	Intelligent Transportation System for Urban Mobility	[189]
	PARAMICS	Parallel Microscopic Simulation	[190]
	VISSIM	Verkehr In Städten - Simulationsmodell	[191]

output of any of those simulations does presumably not differ much, although not being investigated further in this work.

The referenced simulations do not provide for simulation interoperability. They, however, may be extended by a proper HLA module. For SUMO, the steps required to integrate HLA are described in [171]. Latest efforts in designing a distributed simulation platform offering a transportation system simulation *software as a service* in the cloud using HLA are still at a conceptual stage [172]. In [127], a similar concept is presented for the CityMoS platform.

3.8 Conclusions

CityMoS is a distributed simulation platform intended for urban infrastructure planning in which the single components are interoperating using the IEEE Standard 1516-2010, termed HLA. This standard is used for constructing reusable and interoperable distributed system simulations enabling bidirectional communication between joined federates, even spanning across heterogeneous hardware and software platforms. CityMoS is not limited to specific simulations; instead, any component supporting HLA with a compatible SOM may act as a joined federate. In the context of this work, CityMoS is used for investigating the impact of different road transportation electrification scenarios on urban power systems in Chapter 4. The platform therefore comprises the following components:

- **CityMoS Power**

  As an implementation of the PSS framework described in Chapter 2, CityMoS Power allows planning and evaluating PNMs for subsequently conducting power flow studies

on them. The included smart scheduling approach for battery energy storage enables applying different, even price-responsive strategies for charging and discharging PEVs. CityMoS Power is implemented in Java and can operate either standalone using offline data or as a joined federate dynamically exchanging data with other participants of the same federation execution. Its input and output data uses the XML format for which a formal specification in form of an XSD is provided.

- **CityMoS Traffic**

  The agent-based transportation system simulation CityMoS Traffic is able to simulate the movements of a vehicle population as a discrete sequence of events in time. Each vehicle is modeled as an individual agent represented by a driver-vehicle unit comprising own driver behavior and vehicle component models. Those models allow agents to also represent PEVs as required for this work. Agents are routed along a given road network according to their individual trip data. Its output data in a disaggregated form comprises the tempo-spatial position of each single agent. In an aggregated form, tempo-spatial trip data including the required energy and covered distance is provided. Due to storage requirements and processing speed, both the aggregated and disaggregated form uses the CSV format.

- **CityMoS Frontend**

  As an interactive visualization tool, CityMoS Frontend allows participating in and controlling of federation executions and their joined federates in a coupled environment using HLA. User interactions are not limited to the standalone visualization of offline data; instead, they also cover the exchanged data between joined federates at runtime. This way, users are enabled to not only visualize and inspect the output of all joined federates but also actively produce data and thereby interact with them. Visually providing insights into the exchanged data of a federation execution allows users to be more easily attracted to the simulation platform by nurturing their understanding of its functioning and creating confidence in the results. CityMoS Frontend is also implemented in Java. Instead of defining an own data format, the input and output format used by each joined federate is supported.

The functionality offered by the ensemble of the single components of the CityMoS platform is currently unique among the investigated literature. The platform allows evaluating a great variety of large-scale what-if road transportation electrification scenarios on realistically emulated power system infrastructure before they are implemented in a real-world setting. Those scenarios include but are not limited to alternating the design of the power and transportation system infrastructure, varying the CS location and power connection, applying different scheduling strategies, assuming diverse agent charging behavior, diversifying the composition of the vehicle population, as well as applying demand-responsive or vehicle-to-grid charging and discharging schemes. In case further scenarios need to be investigated, CityMoS can be extended by additional federates as, for instance, a railway transportation system simulation. Existing federates can also be replaced by alternative ones in case their functionality better matches the individual use case. In its presented composition, the CityMoS platform is mainly targeting researchers who want to conduct large-scale exploratory simulation experiments to

investigate interdependence between various systems and their components. Moreover, experts of adjacent areas who are not familiar with either transportation or power system simulations are provided a tool with which they are able to conduct interdisciplinary studies targeting the exploration of future road transportation electrification.

4 | Methodology Demonstration on the Example of Singapore

Content

Using the CityMoS platform, realistic power network models are generated and evaluated allowing to simulate power flows induced by different road transportation electrification scenarios on those models. This way, not only the overall impact on the generation capacities but also times and locations of grid congestion are identified.

4.1 Introduction

This chapter provides an application of the methodology presented in Chapter 2 and its implementation described in Chapter 3 in form of two case studies. Their purpose is to finally answer this work's research question which was formulated in Section 1.1 as follows:

Which impact does the power and energy demand induced by a large number of timely and spatially distributed PEVs have on urban power systems?

Concluding on the impact of different road transportation electrification scenarios on power systems requires a PNM which has to be generated and evaluated before relevant power flow calculations can be conducted. Consequently, two case studies are presented addressing both items in the Singapore context:

Case Study 1: Generating and Evaluating Power Network Models (Section 4.2) Realistic PNMs showing topological and electrical properties of real-world power systems are generated based on available data for Singapore. Results, also in the context of a conducted sensitivity analysis to investigate the impact of different parameters and parameter uncertainty, are presented and discussed with respect to the methodology's general applicability.

Case Study 2: Investigating the Power System Impact of Different Road Transportation Electrification Scenarios (Section 4.3) The PNM generated in the context of the previous case study which best matches Singapore is used to investigate different road transportation electrification scenarios. The impact of different PEV population sizes, scheduling strategies, and other parameters is analyzed both on the generation capacities and the utilization of substations and power lines. Results are presented and discussed with regard to limitations of the applied methodology and their significance.

4.2 Case Study 1: Generating and Evaluating Power Network Models

The case study presented in this section is designed to demonstrate the feasibility of the PSS framework presented in Chapter 2 and its implementation described in Chapter 3. It thereby serves as a *proof-of-concept* that despite the framework's limitations, PNMs with topological and electrical properties of real-world power systems can indeed be generated. Based on the available data of the Singapore power system and a set of parameters best accommodating this data which both are described in Section 4.2.1, a PNM of Singapore is planned and discussed in Section 4.2.2. Besides a simple proof-of-concept, detailed investigation in form of ceteris paribus sensitivity analyses help identifying the impact of the different parameters and parameter uncertainty in Section 4.2.3. In Section 4.2.4, the relevance and applicability of

PNMs in general and of the Singapore PNM in particular is discussed, especially when only little information is available for the planning process. Conclusions on the presented findings are drawn in Section 4.2.5.

4.2.1 Input Data

The input data used for generating the PNMs of this study draws on and includes elements of the Singapore power system. A PNM is not an exact representation but instead combines real-world data and those generated by CityMoS Power to match topological and electrical metrics of the real one. Available data of the Singapore power system include the number, location, and specification of substations, power stations, power lines, and consumers on the different voltage levels. They are described in Section 4.2.1.1. CityMoS Power uses this input data to generate the PNMs of this study. The implemented PSP approach can be multi-purposely parametrized to generate PNMs with a large variety of different characteristics. The applied default parameter set is described in Section 4.2.1.2.

4.2.1.1 Singapore Power System

The Singapore power system as shown in Figure 4.1 is divided into the LV grid (0.4 kV), the MV grid (6.6 kV, 22 kV, 66 kV), and the HV grid (230 kV and 400 kV). Substations connect different voltage levels by stepping down the higher of the two voltages. The lower voltage winding of a substation serves as power supply to connected consumers of this voltage level while the upper voltage winding is considered a consumer within the higher voltage layer. For each voltage level, the number of substations [192] as well as their maximum power [193, 194] and efficiency [195] are distinguished. The maximum power rating of substations can be exceeded depending on their thermal design according to the dependency of lifetime and temperature specified in [196] and compactly described in [197]. Additionally, the number [198] and the location [199] of power stations with generation capacities greater than 100 MW, the location [199] of the 400 / 230 kV substations, and the connecting 400 kV power lines are given. The voltage level and precise generation capacities [198] of the given gas- and oil-immersed power stations are provided in Table 4.1. The PSP process also takes this additional information for the manual planning of the 400 kV grid into account as described in Section 2.2. Hereby, the 230 kV winding of each of the 400 / 230 kV substations is connected to the 230 kV winding of the nearest regularly planned 230 / 66 kV substation. The 230 kV power stations are connected to the 230 kV winding of the nearest 230 / 66 kV substation while only allowing one substation to be connected to at maximum one power plant. Voltage regulating devices are installed in all substations of the MV and HV grid [194].

In Singapore, 26 500 km of underground transmission and distribution power cables are installed [192]. In [194], the installed conductor types, their number of cores, insulation, armor, sheath, as well as their material and cross sectional area are given. [200–202] provide additional data on the nominal power rating P_{S}, the maximum cable length at that rating $L_{\max}$, as well as on the conductor resistance R and reactance X. These specifications, distinguished by voltage level, are summarized in Table 4.2.

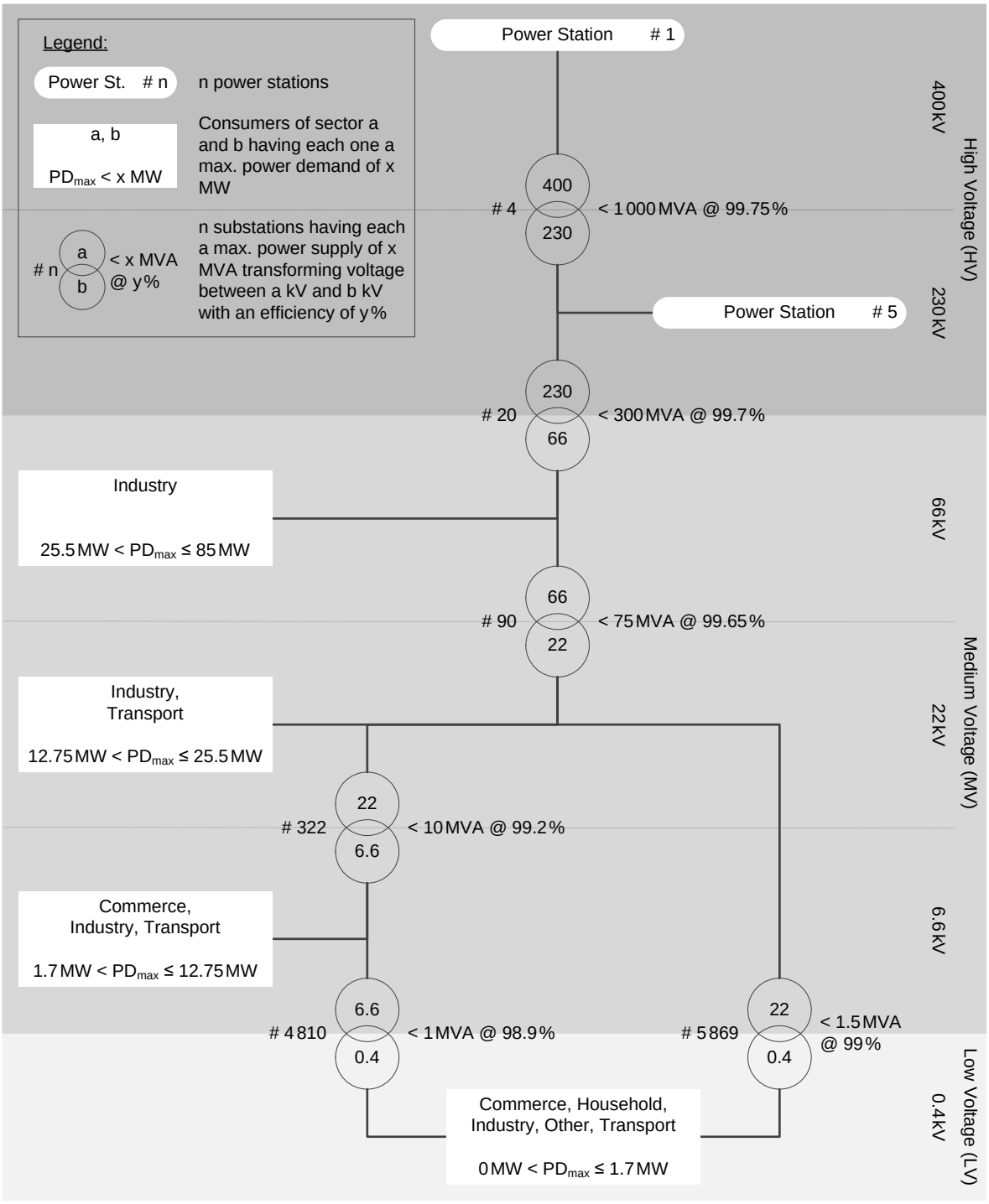

Figure 4.1: Singapore power system.

Table 4.1: Power stations with generation capacities greater than 100 MW in Singapore.

Power station	Voltage level [kV]	Generation capacity [MW]
Tuas Power Generation	400	2 609
Senoko Energy	230	3 300
YTL PowerSeraya	230	3 100
Keppel Merlimau Cogen	230	1 340
PacificLight Power	230	800
SembCorp Cogen	230	785

The power system planning process presented in Section 2.2 requires data on the number [203], locations [204], and power demand [205, 206] of consumers connected to the various voltage levels. The raw data reveals a load curve as illustrated in Figure 4.2. Instead of taking the power demand at any point in time, the peak power demand $P_{\mathrm{D,max}}$ of 6 340 MW is used to ensure proper dimensioning of the installations during the PSP process. This way, satisfaction of the power demand for the 117 852 consumers being geographically distributed over an area spanning 50 km north-south and 30 km east-west can be guaranteed at all other times. Each of these consumers is assigned to one of the sectors *industry* (44 % of total power demand), *commerce* (36 %), *household* (14 %), *transport* (5 %), and *other* (1 %). As there is no related information available, the assignment of consumers to the different voltage levels is estimated based on the combination of the number of substations on each level and their respective maximum power. Consequently, most consumers are connected to the 0.4 kV grid; exceptions of consumers having a higher power demand justifying connecting them to a higher voltage level are made for subway stations, shopping malls, and some commercial buildings which are directly connected to the 6.6 kV grid, the two ferry terminals and checkpoints being connected to the 22 kV, and some industrial buildings being distributed over the voltage levels between 6.6 kV and 66 kV. The calculated mapping of consumers to the different sectors and voltage levels is given in Table 4.3. A topological illustration of the available consumer input data contrasted by sector is shown in Figure 4.3.

Table 4.2: Specification of power cables installed in Singapore.

Voltage level [kV]	Material	Cross sectional area [mm^2]	P_{S} [kVA]	L_{max} [m]	R [Ω/km]	X [Ω/km]
400	Copper	2 000	986 576	145 469	0.0090	0.1093
230	Copper	1 200	374 071	110 519	0.0151	0.1156
66	Copper	1 000	86 651	39 840	0.0176	0.1084
22	Copper	300	23 015	11 163	0.0601	0.0920
22	Aluminum	300	17 909	10 386	0.1000	0.0920
6.6	Copper	185	5 156	3 290	0.0991	0.0900
6.6	Aluminum	120	3 155	2 565	0.2530	0.0950
0.4	Copper	35	94	164	0.5240	0.0750

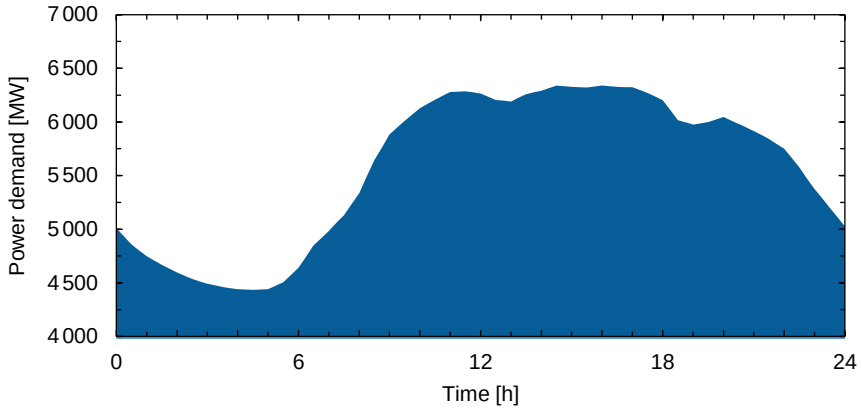

Figure 4.2: Singapore load curve on Monday, 12th January 2015.

Table 4.3: Consumer voltage level and power demand data for Singapore.

Sector	#Nodes				Power demand [MW]			
	0.4 kV	6.6 kV	22 kV	66 kV	0.4 kV	6.6 kV	22 kV	66 kV
Commerce	19 122	983	0	0	611	1 671	0	0
Household	–	–	–	–	–	–	–	–
Condominium	5 443	0	0	0	109	0	0	0
HDB	10 991	0	0	0	727	0	0	0
Landed property	69 447	0	0	0	49	0	0	0
Other	245	0	0	0	3	0	0	0
Industry	5 390	190	125	15	498	323	1 594	375
Other	4 500	0	0	0	63	0	0	0
Transport	1 294	88	4	0	116	150	51	0
Total	117 852				6 340			

Besides the active power demand P_D, the power flow simulation presented in Section 2.3 also requires the reactive power demand Q_D for each consumer. As this data is not available it is derived from the active power demand using the power factor $\varphi = 0.9$ [207] according to

$$Q_D = \frac{P_D}{\cos(\varphi)} \cdot \sqrt{1 - \cos^2(\varphi)} \tag{4.1}$$

4.2.1.2 Power System Planning

The LV (MV) grid is planned with a radial (ring) topology while the HV grid is planned as a partial mesh as motivated in Section 2.2.6. Planning is to some extent done non-regularly. The regular planning process comprises all voltage levels up to and including the 230 kV grid. The non-regular part is restricted to the 400 / 230 kV part for which specific data is available as provided in Section 4.2.1.1. The smallest independent part in the regular power flow simulation

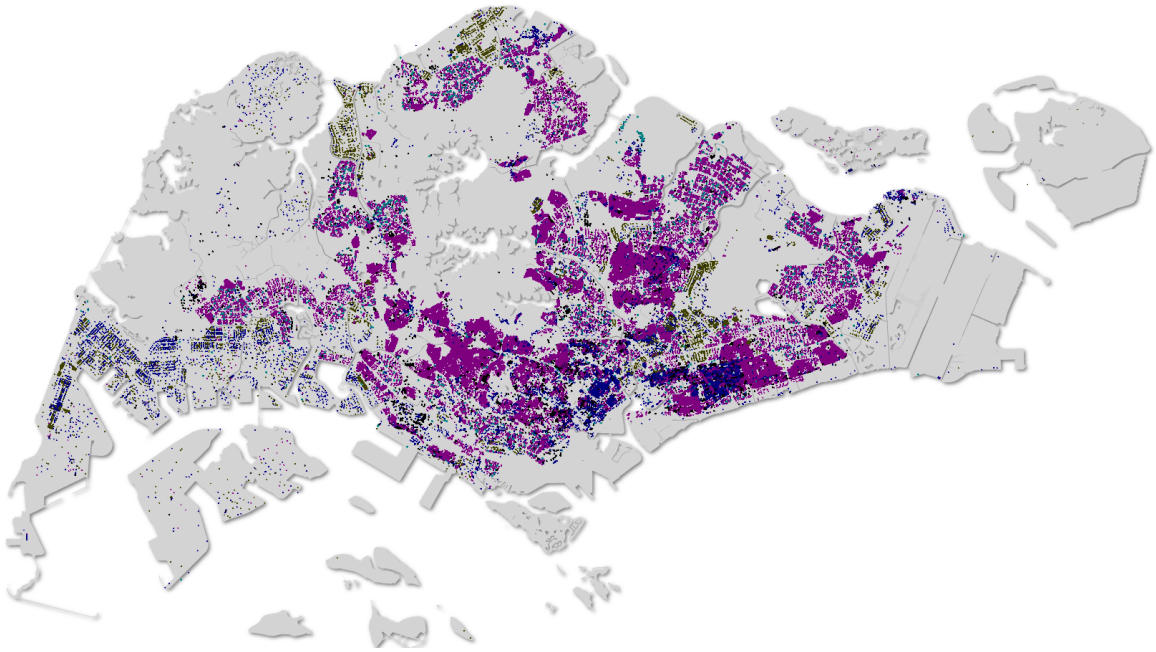

Figure 4.3: Topological illustration of the available consumer input data for the Singapore power system contrasted by sector into commerce (blue), household (purple), industry (dark yellow), other (black), and transport (cyan).

process in the LV (MV) grid is a single tree (ring) while in the HV grid it is the complete mesh. As there are voltage regulating devices installed in the Singapore power system the regular voltage level combination step as described in Section 2.3.2.3 is applied. The 230 kV power stations are considered PV buses and are initialized with 50 % of the generation capacity specified in Table 4.1. The only 400 kV power station is considered the slack bus balancing the remaining power demand and occurring losses resulting in a utilization of 64 % for the assumed peak power demand.

The permitted range of the bus voltage magnitude $|V_i|$ at each consumer i is set to be between 0.95 pu and 1.0 pu in accordance with [208]. The maximum number of nodes for each subregion for the bisection is set to 2 500, the maximum number of iterations for the k-means to 16, the maximum distance between two nodes of a cluster using the DBSCAN algorithm to twice the average distance of each voltage level's PQ bus to its PV bus, and the target mean node degree for the DT to 3.55. Those values are found to be ideal according to the findings presented in Section 4.2.3. The maximum power rating of substations can be exceeded by 25 % assuming proper active cooling. This conservative value accommodates for the wide interval of power demand being similar to the peak power demand and therefore for the long duration this overload lasts as illustrated in Figure 4.2. To account for overcapacities, a maximum power line utilization of 80 % is not exceeded. In case there are power cables of different specification possible for a voltage level, as it is the case in the 6.6 kV and the 22 kV grid, the lower quality is preferably chosen for economical reasons. The higher quality power cable is only used if otherwise an area would become infeasible according to the criteria defined in Section 2.2.1.

Power line stretch factors are set to 3.1 (LV), 2.4 (MV), and 1.5 (HV) to produce a PNM with a total power line length and a number of substations on each voltage level similar to the Singapore power grid and therefore to realistically consider power losses. Values are higher for lower voltage levels to account for a higher branching depth in those layers. Depending on the voltage level, substation and power line costs found in [209] and provided in Table 4.4 are applied to the specification of the Singapore power system found in Figure 4.1 and Table 4.2.

Table 4.4: Substation and power line costs.

Voltage level [kV]	Costs		
	Substation [US$/MW]	Power line [US$/km]	
		Copper	Aluminum
400	24 000	6 546 918	–
230	18 342	2 482 335	–
66	12 884	287 508	–
22	11 419	55 351	32 303
6.6	10 907	7 688	2 288
0.4	10 700	70	–

4.2.2 Results

The PNM generated by CityMoS Power using the described input data is referred to as the *Singapore PNM* in the remainder of this work and is topologically illustrated in Figure 4.4. It includes nodes and edges from both real-world data regarding consumers, substations, power stations, and branches available for Singapore and the ones planned by CityMoS Power on all six voltage levels. Its topological, electrical, and economic properties as defined in Section 2.5 are given in Table 4.5. Metrics are calculated separately for the LV, MV, and HV grid each being considered an individual subgraph of the PNM. This way, aggregation is as fine granular as values of real-world power systems are available, although CityMoS Power can in principal aggregate on a voltage level basis. Generating the Singapore PNM takes place within 13 minutes on an Intel Core i5-2520M using 10 GB RAM. On the same machine, power flows within the entire PNM for one time step are calculated within 11 seconds.

4.2.2.1 Topological Metrics

In the following, observations regarding topological metrics of the Singapore PNM are discussed to allow concluding on their level of consistency with real-world values. Any references to those values of real-world power system originate from Table 2.2.

Number of Substations and Power Lines

By design, the number of substations n_{PV} in all voltage levels exactly matches the target value. The number of edges m directly relates to the number of nodes n and is only dependent on

Table 4.5: Topological, electrical, and economic metrics of the Singapore PNM.

Property	LV	MV	HV
Topological			
Nodes n [#]	127 126	12 516	31
Consumer n_{PQ}	116 447	1 405	0
Substations n_{PV}	10 679	432	4
Per independent part, average $\bar{n}_p$	3.06	20.9	31
Edges m [#]	116 447	13 063	55
Independent parts p [#]	56 452	628	1
Edge length, average $\bar{l}$ [m]	145	684	9 925
Edge length, total l [km]	16 900	8 941	546
Average distance, geographical $\bar{\delta}$ [m]			
Any-to-Any $\bar{\delta}_{\mathrm{g,A2A}}$	191	2 193	20 947
PQ-to-PV $\bar{\delta}_{\mathrm{g,PQ2PV}}$	241	2 205	22 434
Average path length *apl*			
Geodesic apl_{d} [#]	1.34	5.51	3.07
Geographical apl_{g} [m]	196	4 257	27 785
Betweenness b	0.82	0.5	0.16
Clustering coefficient cc	0	0.0019	0.2419
Density d	0	0.0002	0.1183
Diameter $\varnothing$			
Geodesic $\varnothing_{\mathrm{d}}$ [#]	9	61	6
Geographical $\varnothing_{\mathrm{g}}$ [m]	5 682	40 583	66 059
Node degree			
Maximum $deg_{\max}$	140	13	6
Mean deg	1.83	2.09	3.55
Probability distribution $P(k) \sim \beta$ (R^2) [a]	2.37 (0.91)	4.04 (0.73)	–
Pearson correlation coefficient ρ	0.15	0.09	-0.16
Electrical			
Power demand P_{D} [MW] [b]	2 177	6 396	6 661
Power supply P_{S} [MW]	2 233	6 661	6 712
Power loss P_{L} [%]	2.5	3.97	0.76
Utilization, average [%]			
Power line $\bar{u}_{\mathrm{PL}}$	16	5	5
Substation $\bar{u}_{\mathrm{PV}}$	16	71	11
Voltage at consumer, average $\bar{V}$ [pu]	0.9898	0.9801	0.9897
Economic			
Costs [US$·$10^6$]	145	616	2 106
Edge C_{E}	1	407	1 739
Node (Substation) C_{N}	144	209	367

[a] R^2, termed *coefficient of determination*, is a measure how well a regression approximates real data points showing values in the interval $[0, 1]$ whereat 1 indicates a perfect fit.

[b] The value indicates the total power demand of the corresponding voltage level including power losses occurring in lower voltage levels.

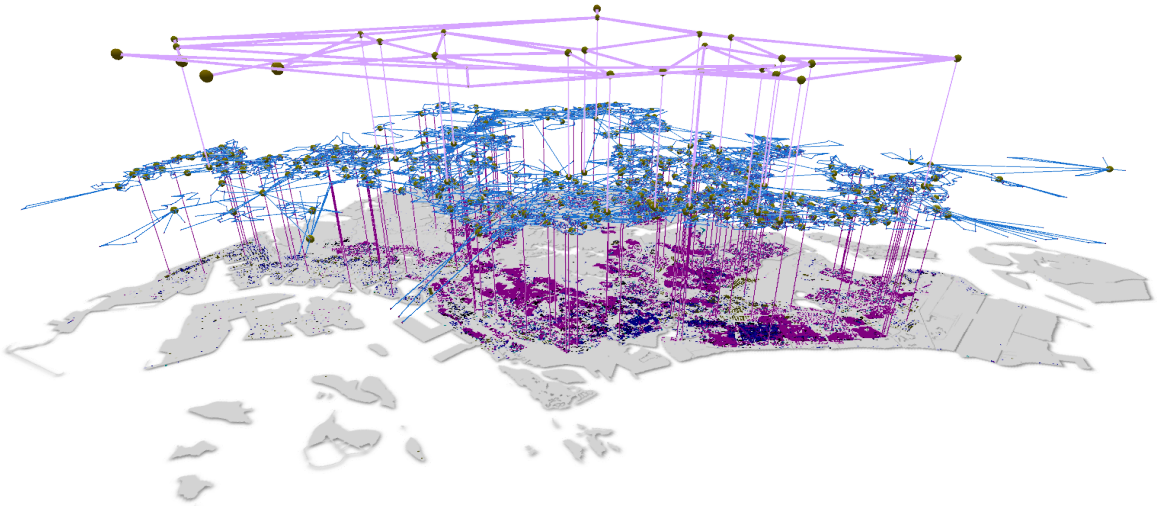

Figure 4.4: Topological illustration of the Singapore PNM aggregating multiple voltage levels to form the LV (bottom), MV (middle), and HV (top) grid.

the topology and the level of redundancy. In the radial and ring topology of the LV and MV grid, respectively, m equals or is slightly higher than the number of consumers n_{PQ} as there is no or only little redundancy. The meshed topology of the HV grid shows a significant level of redundancy and has therefore approximately twice as many edges than nodes. Another measure which is also directly dependent on the redundancy in a network is the density d. The higher the redundancy the more edges exist and therefore the ratio of the number of existing edges to the number of possible edges decreases. With almost no redundancy, the LV and MV grid show a density of virtually 0 whereas the HV grid has a density of around 0.12. In absence of any available data for real-world power systems this measure can only be used to compare different PNMs with each other rather than concluding on the relationship between a PNM and real-world power systems.

Distances

By design, the total power line length l of 26 387 km matches the target value. Stretch factors allow for higher branching depth in lower voltage levels and thereby realistically bypass missing geographical information related to the branch laying. To satisfy the raising power demand in higher voltage levels, the nominal power rating and thus the maximum cable length of the power lines are increasing as specified in Table 4.2. This is why the average power line length $\bar{l}$ is monotonically increasing from 145 m in the LV grid up to 9 925 m in the HV grid.

With the average geographical distance $\bar{\delta}$, average path length apl, and diameter $\varnothing$ there are three different distance measures, the latter two related to path lengths in a network. Distance values are calculated for each independent part and afterwards averaged. Calculating those metrics for the entire voltage level would distort results as there are no connections between the different parts within a voltage level. The values for the three measures are as

expected for the Singapore PNM. Average geographical distances $\bar{\delta}_{\mathrm{g}}$ are increasing with the voltage level. They are always higher when only considering the average distance of a PQ bus to its connected PV bus $\bar{\delta}_{\mathrm{g,PQ2PV}}$ than in the case of connecting any two buses $\bar{\delta}_{\mathrm{g,A2A}}$. Average geodesic path lengths apl_{d} and diameter $\varnothing_{\mathrm{d}}$ can be explained with the prevailing topology. In the radial topology of the LV grid, the only way of connecting the average number of nodes of 3.06 in an independent part is a unary tree resulting in a geodesic path length of 1.34. The average geodesic path length in the MV grid's ring topology is determined to follow the relationship $apl_{\mathrm{d}} = 0.25 \cdot n_p + 0.275$. The length of 5.51 therefore exactly relates to the 20.9 nodes per independent part $\bar{n}_p$. In the meshed HV grid, there is a higher redundancy resulting in less nodes being on the shortest path between any pair of nodes. As expected, the average geographical path lengths apl_{g} and diameter $\varnothing_{\mathrm{g}}$ continuously increase with higher voltage levels. Nodes are more distributed which becomes visible on the longer average edge length being enabled by higher quality power cables.

Lacking any real-world values for the average geographical distance, comparisons can only be done for the average path length and diameter, in the latter case only for the HV grid. For all voltage levels, the average geodesic path length in the Singapore PNM is considerably lower than in related real-world power systems. One reason may be that the higher real-world values stem from some few power systems with very high values. Excluding them when calculating apl_{d} decreases values to 2.02 (LV), 5.98 (MV), and 7.5 (HV). Additionally, considering the still relatively high standard deviation, apl_{d} values of all voltage levels of the Singapore PNM can be considered to be in line with those of real-world power systems as for each voltage level multiple power systems can be found sharing the same characteristic. Especially for the HV grid, the power system of France and Spain exhibit a comparably low average geodesic path length and geodesic diameter.

Betweenness

The node betweenness b and thus the normalized frequency of nodes being on the shortest path between other nodes decreases with higher voltage levels. Higher values indicate a greater relevance to the robustness of the network [210]. The betweenness of the Singapore PNM is as expected and matches other values of related measures. In the LV grid, the radial topology is causative for the relatively high betweenness of 0.82. Nodes are predominantly connected in a unary tree with only little branching in each independent part. In the ring topology of the MV grid, each node is obviously on exactly half the number of shortest paths. The meshed HV grid shows some redundancy as indicated by the clustering coefficient cc which results in a relatively low betweenness of 0.16. With average values of 0.81 for the LV grid and 0.38 for the MV grid, real-world values match those of the Singapore PNM quite well. For the HV grid there are no real-world betweenness values available.

Redundancy

The clustering coefficient cc is a measure of redundancy. As discussed in Section 2.6.6, each tree and every ring in a radial and ring topology, respectively, is currently planned as an

independent part without connections between any of them. In the Singapore PNM, the LV and MV grid each implements one of those two topologies thus resulting in *cc* values of 0 (LV) or close to 0 (MV). The ring topology in the MV grid shows a clustering coefficient unequal to 0 because of the 14 rings comprising only three nodes. In this constellation, each node is connected to every other node. Both PQ buses show a clustering coefficient value of 1 while the value of the PV bus is equal or smaller than 1 depending on the number of nodes in each of its connected rings. As an average number, the clustering coefficient of the MV grid is therefore larger than 0, although only slightly. Both values quite closely match those of real-world power systems indicating that indeed there are no or only scattered connections between independent parts thus exhibiting little redundancy. The HV grid does not fall into the same argument as it is mainly planned manually with a target mean degree *deg* of 3.55 which is above the mean of 2.57 given for real-world power systems. With a value of around 0.24, the clustering coefficient for this part of the PNM indicates a highly connected network which is otherwise only found in the one operated by the *New York Independent System Operator* (NYISO) or in the HV grids of France or Spain.

Node Degree

The mean degree *deg* of 1.83 (2.09) for the LV (MV) grid matches the values for smaller sized real-world power systems. They can be explained with the prevalent topology being either radial or ring. In a radial topology, the connected nodes can either have a degree of 1, being a leaf, a degree of 2, connecting two nodes on the same branch, or a degree higher than 2, being a branching node. In the Singapore PNM, PV buses in the LV grid have a maximum degree $deg_{\max}$ of 140. In a ring topology, each but the PV bus is connected to exactly two other nodes. Some nodes are directly connected to the PV bus only having a degree of 1. In contrast, the PV bus may be connected to multiple rings resulting in a degree being much higher; in case of the MV grid, $deg_{\max}$ is 13. The value for the MV grid is much lower than the one for the LV grid since less PQ buses are connected to a PV bus, though each one having a higher power demand. As with the real-world examples, the node degree probability distribution $P(k)$ of the Singapore PNM tends to follow a power law. With an R^2 value of 0.91, a power law distribution fits quite well for the LV grid whereas an R^2 value of 0.73 for the MV grid just indicates a power law.

The HV grid is planned with a meshed topology showing some redundancy other than the radial or ring topology used for planning the LV and MV grid. By design, the implemented DT of the PSP process produces an HV grid with a target mean degree of, in this case, 3.55 which is above the mean of 2.57 for real-world power systems but still clearly below the upper boundary of 4.47 given for the power system operated by NYISO. There it is also stated that the $P(k)$ in the HV grid tends to follow either an exponential or a power law distribution, especially in the former case exhibiting a relatively high standard deviation. This large uncertainty regarding the exact distribution indicates non-conformance among different real-world power systems at this voltage level. The PSP process is therefore only parametrized to achieve a specific target mean degree and not a specific node degree probability distribution, although possible through the iterative branch removal described in Section 2.2.6.

Assortativity

With Pearson correlation coefficient values ρ between -0.16 and 0.15 the Singapore PNM in general does not show any tendency towards being assortative or dissortative. This means that nodes neither tend to connect to nodes of the same or a similar degree nor to nodes of a degree most different. Instead, nodes are connected to nodes of any other degree with a similar probability. In the HV grid, nodes slightly tend to connect to nodes of other degrees while in the LV grid the situation is inverse. At first glance, those findings may be counterintuitive as most nodes in a radial or ring topology have a degree of 1 or 2. If only considering those nodes reflecting PQ buses, the majority of nodes therefore tends to connect to nodes with an equal or similar degree which would result in much higher coefficient values. PV buses are, however, included in the calculation of the coefficient. Their diverse degrees which are even a magnitude or two higher than the ones of the PQ buses distort overall results to a level which lets this characteristic range over a wide interval in its defined domain. This context is also identified in [211] and can be found in real-world power systems having a high standard deviation of 0.19. The Pearson correlation coefficient can therefore only be used as a metric for comparing different PNMs with each other rather than comparing a PNM with a real-world power system.

4.2.2.2 Electrical Metrics

The total power demand P_{D} of 6 340 MW is satisfied by a total power supply P_{S} of 6 712 MW. This implies an overall power loss P_{L} of 5.5 % which is close to the reference value of 5.3 % given for Singapore [212]. At each consumer the voltage is guaranteed to be between 0.95 pu and 1 pu with an average of 0.98 pu to 0.99 pu, depending on the voltage level.

In Figure 4.5a, the temporal distribution of the average substation utilization $\bar{u}_{\mathrm{PV}}$ is illustrated for the LV grid. With an average daily value of 14 % it is very low. At all times, more than 90 % of the substations are only utilized up to a value of 25 %. For the MV grid shown in Figure 4.5b, the average daily utilization is 63 % which is slightly below the optimal value ranging between 70 and 80 % [213]. Depending on the time of the day, between 56 % and 74 % of the substations are utilized up to a value of 75 % of their maximum power. Only at peak times, a maximum of 31 % are overloaded by up to 25 % as specified in Section 4.2.1.2.

The temporal distribution of the average power line utilization $\bar{u}_{\mathrm{PL}}$ for the LV and MV grid is opposed to the one for substations. In the LV grid shown in Figure 4.6a, at all times at least 70 % of the power lines are utilized up to a value of 20 %. At peak times, a maximum of 8 % are close to their maximum utilization of 80 % as specified in Section 4.2.1.2. The MV grid shown in Figure 4.6b clearly identifies the overdimensioning of the power lines of which 98 % have a utilization of less than 20 %.

Neither for $\bar{u}_{\mathrm{PV}}$ nor for $\bar{u}_{\mathrm{PL}}$ real-world power values are available. Therefore, no conclusions can be drawn on how realistic substation and power line utilization values of the Singapore PNM are. At first glance, utilization values, however, seem to be very low which is a result of incomplete input data. This topic is discussed in more detail in Section 4.2.4.

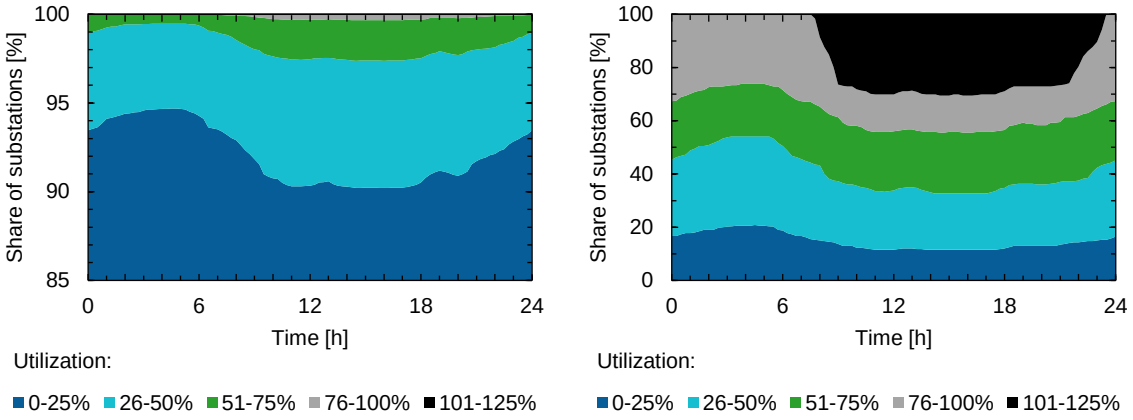

Figure 4.5: Temporal distribution of the substation utilization in the (a) LV and (b) MV grid of the Singapore PNM.

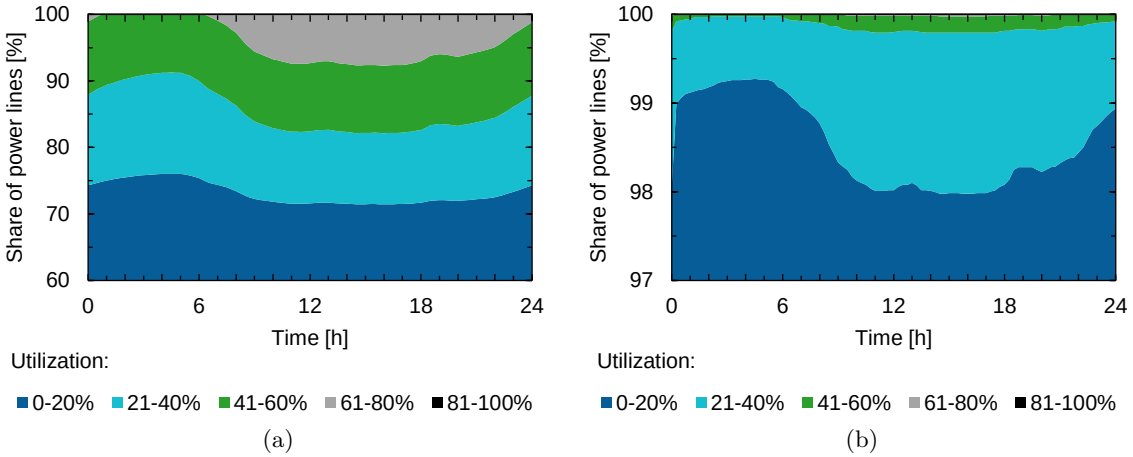

Figure 4.6: Temporal distribution of the power line utilization in the (a) LV and (b) MV grid of the Singapore PNM.

4.2.3 Parametrization

The PSP approach of CityMoS Power can be multi-purposely parametrized to accommodate different sets of input data and thereby generating PNMs with a large variety of different characteristics. Using ceteris paribus sensitivity analyses, the impact of different parameters and parameter uncertainty on the resulting PNM is identified. This section puts the focus on the LV grid; in the MV grid, changes cannot be clearly traced back to specific parameter variations as they may also be the result of changes in the LV grid. For each parameter variation a PNM is generated to identify the impact of the different parameters on the network by

comparing the resulting values for the metrics presented in Table 4.5. Based on the parameter set for the Singapore PNM described in Section 4.2.1.2, parameters are varied and the impact on the resulting PNM is discussed. This impact can be best identified looking at elementary metrics as, for instance, the number of substations, power lines, or independent parts, the total power line length, average size of an independent part, or power losses. The development of the other metrics can in their magnitude mostly be derived from those numbers. They are therefore not specifically discussed but instead only mentioned if they develop unexpectedly. Table 4.6 provides an overview of the findings which are elaborated in the following.

Table 4.6: Impact of different parameters on the resulting PNM.

Parameter	Investigated value range	Direct impact when increasing value
Cost optimization	No, Yes	Yes: $\downarrow n_{\text{Substation}}$, $\uparrow len$
Clustering		
Bisect (# nodes per cluster)	500 - 15 000	$\downarrow n_{\text{Substation}}$
K-means (# iterations)	2 - 48	$\downarrow n_{\text{Substation}}$
DBSCAN (max. node distance)	0 - $\delta_{\text{g,max}}$	$\downarrow p$, $\uparrow n_p$
Maximum utilization (node / edge)	0.8 - 1.5 / 0.8 - 1	$\downarrow n_{\text{Substation}}$,$\downarrow len$,$\downarrow p$, $\uparrow n_p$
Mean degree (HV)	2 - 4.5	$\uparrow m$
Power factor	0.8 - 1	$\downarrow Q$, $\downarrow n_{\text{Substation}}$
Power line quality factor	0.5 - 2	$\downarrow n_{\text{Substation}}$, $\downarrow m$, $\uparrow len$
Power line stretch factor (LV / MV)	3 - 3.3 / 2.1 - 2.6	$\uparrow len$,$\uparrow n_{\text{Substation}}$
Topology	Radial, Ring	Ring: $\uparrow m$,$\downarrow len$,$\downarrow p$,$\uparrow n_p$

Cost-optimized Singapore PNM

In addition to the Singapore PNM, a *cost-optimized Singapore PNM* is planned which is characterized by the metrics provided in Appendix A.2. The planning process builds on the same input data but the network recombination step is executed until no more areas can be consolidated. This way, the cost-minimal solution which can be achieved by this method is found by removing substations and thereby extending the power lines connecting consumers to the next nearest substation. As cost factors the number of substations, the total power line length, and power losses are taken into account. Compared to the Singapore PNM, there is an optimization potential of 3.3 % resulting in total costs to be reduced from $2\,868{\cdot}10^6$ US$ to $2\,772{\cdot}10^6$ US$. This number includes savings from reducing the number of substations for both the LV and MV grid by around 5 % and 28 %, respectively. It also includes additional costs arising from a total power line length growing by 25 % in the LV grid and 42 % in the MV grid as well as from power losses which are increased by 0.2 %[1].

[1] Additional costs due to power losses are calculated by valuing the 203 MWh/day of additionally required energy by the average Singapore electricity price of 0.2 US$/kWh (0.27 S$/kWh) in 2015.

Clustering

Before applying the k-means algorithm, the initial region is divided into subregions each having a maximum number of nodes between 500 and 15 000. This parameter effects the number of initially planned areas, the placement of their substation, and the way PQ buses are connected to the substation as described in Sections 2.2.2 to 2.2.4. The more nodes a subregion contains the better the k-means algorithm can determine clusters of equal size. Regardless of the number of initially planned areas, the network recombination step described in Section 2.2.5 consolidates areas to a user-defined number of areas or a minimal value. This process achieves cost-minimal results if the number of nodes per subregion is set at least to 2 500. Values smaller than this number yield worse results, higher values do not minimize costs any further but instead only increase runtime. Overall, the minimal number of areas differ by 0.8 % depending on the value of this parameter.

The implemented k-means algorithm is an iterative algorithm which stops either after a predefined number of iterations has been reached or no more changes from one iteration to another are realized. The maximum number of iterations effects the initial allocation of PQ buses to areas. The investigated value range is between 2 and 48. As with the bisecting, cost-minimal results in the network recombination step are achieved if the maximum number of iterations is set at least to 16. Smaller values yield worse results, higher values do not further decrease costs. The total variation in the number of substations is with 0.2 % negligibly low.

The DBSCAN algorithm generates clusters of nodes in an area based on a maximum allowed distance between two nodes. Setting this distance to 0 treats each PQ bus as a separate cluster resulting in only planning direct connections between PQ buses and the PV bus. The targeted topology only becomes visible with values larger than 0. Increasing this value therefore results in clusters containing more nodes up to a level where only one cluster is formed in case the distance value is set to the maximum distance between two nodes of this area. The investigated value range is marked by those two borders. The maximum distance parameter directly influences the number of independent parts and thereby the number of nodes per independent part. Avoiding unnecessary laying of branches the number of independent parts should be as low as possible, the number of nodes per independent part as high as possible. This results in an ideal value of twice the average distance between any PQ bus and its connected PV bus. Values larger than this value have only a negligibly low influence on the resulting PNM. Although they produce clusters containing more nodes, those clusters are being split due to violating feasibility criteria preventing a lower number of independent parts or larger sized ones. Values smaller than twice the average distance produce more clusters with a lower average number of independents parts per cluster.

Maximum Utilization of Substations and Power Lines

The maximum power substations can provide depends on their cooling. Assuming a proper implementation, their nominal rating can therefore be exceeded for a limited time period considering their lower efficiency in a higher operating range. Investigated values for the maximum utilization are between 80 % and 150 %. Allowing for higher overloading, less

substations are required resulting in a longer total power line length, more independent parts, less nodes per part, and finally less costs. A 10 % increase in the maximum allowed utilization of all substations results in 0.2 % less substations being required for the LV grid and and 1.5 % for the MV grid. This comes along with the total power line length to be 0.4 % higher and increased power losses of 2.6 %.

Power lines cannot be overloaded as no active cooling mechanism is applied to underground cables. Investigated values for the maximum utilization are therefore between 80 % and 100%. Allowing for a higher utilization does not have a significant direct impact on any of the metrics besides the minimum number of substations. The optimization potential is increased by 0.5 % for every 1 % increase in the maximum utilization. While this correlation is valid for the LV grid, the MV grid does not offer an increased optimization potential. Decreasing the number of substations is already limited by their maximum power.

Mean Degree of the HV Grid

Other than the implemented radial and ring topology of the LV and MV grid, the meshed topology of the HV grid is explicitly designed to exhibit redundancies. Besides the clustering coefficient, the node degree can serve as a simple measure for the redundancy in a network. Changing the number of edges while at the same time keeping the number of nodes without inducing islanding in the network results in a different mean degree which is increasing with the number of edges. Investigated values for the node degree range from 2 to 4.5 which reflect the value range available for real-world power systems. PNMs generated by CityMoS Power behave as expected in all presented metrics. A higher mean degree yields increasing edge lengths as well as higher values for the clustering coefficient, density, and costs. Values for the average path lengths, betweenness, and diameter are decreasing as well as the one for occurring power losses. Although with a lower mean degree the costs for the entire PNM also decrease by approximately 8 % reducing the mean degree by 1, there is no optimal value for the target mean degree of the HV grid. It, instead, reflects a design choice offering the user the possibility to customize the HV grid.

Power Factor

The power factor is the ratio between active and apparent power and implicitly denotes the amount of reactive power which must be provided but which cannot be used to perform work [33, pp. 57]. An ideal power system has a power factor of 1 only providing active power whereas a value of 0.9 is given for Singapore. Investigated values range from 0.8 to 1. The higher the power factor the less reactive power is provided requiring less substations. An increase of the power factor by 1 % results in an average decrease of the reactive power supply by 0.1 % equivalent to 24 MVar while at the same time planning 0.3 % less substations. Power losses are thereby decreased by 0.5 %.

Power Line Quality Factor

Power cables installed in Singapore follow the specifications provided in Table 4.2 which translates to a power line quality factor of 1. Lower factors result in power cables with higher resistance values but lower costs and vice versa. Reactance values are independent of the quality according to the specification of different power cables [200–202]. By scaling the power cable specification with values between 0.5 and 2 at a step size of 0.1, scenarios are investigated where power cables of lower and higher quality are installed. Assuming power cables with a quality 50 % lower than the default, 70 % more substations are required in the LV grid. They have to be connected with 20 % shorter cables resulting in a variation of around 5 % in the total power line length of the entire PNM. This comes along with increased power losses, an increased number of independent parts, and a decreased number of nodes per independent part. With more substations being required, the utilization of each substation is also lower. Higher quality cables show just opposite results. Increasing the quality factor to 2 results in 47 % less required substations in the LV grid. They can be connected by power cables which are in average 25 % longer. The total power line length of the entire PNM is around 7 % higher while power losses are decreased by around 21 %. The power line quality factor is beneficial in case the exact power line specification for the investigated region is not available by applying generic specifications and scaling them to targeted resulting values.

Power Line Stretch Factor

The power line stretch factor virtually extends the length of the power lines to account for non-beeline paths in reality while at the same time realistically considering electrical and economic properties in a generated PNM. Possible values strongly depend on the available data, especially on the number of consumers and GIS information on the branching depth. Based on the data described in Section 4.2.1.1, investigated values range from 3 to 3.3 in the LV grid and from 2.1 to 2.6 in the MV grid while having the HV grid always set to 1.5. The different values are combined to generate PNMs of the target total power line length of 26 500 km while at the same time allow for a higher branching depth in the LV than in the MV grid. The stretch factor has a direct influence on the network recombination potential. The lower the stretch factor, the shorter power lines are. Shorter power line lengths result in more independent parts with less direct connections, a higher average number of nodes per independent part, as well as shorter geographical average path lengths, average distance, and diameter. Additionally, the maximum power flow on each line is increased thereby reducing the required number of substations when recombining areas. It is found that stretch factors have to be set to 3.1 (LV) and 2.4 (MV) to achieve realistic values for the total power line length and power losses in the Singapore PNM.

Topology

Depending on the voltage level, real-world power grids exhibit different topologies, with radial, ring, and meshed networks being most common. While LV and MV grids are planned using a radial or ring topology, meshed networks can be found in HV grids. Investigated topologies are

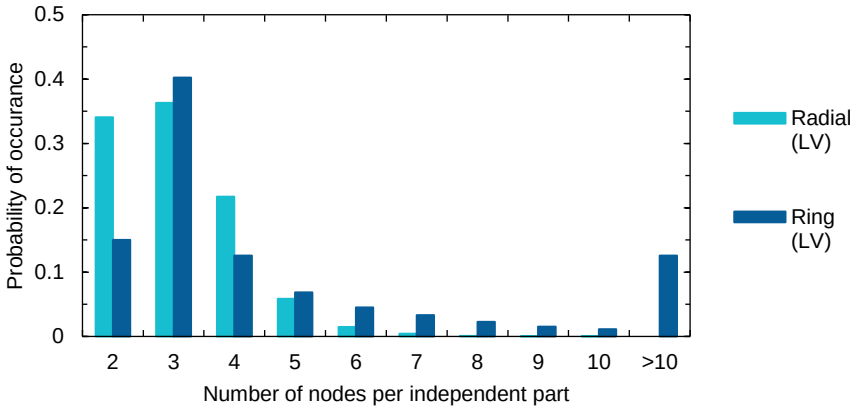

Figure 4.7: Number of nodes per independent part in the LV grid depending on the applied topology.

radial and ring being interchanged in any combination in the LV and MV grid. The applied topology influences almost all metrics. A ring topology varies from a radial one in the way that although the minimum number of possibly planned substations is equal, more power lines are planned which are shorter on average and in total. The number of independent parts is only half the number as for radial networks while each part on average consists of twice the number of nodes. The histogram of the bin size with respect to the number of nodes per independent part shown in Figure 4.7 confirms the latter observation considering the ring and radial topology in the LV grid. Both differences together result in a smaller maximum node degree for substations and a lower betweenness. While there is no redundancy in an LV grid's radial topology, around 40 % of the independent parts are composed of three nodes in an LV grid's ring topology. This results in a clustering coefficient of 0.19 compared to 0 in a radial topology and a higher mean node degree of 2.17 compared to 1.84. Planning the LV grid either with a ring or a radial topology has almost no influence on the total costs although power losses are marginally higher and the average voltage at the consumers is 0.01 pu lower.

4.2.4 Discussion

PNMs are helpful as means for investigating the impact of new types of power system participants. Both a temporal or spatial shift or increase in the power demand of a real-world power system can this way be analyzed before becoming reality. CityMoS Power is able to derive PNMs that realistically emulate the actual power system infrastructure. Those PNMs can be evaluated based on defined metrics for which reference values of real-world power systems are provided. The evaluation is thereby part of the process of generating PNMs tailored to individual requirements. In Section 2.6, several limitations of the PSS framework which is implemented in CityMoS Power and used in this case study have been discussed. They are based on findings resulting from the development of the methodology only. In this section, the discussion is refined, this time considering the findings from the application of the methodology on the example of Singapore.

The design goal of the PSS framework serves as a proof-of-concept that despite its limitations PNMs can be generated by the methodology which are able to satisfy the current power demand specified in the consumer input data and at the same time show aggregated topological, electrical, and economic properties of real-world power systems. This goal has been achieved. Results of this case study indeed demonstrate the methodology's feasibility of processing data available for Singapore to generate realistic PNMs for this region. Realistic in this context refers to matching the defined metrics only without requiring for an exact replica of the target's power system. The framework's limitation of emulating the evolution of real-world power systems while also neglecting placement constraints and inhomogeneities among electrical installations of the same voltage level can be ascribed to a lack of available data. Assessing the importance of those three limitations requires answering the following question:

How realistic are PNMs generated with limited input data?

In general, PNMs are more realistic the more input data is used in the generation process. But whether a PNM is considered realistic or not depends on its purpose. This purpose may not require an exact copy of a real-world power system in all aspects. Instead, specific parts of the system may be modeled in greater detail than others without losing explanatory power when using such a PNM. Calculating power losses, for instance, only requires a power line's length not its exact routing path. While such a model is geographically not very realistic it is exact with respect to its purpose. A sound evaluation of results should thereby always consider its environment: the data, algorithms, and assumptions used to generate a specific PNM. Disrespecting, for instance, specific input data must not allow drawing conclusions from results which would require this data set. This also applies to the results presented in this case study. They should never be taken as-is but always under the presumptions of the input data described in Section 4.2.1. With regard to the framework's above-mentioned limitations the following conclusions can be drawn:

- **Evolution of power systems**

  The set of input data is incomplete and originates from various sources with a slight temporal difference. While data on the number of substations and the total power line length is officially published and hence assumed to be correct, sources for the number and geographical distribution of consumers do not guarantee completeness. This uncertainty also applies to the power demand distribution on each single consumer which has been distinctly averaged on the basis of their belonging to a sector. Due to unavailability, any data about the power system's historical evolution is entirely disregarded.

- **Placement constraints**

  Geographic or environmental constraints are not explicitly considered when placing substations or laying power lines. The exact locations of the PNM's electrical installations are therefore inaccurate compared to their real-world counterparts. Using the location of consumers as input data and applying economically feasible assumptions when placing those installations only approximate realistic locations of substations. Beeline branch

laying results in an unrealistic geography of power lines. Stretch factors accounting for correct line length, however, ensure matching topological and electrical properties.

- **Inhomogeneities of electrical installations**

  Specifications on electrical installations as, for instance, the nominal power rating of substations, their maximum utilization, or the quality of power lines are not distinguished within a voltage level. This results in all substations on the same voltage level providing the same maximum power while all power lines have an equal nominal power rating. For Singapore, a more inhomogeneous and diverging distribution should be applied which was also confirmed by *SP Power*, the energy utility company in Singapore [214], providing excerpts of small parts of the power system. Although the assumed averaging matches the averaging done on the consumer's power demand distribution, temporal or spatial grid congestion may not be realistically identified producing inaccurate results regarding the utilization of electrical installations.

Considering those limitations, PNMs generated by CityMoS Power indeed abstract some parts of real-world power systems to handle unavailability of data while at the same time focus on ensuring matching topological and electrical metrics. Although those PNMs are able to satisfy the power demand of the consumers as specified in the input data, their real-world counterpart can be structurally quite different. Drawing conclusions is thus limited to the investigated PNM. Regarding a PNM's real-world counterpart, assumed abstractions should result in avoiding clear statements of the quality *there IS a problem* but instead allows only indications such as *there MAY BE a problem which needs further investigation.* Moreover, excluding occurrences of other problems which have not been identified using a PNM is also not permitted.

Reaching sound conclusions with respect to the implications for a real-world power system based on findings applying a PNM requires considering the input data, assumptions, and algorithms used for generating the PNM. With respect to the presented metrics, PNMs generated by CityMoS Power are realistic and quite closely match their real-world counterparts. The comprehensive parametrization thereby enables tailoring PNMs to individual requirements allowing to handle different levels of completeness of the input data. Considering the utilization of substations and power lines, abstractions in the PNM especially regarding the homogeneous specification of electrical installations prevent drawing clear conclusions for the PNM's real-world counterpart. Instead, a more detailed investigation of the utilization is required and done in the context of the second case study investigating the power system impact of different road transportation electrification scenarios presented in the following Section 4.3.

4.2.5 Conclusions

In this study, the applicability of the PSS framework presented in Chapter 2 for generating realistic PNMs is investigated. The study is designed to demonstrate that despite the framework's main limitations discussed in Section 4.2.4, PNMs showing topological and electrical properties of real-world power systems can be generated. This is done on the example of Singapore by generating PNMs based on the available data on the power system of that region.

The framework's PSP process is multi-purposely parametrized; thus, many different PNMs are generated and evaluated to explore the impact of the different parameters and parameter uncertainty. In the end, a parameter set is identified that allows generating a PNM best accommodating the available input data and best matching real-world power system properties, the Singapore PNM.

This Singapore PNM combines all available data of the real Singapore power system including the number, location, and specification of substations, power stations, power lines, and consumers on the different voltage levels with those generated by the framework's PSP process. Thus, a PNM is generated most realistically emulating the power system infrastructure of Singapore with respect to values available for the defined properties. Structurally, the real power system of Singapore can, however, be quite different due to a lack of available input data some of the framework's limitations are based on. This apparent contradiction in considering a PNM realistic or not is dissolved scrutinizing its purpose. Drawing conclusions on the power system of Singapore based on the Singapore PNM can therefore not simply be taken for granted. Instead, thorough consideration of the input data used for generating the PNM are required for each specific use case whether they in principle allow drawing a conclusion or not.

4.3 Case Study 2: Investigating the Power System Impact of Different Road Transportation Electrification Scenarios

The case study presented in this section is designed to finally answer this work's research question formulated in Section 1.1. As anticipated in the proposed solution statement, a simulation platform is applied to provide insights into the different aspects of power system impact when implementing road transportation electrification on a large scale. In this case study, all previous findings of this work are combined. The PSP approach presented in Section 2.2 is applied to generate a PNM of Singapore as described in the previous case study in Section 4.2. On this PNM power flow simulations are conducted as described in Section 2.3 using the scheduling strategy presented in Section 2.4 among others. Those power flow simulations are not only based on the load curve of the region but also include the additional power demand induced by PEV populations of different sizes. The former is termed *regular demand* in the context of this study while the latter is referred to as the *additional demand*. Superposing both demands results in the *aggregated demand*. Using the simulation platform presented in Chapter 3, the agent-based transportation system simulation described in Section 3.4 is able to interact with the power system simulation described in Section 3.3 over the simulation coupling standard explained in Section 3.2.

In Section 4.3.1, the input data required for the charging infrastructure, the scheduling algorithm, and the transportation system simulation is described. This data is then used to generate and run a federation execution involving the power and transportation system simulation with a default parameter set. Results especially with respect to the PNM's generation capacities as well as substation and power line utilization are presented in Section 4.3.2. In Section 4.3.3, a sensitivity analysis of the different parameters is conducted and its findings

are presented. Limitations of the case study's setup are discussed in Section 4.3.4, along with a presentation of related power system impact studies. Section 4.3.5 concludes this case study.

4.3.1 Input Data

Investigating the impact of large-scale road transportation electrification on a power system requires both a PNM of the power system under investigation and an agent-based transportation system simulation used to generate the additional power demand induced by the PEVs. As PNM, the Singapore PNM generated in the context of the previous case study presented in Section 4.2 is used. Different scheduling strategies, the placement of CSs, and their power connections are described in Section 4.3.1.1. The scheduling strategy presented as part of the PSS framework in Section 2.4 requires parametrization. The default parameter set as well as the definition of input electricity prices are provided in Section 4.3.1.2. The transportation system simulation is used to generate and simulate the itineraries of a PEV population with trip characteristics as presented in Section 4.3.1.3.

4.3.1.1 Charging Stations

Charging/discharging of PEVs takes place at residential or public electrical installations, each equipped with a number of power connections serving one to many PEVs at the same time. An installation which is able to do both supplying energy to exactly one PEV charging its battery and accepting feedback of energy from the same PEV discharging its battery is termed *charging station* (CS) in this study. The most relevant characteristic of a CS is the maximum power it is limited to. Typical power connections which are used in this case study are defined in Table 4.7.

Table 4.7: Typical power connections for PEV charging/discharging.

Power [kW]	Voltage [V]	Max. current [A]	Type	Charging/discharging time for 20 kWh [a)]
3.6	230	16	AC (single phase)	5.5 h
7.2	230	32	AC (single phase)	2.8 h
11	400	16	AC (three phases)	1.8 h
22	400	32	AC (three phases)	1 h
43	400	63	AC (three phases)	30 min
120	400	300	DC	10 min

[a)] Charging/discharging times are calculated using the *constant current* scheme only. Realistically applying the the *constant voltage* scheme at an *SOC* above 80 % extends this duration by a factor depending on the specific battery [5].

Besides the maximum power a CS can supply or accept, the temporal distribution of the power values at all times during a stop is an influencing factor when assessing the power system impact. The following *scheduling strategies* are therefore investigated:

- **Dumb charging**

  Immediately charging a battery once it is connected to a CS is termed *dumb charging* in the remainder of this work. No information regarding the charging duration is required allowing to charge the battery as fast as possible. Battery aging costs and the impact on the power system are thereby neglected. Besides, the possibility to exploit variable electricity prices is spared.

- **Mean charging**

  With the *mean charging* strategy a battery is evenly charged with the same power over the entire charging period. This strategy requires knowledge of the charging duration and the battery's target *SOC* previous to the beginning of charging. Battery aging costs or the impact on the power grid are as little considered as variable electricity prices.

- **Price-responsive charging**

  The scheduling approach presented in Section 2.4 implements a *price-responsive charging* strategy by adjusting charging power based on temporally resolved price data to minimize charging costs. Besides electricity prices, this strategy again requires knowledge of the charging duration and the battery's target *SOC* previous to the beginning of charging to yield optimal results. Battery aging costs are inherently considered by the optimization algorithm resulting in a cost-minimal charging schedule. To reduce negative impact on the power system's load curve, prices reflecting the system's state have to be defined to allow for lower prices in case of power excess and higher prices in the opposite case. When there are multiple periods with an equal cost-minimization potential, the power demand is equally distributed over all periods equivalent to the mean charging strategy. This is only possible because calendar aging is not considered in the implemented battery model. Otherwise, at each period the *SOC* would have an additional influence on the temporal charging decision as described in [35].

- **Price-responsive charging/discharging**

  Besides price-responsive charging the scheduling approach presented in Section 2.4 also provides the possibility for discharging. This strategy is termed *price-responsive charging/discharging*. The same requirements regarding knowledge of electricity prices, the charging/discharging duration, and the battery's target *SOC* previous to the beginning of charging/discharging apply. As with the price-responsive charging strategy, this strategy can prevent increasing peaks in the regular demand. To some extent it additionally may even decrease those peaks at some points in time at the cost of a demand increase at others.

In the Singapore PNM, there are 117 852 different locations where CSs can be placed, each one in principle allowing for a different maximum power. The proper placement strategy along with the determination of the maximum power is a research area of its own and is discussed on a high level in Section 4.3.4.3. In this study, CSs are installed at all locations. The number of the installed stations at a location equals the maximum number of simultaneously charging/discharging PEVs at this location. This way each PEV can connect to a CS whenever its itinerary allows doing so. Initially, each location is equally equipped with a fast CS supplying

a maximum power of 120 kW. Other power connections defined in Table 4.7 are investigated in the context of the sensitivity analysis in Section 4.3.3.

4.3.1.2 Scheduling of Battery Energy Storage

The scheduling approach for battery energy storage is applied for both demand-responsive charging and energy back-feeding. The dynamic programming algorithm computes a globally optimal solution sufficiently fast for real-time operation of a single PEV. Computing optimal charging/discharging schedules for a PEV population of an entire city, however, requires decreasing computational complexity. Prices are therefore considered ex post and are thus not updated once made available. This way continuous re-calculation after each period of time using the rolling horizon approach can be avoided. Instead, the rolling horizon approach is applied for each stop thereby calculating the profit-maximizing charging/discharging schedule for the entire lookahead horizon while only taking the time periods until the next trip start into account. Further parameters include the duration of a time period for which prices and charging/discharging power are fixed to 15 minutes, a lookahead of 24 hours, a battery capacity of 20 kWh with an initial SOC of 1 and an SOC discretization of 1 %, as well as equal charging and discharging efficiency each of 0.89. In case of demand-responsive charging the minimum power is set to 0 kW, disallowing energy back-feeding. Dropping this restriction and thereby additionally allowing for demand-responsive discharging, the minimum power is set to the negative maximum power of the connected station.

For the price-responsive scheduling strategies electricity prices are set to follow the temporal power demand distribution meaning they have their minimum at the time of the absolute demand valley while the maximum price is only valid for the time period of peak demand. Prices are not calculated only once but instead they are continuously re-calculated after the sequential processing of each trip. Calculations are based on the aggregation of the regular and the additional power demand of the already scheduled agents including the last one but leaving out trips which have not yet been scheduled. This way, the absolute daily demand valley is continuously shifted in time whenever a trip is scheduled allowing for evenly filling the load area around the valley instead of creating a new peak at that very time. Electricity prices are calculated according to

$$p(t) = \left(1 - \frac{P_{\mathrm{D,max}} - P_{\mathrm{D}}(t)}{P_{\mathrm{D,max}} - P_{\mathrm{D,min}}}\right) \cdot (p_{\max} - p_{\min}) + p_{\min} \tag{4.2}$$

having a minimum power demand $P_{\mathrm{D,min}}$ of 4 433 MW, a maximum power demand $P_{\mathrm{D,max}}$ of 6 340 MW, a minimum price $p_{\min}$ of 0.135 S$/kWh[2], and a maximum price $p_{\max}$ of 0.359 S$/kWh. $P_{\mathrm{D,min}}$ and $P_{\mathrm{D,max}}$ result from Figure 4.2, $p_{\min}$ is arbitrarily set to half the consumer *electricity tariff* of Singapore on the day on which the power demand used for planning the Singapore PNM occurred, and $p_{\max}$ is set to the value for which the average of all electricity prices equals the consumer electricity tariff of Singapore of 0.27 S$/kWh. The impact of price variations are discussed in Section 4.3.3. The remuneration for providing energy to the grid equals the electricity price. This way, at times of high power demand, the electricity price is

[2] S$ 1 equals 0.69 US$ (19th December 2016).

high, preventing the PEV to charge, while at the same time the remuneration is also high, incentivizing providing energy to the grid.

4.3.1.3 Transportation System Data

CityMoS Traffic as described in Section 3.4 is used to simulate an agent population over the course of one day. Each agent represents a PEV which starts with a fully charged battery. Limited input data regarding the location or the timing of traffic lights prevents simulating a population size of more than 20 000 agents much less the 540 000 private cars available in Singapore [132]. With an increasing number of agents the transportation system would rapidly become jammed. To still be able to investigate scenarios with a larger vehicle population the following process is applied to the aggregated output resulting from simulating 20 000 agents over the course of one day as described in Section 3.4.2:

1. Each agent including its itinerary is duplicated n times resulting in the desired number of agents.
2. Each trip is randomly modified with respect to the following parameters:
   a) The location where a trip starts and ends is varied within a radius of 1 km of the original location resulting in a different trip length.
   b) The starting time of a trip is uniformly shifted by any value up to ±30 minutes.
   c) The duration and energy demand of a trip are both linearly scaled to the new trip length.

The described process is applied to generate populations of 100 000, 300 000, and 500 000 agents, all with the same characteristics presented in Table 4.8. The extrapolated data thereby reflects the characteristics of the data generated by simulating 20 000 agents with CityMoS Traffic. Limitations coming along with applying this abovementioned process in contrast to directly simulating the transportation system with a larger number of PEVs are discussed in Section 4.3.4.1. While for 20 000 agents only 28 % of the total number of all 117 853 possible locations is covered by the generated trips, 72 %, 94 %, and 98 %, respectively, are covered for the three extrapolated agent populations.

Table 4.8: Trip characteristics.

Characteristic	Value
#Trips per agent	2.15
Trip duration, average [min]	14.07
Trip length, average [km]	10.9
Energy demand, driving per 100 km [kWh]	13.16
Additional constant power demand, aircon [kW]	0.9

To realistically assess the power system impact, a steady state of the transportation system has to be reached. With CityMoS Traffic trips can only be generated and simulated for the course of one day. This would result in inaccuracies determining the temporal power

demand at the beginning and end of the day. In the first couple of hours of a day, no charging/discharging events originating from trips of the previous day would be scheduled although they may span this time period. The same would apply to the the last couple of hours of a day. Charging/discharging events would be scheduled to be finished by the end of the day instead of the lookahead. The power demand at this time period would therefore be unrealistically high. To avoid those inaccuracies, a warm-up and cool-down phase is therefore added by concatenating the generated trips simulated by CityMoS Traffic three times. This way each agent's itinerary spans over three days performing the same trips every day. Charging/discharging events are scheduled for the entire three days. When investigating the impact of the charging/discharging events on the power system only the second day is examined.

4.3.2 Results

Calculating the charging/discharging schedule for 500 000 agents takes place within 8 seconds using the dumb charging strategy and around 3 minutes for the mean charging strategy on the previously mentioned Intel Core i5-2520M using 12 GB RAM. Both price-responsive scheduling strategies are computationally highly expensive even if scheduling is done as described in Section 4.3.1.2. Parallel calculation would take about 1 year on the specified processor and still about 50 days on the 14 available Intel Xeon E5-2670 cores. A sensitivity analysis would this way quickly become infeasible. In the context of the findings presented in this section, 100 000 agents are scheduled for both strategies and results are scaled to the target population size. The scaling does not have a significant impact on the results when investigating the total aggregated power or energy demand as described in Section 4.3.2.1. It, however, distorts results finding grid congestion especially at lower voltage levels as described in Sections 4.3.2.2 and 4.3.2.3. This inaccuracy of using only parts of the total number of possible locations when scaling up results instead of directly using a larger population size is discussed in Section 4.3.4.1.

4.3.2.1 Generation Capacities

The temporally resolved total power demand of 500 000 PEVs and thereby the overall impact of road transportation electrification with regard to existing generation capacities is illustrated in Figure 4.8. Depending on the scheduling strategy the additional daily power and energy demand are summarized in Table 4.9 and explained in the following:

- **Dumb charging (Figure 4.8a)**

  Whenever a PEV stops at a CS, an additional power demand is induced to fully charge the battery as fast as possible. This power demand is not tied to any peaks or valleys in the regular load curve but only depends on the itineraries of the PEVs. This way, an aggregated demand peak is formed which is 104 MW higher than the regular demand peak while valleys remain largely unused. The maximum additional daily power demand is 282 MW of which 139 MW remain unsatisfied affecting 2 074 or 1.8 % of the used

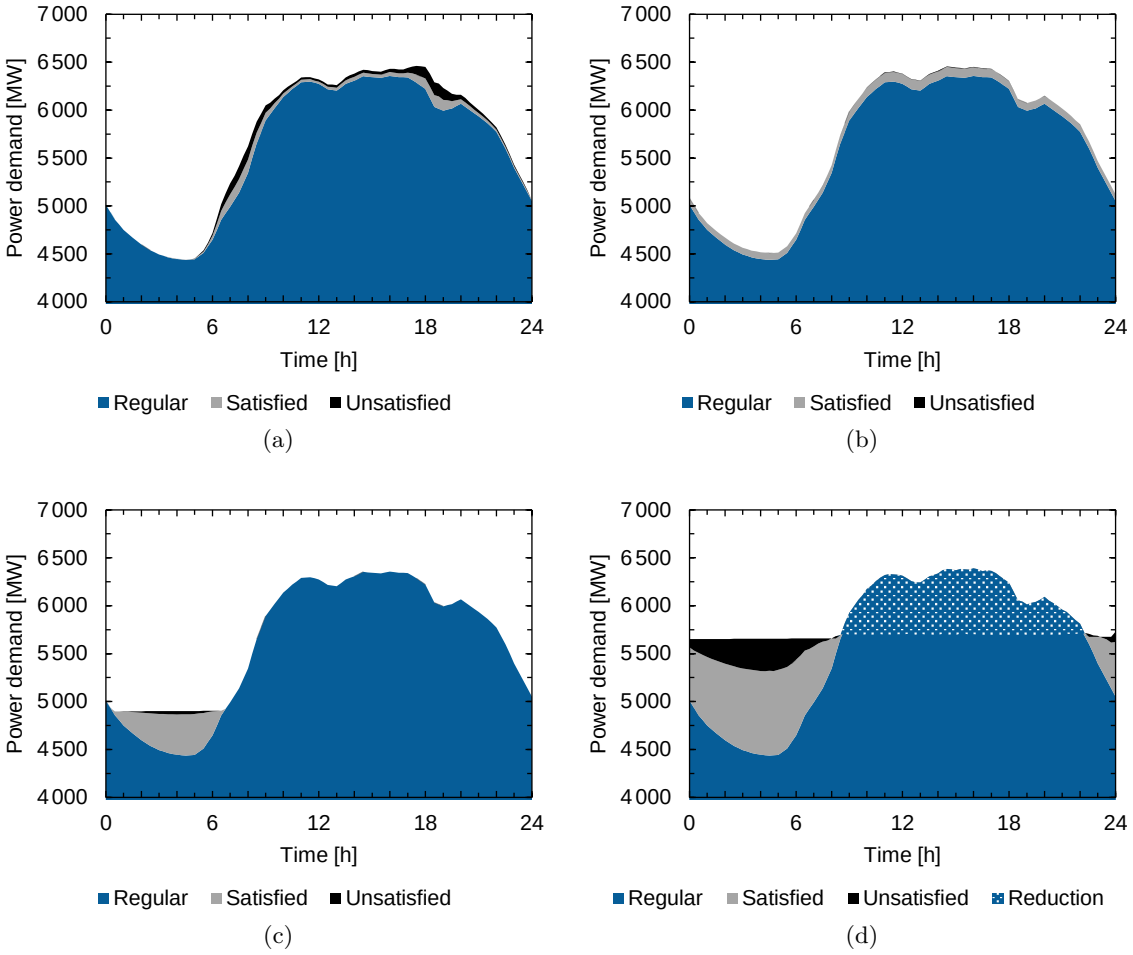

Figure 4.8: Regular load curve including the additional power demand induced by 500 000 PEVs using the (a) dumb, (b) mean, (c) price-responsive charging, and (d) price-responsive charging/discharging strategy. The power demand which cannot be satisfied due to reasons of limited substation or power line capacities is separately shown in black.

115 663 locations. The additional total daily energy demand which cannot be satisfied is 981 MWh and thereby conforms to about half of the total demand[3].

- **Mean charging (Figure 4.8b)**

  The additional power demand induced by each PEV is distributed over its stop's duration. Due to the large number of PEVs the additional power demand of the entire

[3] The additional daily energy demand induced by 500 000 PEVs is 1 978 MWh and is calculated applying the values provided in Table 4.8 as

$$\frac{\text{Total trip length [km]} \cdot \text{Energy demand/km} + \text{Total trip duration [h]} \cdot \text{Energy demand/hour (aircon)}}{\text{Charging efficiency}}$$

Table 4.9: Additional daily power and energy demand induced by 500 000 PEVs from the perspective of the power grid. The demand depends on the applied scheduling strategy.

Scheduling strategy	Additional power demand [MW]			Aggregated peak power demand [MW]	Additional energy demand, unsat. [MWh]	Affected locations [%]
	Min.	Max.	Unsat.			
Dumb charging	0	282	139	6 444	981	1.8
Mean charging	68	106	4	6 442	41	2.4
Pr.-resp. charging	0	464	35	6 340	119	4.7
Pr.-resp. ch./dis.	1 216	-688	417	5 652	–	–

PEV population is temporally evenly distributed. This way, generation capacities are additionally almost equally stressed throughout the day. The aggregated peak power demand is 6 442 MW which is an increase of 102 MW compared to the regular demand peak. The maximum additional power demand is 106 MW of which only 4 MW remain unsatisfied. Due to substation or power line limitations, a total of 2 781 and thus 2.4 % of all used locations are affected by a forced reduction in power demand which is assumed in the power flow model as described in Section 2.3.2.2. The additional total daily unsatisfied energy demand is as low as 41 MWh.

- **Price-responsive charging (Figure 4.8c)**

  The target of scheduling the PEVs' batteries with the price-responsive charging strategy differs from the two previous strategies. While using dumb charging the PEV has to be fully charged as fast as possible; mean charging targets a full battery at the end of each stop. Using price-responsive charging the battery has to be fully charged within the lookahead while at the same time guaranteeing a sufficient charge for conducting each trip. This allows choosing the least cost time periods for charging within the lookahead. By defining prices reflecting the current load, peaks are not further increased but instead charging happens at demand valleys only. The maximum additional power demand is 464 MW of which 35 MW remain unsatisfied. A total of 4.7 % of all used locations[4] are affected by the applied reduction of their power demand. The additional total daily energy demand which is left unsatisfied is 119 MWh.

- **Price-responsive charging/discharging (Figure 4.8d)**

  Again, the target of this scheduling strategy has shifted compared to other strategies. While it is still the goal to fully charge the battery within the lookahead by using least cost time periods, discharging the battery to provide energy to the grid is allowed. This way, demand valleys are not only used for charging the battery but also demand

[4] As explained in Section 4.3.2, only 100 000 agents are scheduled for the price-responsive charging strategy. The power demand of each agent is thereby scaled by a factor of 5 to emulate a scenario with 500 000 PEVs. This results in each of the 84 383 locations having to satisfy a higher power demand than in the case of directly scheduling 500 000 PEVs. A load reduction is therefore more likely making the ratio of affected locations using this strategy not comparable with the ratio involving 500 000 agents.

peaks are used for discharging. This allows reducing daily peak demands by more than 10 % (indicated by the blue-white dotted area in Figure 4.8d). Using this strategy, the load curve can be totally flattened showing a constant temporal aggregated power demand of 5 652 MW throughout the day. The total and unsatisfied additional daily energy demand are distorted due to additional charging/discharging cycles targeting the flattening of the daily power demand. Each of those cycles additionally incur power losses resulting in a further energy demand matching the batteries' charging/discharging efficiency. Respective numbers are not separable into the demand resulting from driving and the one from simply shifting power. They are therefore incomparable with those of previous scheduling strategies which is why they are not provided in Table 4.9.

The price-responsive charging/discharging strategy was implemented as a proof-of-concept that applying a matching strategy a total load curve flattening effect can be achieved only by varying electricity prices and remunerations while still considering battery depreciation. Remunerations as assumed in this study correlate to the electricity prices and are therefore unrealistically high. By implementing current prices for providing energy to the grid, this scheduling strategy would only marginally differ from the price-responsive charging strategy. It is the costs arising through battery depreciation and the auxiliary demand caused by conversion losses that currently restrict an economically feasible application of this strategy to mainly providing *ancillary services* [215] and only in exceptional cases for *peak shaving* as described in [15]. Although it is beneficial to provide a total load curve flattening effect, the price-responsive charging/discharging strategy is therefore not further considered in the remainder of this study. In this work, the focus is put to the price-responsive charging strategy with its positive load curve valley filling effect.

Both power and energy demand need to be considered when investigating the impact on generation capacities. From the perspective of power generation capacities necessary to compensate the higher peak power demand, the increased requirement is with 1.6 % rather moderate when applying the dumb or mean charging strategy, especially when considering current spare capacities of around 47 %. Using any of the price-responsive scheduling strategies, there is no additional power demand which further increases the maximum power supply. Regardless of the applied strategy, the additional daily energy demand induced by 500 000 PEVs is about 2 GWh which is as little as 1.5 % of the regular daily demand. Some fraction of this demand depending on the strategy can, however, not be satisfied. Although only small parts of the PNM are affected, detailed investigation on the substation and power line utilization, especially in those parts, is required and provided in the following Sections 4.3.2.2 and 4.3.2.3.

4.3.2.2 Substation Utilization

Road transportation electrification at first affects the part of the power system where the CSs are connected to. Although in the Singapore PNM 98.8 % of all locations are connected to the LV grid leaving the remaining 1.2 % to the MV grid, the entire additional demand applies to the LV grid as all CSs are connected to this part. Any additional power demand in the LV grid which can be satisfied by the directly connected substations and power lines also has to be satisfied by the electrical installations at higher voltage levels. Power demand which cannot

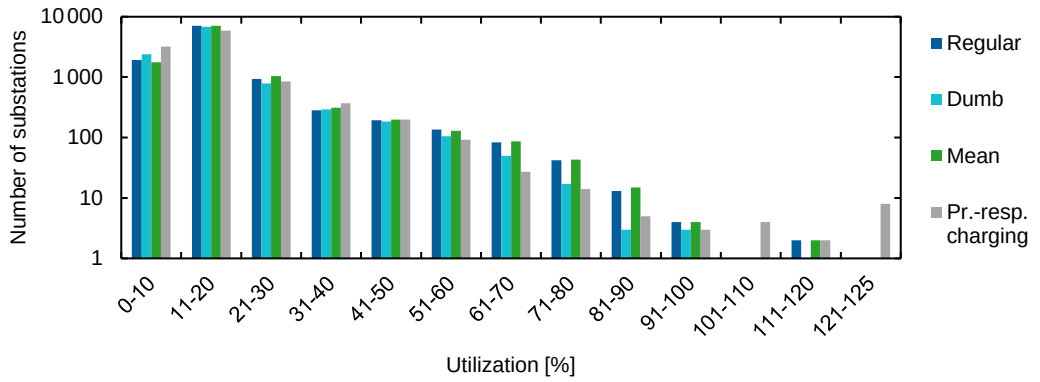

(a)

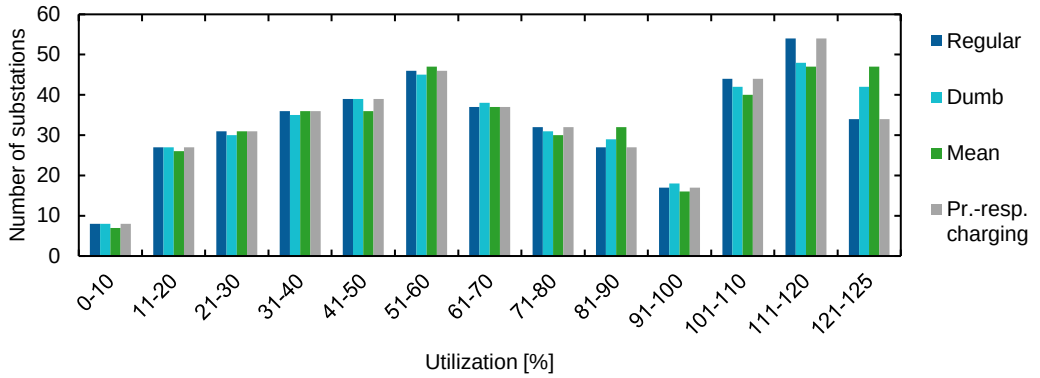

(b)

Figure 4.9: Distribution of the substation utilization based on the aggregated power demand in the (a) LV and (b) MV grid using different scheduling strategies, each at the time of their additional peak demand.

be satisfied at the same voltage level is curtailed. The power excess is therefore not applicable to be served by installations at higher levels as described in Section 2.3.2.2. The maximum additional power demand induced by PEV charging and its time of occurrence depends on the scheduling strategy and is provided in Table 4.9. For the time periods exhibiting this maximum demand, the distribution of the substation utilization using different scheduling strategies is illustrated in Figure 4.9. In the following, the LV and MV grid are separately investigated:

- **LV grid**

  The distribution of the substation utilization for the LV grid is shown in Figure 4.9a. Deviations between both scenarios with and without PEVs are rather small resulting in a temporal substation utilization not significantly different from the one illustrated in Figure 4.5a. With an average demand increase of about 26 kW (dumb charging),

10 kW (mean charging), and 43 kW (price-responsive charging) at every substation, those small deviations are as expected. There are, however, also almost no changes in the number of substations having a utilization larger than 120 % except for the price-responsive charging strategy. Both for the dumb and mean charging strategy this number remains 0 whereas for the price-responsive charging strategy it increases to eight. Given the ample unused substation capacities, the unsatisfied power demand of 139 MW (dumb charging), 4 MW (mean charging), and 35 MW (price-responsive charging) cannot be explained with a restriction related to substations. Instead, the unsatisfied demand indicates a power line limitation in the LV grid which is investigated in the following Section 4.3.2.3.

- **MV grid**

  The distribution of the substation utilization for the MV grid is shown in Figure 4.9b. Deviations between both scenarios with and without PEVs applying different scheduling strategies are again rather small showing a similar temporal substation utilization than the one illustrated in Figure 4.5a. In the MV grid, as opposed to the LV grid, the number of substations which are utilized at or close to their maximum capacity increases from around 8 % (regular demand) to 10 % (dumb charging) and 11 % (mean charging), respectively, while not changing applying the price-responsive charging strategy. Showing an unsatisfied power demand of 3 MW (dumb charging) and 4 MW (mean charging) while having all demand satisfied applying the price-responsive charging strategy, this indicates substations to at least partly restrict a power demand increase. In the following Section 4.3.2.3, a possible impact of power lines on this limitation is investigated.

Further increasing the additional demand is restricted by limited power line capacities in the LV grid while in the MV grid substation capacities are the limiting factor. This conclusion based on the findings of investigating the substation utilization of the aggregated power demand is further substantiated by analyzing the power line utilization in the following Section 4.3.2.3.

4.3.2.3 Power Line Utilization

As concluded in the previous Section 4.3.2.2, the unsatisfied power demand especially in the LV grid indicates a power line restriction as there are still ample unused substation capacities both temporally and spatially. For each scheduling strategy, the distribution of the substation utilization for the time period of each strategy's additional peak demand is illustrated in Figure 4.10. In the following, the power line utilization both for the LV and MV grid are separately investigated:

- **LV grid**

  The distribution of the power line utilization for the LV grid is shown in Figure 4.10a. Although deviations between both scenarios with and without PEVs are rather small for the power lines with a lower utilization, they significantly differ for higher utilized power lines, especially for those operating at or close to their maximum utilization. This emphasizes the previously suggested limitation of the power line capacities. Temporally, the power line utilization illustrated in Figure 4.11 also relates to the additional and

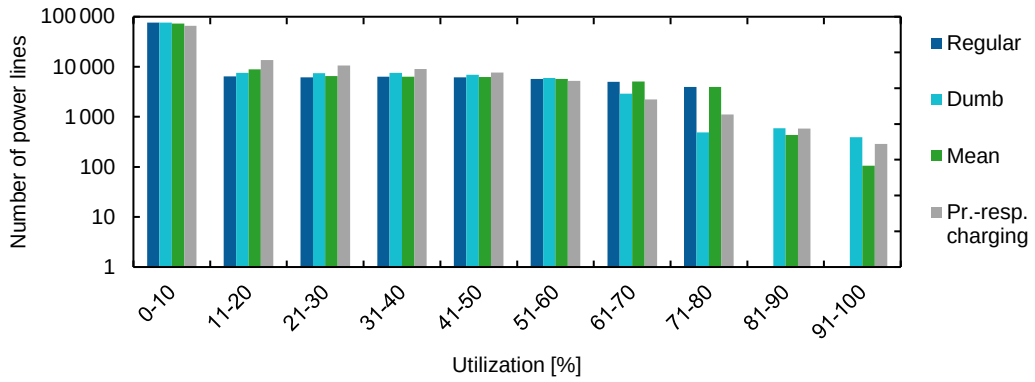

(a)

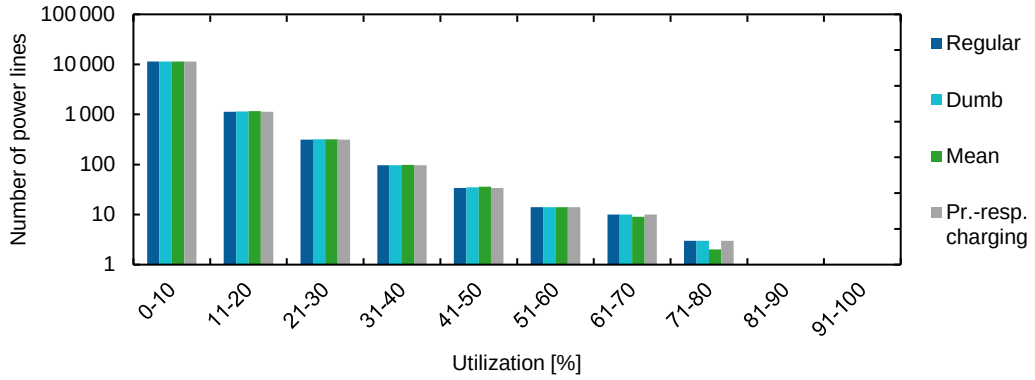

(b)

Figure 4.10: Distribution of the power line utilization based on the aggregated power demand in the (a) LV and (b) MV grid using different scheduling strategies, each at the time of their additional peak demand.

the unsatisfied power demand shown in Figure 4.8. This is especially noticeable on the distribution of the ratio of power lines which are utilized close to 100 %. This ratio is at its maximum at the time of the unsatisfied power demand peak at each scheduling strategy. With an average power flow increase of about 2.4 kW (dumb charging), 0.9 kW (mean charging), and 4 kW (price-responsive charging) at each power line, neither the increased number of fully loaded power lines nor the unsatisfied power demand can be explained. The spatial power demand distribution is therefore considerably inhomogeneous.

In Figure 4.12a, the spatially distributed additional power demand using the mean charging strategy at the time of the aggregated peak demand is illustrated. A similar figure would have been the result of both the dumb and price-responsive charging strategy[5]. It

[5] In Figure 4.12a, the mean charging strategy was preferred over the price-responsive one due to the scaling of the results for the latter strategy as explained in Section 4.3.2.

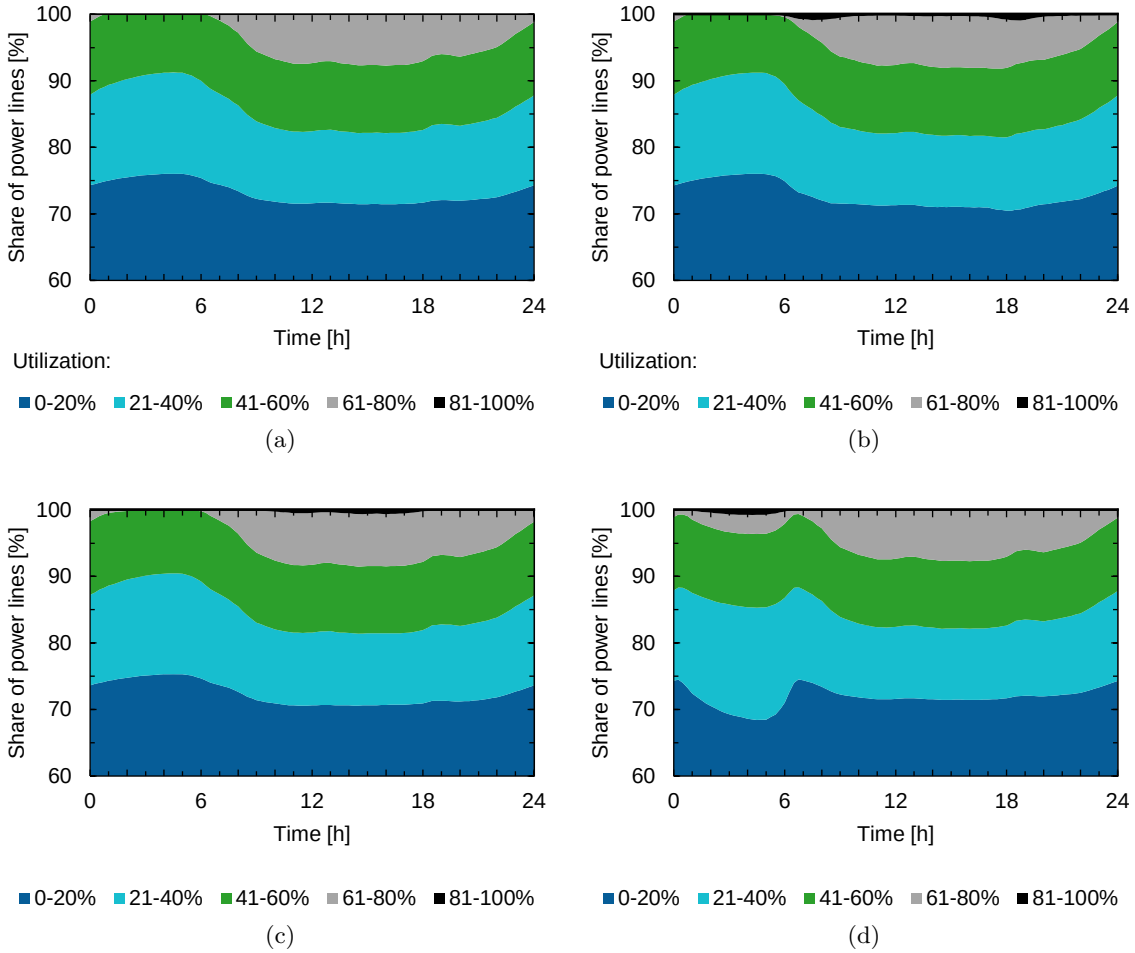

Figure 4.11: Temporal distribution of the power line utilization in the LV grid for the (a) regular and (b) - (d) aggregated power demand using the (b) dumb, (c) mean, and (d) price-responsive charging strategy.

can be seen that the additional power demand is inhomogeneously distributed. Regions with a higher color intensity indicate a higher demand which is with 775 kW (dumb charging), 89 kW (mean charging), and 102 kW (price-responsive charging) at its maximum. The spatially distributed power line utilization at the time of the aggregated peak power demand using the mean charging strategy is illustrated in Figure 4.12b. Again, the figure would look similar using the dumb or price-responsive charging strategy. It can be seen that the power line utilization is also inhomogeneously distributed. The distribution thereby reflects the one of the additional power demand shown in Figure 4.12a. Power lines operating at or close to their maximum utilization can almost exclusively be found in regions having a high additional demand while those with a lower additional demand are only accommodating power lines still having some unutilized capacity. For each of the different scheduling strategies, the total number of power lines that would have been

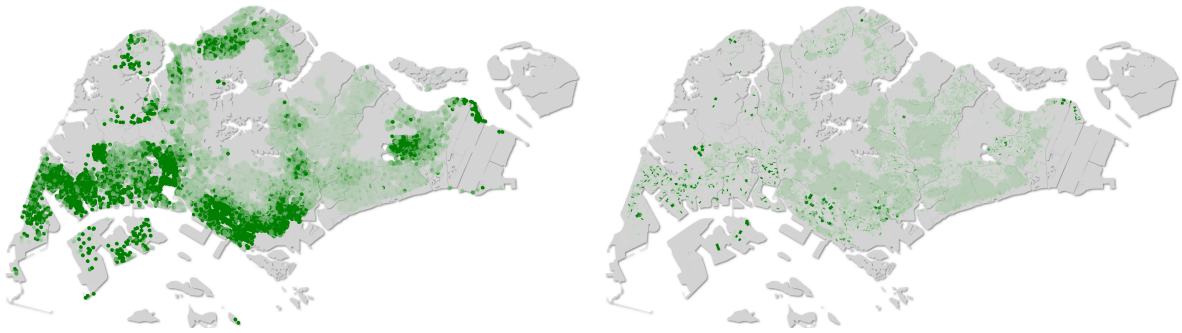

(a) (b)

Figure 4.12: Spatially distributed (a) additional power demand induced by 500 000 PEVs and (b) power line utilization in the LV grid, both using the mean charging strategy at the time of the aggregated peak power demand. The color intensity thereby reflects the (a) additional power demand and (b) power flow.

overloaded given the additional power demand is with less than 1 % rather low. This especially stands out compared to the ratio of unsatisfied to total additional demand of 47 % (dumb charging), 3 % (mean charging), and 8 % (price-responsive charging), respectively. This supports the previous conclusion that substations in the LV grid do not pose a limitation in satisfying the additional power demand but instead only some few power lines are insufficiently designed preventing satisfying the entire additional demand.

- **MV grid**

  The distribution of the power line utilization for the MV grid is shown in Figure 4.10b. Deviations between the two scenarios with and without PEVs applying different scheduling strategies are almost non-existing. And although at least for the dumb and mean charging strategy there is an unsatisfied power demand of 3 MW and 4 MW, respectively, there are no power lines operating at a maximum utilization larger than 80 %. This supports the previous conclusion that in the MV grid, limited substation capacities further restrict a power demand increase while power lines are sufficiently designed.

The findings presented in the previous Section 4.3.2.2 allowed drawing the conclusion, that power line capacities are limiting an additional power demand increase in the LV grid while substation capacities are preventing increasing the additional demand in the MV grid. The results discussed in this section confirm this conclusion. In the following Section 4.3.3, the impact of road transportation electrification both on the generation capacities as well as substation and power line utilization is investigated varying different parameters.

4.3.3 Parametrization

When investigating the impact of 500 000 PEVs on the Singapore PNM, different parameters as defined in Section 4.3.1 can be varied. Sweeping through the most influencing parameters, a ceteris paribus sensitivity analysis is conducted. Its results are elaborated in the following.

Power and Energy Demand

There are three parameters which have the most influence on the overall power and energy demand of road transportation electrification: the size of the PEV population, the length of the daily itinerary, and the energy consumption per kilometer. Investigating large-scale road transportation electrification with hundreds of thousands of PEVs, the three parameters have an equal impact, i.e., doubling the population size has the same impact as doubling the length of the daily itinerary or doubling the energy consumption per kilometer. This only applies to the presented results using the transportation system data as described in Section 4.3.1.3; in reality, there are non-linear effects resulting from the interaction of agents which can only be partially simulated with CityMoS Traffic due to its limitations regarding the population size. The linear effect, however, allows transferring conclusions from investigating the impact of one of the parameters to any of the other two. In this case study, only the size of the PEV population is therefore varied. While a value around 0 marks the lower boundary estimating the size of the current PEV population in Singapore [216], an entire electrification of the currently around 540 000 private cars can in principle be realized in Singapore within 10 years due to the limited validity of the *Certificate of Entitlement* [217]. More realistic, however, is the plan of having a vehicle population consisting of at least 50 % and thus of around 300 000 PEVs by 2050 [218].

Contradicting information on, for instance, the mentioned number of PEVs or the average daily mileage as mentioned in Section 3.4.1 certainly require a consideration of the sensitivity. For the different scheduling strategies, Table 4.10 provides functional dependencies of the properties defined in Table 4.9 on PEV populations sized between 20 000 and 500 000 agents. For all properties, results show a linear scale with the number of PEVs each having a coefficient of determination of $R^2 > 0.96$ when performing a regression. A commitment to any specific population size is therefore not necessary at this point. Instead, those dependencies allow scaling results presented in Section 4.3.2.1 to any target number of PEVs, length of the daily itinerary, and energy consumption per kilometer.

Charging Power

By default, each location is equally equipped with a fast CS having a maximum power of 120 kW as defined in Section 4.3.1.1. Besides, continuing along the typical power connections defined in Table 4.7, the following distributions are investigated in this section:

- **Slow**

  Each location is equally equipped with a slow CS having a maximum power of 3.6 kW.

Table 4.10: Dependency of the properties defined in Table 4.9 on the PEV population size x using different scheduling strategies.

Scheduling strategy	Max. additional power demand [kW]	Max. aggregated peak power demand increase [kW]	Additional energy demand, unsat.[kWh]	Affected locations [%]
Dumb charging	$0.57x$	$0.13x$	$1.92x$	$0.37E^{-5}x$
Mean charging	$0.21x$	$0.19x$	$0.07x$	$0.44E^{-5}x$
Pr.-resp. ch.	$0.96x$	_ [a)]	_ [a)]	_ [a)]

[a)] Within the investigated range of up to 100 000 PEVs, the price-responsive charging strategy does neither increase the peak power demand nor does it result in any unsatisfied additional energy demand. The latter starts to occur when further increasing the agent population size.

- **Slow-Fast**

  The maximum power of each location depends on its sector and is set to 3.6 kW for *Household* and 120 kW otherwise allowing for private slow and public fast charging.

- **Mix**

  The maximum power of each location is randomly selected with a probability of 0.25 each for having a 3.6 kW or 7.2 kW charging power, 0.15 each for 11 kW, 22 kW, or 43 kW, and 0.05 for 120 kW. 25 simulation runs are performed to average results.

Applying the dumb, mean, and price-responsive charging strategy on the different distributions results in only the dumb charging strategy to show significant differences. For the price-responsive charging strategy prices are re-calculated after the sequential processing of each trip. Different power connections therefore only make a difference if the duration of the valley to be filled is shorter than required to fully charge all PEVs which does not happen for the assumed PEV population. For the mean charging strategy the lowest possible power is applied at all times. Results would thus only be distorted by a less powerful connection in case of very short stops which rarely happens. The power demand of each PEV using the dumb charging strategy, however, directly depends on the available power connection. In Figure 4.13, the additional power demand using this strategy is illustrated applying different power connection distributions. Regardless of the distribution the demand is naturally equal. Only considering the unsatisfied power demand, however, reveals a dependency from the average power connection which is the higher the more fast CSs are used. Having each location equipped with slow CSs results with 98 MWh in an additional daily unsatisfied energy demand of only 10 % of the amount as for fast CSs. This indicates that applying the dumb charging strategy, limits with respect to overloaded substations or power lines may be dissolved or at least reduced. This can be achieved by only restricting the maximum power connection of selected CSs without requiring for upgrading affected electrical installations. It may, however, be inevitable to not place CSs at all location as discussed in Section 4.3.4.3.

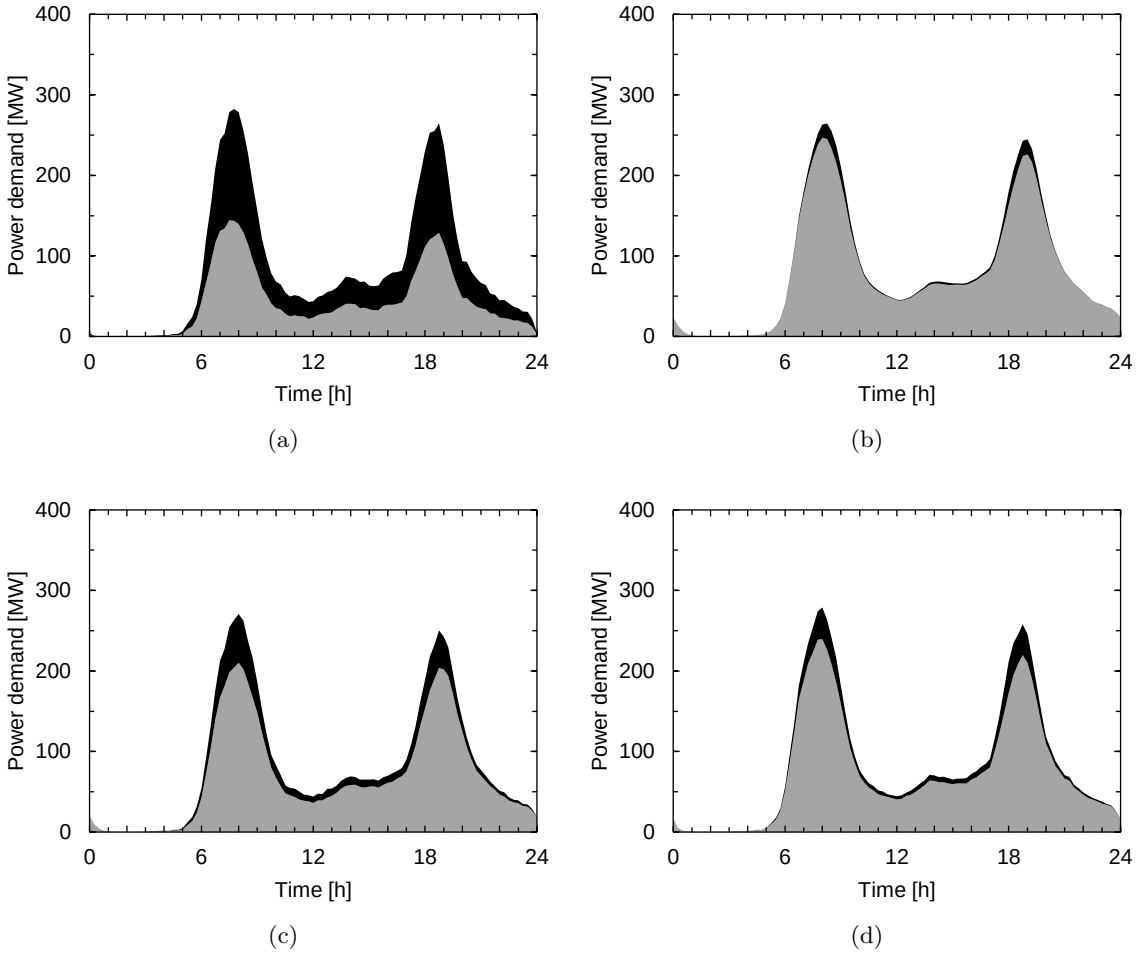

Figure 4.13: Additional satisfied (gray) and unsatisfied (black) power demand induced by 500 000 PEVs using the dumb charging strategy following the (a) fast, (b) slow, (c) slow-fast, and (d) mix maximum charging power distribution.

Electricity Prices

The price-responsive charging strategy is, as suggested by the name, sensitive to electricity price variations. Three different cases for defining those prices can be distinguished and are discussed in the following:

- **Constant prices**

  In case the electricity price is constant over the course of a day, the price-responsive charging strategy is indifferent when to charge. Besides a PEV's itinerary and the maximum power a CS can provide, the actual time and power of charging the battery is therefore only restricted by the battery model. As described in Section 4.3.1.1, the provided battery model produces a charging schedule which in the case of constant prices

is almost identical to the one of the mean charging strategy. It is even equal to it when only having a lookahead until each agent's next trip starts.

- **Time-dependent prices defined once**

  Time-dependent prices which are defined only once at the beginning of a simulation and which are equal for all PEVs may be worse from a power grid perspective than constant ones, depending on the temporal price distribution. The most simple case distinguishing this pricing strategy from the previous one is discriminating prices into two different groups. In Figure 4.14a, electricity prices are constant but different during day and night. They are set to 0.304 S$/kWh from 8:30 am to 11:15 pm and 0.216 S$/kWh otherwise, resulting in an average price of 0.27 S$/kWh reflecting the consumer electricity tariff of Singapore[6]. It can be seen that the price-responsive charging strategy exploits available price information to produce a cost-minimal charging schedule using only nighttime periods. This way, a further increase of demand peaks during the day can be avoided. At night, however, the valley is not flattened but instead the demand is evenly increased. Results for this pricing strategy are equal no matter the absolute prices or the size of the spread between day and night prices.

  In Figure 4.14b, the most complex case for this pricing strategy is illustrated. Prices are discriminated into 96 groups and thereby into the maximum number allowed by a time discretization of 15 minutes. They follow the regular load curve, are defined as described in Section 4.3.1.2, and therefore have exactly one price valley at 4:30 am. Since all agents have the same information about the price distribution the entire additional power demand is shifted to the time of the absolute price valley. Neighboring low price periods ranging from 1:30 until 6:15 am are supplementally used to allow for a PEV to fully charge. This way, the additional power demand is normally distributed increasing the global demand at 4:30 am by 900 MW. Although a further increase of daily demand peaks can also be avoided in this case, an additional load peak at the period previously showing a demand valley occurs. The exact price distribution is thereby irrelevant, implying that the occurrence of this peak is independent of the absolute prices or the spread between the prices of different periods. Peaks are always occurring at lowest price periods which are less distinct the less PEVs are charging at those periods. This can be achieved, for instance, by extending the duration of those periods and thereby offering the lowest price over a longer time span as illustrated in Figure 4.14a having the lowest price over the entire night time.

- **Time-dependent prices continuously re-calculated**

  A solution resulting in a temporal power demand evenly filling valleys while not increasing daily demand peaks are time-dependent prices which are temporally different for each agent. This behavior, whose real-world applicability is discussed in more detail in Section 4.3.4.2, is emulated by time-dependent prices which are continuously re-calculated based on the aggregated power demand. Results presented in Section 4.3.2 are based on this continuous re-calculation allowing the prices to follow the aggregated demand.

[6] Prices are calculated according to Equation (4.2) having a minimum price $p_{\min}$ of 0.216 S$/kWh which is equal to 80 % of the consumer electricity tariff of Singapore.

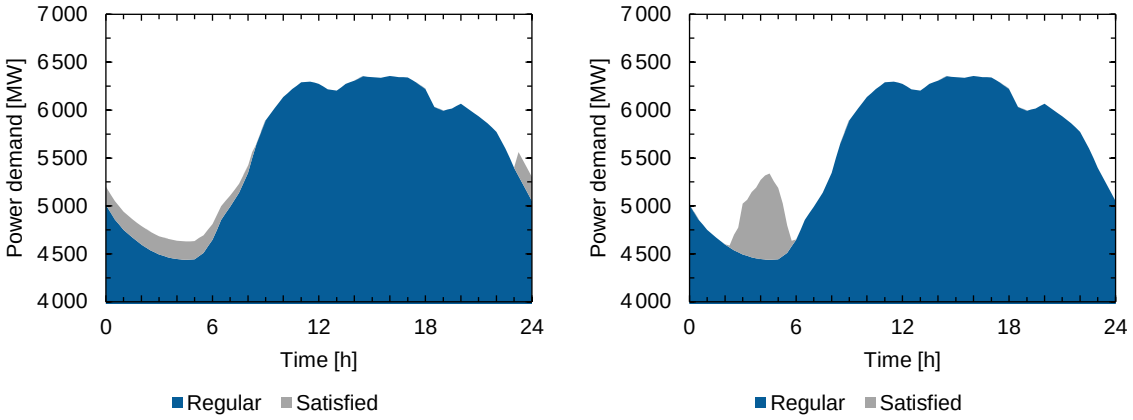

Figure 4.14: Regular load curve including the additional power demand induced by 500 000 PEVs using the price-responsive charging strategy and time-dependent prices defined once. Prices are either (a) constant but differing during the day and at night or (b) follow the regular load curve.

As long as prices reflect the power demand, higher or lower prices or a larger spread between those of different periods than assumed in Section 4.3.1.2 have no influence on the results. Thereby, only prices defined for the periods actually used for charging, in this case from midnight to 7 am, have to follow the aggregated demand. Prices for periods not considered for charging do not have an effect on the results and can therefore be arbitrarily set to any value higher than the prices in the periods considered for charging. Applying this pricing strategy, the temporal impact of charging PEVs on the power system can be controlled assuming rational agents. More complex behavior models can alternatively be implemented for each single agent in CityMoS Traffic. This, however, would then require adapting the described definition of prices and their dissemination in a real-world scenario.

Lookahead

Besides electricity prices discussed in the previous paragraph, the lookahead is the second of two parameters which heavily affect results using the price-responsive scheduling strategy. As described in Section 2.4.2.2, it relates to the number of used price forecast periods when deriving the profit-maximizing charging schedule. By planning ahead his daily itinerary, the PEV owner has a direct influence on his lookahead, unlike on externally provided prices. With a lookahead of 0, the scheduling strategy produces the same results as the dumb charging one; a lookahead until the beginning of the next trip equals the mean charging strategy. Increasing the value allows more information to be included in the process of calculating the charging schedule. This yields a higher potential of temporally shifting charging within the time horizon and thereby allowing power values to be adapted more fine-grained.

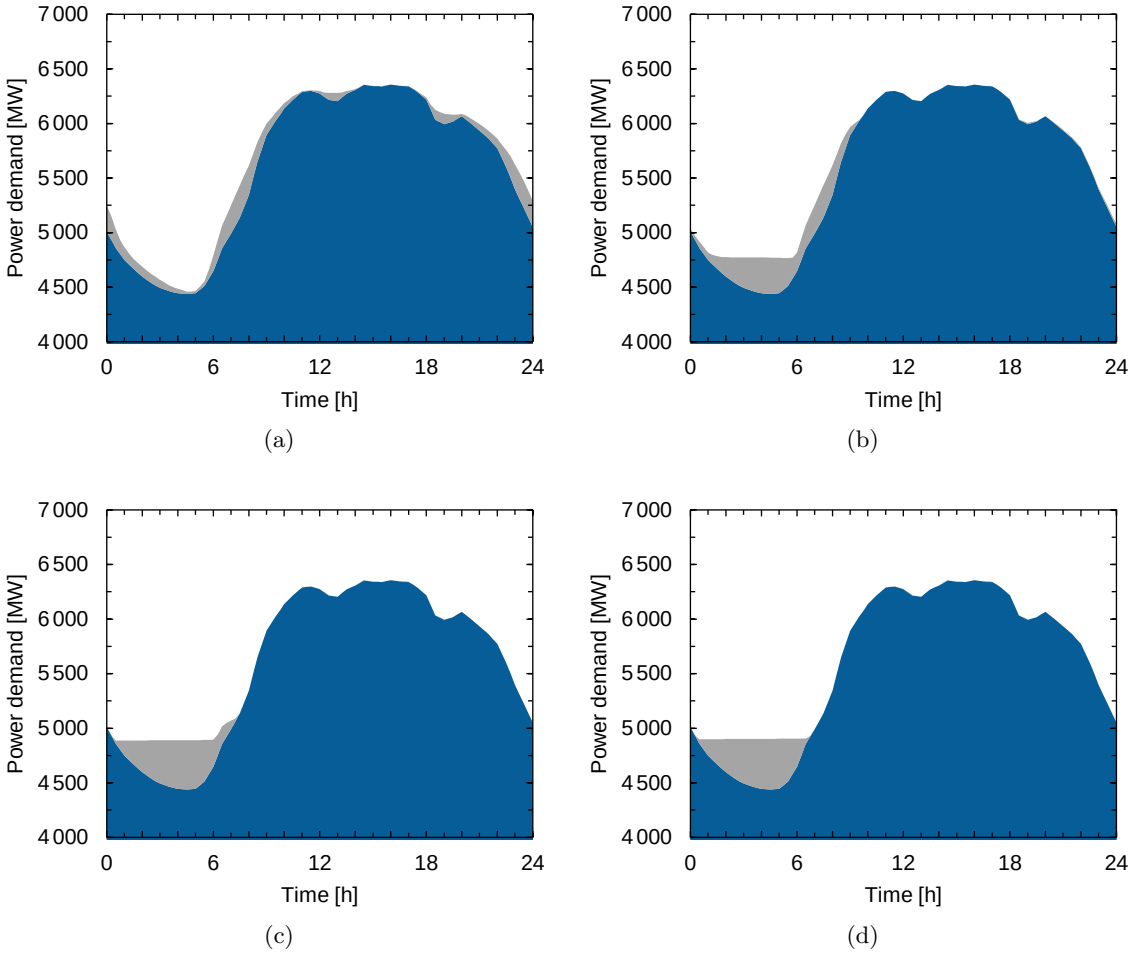

Figure 4.15: Regular load curve including the additional power demand induced by 500 000 PEVs using the price-responsive charging strategy with a characteristic lookahead of (a) 6 hours, (b) 12 hours, (c) 18 hours, and (d) 21 hours.

In Figure 4.15, the regular load curve including the additional power demand using the price-responsive charging strategy with different characteristic lookahead values between 6 and 21 hours is illustrated. The results for a lookahead of 24 hours have already been shown in Figure 4.8. It can be seen that the larger the lookahead the more of the additional power demand is shifted into the global demand valley between midnight and 7 am. A value of 7 hours is thereby sufficient to not further increase the regular peak demand but instead shifting charging into neighboring time periods. An optimal result totally flattening the valley can only be achieved with a lookahead of at least 21 hours.

With regard to the utilization of electrical installations, Figure 4.16 illustrates that the number of those installations operating at or close to their maximum utilization follows the additional power demand. Figure 4.16a shows that with an increasing shift of the additional power demand to the global demand valley, the number of overloaded power lines in the LV

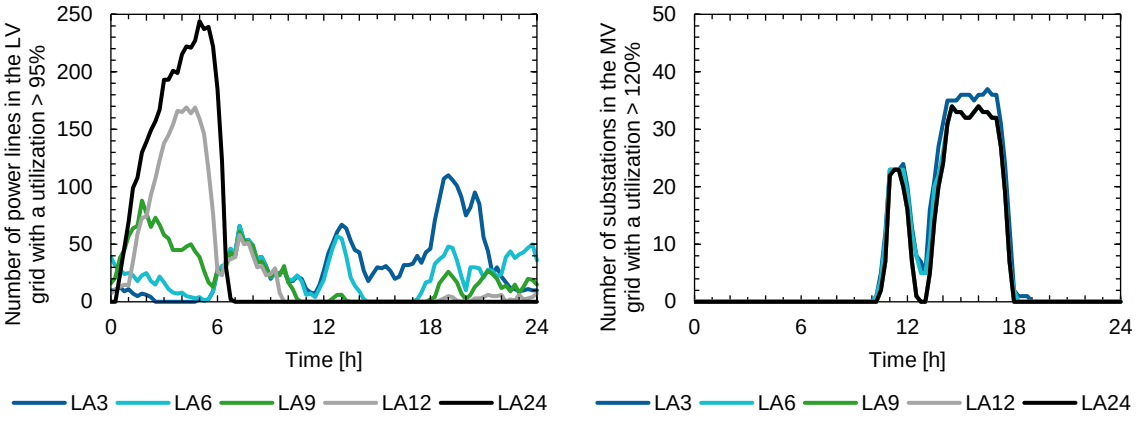

(a) (b)

Figure 4.16: Temporal distribution of the number of (a) power lines in the LV grid and (b) substation in the MV grid both operating at or close to their maximum utilization based on the aggregated power demand using the price-responsive charging strategy and different lookahead values.

grid at those time periods also increase. The number of overloaded substations in the MV grid as shown in Figure 4.16b reflects this trend by indicating a decrease in the number during times of aggregated demand peaks. Consistently with the discussion of the results presented in Section 4.3.2, the effect on the LV power line utilization is more intense than the one on MV substations.

4.3.4 Discussion and Related Work

Following the argument in Section 4.2.4, reaching definite conclusions with respect to transferring the findings of this study to the real-world power system the Singapore PNM is based on is a sensitive issue. First and foremost, this is due to the discussed limitations of the PSP process generating the used PNM. Among them is the limitation of realistically emulating the evolution of real-world power systems while also including placement constraints and inhomogeneities among electrical installations of the same voltage level due to a lack of available data. Apart from the PNM, there are further limitations of the applied setup. First, the impact of scaling the agent population size due to both limitations in CityMoS Traffic and performance restrictions when applying any price-responsive scheduling strategy is discussed in Section 4.3.4.1. Second, the way of defining electricity prices influences results which is described in Section 4.3.4.2. Last, the choice of locations where to place CSs and thereby the spatial distribution of the additional power demand heavily influences results as discussed in Section 4.3.4.3. To place the findings of this study in a broader context, related work on quantifying the power system impact of PEV charging is presented in Section 4.3.4.4.

4.3.4.1 Scaling of the Agent Population Size

In Singapore, over the past 8 years, measures have been implemented to keep the number of vehicles constant [216] despite a population growth of about 16 % [219]. The scenario of having 500 000 PEVs on the road is therefore likely to impose an upper boundary of what is to be expected in Singapore within the next few decades. This upper boundary is taken as the target agent population size in the presented case study. Two limitations, one in CityMoS Traffic and one in CityMoS Power, require scaling of either input or output data. Both limitations are described in the following:

- **Scaling the output of the transportation system simulation**

  CityMoS Traffic is only able to concurrently simulate 20 000 agents as explained in Section 4.3.1.3. The process defined in Section 3.4.2 scales the aggregated output to the target number of agents while preserving the trip characteristics. This way, the scaled aggregated output is similar to the one that would have been the result of simulating this target number of agents while dropping the limitation that prevents CityMoS Traffic to simulate larger PEV population sizes. The scaled and non-scaled output, however, are not equal. By scaling the output, non-linear effects resulting from the interaction of agents are neglected. Those interactions cause traffic to slow down and may produce traffic jams. The effects are naturally the larger the more agents are simulated. In general, they result in a longer average trip duration and thereby in a higher average energy demand per trip. Neglecting those effects therefore underestimates each agent's energy demand and thus also its investigated impact on the power system.

- **Scaling the input for the price-responsive scheduling strategies**

  In scenarios involving hundreds of thousands of PEVs, the dumb and mean scheduling strategies are both uncritical in terms of performance. Applying any of the price-responsive strategies in such scenarios, however, requires intensive computational resources. Due to limited resources available for conducting this case study, the agent population size for those strategies is restricted to 100 000 PEVs. Still allowing for an evaluation of the power system impact of a larger number of PEVs therefore requires scaling the tempo-spatial power demand of each single agent, in case of a target population size of 500 000 PEVs by the factor of 5. This way, the total power demand of the larger population is correctly emulated while for the temporal and spatial power demand inaccuracies may occur.

  Temporally, results are not expected to show any significant difference. Scaling power demand values by a factor of 100 when applying any price-responsive scheduling strategy to 1 000 PEVs produces temporal power demand deviations of less than 0.1 % at all times compared to directly simulating 100 000 PEVs; coming from 20 000 PEVs deviations are even as low as 0.01 %. Using a factor of 5 when scheduling 100 000 PEVs is therefore not expected to show any significant difference, especially considering the limitations regarding the scaling of the transportation system simulation's output discussed above.

  Spatially, things turn out differently. As described in Section 4.3.1.3, only 84 383 of the 117 853 possible locations are covered by the generated trips when simulating

100 000 PEVs whereas with 115 663 almost all locations are covered for 500 000 agents. This mismatch in the number of used locations results in distributing a power demand to each of the 84 383 locations which is on average 27 % higher than in the non-scaled scenario while at the same time neglecting the remaining 31 280 locations. Conclusions regarding the substation or power line utilization should therefore be made conservatively allowing only indications of spatial grid congestion rather than definite statements.

4.3.4.2 Information Dissemination of Electricity Prices

As shown in Section 4.3.3, there are in principle two strategies for defining electricity prices which are further discussed in this section. Considering a third possibility, implementing *auctions*, would detract from the focus of this work which is why it is referred to [220]. The first strategy defines prices once which are then equally made available to all agents. In the best case of having defined only one constant price, this results in an additional demand which is equal throughout the entire day. In the worst case of having multiple but at least two different prices, an additional demand peak is generated at the time of the absolute price valley. The second strategy targets evenly filling demand valleys while not increasing peaks by disseminating different information to each single agent. *Information dissemination* in this context is the process of providing real-time information about electricity prices and price forecasts to the agents [221]. They, in turn, are themselves participants in the information generation process as prices do not only reflect the daily load curve of traditional consumers but also depend on their own and on the power demand of other agents. An agent always makes decisions based on the information disseminated to him or her. If, for instance, a rational agent has information on the exact time or location of the lowest electricity price, he or she will use it to least cost charge at that very time or location as long as this fits his or her itinerary. Depending on their behavior, some agents might also delay charging or take a detour to minimize charging costs which, in turn, allows agents' charging behavior to be externally controlled within limits. Disseminating the same electricity price information to the entire set of agents allows each single one of them to equally exploit this information resulting in all agents charging at the least cost time or location. This leads to an unintended additional load peak as shown in Figure 4.14b in the context of time-dependent prices defined only once. It is therefore desirable to provide different information to each single agent or groups of them. This way, prices can individually be determined and disseminated to allow for load valley filling while at the same time avoid load peak amplification or even provide peak shaving.

This approach has been demonstrated in this case study applying the price-responsive charging strategy emulating non-equally disseminated information with continuously re-calculated electricity prices. It thereby has been shown that although the overall energy demand is fixed, the entire daily power demand induced by road transportation electrification can be temporally controlled by means of intelligently disseminated electricity price information. Disseminating spatially different prices may result in shifting at least parts of the additional power demand from congested to non-congested locations. This depends on the absolute price spread but even more requires proper charging behavior models as, for instance, developed in [222]. In reality, it still remains an open task to calculate and disseminate electricity prices in a non-discriminating way accomplishing a similar impact on the power system. There is much more uncertainty

in real agents' itineraries, their specific charging behavior, and rationality than assumed in this section, not to mention the requirement of implementing real-time electricity prices and broadly employing algorithmic scheduling approaches for exploiting them.

4.3.4.3 Charging Station Locations

In this study, CSs are installed at all of the 117 852 locations offered in the Singapore PNM, only varying the stations' maximum power connection. This allows each PEV to recharge whenever it is not in use for driving purposes. Placing CSs at all locations is rather unrealistic considering infrastructure costs. Instead, hotspots have to be identified where the charging need is sufficiently high to economically justify installing a CS while ensuring a short enough distance to the PEV owner's preferred parking location. This trade-off between minimal infrastructure costs and a maximum coverage constitutes an optimization problem which has already been approached considering different aspects. Those aspects include operation, maintenance, and costs due to power loss [223], coverage and driver convenience [224], energy costs for detours [225], drivers' time costs in terms of charging delays [226], driving time spent for reaching a CS [227], or queuing time [228].

The CS placement problem can also be solved using the CityMoS platform. In the setup described in Chapter 3, the relevant environment consisting of a transportation and a power system simulation using tempo-spatially resolved electricity prices is considered. This way, minimizing the impact of the CS distributions on the power system can be used as the objective function. Conducting studies on this topic is left subject to future work. In lieu thereof, a possible heuristic algorithm tackling this problem is outlined in the following:

1. Install CSs at all locations.
2. Run a federation execution for a period of 24 hours to generate a tempo-spatial pattern of charging demand (CityMoS Traffic) and power supply (CityMoS Power) using the current station placement.
3. Consolidate infrastructure guaranteeing the following feasibility criteria: the agents' total energy demand is satisfied, a previously defined convenience criterion of acceptable detours is met, and further grid congestion is prevented. Consolidation is as follows:
   a) Cluster CSs in a certain vicinity which have complementary temporal usage patterns to decrease the number of stations while increasing their utilization without increasing their maximum power demand.
   b) Remove a certain previously defined percentile of CSs with the lowest overall energy demand.
4. Repeat steps 2 and 3 until no more CSs can be consolidated without violating the feasibility criteria. The modified distribution of the CSs requires agents to adapt to the changed conditions by shifting charging temporally, spatially, or both. This results in a different tempo-spatial pattern of charging demand and power supply generated by CityMoS Traffic and CityMoS Power, respectively.

The consolidation of CSs reduces their number from the maximum possible having stations placed at all locations to an optimal value as, for instance, provided by the outcome of the algorithm presented above. This results in an entirely different distribution of the electrical installations' utilization. There are less locations which can be used for PEV charging. Still allowing each PEV to fully charge its battery requires every station to in principal provide a higher power than determined in the context of this case study. This, in turn, may result in even more grid congestion if no proper measures for upgrading electrical installations at those new hotspots are taken. As an application of the CityMoS platform, conducting a study to identify the optimal placement of CSs thereby minimizing the power system impact while considering the real-time development of queues at the stations is left subject to further research.

4.3.4.4 Related Power System Impact Studies

Investigating the impact of road transportation electrification on the different aspects of urban power systems is subject of a multitude of studies. As a primer, several current review papers found in [229–233] describe the findings of a wide range of available studies. In addition, several other relevant studies of the past three years are categorized in Tables 4.11 and 4.12. In this section, the findings of both sets of studies including those found in the referred review papers and those provided in the mentioned tables are discussed. The studies widely differ in their applied methodology as well as in the used input data and models which is why their results can hardly exactly be compared with each other. The mentioned studies mostly differ in three aspects:

- **Transportation system**

  There are two main differences in the way the transportation system is investigated. First, each study defines its own PEV population size. The number of PEVs thereby ranges from only a few PEVs which are currently registered to some percentage for the next decade which may come up to a scenario of an entire road transportation electrification. The definition of the reference value for the percentage is heterogeneous and includes the current and estimated future vehicle population, the targeted PEV share announced by the government, the consumer population, or it remains undefined.

  The second difference in the transportation system investigation is the way of generating the power demand induced by the PEVs for which there are three different possibilities. First, some estimate on the number of concurrently charging PEVs is applied. Worst-case estimations unrealistically act on the assumption of total concurrency. Second, an observed travel pattern is applied to the entire PEV population using some average energy consumption per distance driven. Third, traffic is simulated using an agent-based transportation system simulation realistically emulating interactions between the PEVs influencing their energy demand. Some studies do not reveal their methodology at all.

- **Power system**

  The applied PNM is either a real-world transmission grid, a small part of a distribution grid, or an IEEE test system [254], all limited to a few thousand nodes mostly spanning

Table 4.11: Characteristics of power system studies.

	Transportation system		Power system			Charging		
	# PEVs [%]	Trip generation [a]	n_{PV}	n_{PQ}	Voltage level [kV]	Strategy [b]	Power [kW]	Time [min]
[234]	30, 60	–	IEEE 37		0.48, 4.8	U, O	–	60
[235]	5, 10, 20	–	38	3 992	0.4, 10.5, 35	U, C, V2G	3.7, 22, 50	60
[236]	30	SMP	12	9 000	20, 90	U, C	3.7	10
[237]	10, 30	–	–	–	110, 330	U, C	3.7, 43	60
[238]	100	ABS	4	–	–	U, C	–	15
[239]	90	–	–	–	–	U, C	5	–
[240]	10	MDMP	3	155	0.23	U	2.3, 3.7, 22	1
[241]	100	MDMP	–	–	–	U, M, C, V2G	5.75	30
[242]	170 000 PEVs	HRTV	IEEE 30		1, 11	U, M	3.3, 6.6	15
[243]	300, 1 000 PEVs	MDMP	35	20	–	U, C	3.6, 11, 30	60
[244]	100	–	1	3	0.24, 7.2	U, C	18, 25	30
[245]	10, 25, 45	MDMP	1	20	MV	U, C	3.3, 7.2	5
[246]	50	–	1	12	LV	U, O	3.7, 22	60
[247]	20	random	–	–	LV / MV	U	–	15
[248]	40	HRTV	–	–	–	U, O	3.3, 6.6	10
[249]	20, 100	SMP	3	96	0.43, 11, 33	U	3.6	30
[250]	10, 20, ..., 100	MDMP	1	42	0.4, 11	V2G	2.4, 7.4	10
[251]	10	ABS	1500	895	11, 22, 150, 220, 380	U, C	3.5, 11	15
[252]	284 PEVs	MDMP	IEEE 34		25	U, M	1.7, 17, 40, 100	10
[253]	25, 50, 100	MDMP	–	–	–	U, C, O	3.3, 6.6	10

[a] ABS: agent-based simulation, HRTV: Hourly road traffic volume, MDMP: multiple different mobility pattern, SMP: single mobility pattern.

[b] C: controlled, M: mean, O: off-peak, U: uncontrolled, V2G: vehicle-to-grid.

Table 4.12: Investigated impact of power system studies.

	Peak load	Substation util.	Power line util.	Voltage	Power loss
[234]	–	–	–	x	x
[235]	x	x	x	x	x
[236]	x	–	–	x	–
[237]	x	x	x	x	x
[238]	x	–	–	–	–
[239]	–	–	–	x	x
[240]	x	x	x	x	x
[241]	x	–	–	–	–
[242]	x	–	–	–	–
[243]	x	–	x	x	x
[244]	–	x	–	x	–
[245]	–	x	–	–	–
[246]	–	–	–	x	–
[247]	–	x	–	x	–
[248]	x	–	–	–	–
[249]	–	x	–	x	x
[250]	x	–	x	–	–
[251]	x	x	x	–	–
[252]	–	x	x	x	x
[253]	x	–	–	–	–

over two different voltage levels. Some studies do not provide information on their used power system or only investigate the impact on generation capacities. An entire city's PNM in the level of detail as investigated in this work is not applied in any study.

- **Charging**

  Different scheduling strategies are applied throughout the different studies. They can mostly be differentiated into *uncontrolled* or *controlled* strategies. The former refers to the dumb charging strategy of this work while the latter relates to some smart charging strategy. The target of the applied smart charging strategy differs and includes price responsiveness, matching renewable energies' output, demand valley filling, or energy source optimization. Some studies also include the mean charging strategy, shifting charging into off-peak times, or offer the possibility of back-feeding energy to the grid. An excellent overview of the different scheduling strategies which are applied in many studies and which are reflected in this work is provided in [255].

  The investigated studies can also be differentiated by their used charging power. While most studies consider only slow charging up to 7.2 kW, very few analyze the impact of fast charging with a connecting power larger than 50 kW. Studies also apply a different time resolution investigating the impact of PEV charging on the daily load curve ranging from 1 minute to 1 hour.

Abstracting from those differences, most of the studies agree in their general conclusions which conform to the findings of this case study summarized in Section 4.3.5. The following consensus differentiated into an *aggregated* level, conforming to generation capacities, and a *disaggregated* level, conforming to individual substations and power lines, can be phrased:

- **Aggregated**

  The power and energy demand induced by the PEVs is both with less than 5 % of the current demand very little. The additional power demand at times of the daily demand peak is of particular relevance as it requires providing additional generation capacities. The provision does not apply or can at least be reduced by a significant amount if some kind of controlled charging strategy is applied. In case such a strategy includes the possibility for V2G, current generation capacities can even be reduced.

- **Disaggregated**

  Both substation and power line capacities are mostly sufficiently planned to serve a PEV population up to 20 % of the respective vehicle population, even using uncontrolled charging. Applying a controlled scheduling strategy no overloading or significant voltage drops occur until the PEV population grows beyond 40 %. Regardless of the scheduling strategy, some studies, however, indicate insufficient dimensioning of individual substations or power lines.

In conclusion, there is a wide variety of different approaches investigating the impact of road transportation electrification on power systems. Most of the investigated studies focus on introducing a controlled scheduling strategy to mitigate power system impact. Implementing such a strategy indeed defers investments for upgrading the power system infrastructure. It, however, does not prevent investments at all as those strategies require implementing a communication infrastructure. The common statement of most of the studies is that there are little to no problems expected regarding generation capacities while especially using an uncontrolled charging strategy substation or power line overloading may occur at certain times or places. As overloading or voltage drops may in some cases already occur with a couple of thousand of PEVs more detailed investigation on individual use cases are advised.

4.3.5 Conclusions

In this study, the power and energy demand of a PEV population of up to 500 000 PEVs is analyzed with regard to existing generation capacities as well as substation and power line utilization on all voltage levels in the Singapore PNM. The different availability of information regarding the agent's itineraries and electricity prices enable various scheduling strategies all having a different impact on the generation capacities. Applying dumb charging, PEVs are immediately charged with the maximum available power without considering intermittently increasing demand peaks. The mean charging strategy evenly increases the regular load curve by charging with the minimum possible power while requiring a fully charged battery right before a trip starts. The price-responsive charging strategy uses price information tied to the aggregated load curve to shift charging into times of demand valleys thereby not increasing demand peaks. The price-responsive charging/discharging strategy further flattens

the aggregated load curve at the cost of accepting energy conversion losses. This is done by allowing PEVs to provide energy to the grid at times of peak demands which was previously provided to the PEVs by the grid at times of demand valleys. In reality, a mix of those or other strategies applies depending on the agents' charging behavior.

In Singapore, having 500 000 PEVs on the road is in principle possible within 10 years; with regard to the official plan of only having half this number by 2050, it, however, imposes an upper boundary of what is to be expected in Singapore within the next few decades. With respect to the requirement for additional power generation capacities, it is found that even for this large number of PEVs values of up to 100 MW or 1.6 % of the current maximum power supply apply as found in Section 4.3.2.1. Those values are negligibly low considering current spare capacities of around 47 %. Furthermore, with a proper scheduling strategy, a smart policy on disseminating electricity price information, and a sufficiently large trip planning horizon on the side of the PEV owners, regular demand valleys can be evenly filled while not further increasing peak demands. A similar moderate effect as for the requirements of additional power generation capacities can be observed for the additional daily energy demand which is about 2 GWh or 1.5 % of the regular demand, independent of the scheduling strategy.

There is, however, a temporally and spatially varying, non-negligible unsatisfied power demand which is the higher the larger the maximum power connection of CSs is. Unlike power stations which have large spare capacities, a number of substations and power lines are utilized at or close to their maximum capacity. In the applied power flow simulation, those overloaded electrical installations result in load curtailments of connected consumers and thus in an unsatisfied power demand. This unsatisfied power demand follows from limited power line capacities in the LV grid while in the MV grid substation capacities are preventing an additional power demand increase at some locations. With up to 5 % of all locations a significant part of the Singapore PNM is affected. This part primarily represents locations which are more often used as a trip's origin and destination than others and thus show an increased additional power demand. The spatial distribution of the electrical installations' utilization thereby reflects the likewise spatially inhomogeneously distributed additional power demand. This allows drawing the conclusion that substations or power lines in general do not pose a limitation in satisfying the additional power demand but instead only a few installations are insufficiently designed preventing satisfying the entire additional demand. Different measures may result in shifting parts of the additional power demand from affected locations to those having spare capacities and thus mitigate grid congestion. Among them are, for instance, selectively limiting the number of locations equipped with CSs, limiting affected station's maximum power connection, or defining spatially different electricity prices. Implementing those measures is subject to further research and is not investigated in this work.

Based on the findings of this study, the answer to the question of quantifying the impact of road transportation electrification on urban power systems posed in Section 1.1 is twofold. A distinction is required between the utilization of existing generation capacities on the one hand as well as substations and power lines on the other hand. Additionally, the discussion in Section 4.2.4 suggests to differentiate conclusions related to a real power system and a model of it. For both environments, conclusions are drawn in the remainder of this section.

Applying the **Singapore PNM** in the presented simulation environment, the answer to the research question is composed of the following two conclusions:

1. *From the perspective of existing generation capacities, the impact of a large number of PEVs on a simulated environment of Singapore with respect to a peak power and daily energy demand increase is in both cases with up to 1.5 % negligibly low, especially considering spare capacities of 47 %. Furthermore, by applying proper scheduling and electricity pricing strategies, the additional power demand can entirely be shifted to times of demand valleys resulting in a load curve flattening effect.*

2. *Existing substation and power line capacities are partially insufficient to fully satisfy the additional power demand induced by a large number of timely and spatially distributed PEVs. While in the LV grid around 1 % of the power lines are insufficiently designed, capacities of up to 3 % of all substations are the limiting factor in the MV grid. This results in up to 50 % of the additional power demand remaining unsatisfied, depending on the applied scheduling strategy.*

Drawing conclusions on the implications for the real Singapore power system based on those findings requires considering the limitations of the applied simulation environment. On the power system simulation side, the PSS framework is limited with respect to emulating the evolution of real-world power systems while also neglecting placement constraints and inhomogeneities among electrical installations of the same voltage level. On the transportation system simulation side, the number of concurrently simulated agents and thus the interactivity between them is limited while there is also a large uncertainty in the data the trip generation process is based on. Besides, the applied CS placement including the CSs' power connection is unrealistic and does not account for minimizing power system impact. Considering those simplifications and limitations of the applied simulation environment and the uncertainties in the used input data, the answer to the research question with respect to the **real power system of Singapore** therefore comprises the following conclusions:

1. *From the perspective of existing generation capacities, the impact of large-scale road transportation electrification on the Singapore power system is negligibly low and can be compensated by available spare capacities.*

2. *Considering little spare capacities of power lines in the LV grid and of substations in the MV grid, the impact of even a small number of tempo-spatially concentrated PEVs is, however, significant for individual electrical installations. It is likely to be large enough to perturb the seamless integration of both transportation and power system therefore requiring further investigation using refined simulation models and more realistic data.*

5 | Conclusions

Content

From the perspective of existing generation capacities, the impact of large-scale road transportation electrification on the Singapore power system is negligibly low and can be compensated by available spare capacities.

Considering little spare capacities of power lines in the LV grid and of substations in the MV grid, the impact of even a small number of tempo-spatially concentrated PEVs is, however, significant for individual electrical installations. It is likely to be large enough to perturb the seamless integration of both transportation and power system therefore requiring further investigation using refined simulation models and more realistic data.

5.1 Summary

Plug-in electric vehicles (PEV) have the potential to reduce the transportation sector's dependency on fossil fuels, thereby diversifying its sources of primary energy supply. The implications of a large-scale introduction on their environment, in particular on the power system, is yet to be determined. This work is therefore motivated by concluding on the following **research question**:

Which impact does the power and energy demand induced by a large number of timely and spatially distributed PEVs have on urban power systems?

PEVs currently exist only on a small scale. The impact of road transportation electrification on power systems is therefore negligibly low. Studying its impact on a large scale is, however, cumbersome as the conditions precedent are not given in reality. It is therefore the following **problem statement** that is addressed in this work:

How to study the electrification of the road transportation system in an environment of interdependent systems that does not yet exist?

Both the electrified road transportation and the power system show tempo-spatial interdependence yielding unrealistic results if each individual system is studied in isolation. An integrated approach conjointly simulating both systems is thus essential. Focusing on the power system part of the environment, a methodology is initially required to generate specific data models of the system, termed *power network models* (PNM). Those PNMs can be used by an integrated simulation platform to investigate the impact of new types of power system participants before they become reality. The **proposed solution** to this work's problem statement is therefore as follows:

A simulation platform is developed allowing to microscopically evaluate the impact of road transportation electrification on power systems.

Applying the implemented distributed simulation platform to the generated PNM best matching Singapore using a price-responsive scheduling strategy allows answering this work's research question with respect to the **simulated environment** by the following quantitative **conclusions**:

1. *From the perspective of existing generation capacities, the impact of a large number of PEVs on a simulated environment of Singapore with respect to a peak power and daily energy demand increase is in both cases with up to 1.5 % negligibly low, especially considering spare capacities of 47 %. Furthermore, by applying proper scheduling and electricity pricing strategies, the additional power demand can entirely be shifted to times of demand valleys resulting in a load curve flattening effect.*

2. *Existing substation and power line capacities are partially insufficient to fully satisfy the additional power demand induced by a large number of timely and spatially distributed PEVs. While in the LV grid around 1 % of the power lines are insufficiently designed, capacities of up to 3 % of all substations are the limiting factor in the MV grid. This results in up to 50 % of the additional power demand remaining unsatisfied, depending on the applied scheduling strategy.*

Considering simplifications and limitations of the applied simulated environment and uncertainties in the used input data, the answer to the research question with respect to the **real power system of Singapore** therefore comprises the following qualitative **conclusions**:

1. *From the perspective of existing generation capacities, the impact of large-scale road transportation electrification on the Singapore power system is negligibly low and can be compensated by available spare capacities.*

2. *Considering little spare capacities of power lines in the LV grid and of substations in the MV grid, the impact of even a small number of tempo-spatially concentrated PEVs is, however, significant for individual electrical installations. It is likely to be large enough to perturb the seamless integration of both transportation and power system therefore requiring further investigation using refined simulation models and more realistic data.*

To derive those conclusions, this work was framed into several chapters as follows:

In Chapter 1, PEVs were introduced as either chance or risk to the power system, depending on their integration. The question of quantifying the impact of road transportation electrification on power systems on a large scale was raised as this work's research question in Section 1.1. It was argued that models of the involved systems, especially PNMs considering power systems to be the focus of this work, are essential to emulate the required, currently non-existing environment. In Section 1.2, simulation was identified as this work's favored approach to determine the tempo-spatial electricity demand of a large

number of PEVs and its impact on power systems' electrical installations. Section 1.3 outlined this work thereby describing each chapter's main contribution.

In Chapter 2, the methodological part of this work was presented describing a *power system simulation* (PSS) framework. In Section 2.2, a *power system planning* (PSP) approach for generating PNMs of any scale was described. This approach uses a combination of algorithms to generate PNMs realistically emulating the actual power system infrastructure. It was stated that it can be multi-purposely parametrized to generate PNMs tailored to individual requirements and thus works around usual limitations on the availability of input data. In Section 2.3, the framework's built-in possibility to simulate power flows on the previously generated PNMs was explained. The applied network decomposition approach is able to realistically solve AC power flow problems within seconds even for large-scale PNMs. It was further described that the power flow simulation is not only used during the PSP process to ensure that the generated PNMs are functional but also allows conducting studies simulating power flows under arbitrary tempo-spatial load profiles. By calculating the capacity utilization at every bus and branch as well as the voltage at each consumer and substation, times and locations of grid congestion and voltage drops can be identified. For investigating the impact of charging a large number of PEVs on a power system, a price-responsive scheduling approach for battery energy storage was presented as part of the PSS framework in Section 2.4. Battery degradation and electricity price forecasts are considered to shift charging/discharging into time periods least influencing power grid stability while guaranteeing an economically optimal scheduling process for the battery owner. In Section 2.5 it was argued that prior to conducting studies on any generated PNMs, their applicability for specific use cases should be evaluated. Using the framework's topological, electrical, and economic metrics, different PNMs can be compared with each other and with real-world power systems. This chapter ended with a discussion of the applicability and limitations of the PSS framework in Section 2.6.

In Chapter 3, the implementation part of this work, the *City Mobility Simulation* (CityMoS) platform, was introduced. CityMoS was intended as the infrastructure required for analytically and visually investigating different road transportation electrification scenarios by providing a platform for multiple, possibly distributed simulations to interact with each other. With the IEEE Standard 1516-2010 called *High Level Architecture* (HLA) the mechanism to construct such interoperable distributed system simulations was described in Section 3.2. It was stated that in this work's use case, CityMoS comprises three components. At first, as an implementation of the previously described PSS framework, CityMoS Power was presented in Section 3.3. Second, the characteristics of CityMoS Traffic, an agent-based transportation system simulation, were introduced in Section 3.4. Third, CityMoS Frontend as an interactive tool allowing to visualize the status and control interactions between the other platform's system simulations was described in Section 3.5. Subsequently, the platform's architecture, each simulation's specific requirements to participate in a distributed simulation, and the exchanged interactions were explained in Section 3.6. This chapter concluded with a discussion on alternatives to both HLA as the implemented distributed system simulation standard as well as the power and transportation system simulation in Section 3.7.

In Chapter 4, the application part of this work was presented. Two case studies were conducted to answer this work's research question motivated in Chapter 1 by using the methodology explained in Chapter 2 and its implementation described in Chapter 3. In the first study in Section 4.2, different PNMs of Singapore were generated and evaluated with respect to the framework's defined topological, electrical, and economic metrics. Reflecting on the limited availability of input data it was shown that despite the discussed limitations realistic PNMs for Singapore can be generated. The PNM best matching Singapore was used in the second study in Section 4.3. Several road transportation electrification scenarios were evaluated to analyze the tempo-spatial impact of different parameters both on the generation capacities as well as on the utilization of substations and power lines. This way, a comprehensive answer to the research question was given for both the simulation environment and the real power system of Singapore highlighting the power system impact from multiple perspectives.

5.2 Outlook

CityMoS is a promising platform and in its presented form comprising a transportation system simulation interacting with a power system simulation enables investigating future scenarios in the realm of transportation electrification. This way, the impact of possibly large-scale what-if urban mobility scenarios on realistically emulated power system infrastructure can be analyzed before the scenarios are implemented in a real-world setting. In this work, CityMoS is used to conduct transportation electrification studies to draw specific conclusions with respect to the research question for the case of Singapore. There is, however, the need for further research to make results more realistic and to expand the scope of the investigation to other areas. For this reason, the potential for both methodological and implementation improvements are presented in Section 5.2.1. Those improvements are limited to the most influencing ones making results more realistic, especially concerning the generated PNMs. Subsequently, extended areas of research are outlined in Section 5.2.2.

5.2.1 Methodological and Implementation Improvements

The methodology and implementation of both CityMoS Power and CityMoS Traffic can be improved to make results more realistic. As the implementation of CityMoS Traffic was not part of this work, possible improvements neglect technical details such as, for instance, extending the current unidirectional HLA module to allow for bidirectional communication. Instead, the focus is put on limitations discussed in the context of this work's studies. In the following, an outlook on future work to improve the accuracy of results is provided:

- **CityMoS Power**

  The missing functionality most limiting results from being more realistic is the planning of substations and power lines which are inhomogeneous within a voltage level. Even if there is no data on the particular specification of each substation available, future work has not only to deal with finding the geographical placement of a set of substations;

it also has to discover a matching distribution of the differently specified substations to the geographical locations. Without real-world data on the historic evolution of a power system and a way to include them via dynamic multi-stage expansion planning, resulting PNMs still differ from their real-world counterparts. Although being more realistic than the current approach, this still requires detailed examination of the results before drawing conclusions.

Expansion planning has not only to include possibilities to extend an existing network by adding additional components but instead also needs to allow for upgrading existing ones. Enhancing an existing substation may probably economically be the preferred option instead of newly building a substation next to an existing one. This way, the current way of generating a PNM reproducing the present state can be extended by providing decision support for future extensions of a power system.

Current PNMs are limited to nodes being either PQ (consumers) or PV buses (power plants), except for substations which can act as either a consumer or a producer of electricity depending on the voltage level. Prosuming PQ-PV buses which both consume and provide electricity from and to connected buses, respectively, especially those doing both at the same point in time on the same voltage level are not supported. Including distributed generation particularly in the LV and MV grid requires the applied network decomposition approach for simulating power flows to be refined to still be able to solve AC power flow problems for large-scale, multi-level PNMs. This may simultaneously allow for including redundancies within different parts of the PNM.

The accuracy of the generated PNMs compared to their real-world counterpart can also be increased by two other measures. First, power system components other than power lines, substations, and power plants such as circuit breakers or energy storage devices can be included. Second, existing components can be modeled on a higher level of detail. Especially including realistic unit commitment models for power stations is beneficial.

Considering the scheduling for battery energy storage approach, future work is necessary on modeling battery depreciation costs for different types of cells, also with respect to calendar aging. By knowing the exact costs of charging and discharging, agents can be integrated in power system-wide price-responsive scheduling schemes. This allows influencing the charging behavior of a large number of PEVs by just modifying one single parameter. Price-responsive scheduling schemes, however, do not only require knowledge of current but also of future electricity prices. Ways of dealing with price uncertainties have therefore to be further investigated.

- **CityMoS Traffic**

  The most severe limitation when simulating the transportation system with CityMoS Traffic is related to the missing implementation of a traffic control system which is restricting the maximum number of concurrently simulated agents. Several adaptive and coordinated traffic control systems are installed in the various cities worldwide such as, for instance, the *Sydney Coordinated Adaptive Traffic System* [256] in Singapore. Future work has therefore not necessarily to deal with improved ways of intelligently controlling traffic;

instead, emulating the respective system in place of the investigated region already helps improving accuracy of the simulation.

Further limitations can be resolved by diversifying charging behavior models realistically corresponding to the driver population. Agents may tempo-spatially charge differently depending on their current *state of charge* (SOC), distance to target, accepted detours, charging duration, and electricity prices. Additionally, the composition of the PEV population with respect to their energy consumption has also to be diversified to represent the current or any realistic future vehicle population. This includes different types of vehicles and matching driver behavior models.

Most of the current limitations in the methodology or the implementation, especially in the power system simulation, can be ascribed to a lack of available real-world data. Producing a more detailed replica of a target's power system still depends on available data and is mostly foiled for a lack of it. Individual locations and specifications of power lines and substations are typically rare requiring approximating them which results in PNMs diverging from reality. Findings of this work indicating grid congestion in parts of the power system should therefore incentivize authorities to make the required real-world data available to further improve platforms such as the presented one. This way, the impact of road transportation electrification on urban power systems can not only be more realistically investigated. Further research in adjacent areas is additionally facilitated allowing, for instance, identifying the optimal *charging station* (CS) placement, finding ways of most beneficially determining and disseminating electricity prices, or even evaluating a power system's robustness against faults or attacks as outlined in the following Section 5.2.2.

The extensions named above target the improvement of the accuracy of the results towards more realistically emulating the transportation and power system infrastructure. In addition, there are ways to improve the simulation platform to address a broader user group. Those improvements include offering the functionality of the entire CityMoS platform as an integrated service in the cloud. The platform comprises both system simulations as well as the interactive visualization and not just the transportation system simulation as proposed in [127]. Additional research is required to allow users to dynamically include further federates in a distributed federation execution using HLA. Those federates thereby do not necessarily have to be executed on the same hardware. They do not even have to run in the same network. This way, users are enabled to run arbitrary studies not only using the provided simulation environment but instead using their individually extended one.

5.2.2 Extended Areas of Research

The CityMoS platform does not only enable power system impact studies as conducted in this work. Instead, a broad range of possible topics in the wider area of electrified urban mobility can be investigated. Limits are only set by the platform's joined federates. Research areas can be extended by, for instance, including a *railway transportation system* simulation or an agent heat emission model. Besides computer simulations, HLA allows federates also to be *live* as in *live, virtual, and constructive* (LVC) systems. Including those systems as federates in the platform on the one hand allows real-time data to be integrated in the simulation

and on the other hand provide real-time information feedback to enable simulation-based decision support for the live system. In the following, three research questions are outlined which can be investigated with the current CityMoS platform including the improvements described in Section 5.2.1 where necessary. Areas of further research are thereby not limited to those questions. Instead, the questions provide an idea for topics suggesting themselves to be investigated as a logical next step to this work's research.

- **What are optimal spots for placing charging stations?**

  Transportation electrification requires the installation of CSs. Several constraints have to be considered to determine their optimal number, maximum power connection, and geographical placement. The basic problem thereby is trading coverage for costs. By decreasing the number of CSs, their total costs of installation are naturally also lower. At the same time, costs in terms of time investments for detours or queuing arise for the drivers. From a power system perspective, the charging impact is spatially clustered which may require strong selective infrastructure enhancements. Repeatedly simulating the transportation system starting with CSs placed at every location each time consolidating neighboring CSs with complementary charging pattern results in identifying charging hotspots. At those hotspots, the charging need is sufficiently high to economically justify installing a CS while at the same time ensuring low time investment costs for the drivers.

- **Do tempo-spatially different electricity prices influence the electrified traffic?**

  Besides the CSs' location and their maximum power, electricity prices may be the one parameter allowing to control the power system impact. Prices can be both temporally and spatially different and may even be different depending on the maximum power drawn by a PEV. They do not necessarily have to correspond to real electricity market prices. Instead, they can be arbitrarily set to control the charging behavior of PEV drivers targeting different purposes, e.g., controlling the power demand to selectively regulate the power system impact or influencing itineraries of agents to some extent.

  There are two research topics involved to comprehensively answer the posed question. First, agent charging behavior has to be realistically modeled including price-responsiveness to a certain degree. Agents may be differently motivated when, where, and with which strategy to charge. Maximizing their convenience while minimizing their costs is certainly a valid assumption though requiring some variation within the entire agent population. Second, prices have to be tempo-spatially modeled considering forecasts and uncertainties to achieve specific objectives, e.g., selectively relieving the power system infrastructure when necessary. Discriminating prices among different agents allows to better control the charging behavior of the entire agent population. The strategy of disseminating information on electricity prices is certainly as important as determining prices itself. It is not only a question of whom to provide with which information but also a technical one of how to do this thereby not discriminating against single agents.

  The topic for both the agent behavior as well as the price determination and dissemination is getting more complex if in addition to charging also discharging is considered. Distributed power sources and storage are promoting demand-responsive and *battery-to-*

grid (B2G) scheduling schemes. They certainly also have an impact on the electricity prices set for PEV charging and discharging.

- **How to evaluate the robustness and resilience of a power system against faults as well as random or targeted attacks?**

  A power system is designed to faultlessly satisfy the demand of its consumers at all times. Faults in any of its components may result in not fulfilling this obligation. They may be the result of a technical malfunctioning or an attack against the power system and may occur either randomly or targeted. The latter aims at wreaking most damage by first targeting electrical installations having the highest influence on satisfying the power demand. While a power system is robust if it in principle continues functioning after a fault or cascading outages without fundamental changes to the system, the resilience refers to the power system's capability to adapt to a fault by changing the system's operation [257]. Using CityMoS Power, a robustness or resilience metric can be calculated by selectively removing buses or branches and subsequently conducting power flow simulations. Alternatively, it can roughly be approximated by the node degree or the betweenness [210]. The robustness and resilience of each electrical installation allows to evaluate its importance with regard to the proper functioning of the system. It may even allow identifying possible bottlenecks and targets worthwhile to be attacked. This, in turn, offers the possibility to enhance the system by selectively expanding it thereby including redundancy to some degree.

A | Appendix

Content

A.1 CityMoS Power XSD

```
<?xml version="1.0" encoding="UTF-8"?>

<!--
  Author:  David Ciechanowicz
  Date:    2017-01-01
  Version: 1.0

  Description:
    This XML Schema describes the input data required
    and output data generated by CityMoS Power v1.0.
    It includes input and output data for the power
    system planning and power flow simulation.
-->

<xs:schema

  targetNamespace="http://rp5.info"
  xmlns:sp="http://rp5.info"
  xmlns:xs="http://www.w3.org/2001/XMLSchema"
  elementFormDefault="qualified">



  <!--                -->
  <!-- POWER SYSTEM -->
  <!--                -->

  <xs:element name="PowerSystem">
    <xs:complexType>
      <xs:sequence>
        <xs:element name="Node" type="sp:NodeType" minOccurs="2" maxOccurs="
            unbounded" />
        <xs:element name="Edge" type="sp:EdgeType" minOccurs="0" maxOccurs="
            unbounded" />
        <xs:element name="Area" type="sp:AreaType" minOccurs="0" maxOccurs="
            unbounded" />
      </xs:sequence>
      <xs:attribute name="Author" use="required">
        <xs:simpleType>
          <xs:restriction base="xs:string">
            <xs:pattern value="[a-zA-Z ]+" />
          </xs:restriction>
        </xs:simpleType>
      </xs:attribute>
      <xs:attribute name="Version" use="required">
        <xs:simpleType>
          <xs:restriction base="xs:decimal">
            <xs:pattern value="[0-9]*.[0-9]*" />
          </xs:restriction>
        </xs:simpleType>
      </xs:attribute>
      <xs:attribute name="Date" use="required">
        <xs:simpleType>
          <xs:restriction base="xs:date">
            <xs:minInclusive value="2016-01-01" />
            <xs:maxInclusive value="2029-12-31" />
          </xs:restriction>
        </xs:simpleType>
      </xs:attribute>
    </xs:complexType>
```

```
58      <!--                          -->
59      <!-- KEY, KEYREF & UNIQUE -->
60      <!--                          -->
61
62      <!--       -->
63      <!-- NODE -->
64      <!--       -->
65
66      <!-- KEY -->
67
68      <xs:key name="Node_IdNode_Key">
69        <xs:selector xpath="sp:Node" />
70        <xs:field xpath="@IdNode" />
71      </xs:key>
72
73      <!-- KEYREF -->
74
75      <!-- UNIQUE -->
76
77      <xs:unique name="Node_Location_Key">
78        <xs:selector xpath="sp:Node" />
79        <xs:field xpath="@Longitude" />
80        <xs:field xpath="@Latitude" />
81      </xs:unique>
82
83
84
85      <!--       -->
86      <!-- EDGE -->
87      <!--       -->
88
89      <!-- KEY -->
90
91      <xs:key name="Edge_IdEdge_Key">
92        <xs:selector xpath="sp:Edge" />
93        <xs:field xpath="@IdEdge" />
94      </xs:key>
95
96      <!-- KEYREF -->
97
98      <xs:keyref name="Edge_IdNode1_Ref" refer="sp:Node_IdNode_Key">
99        <xs:selector xpath="sp:Edge" />
100       <xs:field xpath="@IdNode1" />
101     </xs:keyref>
102
103     <xs:keyref name="Edge_IdNode2_Ref" refer="sp:Node_IdNode_Key">
104       <xs:selector xpath="sp:Edge" />
105       <xs:field xpath="@IdNode2" />
106     </xs:keyref>
107
108     <!-- UNIQUE -->
109
110     <xs:unique name="Edge_IdNodes_Uni">
111       <xs:selector xpath="sp:Edge" />
112       <xs:field xpath="@IdNode1" />
113       <xs:field xpath="@IdNode2" />
114     </xs:unique>
```

```
115       <!--       -->
116       <!-- AREA -->
117       <!--       -->
118
119       <!-- KEY -->
120
121       <xs:key name="Area_IdArea_Key">
122         <xs:selector xpath="sp:Area" />
123         <xs:field xpath="@IdArea" />
124       </xs:key>
125
126       <xs:key name="Area_NodeList_IdNode_Key">
127         <xs:selector xpath="sp:Area/sp:NodeList/sp:Node" />
128         <xs:field xpath="@IdNode" />
129       </xs:key>
130
131       <xs:key name="Area_EdgeList_IdEdge_Key">
132         <xs:selector xpath="sp:Area/sp:EdgeList/sp:Edge" />
133         <xs:field xpath="@IdEdge" />
134       </xs:key>
135
136       <!-- KEYREF -->
137
138       <xs:keyref name="Area_IdNodeSubstation_Ref" refer="sp:Node_IdNode_Key">
139         <xs:selector xpath="sp:Area" />
140         <xs:field xpath="@IdNodeSubstation" />
141       </xs:keyref>
142
143       <xs:keyref name="Area_NodeList_IdNode_Ref" refer="sp:Node_IdNode_Key">
144         <xs:selector xpath="sp:Area/sp:NodeList/sp:Node" />
145         <xs:field xpath="@IdNode" />
146       </xs:keyref>
147
148       <xs:keyref name="Area_NodeLoopList_IdNode_Ref" refer="sp:
              Area_NodeList_IdNode_Key">
149         <xs:selector xpath="sp:Area/sp:NodeLoopList/sp:Loop/sp:Node" />
150         <xs:field xpath="@IdNode" />
151       </xs:keyref>
152
153       <xs:keyref name="Area_EdgeList_IdEdge_Ref" refer="sp:Edge_IdEdge_Key">
154         <xs:selector xpath="sp:Area/sp:EdgeList/sp:Edge" />
155         <xs:field xpath="@IdEdge" />
156       </xs:keyref>
157
158       <xs:keyref name="Area_EdgeLoopList_IdEdge_Ref" refer="sp:
              Area_EdgeList_IdEdge_Key">
159         <xs:selector xpath="sp:Area/sp:EdgeLoopList/sp:Loop/sp:Edge" />
160         <xs:field xpath="@IdEdge" />
161       </xs:keyref>
162
163       <!-- UNIQUE -->
164
165       <xs:unique name="Area_NodeLoopList_IdNode_Uni">
166         <xs:selector xpath="sp:Area/sp:NodeLoopList/sp:Loop/sp:Node" />
167         <xs:field xpath="@IdNode" />
168       </xs:unique>
169
170       <xs:unique name="Area_EdgeLoopList_IdEdge_Uni">
171         <xs:selector xpath="sp:Area/sp:EdgeLoopList/sp:Loop/sp:Edge" />
172         <xs:field xpath="@IdEdge" />
173       </xs:unique>
174
175     </xs:element>
```

```
176   <!--       -->
177   <!-- NODE -->
178   <!--       -->
179
180   <xs:complexType name="NodeType">
181     <!-- SUB-ELEMENTS -->
182     <xs:sequence>
183       <xs:element name="Input" type="sp:NodeInputType" minOccurs="0" maxOccurs="
              unbounded" />
184       <xs:element name="Output" type="sp:NodeOutputType" minOccurs="0" maxOccurs="
              unbounded" />
185     </xs:sequence>
186     <!-- REQUIRED -->
187     <xs:attribute name="IdNode" type="xs:int" use="required" />
188     <xs:attribute name="Latitude" type="xs:decimal" use="required" />
189     <xs:attribute name="Longitude" type="xs:decimal" use="required" />
190     <xs:attribute name="VoltageLevel" type="sp:VoltageLevelType" use="required" />
191     <!-- OPTIONAL -->
192     <xs:attribute name="Description" type="xs:string" use="optional" default="" />
193     <xs:attribute name="IdBuildingType" type="xs:int" use="optional" default="-1"
            />
194     <xs:attribute name="IdNodeParent" type="xs:int" use="optional" default="-1" />
195     <xs:attribute name="IdNodeType" type="xs:int" use="optional" default="0" />
196     <xs:attribute name="IdSector" type="xs:int" use="optional" default="-1" />
197     <xs:attribute name="Name" type="xs:string" use="optional" default="" />
198     <xs:attribute name="PowerSupplyActiveMin" type="xs:decimal" use="optional"
            default="0" />
199     <xs:attribute name="PowerSupplyActiveMax" type="xs:decimal" use="optional"
            default="0" />
200     <xs:attribute name="PowerSupplyReactiveMin" type="xs:decimal" use="optional"
            default="0" />
201     <xs:attribute name="PowerSupplyReactiveMax" type="xs:decimal" use="optional"
            default="0" />
202     <xs:attribute name="VoltageLevelUpper" type="sp:VoltageLevelType" use="
            optional" default="6.6" />
203     <!-- ADDITION -->
204     <xs:anyAttribute processContents="lax" />
205   </xs:complexType>
206
207   <xs:complexType name="NodeInputType">
208     <!-- REQUIRED -->
209     <xs:attribute name="TimePeriod" type="xs:int" use="required" />
210     <xs:attribute name="PowerDemandBaseloadActiveRequired" type="xs:decimal" use="
            optional" default="0" />
211     <xs:attribute name="PowerDemandBaseloadReactiveRequired" type="xs:decimal" use
            ="optional" default="0" />
212     <xs:attribute name="PowerDemandTrafficActiveRequired" type="xs:decimal" use="
            optional" default="0" />
213     <xs:attribute name="PowerDemandTrafficReactiveRequired" type="xs:decimal" use=
            "optional" default="0" />
214   </xs:complexType>
215
216   <xs:complexType name="NodeOutputType">
217     <!-- REQUIRED -->
218     <xs:attribute name="TimePeriod" type="xs:int" use="required" />
219     <xs:attribute name="PowerDemandBaseloadActiveGranted" type="xs:decimal" use="
            required" />
220     <xs:attribute name="PowerDemandBaseloadReactiveGranted" type="xs:decimal" use=
            "required" />
221     <xs:attribute name="VoltageAngle" type="xs:decimal" use="required" />
222     <xs:attribute name="VoltageMagnitude" type="xs:decimal" use="required" />
223     <xs:attribute name="VoltageMagnitudeIncrease" type="xs:decimal" use="required"
            />
```

```
224       <!-- OPTIONAL -->
225       <xs:attribute name="PowerDemandTrafficActiveGranted" type="xs:decimal" use="
              optional" default="0" />
226       <xs:attribute name="PowerDemandTrafficReactiveGranted" type="xs:decimal" use="
              optional" default="0" />
227       <xs:attribute name="PowerSupplyActive" type="xs:decimal" use="optional"
              default="0" />
228       <xs:attribute name="PowerSupplyReactive" type="xs:decimal" use="optional"
              default="0" />
229     </xs:complexType>
230
231
232
233     <!--       -->
234     <!-- EDGE -->
235     <!--       -->
236
237     <xs:complexType name="EdgeType">
238       <!-- SUB-ELEMENTS -->
239       <xs:sequence>
240         <xs:element name="PowerFlow" type="sp:PowerFlowType" minOccurs="0" maxOccurs
                ="unbounded" />
241       </xs:sequence>
242       <!-- REQUIRED -->
243       <xs:attribute name="IdEdge" type="xs:int" use="required" />
244       <xs:attribute name="IdNode1" type="xs:int" use="required" />
245       <xs:attribute name="IdNode2" type="xs:int" use="required" />
246       <!-- OPTIONAL -->
247       <xs:attribute name="Description" type="xs:string" use="optional" default="" />
248       <xs:attribute name="IdEdgeType" type="xs:int" use="optional" default="0" />
249       <xs:attribute name="Length" type="xs:decimal" use="optional" default="0" />
250       <xs:attribute name="Name" type="xs:string" use="optional" default="" />
251       <xs:attribute name="Reactance" type="xs:decimal" use="optional" default="0" />
252       <xs:attribute name="Resistance" type="xs:decimal" use="optional" default="0"
              />
253       <xs:attribute name="VoltageLevel" type="sp:VoltageLevelType" use="optional"
              default="0.4" />
254       <!-- ADDITION -->
255       <xs:anyAttribute processContents="lax" />
256     </xs:complexType>
257
258     <xs:complexType name="PowerFlowType">
259       <!-- REQUIRED -->
260       <xs:attribute name="TimePeriod" type="xs:int" use="required" />
261       <xs:attribute name="PowerFlowActive" type="xs:decimal" use="required" />
262       <xs:attribute name="PowerFlowReactive" type="xs:decimal" use="required" />
263       <xs:attribute name="PowerFlowApparent" type="xs:decimal" use="required" />
264     </xs:complexType>
265
266
267
268     <!--       -->
269     <!-- Area -->
270     <!--       -->
271
272     <xs:complexType name="AreaType">
273       <!-- SUB-ELEMENTS -->
274       <xs:sequence>
275         <xs:element name="NodeList" type="sp:NodeListType" minOccurs="1" maxOccurs="
                1" />
276         <xs:element name="EdgeList" type="sp:EdgeListType" minOccurs="1" maxOccurs="
                1" />
```

```
277         <xs:element name="NodeLoopList" type="sp:NodeLoopListType" minOccurs="1"
                maxOccurs="1" />
278         <xs:element name="EdgeLoopList" type="sp:EdgeLoopListType" minOccurs="1"
                maxOccurs="1" />
279       </xs:sequence>
280       <!-- REQUIRED -->
281       <xs:attribute name="IdArea" type="xs:int" use="required" />
282       <xs:attribute name="IdNodeSubstation" type="xs:int" use="required" />
283       <!-- ADDITION -->
284       <xs:anyAttribute processContents="lax" />
285     </xs:complexType>
286
287     <xs:complexType name="NodeListType">
288       <!-- SUB-ELEMENTS -->
289       <xs:sequence>
290         <xs:element name="Node" minOccurs="1" maxOccurs="unbounded">
291           <xs:complexType>
292             <xs:attribute name="IdNode" type="xs:int" use="required" />
293           </xs:complexType>
294         </xs:element>
295       </xs:sequence>
296     </xs:complexType>
297
298     <xs:complexType name="NodeLoopListType">
299       <!-- SUB-ELEMENTS -->
300       <xs:sequence>
301         <xs:element name="Loop" type="sp:NodeListType" minOccurs="1" maxOccurs="
                unbounded" />
302       </xs:sequence>
303     </xs:complexType>
304
305     <xs:complexType name="EdgeListType">
306       <!-- SUB-ELEMENTS -->
307       <xs:sequence>
308         <xs:element name="Edge" minOccurs="1" maxOccurs="unbounded">
309           <xs:complexType>
310             <xs:attribute name="IdEdge" type="xs:int" use="required" />
311           </xs:complexType>
312         </xs:element>
313       </xs:sequence>
314     </xs:complexType>
315
316     <xs:complexType name="EdgeLoopListType">
317       <!-- SUB-ELEMENTS -->
318       <xs:sequence>
319         <xs:element name="Loop" type="sp:EdgeListType" minOccurs="1" maxOccurs="
                unbounded" />
320       </xs:sequence>
321     </xs:complexType>
322
323
324
325     <!--          -->
326     <!-- GENERAL -->
327     <!--          -->
328
329     <xs:simpleType name="VoltageLevelType">
330       <xs:restriction base="xs:decimal">
331         <xs:pattern value="0.4|6.6|22|66|230|400" />
332       </xs:restriction>
333     </xs:simpleType>
334
335 </xs:schema>
```

A.2 Topological, Electrical, and Economic Metrics of the Cost-optimized Singapore PNM

Property	LV	MV	HV
Topological			
Nodes n [#]	126 571	11 842	33
Consumer n_{PQ}	116 447	1 405	0
Substations n_{PV}	10 124	313	4
Per independent part, average $\bar{n}_p$	3	15.24	33
Edges m [#]	116 447	12 557	59
Independent parts p [#]	58 131	830	1
Edge length, average $\bar{l}$ [m]	181	1 015	8 674
Edge length, total l [km]	21 053	12 740	512
Average distance, geographical $\bar{\delta}$ [m]			
Any-to-Any $\bar{\delta}_{\mathrm{g,A2A}}$	242	2 714	21 129
PQ-to-PV $\bar{\delta}_{\mathrm{g,PQ2PV}}$	316	2 808	22 598
Average path length apl			
Geodesic apl_{d} [#]	1.32	4.1	3.12
Geographical apl_{g} [m]	237	4 516	26 350
Betweenness b	0.83	0.51	0.18
Clustering coefficient cc	0	0.0079	0.2636
Density d	0	0.0002	0.1117
Diameter $\varnothing$			
Geodesic $\varnothing_{\mathrm{d}}$ [#]	10	44	6
Geographical $\varnothing_{\mathrm{g}}$ [m]	8 122	30 743	63 754
Node degree			
Maximum $deg_{\max}$	221	20	6
Mean deg	1.84	2.12	3.58
Probability distribution $P(k) \sim \beta$ (R^2)	2.59 (0.93)	–	–
Pearson correlation coefficient ρ	0.16	-0.02	-0.04
Electrical			
Power demand P_{D} [MW]	2 177	6 400	6 677
Power supply P_{S} [MW]	2 236	6 677	6 723
Power loss P_{L} [%]	2.5	3.97	0.76
Utilization, average [%]			
Power line $\bar{u}_{\mathrm{PL}}$	18	6	4
Substation $\bar{u}_{\mathrm{PV}}$	17	97	11
Voltage at consumer, average $\bar{V}$ [pu]	0.9886	0.9803	0.99
Economic			
Costs [US\$·10^6]	139	596	2 021
Edge C_{E}	1	406	1 654
Node (Substation) C_{N}	138	190	367

Bibliography

[1] Navigant Research. Transportation forecast: Light duty vehicles: Global market forecasts, 2015-2035. Technical report, 2015.

[2] Umweltbundesamt. Daten zum Verkehr. https://www.umweltbundesamt.de/sites/default/files/medien/publikation/long/4364.pdf, 2012. Last accessed 19th December 2016.

[3] BMW. Der BMW i3. http://www.bmw.de/dam/brandBM/marketDE/countryDE/newvehicles/allfacts/catalogue/BMW_i3_Katalog.pdf?download.1424447309599.pdf. Last accessed 19th December 2016.

[4] P. Icha and G. Kuhs. Entwicklung der spezifischen Kohlendioxid-Emissionen des deutschen Strommix in den Jahren 1990 bis 2015. *Climate Change*, 26, 2016. https://www.umweltbundesamt.de/sites/default/files/medien/378/publikationen/climate_change_26_2016_entwicklung_der_spezifischen_kohlendioxid-emissionen_des_deutschen_strommix.pdf.

[5] K. Young, C. Wang, L.Y. Wang, and K. Strunz. Electric vehicle battery technologies. In *Electric Vehicle Integration into Modern Power Networks*, pages 15–56. Springer Nature, Oct 2013. doi: 10.1007/978-1-4614-0134-6_2.

[6] Z. Kravanja, P.S. Varbanov, and J.J. Klemeš. Recent advances in green energy and product productions, environmentally friendly, healthier and safer technologies and processes, CO2 capturing, storage and recycling, and sustainability assessment in decision-making. *Clean Technologies and Environmental Policy*, 17(5):1119–1126, Jun 2015. ISSN 1618-9558. doi: 10.1007/s10098-015-0995-9.

[7] Wikipedia. Government incentives for plug-in electric vehicles. https://en.wikipedia.org/wiki/Government_incentives_for_plug-in_electric_vehicles. Last accessed 19th December 2016.

[8] L. Gustafsson and M. Sternad. Consistent micro, macro and state-based population modelling. *Mathematical Biosciences*, 225(2):94–107, Jun 2010. doi: 10.1016/j.mbs.2010.02.003.

[9] E. Bonabeau. Agent-based modeling: Methods and techniques for simulating human systems. *Proceedings of the National Academy of Sciences*, 99(Supplement 3):7280–7287, May 2002. doi: 10.1073/pnas.082080899.

[10] D. Ciechanowicz, H. Aydt, M. Lees, A. Knoll, and T. Hamacher. A universal scheme for modeling energy systems. Technical Report TUM-I1341, Technische Universität München, 2013.

[11] H. Seifi and M. Sadegh Sepasian. *Electric Power System Planning: Issues, Algorithms and Solutions*. Springer, Berlin, Heidelberg, 2011. doi: 10.1007/978-3-642-17989-1.

[12] D. Ciechanowicz, D. Pelzer, B. Bartenschlager, and A. Knoll. A modular power system planning and power flow simulation framework for generating and evaluating power network models. *IEEE Transactions on Power Systems*, 32(3):2214–2224, 2017. ISSN 0885-8950. doi: 10.1109/tpwrs.2016.2602479.

[13] D. Pelzer, D. Ciechanowicz, H. Aydt, and A. Knoll. A price-responsive dispatching strategy for vehicle-to-grid: An economic evaluation applied to the case of Singapore. *Journal of Power Sources*, 256:345–353, Jun 2014. ISSN 0378-7753. doi: 10.1016/j.jpowsour.2014.01.076.

[14] D. Ciechanowicz, A. Knoll, P. Osswald, and D. Pelzer. Towards a business case for vehicle-to-grid—maximizing profits in ancillary service markets. In S. Rajakaruna, F. Shahnia, and A. Ghosh, editors, *Plug In Electric Vehicles in Smart Grids: Energy Management*, pages 203–231. Springer Nature, Singapore, Nov 2015. ISBN 978-981-287-302-6. doi: 10.1007/978-981-287-302-6_8.

[15] D. Pelzer, D. Ciechanowicz, and A. Knoll. Energy arbitrage through smart scheduling of battery energy storage considering battery degradation and electricity price forecasts. In *Proceedings of PES Innovative Smart Grid Technologies Asian Conference (ISGT)*. Institute of Electrical and Electronics Engineers (IEEE), 2016.

[16] K.U. Rao. *Elements of Electrical Engineering*. I.K. International Publishing House, 2015. ISBN 978-93-84588-21-2.

[17] J. Wu. *Advances in K-means Clustering: A Data Mining Thinking*. Springer, Berlin, Heidelberg, 2012. doi: 10.1007/978-3-642-29807-3.

[18] P.-D. Belanger. Equal k-means clustering in java. `https://code.google.com/archive/p/ekmeans/`. Last accessed 19th December 2016.

[19] ELKI. Same-size k-means variation. `http://elki.dbs.ifi.lmu.de/wiki/Tutorial/SameSizeKMeans/`. Last accessed 19th December 2016.

[20] H. Barati, M.A. Sabzivand, M. Joorabian, and K. Sheikhi. Optimal location and sizing of HV/MV substation using the branch and bound method in distribution network of dezful city. *International Journal on Technical and Physical Problems of Engineering (IJTPE)*, 5(15):44–55, Jun 2013.

[21] M. Ester, H.P. Kriegel, J. Sander, and X. Xu. A density-based algorithm for discovering clusters in large spatial databases with noise. In E. Simoudis, J. Han, and U. Fayyad, editors, *2nd International Conference on Knowledge Discovery and Data Mining*, pages 226–231, Portland, Oregon, 1996. AAAI Press.

[22] Apache. DBSCAN (density-based spatial clustering of applications with noise) algorithm. `https://commons.apache.org/proper/commons-math/apidocs/org/apache/`

commons/math3/ml/clustering/DBSCANClusterer.html. Last accessed 31st March 2016.

[23] W.J. Cook. *In Pursuit of the Traveling Salesman: Mathematics at the Limits of Computation*. Walter de Gruyter GmbH, Jan 2014. doi: 10.1515/9781400839599.

[24] P. Stubbings. Fast local search for travelling salesman problem. https://github.com/phil8192/tsp-java. Last accessed 19th December 2016.

[25] R.E. Neapolitan. *Foundations of Algorithms*. Jones & Bartlett Learning, 2014.

[26] F. Aurenhammer, R. Klein, and D.-T. Lee. *Voronoi Diagrams and Delaunay Triangulations*. World Scientific Publishing, Nov 2013. ISBN 9814447633. doi: 10.1142/8685.

[27] P. Chew. Delaunay triangulation. http://www.cs.cornell.edu/home/chew/Delaunay.html. Last accessed 19th December 2016.

[28] B. Saravanan, S. Das, S. Sikri, and D.P. Kothari. A solution to the unit commitment problem—a review. *Frontiers in Energy*, 7(2):223–236, Apr 2013. ISSN 2095-1698. doi: 10.1007/s11708-013-0240-3.

[29] B. Stott, J. Jardim, and O. Alsac. DC power flow revisited. *IEEE Transactions on Power Systems*, 24(3):1290–1300, Aug 2009. ISSN 0885-8950. doi: 10.1109/tpwrs.2009.2021235.

[30] C. Coffrin and P. Van Hentenryck. A linear-programming approximation of AC power flows. *INFORMS Journal on Computing*, 26(4):718–734, Nov 2014. doi: 10.1287/ijoc.2014.0594.

[31] R. Lincoln. JPOWER - a software package for solving electrical power flow and optimal power flow problems. https://github.com/rwl/JPOWER/. Last accessed 19th December 2016.

[32] R.D. Zimmerman, C.E. Murillo-Sánchez, and R.J. Thomas. MATPOWER: Steady-state operations, planning, and analysis tools for power systems research and education. *IEEE Transactions on Power Systems*, 26(1):12–19, Feb 2011. doi: 10.1109/tpwrs.2010.2051168.

[33] B.M. Weedy, B.J. Cory, N. Jenkins, J.B. Ekanayake, and G. Strbac. *Electric Power Systems*. Wiley, 2012. ISBN 9781118361092.

[34] T. Tingting, L. Yang, L. Ying, and J. Tong. The analysis of the convergence of Newton-Raphson method based on the current injection in distribution network case. *International Journal of Computer and Electrical Engineering*, 5(3):288–290, 2013. doi: 10.7763/ijcee.2013.v5.714.

[35] D. Pelzer. *A Modular Framework for Optimizing Grid Integration of Mobile and Stationary Battery Energy Storage in Smart Grids*. PhD thesis, Technische Universität München, Munich, Germany, 2018.

[36] M. Ecker, N. Nieto, S. Käbitz, J. Schmalstieg, H. Blanke, A. Warnecke, and D.U. Sauer. Calendar and cycle life study of Li(NiMnCo)O2-based 18650 lithium-ion batteries. *Journal of Power Sources*, 248:839–851, Feb 2014. ISSN 03787753. doi: 10.1016/j.jpowsour.2013.09.143.

[37] J. Schmalstieg, S. Käbitz, M. Ecker, and D.U. Sauer. A holistic aging model for Li(NiMnCo)O2 based 18650 lithium-ion batteries. *Journal of Power Sources*, 257: 325–334, Jul 2014. ISSN 0378-7753. doi: 10.1016/j.jpowsour.2014.02.012.

[38] D.P. Bertsekas. *Dynamic Programming and Optimal Control*. Athena Scientific, Belmont, Massachusetts, 4th edition, 2012. ISBN 1886529086.

[39] E. Estrada. Introduction to complex networks: Structure and dynamics. In *Lecture Notes in Mathematics*, pages 93–131. Springer Nature, Oct 2015. doi: 10.1007/978-3-319-11322-7_3.

[40] G.A. Pagani and M. Aiello. Towards decentralization: A topological investigation of the medium and low voltage grids. *IEEE Transactions on Smart Grid*, 2(3):538–547, Sep 2011. ISSN 1949-3053. doi: 10.1109/tsg.2011.2147810.

[41] G.A. Pagani and M. Aiello. Power grid network evolutions for local energy trading. *arXiv preprint arXiv:1201.0962*, 2012.

[42] G.A. Pagani and M. Aiello. From the grid to the smart grid, topologically. *Physica A: Statistical Mechanics and its Applications*, 449:160–175, May 2013. doi: 10.1016/j.physa.2015.12.080.

[43] R. Albert, I. Albert, and G.L. Nakarado. Structural vulnerability of the North American power grid. *Physical Review E*, 69(2), Feb 2004. doi: 10.1103/physreve.69.025103.

[44] P. Crucitti, V. Latora, and M. Marchiori. A topological analysis of the Italian electric power grid. *Physica A: Statistical Mechanics and its Applications*, 338(1-2):92–97, Jul 2004. doi: 10.1016/j.physa.2004.02.029.

[45] K. Sun. Complex networks theory: A new method of research in power grid. In *Transmission & Distribution Conference & Exposition: Asia and Pacific*, pages 1–6. Institute of Electrical and Electronics Engineers (IEEE), 2005. doi: 10.1109/tdc.2005.1547099.

[46] A.J. Holmgren. Using graph models to analyze the vulnerability of electric power networks. *Risk Analysis*, 26(4):955–969, Aug 2006. doi: 10.1111/j.1539-6924.2006.00791.x.

[47] J. Ding, X. Bai, W. Zhao, Z. Fang, Z. Li, and M. Liu. The improvement of the small-world network model and its application research in bulk power system. In *International Conference on Power System Technology*, pages 1–5. Institute of Electrical and Electronics Engineers (IEEE), Oct 2006. doi: 10.1109/icpst.2006.321710.

[48] V. Rosato, S. Bologna, and F. Tiriticco. Topological properties of high-voltage electrical transmission networks. *Electric Power Systems Research*, 77(2):99–105, Feb 2007. doi: 10.1016/j.epsr.2005.05.013.

[49] R.V. Solé, M. Rosas-Casals, B. Corominas-Murtra, and S. Valverde. Robustness of the european power grids under intentional attack. *Physical Review E*, 77(2), Feb 2008. doi: 10.1103/physreve.77.026102.

[50] M. Rosas-Casals and B. Corominas-Murtra. Assessing european power grid reliability by means of topological measures. In *Energy and Sustainability II*. WITPRESS LTD., Jun 2009. doi: 10.2495/esu090471.

[51] P. Hines, S. Blumsack, E. Cotilla-Sanchez, and C. Barrows. The topological and electrical structure of power grids. In *43rd Hawaii International Conference on System Sciences*, pages 1–10. Institute of Electrical and Electronics Engineers (IEEE), 2010. doi: 10.1109/hicss.2010.398.

[52] Z. Wang, A. Scaglione, and R. J. Thomas. Generating statistically correct random topologies for testing smart grid communication and control networks. *IEEE Transactions on Smart Grid*, 1(1):28–39, Jun 2010. ISSN 1949-3053. doi: 10.1109/tsg.2010.2044814.

[53] P. Han and S. Zhang. Analysis of cascading failures in small-world power grid. *International Journal of Energy Science*, 1(2), 2011.

[54] C.D. Brummitt, R.M. D'Souza, and E.A. Leicht. Suppressing cascades of load in interdependent networks. *Proceedings of the National Academy of Sciences*, 109(12): E680–E689, Feb 2012. doi: 10.1073/pnas.1110586109.

[55] B. Cloteaux. Limits in modeling power grid topology. In *2nd Network Science Workshop (NSW)*, pages 16–22. Institute of Electrical and Electronics Engineers (IEEE), Apr 2013. doi: 10.1109/nsw.2013.6609189.

[56] J. Hu, L. Sankar, and D.J. Mir. Cluster-and-connect: A more realistic model for the electric power network topology. In *International Conference on Smart Grid Communications (SmartGridComm)*, pages 85–90. Institute of Electrical and Electronics Engineers (IEEE), Nov 2015. doi: 10.1109/smartgridcomm.2015.7436281.

[57] S. Soltan and G. Zussman. A statistical method for synthetic power grid generation based on the US western interconnection. *SIAM Workshop on Network Science*, 15, 2015.

[58] N.T. Vempati and R.T. Mitta. Small world network. `http://best.eng.buffalo.edu/teaching.html`. Last accessed 19$^{\text{th}}$ December 2016.

[59] M.E.J. Newman. *Networks: An Introduction*. Oxford University Press (OUP), New York, NY, Mar 2010. ISBN 9780199206650. doi: 10.1093/acprof:oso/9780199206650.001.0001.

[60] K. Thulasiraman and M.N.S. Swamy. *Graphs: Theory and algorithms*. Wiley-Blackwell, Mar 2011. doi: 10.1002/9781118033104.

[61] L. Lovász. *Large Networks and Graph Limits*. American Mathematical Society, Dec 2012. doi: 10.1090/coll/060.

[62] E. Estrada. *The Structure of Complex Networks: Theory and Applications*. Oxford University Press (OUP), Oct 2012. doi: 10.1093/acprof:oso/9780199591756.001.0001.

[63] J.A.G. Conejo, G.T. Bartolome, A.G. Exposito, and M.R. Montanes. ANETO: A system for the automatic generation of theoretical network models. In *9th International Conference on Electrical Power Quality and Utilisation*, pages 1–6. Institute of Electrical and Electronics Engineers (IEEE), Oct 2007. doi: 10.1109/epqu.2007.4424189.

[64] A. Navarro and H. Rudnick. Large-scale distribution planning – part I: Simultaneous network and transformer optimization. *IEEE Transactions on Power Systems*, 24(2): 744–751, May 2009. ISSN 0885-8950. doi: 10.1109/tpwrs.2009.2016593.

[65] A. Navarro and H. Rudnick. Large-scale distribution planning – part II: Macro-optimization with voronoi's diagram and tabu search. *IEEE Transactions on Power Systems*, 24(2):752–758, May 2009. ISSN 0885-8950. doi: 10.1109/tpwrs.2009.2016594.

[66] C.M. Domingo, T.G.S. Román, A. Sánchez-Miralles, J.P.P. González, and A.C. Martiánez. A reference network model for large-scale distribution planning with automatic street map generation. *IEEE Transactions on Power Systems*, 26(1):190–197, Feb 2011. ISSN 0885-8950. doi: 10.1109/tpwrs.2010.2052077.

[67] T. Gomez, C. Mateo, A. Sanchez, P. Frias, and R. Cossent. Reference network models: A computational tool for planning and designing large-scale smart electricity distribution grids. In S.K. Khaitan and A. Gupta, editors, *High Performance Computing in Power and Energy Systems*, Power Systems, pages 247–279. Springer Nature, Berlin, Heidelberg, 2013. ISBN 978-3-642-32682-0. doi: 10.1007/978-3-642-32683-7_9.

[68] L. González-Sotres, C. Mateo Domingo, A. Sánchez-Miralles, and M. Alvar Miró. Large-scale MV/LV transformer substation planning considering network costs and flexible area decomposition. *IEEE Transactions on Power Delivery*, 28(4):2245–2253, Oct 2013. ISSN 0885-8977. doi: 10.1109/tpwrd.2013.2258944.

[69] P.S. Georgilakis and N.D. Hatziargyriou. A review of power distribution planning in the modern power systems era: Models, methods and future research. *Electric Power Systems Research*, 121:89–100, Apr 2015. ISSN 0378-7796. doi: 10.1016/j.epsr.2014.12.010.

[70] S. Haffner, L.F.A. Pereira, L.A. Pereira, and L.S. Barreto. Multistage model for distribution expansion planning with distributed generation – part I: Problem formulation. *IEEE Transactions on Power Delivery*, 23(2):915–923, 2008.

[71] R.C. Lotero and J. Contreras. Distribution system planning with reliability. *IEEE Transactions on Power Delivery*, 26(4):2552–2562, Oct 2011. doi: 10.1109/tpwrd.2011.2167990.

[72] J. Shu, L. Wu, Z. Li, M. Shahidehpour, L. Zhang, and B. Han. A new method for spatial power network planning in complicated environments. *IEEE Transactions on Power Systems*, 27(1):381–389, Feb 2012. ISSN 0885-8950. doi: 10.1109/tpwrs.2011.2161351.

[73] A.S. Bin Humayd and K. Bhattacharya. Comprehensive multi-year distribution system planning using back-propagation approach. *IET Generation, Transmission & Distribution*, 7(12):1415–1425, Dec 2013. doi: 10.1049/iet-gtd.2012.0706.

[74] R.H. Fletcher and K. Strunz. Optimal distribution system horizon planning – part I: Formulation. *IEEE Transactions on Power Systems*, 22(2):791–799, 2007.

[75] H.M. Khodr, Z.A. Vale, and C. Ramos. A benders decomposition and fuzzy multicriteria approach for distribution networks remuneration considering DG. *IEEE Transactions on Power Systems*, 24(2), 2009.

[76] S. Wong, K. Bhattacharya, and J.D. Fuller. Electric power distribution system design and planning in a deregulated environment. *IET Generation, Transmission & Distribution*, 3(12):1061–1078, Dec 2009. ISSN 1751-8687. doi: 10.1049/iet-gtd.2008.0553.

[77] X. Lin, J. Sun, S. Ai, X. Xiong, Y. Wan, and D. Yang. Distribution network planning integrating charging stations of electric vehicle with V2G. *International Journal of Electrical Power & Energy Systems*, 63:507–512, Dec 2014. doi: 10.1016/j.ijepes.2014.06.043.

[78] Ž.N. Popović and D.S. Popović. Graph theory based formulation of multi-period distribution expansion problems. *Electric Power Systems Research*, 80(10):1256–1266, Oct 2010. doi: 10.1016/j.epsr.2010.04.009.

[79] S. Ganguly, N.C. Sahoo, and D. Das. Multi-objective planning of electrical distribution systems using dynamic programming. *International Journal of Electrical Power & Energy Systems*, 46:65–78, Mar 2013. doi: 10.1016/j.ijepes.2012.10.030.

[80] J.E. Mendoza, M.E. López, S.C. Fingerhuth, H.E. Peña, and C.A. Salinas. Low voltage distribution planning considering micro distributed generation. *Electric Power Systems Research*, 103:233–240, Oct 2013. doi: 10.1016/j.epsr.2013.05.020.

[81] T.-H. Chen, E.-H. Lin, N.-C. Yang, and T.-Y. Hsieh. Multi-objective optimization for upgrading primary feeders with distributed generators from normally closed loop to mesh arrangement. *International Journal of Electrical Power & Energy Systems*, 45(1):413–419, Feb 2013. doi: 10.1016/j.ijepes.2012.09.017.

[82] A. Zidan, M.F. Shaaban, and E.F. El-Saadany. Long-term multi-objective distribution network planning by DG allocation and feeders' reconfiguration. *Electric Power Systems Research*, 105:95–104, Dec 2013. ISSN 0378-7796. doi: 10.1016/j.epsr.2013.07.016.

[83] B. Zeng, J. Zhang, X. Yang, J. Wang, J. Dong, and Y. Zhang. Integrated planning for transition to low-carbon distribution system with renewable energy generation and demand response. *IEEE Transactions on Power Systems*, 29(3):1153–1165, May 2014. doi: 10.1109/tpwrs.2013.2291553.

[84] L.W. Oliveira, F.V. Gomes, E.J. Oliveira, A.R. Oliveira, A.M. Variz, and H.A. Silva. Power distribution systems planning with distributed thermal and wind generation. In *PowerTech*, pages 1–6, Eindhoven, Netherlands, Jun 2015. Institute of Electrical and Electronics Engineers (IEEE). doi: 10.1109/ptc.2015.7232827.

[85] W. Yao, J. Zhao, F. Wen, Z. Dong, Y. Xue, Y. Xu, and K. Meng. A multi-objective collaborative planning strategy for integrated power distribution and electric vehicle charging systems. *IEEE Transactions on Power Systems*, 29(4):1811–1821, Jul 2014. doi: 10.1109/tpwrs.2013.2296615.

[86] D. Kumar, S.R. Samantaray, and G. Joos. A reliability assessment based graph theoretical approach for feeder routing in power distribution networks including distributed generations. *International Journal of Electrical Power & Energy Systems*, 57:11–30, May 2014. doi: 10.1016/j.ijepes.2013.11.039.

[87] D. Kumar and S.R. Samantaray. Design of an advanced electric power distribution systems using seeker optimization algorithm. *International Journal of Electrical Power & Energy Systems*, 63:196–217, Dec 2014. doi: 10.1016/j.ijepes.2014.05.073.

[88] V.A. Evangelopoulos and P.S. Georgilakis. Optimal distributed generation placement under uncertainties based on point estimate method embedded genetic algorithm. *IET Generation, Transmission & Distribution*, 8(3):389–400, Mar 2014. doi: 10.1049/iet-gtd.2013.0442.

[89] K. Rajesh, A. Bhuvanesh, S. Kannan, and C. Thangaraj. Least cost generation expansion planning with solar power plant using differential evolution algorithm. *Renewable Energy*, 85:677–686, Jan 2016. doi: 10.1016/j.renene.2015.07.026.

[90] I.J. Ramirez-Rosado and J.A. Dominguez-Navarro. New multiobjective tabu search algorithm for fuzzy optimal planning of power distribution systems. *IEEE Transactions on Power Systems*, 21(1):224–233, Feb 2006. ISSN 0885-8950. doi: 10.1109/tpwrs.2005.860946.

[91] A.M. Cossi, R. Romero, and J.R.S. Mantovani. Planning and projects of secondary electric power distribution systems. *IEEE Transactions on Power Systems*, 24(3):1599–1608, Aug 2009. ISSN 0885-8950. doi: 10.1109/tpwrs.2009.2021208.

[92] B.R. Pereira Junior, A.M. Cossi, J. Contreras, and J.R. Sanches Mantovani. Multiobjective multistage distribution system planning using tabu search. *IET Generation, Transmission & Distribution*, 8(1):35–45, Jan 2014. ISSN 1751-8687. doi: 10.1049/iet-gtd.2013.0115.

[93] N.C. Koutsoukis, P.S. Georgilakis, and N.D. Hatziargyriou. A tabu search method for distribution network planning considering distributed generation and uncertainties. In *International Conference on Probabilistic Methods Applied to Power Systems (PMAPS)*, pages 1–6. Institute of Electrical and Electronics Engineers (IEEE), Jul 2014. doi: 10.1109/pmaps.2014.6960627.

[94] I. Ziari. *Planning of distribution network for medium voltage and low voltage*. PhD thesis, Queensland University of Technology, 2011.

[95] I. Ziari, G. Ledwich, and A. Ghosh. Optimal integrated planning of MV–LV distribution systems using DPSO. *Electric Power Systems Research*, 81(10):1905–1914, Oct 2011. ISSN 0378-7796. doi: 10.1016/j.epsr.2011.05.015.

[96] M. Gomez-Gonzalez, A. López, and F. Jurado. Optimization of distributed generation systems using a new discrete PSO and OPF. *Electric Power Systems Research*, 84(1):174–180, Mar 2012. doi: 10.1016/j.epsr.2011.11.016.

[97] M.E. Samper and A. Vargas. Investment decisions in distribution networks under uncertainty with distributed generation – part I: Model formulation. *IEEE Transactions on Power Systems*, 28(3):2331–2340, Aug 2013. ISSN 0885-8950. doi: 10.1109/tpwrs.2013.2239666.

[98] M.E. Samper and A. Vargas. Investment decisions in distribution networks under uncertainty with distributed generation – part II: Implementation and results. *IEEE*

Transactions on Power Systems, 28(3):2341–2351, Aug 2013. ISSN 0885-8950. doi: 10.1109/tpwrs.2013.2239667.

[99] M. Sedghi, M. Aliakbar-Golkar, and M.R. Haghifam. Distribution network expansion considering distributed generation and storage units using modified PSO algorithm. *International Journal of Electrical Power & Energy Systems*, 52:221–230, Nov 2013. doi: 10.1016/j.ijepes.2013.03.041.

[100] M. Gitizadeh, A.A. Vahed, and J. Aghaei. Multistage distribution system expansion planning considering distributed generation using hybrid evolutionary algorithms. *Applied Energy*, 101:655–666, Jan 2013. doi: 10.1016/j.apenergy.2012.07.010.

[101] R. Hemmati, R.-A. Hooshmand, and N. Taheri. Distribution network expansion planning and DG placement in the presence of uncertainties. *International Journal of Electrical Power & Energy Systems*, 73:665–673, Dec 2015. doi: 10.1016/j.ijepes.2015.05.024.

[102] J.M. Nahman and D.M. Peric. Optimal planning of radial distribution networks by simulated annealing technique. *IEEE Transactions on Power Systems*, 23(2):790–795, May 2008. ISSN 0885-8950. doi: 10.1109/tpwrs.2008.920047.

[103] Ž.N. Popović, V.D. Kerleta, and D.S. Popović. Hybrid simulated annealing and mixed integer linear programming algorithm for optimal planning of radial distribution networks with distributed generation. *Electric Power Systems Research*, 108:211–222, Mar 2014. doi: 10.1016/j.epsr.2013.11.015.

[104] S. Verma and V. Mukherjee. Transmission expansion planning: A review. In *International Conference on Energy Efficient Technologies for Sustainability (ICEETS)*, pages 350–355. Institute of Electrical and Electronics Engineers (IEEE), Apr 2016. doi: 10.1109/iceets.2016.7583779.

[105] N. Voropai. Power system expansion planning - state of the problem. *Global Journal of Technology and Optimization*, 6(2), 2015. doi: 10.4172/2229-8711.1000176.

[106] R.Y. Rubinstein and D.P. Kroese. *Simulation and the Monte Carlo Method*. Wiley Series in Probability and Statistics. John Wiley & Sons, Inc., 3rd edition, Dec 2016. doi: 10.1002/9780470230381.

[107] A. Reutlinger, G. Schurz, and A. Hüttemann. Ceteris paribus laws. In E.N. Zalta, editor, *The Stanford Encyclopedia of Philosophy*. Fall edition, 2015.

[108] R. Koch, R. Kuhn, I. Zilberman, and A. Jossen. Electrochemical impedance spectroscopy for online battery monitoring - power electronics control. In *16th European Conference on Power Electronics and Applications*, pages 1–10. Institute of Electrical and Electronics Engineers (IEEE), Aug 2014. doi: 10.1109/epe.2014.6910907.

[109] O. Topçu, U. Durak, H. Oğuztüzün, and L. Yilmaz. *Distributed Simulation: A Model Driven Engineering Approach (Simulation Foundations, Methods and Applications)*. Springer, 2nd edition, 2016.

[110] Modeling & Simulation Coordination Office (M&S CO). High Level Architecture (HLA). `http://msco.mil/hla.html`. Last accessed 19th December 2016.

[111] IEEE. IEEE standard for Modeling and Simulation (M&S) High Level Architecture (HLA)– framework and rules. *IEEE Std. 1516-2000*, 2000. doi: 10.1109/ieeestd.2000.92296.

[112] IEEE. IEEE standard for Modeling and Simulation (M&S) High Level Architecture (HLA)– framework and rules. *IEEE Std. 1516-2010 (Revision of IEEE Std 1516-2000)*, pages 1–38, Aug 2010. doi: 10.1109/ieeestd.2010.5553440.

[113] IEEE. IEEE standard for Modeling and Simulation (M&S) High Level Architecture (HLA)– object model template (OMT) specification. *IEEE Std 1516.2-2010 (Revision of IEEE Std 1516.2-2000)*, pages 1–112, Aug 2010. doi: 10.1109/ieeestd.2010.5953408.

[114] T. Bray, J. Paoli, C.M. Sperberg-McQueen, E. Maler, and F. Yergeau. W3C extensible markup language (XML) 1.0. *W3C Recommendation*, 2008.

[115] S. Gao, C.M. Sperberg-McQueen, and H.S. Thompson. W3C XML Schema Definition Language (XSD) 1.1 Part 1: Structures. *W3C Recommendation*, 2012.

[116] D. Peterson, S. Gao, A. Malhotra, C.M. Sperberg-McQueen, and H.S. Thompson. W3C XML Schema Definition Language (XSD) 1.1 Part 2: Datatypes. *W3C Recommendation*, 2012.

[117] ISO/IEC. ISO/IEC Document Schema Definition Languages (DSDL) – rule-based validation - schematron. *ISO/IEC Std. 19757-3:2006*, 2006.

[118] IEEE. IEEE standard for Modeling and Simulation (M&S) High Level Architecture (HLA)– federate interface specification. *IEEE Std 1516.1-2010 (Revision of IEEE Std 1516.1-2000)*, pages 1–378, Aug 2010. doi: 10.1109/ieeestd.2010.5954120.

[119] P. Ross. Comparison of high level architecture run-time infrastructure wire protocols – part one. In *SimTecT 2012*, 2012.

[120] P. Ross. Comparison of high level architecture run-time infrastructure wire protocols – part two. In *Fall Simulation Interoperability Workshop*, pages 8–12, Florida Mall Conference Center, Orlando, United States, 2014.

[121] S. Ghosh. *Distributed Systems: An Algorithmic Approach*. Chapman and Hall/CRC, 2014. doi: 10.1201/9781420010848.

[122] Modeling & Simulation Coordination Office (M&S CO). Test procedures for RTIs. `http://www.msco.mil/procedures1516.html`. Last accessed 31st March 2016.

[123] M. Dawson, G. Johnson, and A. Low. Best practices for using the Java Native Interface. `http://www.ibm.com/developerworks/library/j-jni/j-jni-pdf.pdf`, 2009. Last accessed 19th December 2016.

[124] B. Watrous, L. Granowetter, and D. Wood. HLA federation performance: What really matters. In *Proceedings of the Fall Simulation Interoperability Workshop*, 2006.

[125] S. Nandi, F. Rodriguez, D.D. Wood, and L. Granowetter. The MÄK high-performance RTI : Performance by design. 2015.

[126] B.K. Choi and D. Kang. *Modeling and Simulation of Discrete-Event Systems*. Wiley-Blackwell, Aug 2013. doi: 10.1002/9781118732793.

[127] D. Zehe, A. Knoll, W. Cai, and H. Aydt. SEMSim cloud service: Large-scale urban systems simulation in the cloud. *Simulation Modelling Practice and Theory*, 58:157–171, Nov 2015. ISSN 1569-190X. doi: 10.1016/j.simpat.2015.05.005.

[128] V. Viswanathan, D. Zehe, J. Ivanchev, D. Pelzer, A. Knoll, and H. Aydt. Simulation-assisted exploration of charging infrastructure requirements for electric vehicles in urban environments. *Journal of Computational Science*, 12:1–10, Jan 2016. ISSN 1877-7503. doi: 10.1016/j.jocs.2015.10.012.

[129] Navteq. We are HERE. `http://www.navteq.com/`. Last accessed 19th December 2016.

[130] H. Ortega-Arranz, D.R. Llanos, and A. Gonzalez-Escribano. The shortest-path problem: Analysis and comparison of methods. *Synthesis Lectures on Theoretical Computer Science*, 1(1):1–87, Dec 2014. doi: 10.2200/s00618ed1v01y201412tcs001.

[131] LTA. Household interview travel survey. `http://www.lta.gov.sg/apps/news/page.aspx?c=2&id=1b6b1e1e-f727-43bb-8688-f589056ad1c4`, 2012. Last accessed 19th December 2016.

[132] Land Transport Authority (LTA). Singapore land transport statistics in brief. `https://www.lta.gov.sg/content/dam/ltaweb/corp/PublicationsResearch/files/FactsandFigures/Statistics%20in%20Brief%202015%20FINAL.pdf`, 2015. Last accessed 19th December 2016.

[133] C. Reas and B. Fry. *Getting Started with Processing: A Hands-On Introduction to Making Interactive Graphics*. Maker Media, Inc., 2nd edition, 2015.

[134] OpenGL. The industry's foundation for high performance graphics. `https://www.opengl.org/`. Last accessed 19th December 2016.

[135] R. Smith. *Simulation Interoperability: Challenges in Linking Live, Virtual, and Constructive Systems*. Modelbenders Press, 2009. ISBN 9780982304051.

[136] J.W. Hollenbach. Inconsistency, neglect, and confusion: A historical review of DoD distributed simulation architecture policies. In *Proceedings of the Spring Simulation Interoperability Workshop*, pages 23–27, 2009.

[137] VT MÄK. VR-Exchange: Protocol translation & bridging. `http://www.mak.com/products/link/vr-exchange`. Last accessed 19th December 2016.

[138] R.M. Weatherly, A.L. Wilson, B.S. Canova, E.H. Page, A.A. Zabek, and M.C. Fischer. Advanced distributed simulation through the aggregate level simulation protocol. In *29th Hawaii International Conference on System Sciences (HICSS)*, volume 1, pages 407–4151. Institute of Electrical and Electronics Engineers (IEEE), Jan 1996. doi: 10.1109/hicss.1996.495488.

[139] OMG. Common object request broker architecture (CORBA) specification – part 1: Corba interfaces. *OMG Specifications*, 2012.

[140] OMG. Common object request broker architecture (CORBA) specification – part 2: Corba interoperability. *OMG Specifications*, 2012.

[141] OMG. Common object request broker architecture (CORBA) specification – part 3: Corba component model. *OMG Specifications*, 2012.

[142] ISO/IEC. Common object request broker architecture (CORBA) – part 1: Interfaces. *ISO/IEC Std. 19500-1:2012*, 2012.

[143] ISO/IEC. Common object request broker architecture (CORBA) – part 2: Interoperability. *ISO/IEC Std. 19500-2:2012*, 2012.

[144] ISO/IEC. Common object request broker architecture (CORBA) – part 3: Components. *ISO/IEC Std. 19500-3:2012*, 2012.

[145] OMG. Interface definition language, version 3.5. *OMG Specifications*, 2014.

[146] A. D'Ambrogio and D. Gianni. Using CORBA to enhance HLA interoperability in distributed and web-based simulation. In C. Aykanat, T. Dayar, and İ. Körpeoğlu, editors, *Lecture Notes in Computer Science*, pages 696–705. Springer Nature, 2004. ISBN 978-3-540-30182-0. doi: 10.1007/978-3-540-30182-0_70.

[147] OMG. CORBA. `http://www.corba.org`. Last accessed 19th December 2016.

[148] OMG. OMG standard for Data Distribution Service (DDS). *OMG Specifications*, 2015.

[149] OMG. OMG DDS interoperability demo. `https://community.rti.com/content/presentation/omg-dds-interoperability-demo-2012`, 2012. Last accessed 19th December 2016.

[150] R. Joshi and G.-P. Castellote. A comparison and mapping of data distribution service and high-level architecture. *Technology, The Netherlands*, 2006.

[151] M.-S. Oh, Y.-H. Son, and K.-C. Lee. An ontology system for interoperation between DDS and HLA. *Indian Journal of Science and Technology*, 8(27), Oct 2015. doi: 10.17485/ijst/2015/v8i27/81175.

[152] J.M. Lopez-Rodriguez, R. Martin, and P. Jimenez. How to develop true distributed real time simulations? Mixing IEEE HLA and OMG DDS standards. *Nextel Aerospace Defense & Security (NADS)*, 2011.

[153] IEEE. IEEE standard for distributed interactive simulation–application protocols. *IEEE Std 1278.1-2012 (Revision of IEEE Std 1278.1-1995)*, pages 1–747, Dec 2012. doi: 10.1109/ieeestd.2012.6387564.

[154] IEEE. IEEE standard for distributed interactive simulation (DIS) – communication services and profiles. *IEEE Std 1278.2-2015 (Revision of IEEE Std 1278.2-1995)*, pages 1–42, Nov 2015. doi: 10.1109/ieeestd.2015.7323777.

[155] IEEE. IEEE recommended practice for distributed interactive simulation - exercise management and feedback. *IEEE Std 1278.3-1996*, 1997. doi: 10.1109/ieeestd.1997.82357.

[156] IEEE. IEEE recommended practice for Distributed Interactive Simulation– verification, validation, and accreditation. *IEEE Std 1278.4-2003 (Reaff 2010)*, pages 1–78, Sep 2013. doi: 10.1109/ieeestd.2013.6595010.

[157] The FMI development group. Functional mock-up interface (FMI). `https://www.fmi-standard.org/`. Last accessed 19th December 2016.

[158] T. Blochwitz, M. Otter, M. Arnold, C. Bausch, C. Clauss, H. Elmqvist, A. Junghanns, J. Mauss, M. Monteiro, T. Neidhold, D. Neumerkel, H. Olsson, J.-V. Peetz, and S. Wolf. The functional mockup interface for tool independent exchange of simulation models. In *Proceedings from the 8th International Modelica Conference*, number 63, pages 105–114, Dresden, Germany, Jun 2011. Linkoping University Electronic Press. doi: 10.3384/ecp11063105.

[159] M.U. Awais, P. Palensky, A. Elsheikh, E. Widl, and S. Matthias. The high level architecture RTI as a master to the functional mock-up interface components. In *International Conference on Computing, Networking and Communications (ICNC)*, pages 315–320. Institute of Electrical and Electronics Engineers (IEEE), Jan 2013. doi: 10.1109/iccnc.2013.6504102.

[160] F. Yilmaz, U. Durak, K. Taylan, and H. Oğuztüzün. Adapting functional mockup units for HLA-compliant distributed simulation. In *10th International Modelica Conference*, pages 247–257, Lund, Sweden, Mar 2014. Linkoping University Electronic Press. doi: 10.3384/ecp14096247.

[161] United States Department of Defense. The test and training enabling architecture: Architecture reference document. Technical report, Foundation Initiative 2010 Project Office, 2002.

[162] E.T. Powell and J.R. Noseworthy. The test and training enabling architecture (TENA). In *Engineering Principles of Combat Modeling and Distributed Simulation*, pages 449–477. Wiley-Blackwell, Feb 2012. doi: 10.1002/9781118180310.ch20.

[163] TENA. Test and training enabling architecture (TENA). `https://www.tena-sda.org/`. Last accessed 19th December 2016.

[164] D.F. Allan and A.M. Farid. A benchmark analysis of open source transportation-electrification simulation tools. In *18th International Conference on Intelligent Transportation Systems*, pages 1202–1208. Institute of Electrical and Electronics Engineers (IEEE), Sep 2015. doi: 10.1109/itsc.2015.198.

[165] Open Electrical. Power systems analysis software. `http://www.openelectrical.org/wiki/index.php?title=Power_Systems_Analysis_Software`. Last accessed 19th December 2016.

[166] Power Systems Simulation Laboratory. Power systems analytical software tools. `http://www.itee.uq.edu.au/pssl/drupal7_with_innTheme/?q=node/34`. Last accessed 19th December 2016.

[167] D. Ni. Multiscale traffic flow modeling. In *Traffic Flow Theory*, volume 1, pages 361–377. Elsevier BV, 2011. doi: 10.1016/b978-0-12-804134-5.00024-6.

[168] G. Papageorgiou and A. Maimaris. Modelling, simulation methods for intelligent transportation systems. In *Intelligent Transportation Systems*. InTech, Mar 2012. doi: 10.5772/26013.

[169] H. Zheng, Y.-J. Son, Y.-C. Chiu, L. Head, Y. Feng, H. Xi, S. Kim, and M. Hickman. A primer for agent-based simulation and modeling in transportation applications. Technical Report FHWA-HRT-13-054, Federal Highway Administration (FHWA), 2013.

[170] L.S. Passos, R.J.F. Rossetti, and Z. Kokkinogenis. Towards the next-generation traffic simulation tools: A first appraisal. In *6th Iberian Conference on Information Systems and Technologies (CISTI)*, pages 1–6. Institute of Electrical and Electronics Engineers (IEEE), 2011.

[171] J. Macedo, Z. Kokkinogenis, G. Soares, D. Perrotta, and R.J.F. Rossetti. A HLA-based multi-resolution approach to simulating electric vehicles in simulink and SUMO. In *16th International Conference on Intelligent Transportation Systems (ITSC 2013)*, pages 2367–2372. Institute of Electrical and Electronics Engineers (IEEE), Oct 2013. doi: 10.1109/itsc.2013.6728581.

[172] T. Azevedo, R.J.F. Rossetti, and J.G. Barbosa. A state-of-the-art integrated transportation simulation platform. In *International Conference on Models and Technologies for Intelligent Transportation Systems (MT-ITS)*, pages 340–347. Institute of Electrical and Electronics Engineers (IEEE), Jun 2015. doi: 10.1109/mtits.2015.7223277.

[173] JaamSim Development Team. JaamSim: Discrete-event simulation software release 2016-04. 2016. doi: 10.5281/zenodo.57118.

[174] D.H. King and H.S. Harrison. Open-source simulation software JaamSim. In *Proceedings of the Winter Simulation Conference: Simulation: Making Decisions in a Complex World*, pages 2163–2171. Institute of Electrical and Electronics Engineers (IEEE), 2013.

[175] J. Dallmeyer and I.J. Timm. MAINSIM–MultimodAl INnercity SIMulation. In *35th German Conference on Artificial Intelligence (KI2012)*, pages 125–129, 2012.

[176] A. Horni, K. Nagel, and K.W. Axhausen. The multi-agent transport simulation MATSim. *Ubiquity, London*, 9, 2016.

[177] M. Ben-Akiva, H.N. Koutsopoulos, T. Toledo, Q. Yang, C.F. Choudhury, C. Antoniou, and R. Balakrishna. Traffic simulation with MITSIMLab. In J. Barceló, editor, *Fundamentals of Traffic Simulation*, pages 233–268. Springer Nature, New York, NY, 2010. ISBN 978-1-4419-6142-6. doi: 10.1007/978-1-4419-6142-6_6.

[178] M. Treiber and A. Kesting. Model-based traffic flow optimization. In *Traffic Flow Dynamics: Data, Models and Simulation*, pages 403–422. Springer Nature, Berlin, Heidelberg, Oct 2013. ISBN 978-3-642-32460-4. doi: 10.1007/978-3-642-32460-4_21.

[179] N.T. Collier and M.J. North. Parallel agent-based simulation with repast for high performance computing. *SIMULATION*, 89(10):1215–1235, Nov 2012. doi: 10.1177/0037549712462620.

[180] M.J. North, N.T. Collier, J. Ozik, E.R. Tatara, C.M. Macal, M. Bragen, and P. Sydelko. Complex adaptive systems modeling with repast simphony. *Complex Adaptive Systems Modeling*, 1(1), 2013. doi: 10.1186/2194-3206-1-3.

[181] M. Behrisch, L. Bieker, J. Erdmann, and D. Krajzewicz. SUMO–simulation of urban mobility: an overview. In *3rd International Conference on Advances in System Simulation (SIMUL)*. ThinkMind, 2011.

[182] D. Krajzewicz, J. Erdmann, M. Behrisch, and L. Bieker. Recent development and applications of SUMO–simulation of urban mobility. *International Journal On Advances in Systems and Measurements*, 5(3&4), 2012.

[183] C.L. Barrett, R. Beckman, K. Berkbigler, K. Bisset, B. Bush, K. Campbell, S. Eubank, K. Henson, J. Hurford, and D. Kubicek. TRANSIMS: Transportation analysis and simulation system. Technical report, Jul 2001.

[184] K. Nagel and M. Rickert. Parallel implementation of the TRANSIMS micro-simulation. *Parallel Computing*, 27(12):1611–1639, Nov 2001. doi: 10.1016/s0167-8191(01)00106-5.

[185] C. Sommer, R. German, and F. Dressler. Bidirectionally coupled network and road traffic simulation for improved IVC analysis. *IEEE Transactions on Mobile Computing*, 10(1):3–15, Jan 2011. doi: 10.1109/tmc.2010.133.

[186] S. Schellenberg, R. Berndt, R. German, and D. Eckhoff. Evaluating the electrification of vehicle fleets using the veins framework. Technical Report 1409.1003, arXiv, September 2014.

[187] J. Casas, J.L. Ferrer, D. Garcia, J. Perarnau, and A. Torday. Traffic simulation with AIMSUN. In J. Barceló, editor, *Fundamentals of Traffic Simulation*, pages 173–232. Springer Nature, New York, NY, 2010. ISBN 978-1-4419-6142-6. doi: 10.1007/978-1-4419-6142-6_5.

[188] S. Kim, W. Suh, and J. Kim. Traffic simulation software: Traffic flow characteristics in CORSIM. In *International Conference on Information Science & Applications (ICISA)*, pages 1–3. Institute of Electrical and Electronics Engineers (IEEE), May 2014. doi: 10.1109/icisa.2014.6847475.

[189] A.L.C. Bazzan, M. de Brito do Amarante, T. Sommer, and A.J. Benavides. ITSUMO: An agent-based simulator for its applications. In *4th Workshop on Artificial Transportation Systems and Simulation*, page 8. Institute of Electrical and Electronics Engineers (IEEE), 2010.

[190] P. Sykes. Traffic simulation with paramics. In *Fundamentals of Traffic Simulation*, pages 131–171. Springer Nature, 2010. doi: 10.1007/978-1-4419-6142-6_4.

[191] M. Fellendorf and P. Vortisch. Microscopic traffic flow simulator VISSIM. In *Fundamentals of Traffic Simulation*, pages 63–93. Springer Nature, 2010. doi: 10.1007/978-1-4419-6142-6_2.

[192] Singapore Power. Facts and figures. `http://www.singaporepower.com.sg/irj/servlet/prt/portal/prtroot/docs/guid/106b5b67-d148-2f10-14a7-`

a6b7bbef1871?sppatab=About%20SP%20PowerAssets, 2014. Last accessed 31st March 2016.

[193] Singapore Power. Powering the nation, annual report. http://www.singaporepower.com.sg/irj/go/km/docs/documents/SP%20Content/Sites/Singapore%20Power/Site%20Contents/Annual%20Reports/documents/2012/SPower%20AR2012.pdf, 2012. Last accessed 19th December 2016.

[194] Singapore Power. Major procurement items. http://www.singaporepower.com.sg/irj/servlet/prt/portal/prtroot/docs/guid/80da751a-8fb6-2e10-93a3-ff21cfff0e4c?sppgtab=Procurement, 2016. Last accessed 31st March 2016.

[195] S. Fassbinder. Efficiency and loss evaluation of large power transformers. *ECI Publication No Cu0144*, 2013.

[196] IEEE. IEEE guide for loading mineral-oil-immersed transformers and step-voltage regulators. *IEEE Std C57.91-2011 (Revision of IEEE Std C57.91-1995)*, pages 1–123, Mar 2012. doi: 10.1109/ieeestd.2012.6166928.

[197] J. Perez. Fundamental principles of transformer thermal loading and protection. In *63rd Annual Conference for Protective Relay Engineers*, pages 1–14. Institute of Electrical and Electronics Engineers (IEEE), Mar 2010. doi: 10.1109/cpre.2010.5469518.

[198] Energy Market Authority (EMA) of Singapore. Licensed generation capacity by generation company. https://www.ema.gov.sg/cmsmedia/Publications_and_Statistics/Statistics/MSA19b.pdf, 2015. Last accessed 31st March 2016.

[199] Google. Maps. http://maps.google.com.sg. Last accessed 19th December 2016.

[200] Bahra Cables Company. Low, medium, and high voltage power cables. http://www.bahra-cables.com/downloads.aspx. Last accessed 19th December 2016.

[201] Nexans. Starkstromkabel 1 - 30kV. http://www.nexans.de/eservice/Germany-de_DE/fileLibrary/Download_540171919/Germany/files/Starkstrom_DuGB_12okt12_klein.pdf, 2012. Last accessed 19th December 2016.

[202] Nexans. Höchstspannungskabel zur energieübertragung. http://www.nexans.de/Germany/2007/HS-Katalog%20mit%20Elcufilt.pdf, 2007. Last accessed 19th December 2016.

[203] Streetdirectory. SG & Singapore map. http://www.streetdirectory.com. Last accessed 31st March 2016.

[204] SLA. Onemap. http://www.onemap.sg. Last accessed 19th December 2016.

[205] Energy Market Authority (EMA) of Singapore. Monthly electricity consumption by sector (total). https://www.ema.gov.sg/cmsmedia/Publications_and_Statistics/Statistics/MSA5.pdf, 2015. Last accessed 31st March 2016.

[206] Energy Market Authority (EMA) of Singapore. Half-hourly system demand data. http://www.ema.gov.sg/statistic.aspx?sta_sid=20140826Y84sgBebjwKV, 2015. Last accessed 19th December 2016.

[207] Energy Market Authority (EMA) of Singapore. Transmission code. https://www.ema.gov.sg/cmsmedia/About-Us/transmission%20code.pdf, 2014. Last accessed 19th December 2016.

[208] IEC. IEC 60364-5-52:2009 low-voltage electrical installations – part 5-52: Selection and erection of electrical equipment - wiring systems. *IEC Std. 60364*, 2009.

[209] M.M. Hand, S. Baldwin, E. DeMeo, J.M. Reilly, T. Mai, D. Arent, G. Porro, M. Meshek, and D. Sandor. Renewable electricity futures study: Exploration of high-penetration renewable electricity futures. Technical report, National Renewable Energy Laboratory (NREL), Jun 2012.

[210] D. Deka, S. Vishwanath, and R. Baldick. Analytical models for power networks: The case of the western US and ERCOT grids. *IEEE Transactions on Smart Grid*, (99):1–1, 2016. ISSN 1949-3053. doi: 10.1109/tsg.2016.2540439.

[211] D.E. Whitney and D. Alderson. Are technological and social networks really different? In *Unifying Themes in Complex Systems*, pages 74–81. Springer Nature, 2010. doi: 10.1007/978-3-540-85081-6_10.

[212] Trading Economics. Electric power transmission and distribution losses (percentage of output) in Singapore. http://www.tradingeconomics.com/singapore/electric-power-transmission-and-distribution-losses-percent-of-output-wb-data.html. Last accessed 19th December 2016.

[213] Siemens. Totally integrated power: Planung der elektrischen Energieverteilung. https://w3.siemens.com/powerdistribution/global/DE/consultant-support/download-center/tabcardseiten/Documents/Planungshandbuecher/Planung_der_elektrischen_Energieverteilung_Technische_Grundlagen.pdf, 2015. Last accessed 19th December 2016.

[214] Singapore Power. The leading energy utility company in Asia pacific. http://www.singaporepower.com.sg, 2016. Last accessed 19th December 2016.

[215] C. Peng, J. Zou, and L. Lian. Dispatching strategies of electric vehicles participating in frequency regulation on power grid: A review. *Renewable and Sustainable Energy Reviews*, 68:147–152, Feb 2017. doi: 10.1016/j.rser.2016.09.133.

[216] Land Transport Authority (LTA). Annual vehicle statistics 2015: Motor vehicle population by type of fuel used. https://www.lta.gov.sg/content/dam/ltaweb/corp/PublicationsResearch/files/FactsandFigures/MVP01-4_MVP_by_fuel.pdf, 2015. Last accessed 19th December 2016.

[217] Land Transport Authority (LTA). Certificate of entitlement (COE). https://www.lta.gov.sg/content/ltaweb/en/roads-and-motoring/owning-a-vehicle/vehicle-quota-system/certificate-of-entitlement-coe.html, 2016. Last accessed 19th December 2016.

[218] Land Transport Authority (LTA). E-mobility technology roadmap. https://www.nccs.gov.sg/sites/nccs/files/Roadmap_E-M_1.pdf, 2015. Last accessed 19th December 2016.

[219] Singapore Department of Statistics. Population trends. http://www.singstat.gov.sg/docs/default-source/default-document-library/publications/publications_and_papers/population_and_population_structure/population2016.pdf. Last accessed 19th December 2016.

[220] P. del Río and P. Linares. Back to the future? Rethinking auctions for renewable electricity support. *Renewable and Sustainable Energy Reviews*, 35:42–56, Jul 2014. ISSN 1364-0321. doi: 10.1016/j.rser.2014.03.039.

[221] S. Litescu, V. Viswanathan, M. Lees, A. Knoll, and H. Aydt. Information impact on transportation systems. *Journal of Computational Science*, 9:88–93, Jul 2015. ISSN 1877-7503. doi: 10.1016/j.jocs.2015.04.019.

[222] R. Bi, J. Xiao, V. Viswanathan, and A. Knoll. Influence of charging behaviour given charging station placement at existing petrol stations and residential car park locations in Singapore. *Procedia Computer Science*, 80:335–344, 2016. doi: 10.1016/j.procs.2016.05.347.

[223] Z. Liu, F. Wen, and G. Ledwich. Optimal planning of electric-vehicle charging stations in distribution systems. *IEEE Transactions on Power Delivery*, 28(1):102–110, Jan 2013. doi: 10.1109/tpwrd.2012.2223489.

[224] A.Y.S. Lam, Y.-W. Leung, and X. Chu. Electric vehicle charging station placement: Formulation, complexity, and solutions. In *International Conference on Smart Grid Communications (SmartGridComm)*. Institute of Electrical and Electronics Engineers (IEEE), Oct 2013. doi: 10.1109/smartgridcomm.2013.6688009.

[225] F. Baouche, R. Billot, R. Trigui, and N.-E. el Faouzi. Electric vehicle charging stations allocation model. In *ROADEF - 15ème congrès annuel*, Bordeaux, France, Feb 2014. Société française de recherche opérationnelle et d'aide à la décision.

[226] Y. Ahn and H. Yeo. An analytical planning model to estimate the optimal density of charging stations for electric vehicles. *PLOS ONE*, 10(11), Nov 2015. doi: 10.1371/journal.pone.0141307.

[227] Y. Xiong, J. Gan, B. An, C. Miao, and A.L.C. Bazzan. Optimal electric vehicle charging station placement. pages 2662–2668, Jan 2015.

[228] M.T. Sebastiani, R. Luders, and K.V.O. Fonseca. Allocation of charging stations in an electric vehicle network using simulation optimization. In *Proceedings of the Winter Simulation Conference 2014*, pages 1073–1083. Institute of Electrical and Electronics Engineers (IEEE), Dec 2014. doi: 10.1109/wsc.2014.7019966.

[229] S. López, J. Caicedo, M. Mamaní, A.A. Romero, and G. Rattá. Literature review: Potential impacts of plug-in electric vehicles on electric power systems. In *PES Transmission & Distribution Conference & Exposition - Latin America (PES T&D-LA)*, pages 1–6. Institute of Electrical and Electronics Engineers (IEEE), Sep 2014. doi: 10.1109/tdc-la.2014.6955255.

[230] P. Maheshwari, Y. Tambawala, H.K. Nunna, and S. Doolla. A review on plug-in electric vehicles charging: Standards and impact on distribution system. In *International*

Conference on Power Electronics, Drives and Energy Systems (PEDES), pages 1–6. Institute of Electrical and Electronics Engineers (IEEE), Dec 2014. doi: 10.1109/pedes.2014.7042147.

[231] A. Aljanad and A. Mohamed. Impact of plug-in hybrid electric vehicle on power distribution system considering vehicle to grid technology: A review. *Research Journal of Applied Sciences, Engineering and Technology*, 10(12):1404–1413, Aug 2015. doi: 10.19026/rjaset.10.1841.

[232] S. Habib, M. Kamran, and U. Rashid. Impact analysis of vehicle-to-grid technology and charging strategies of electric vehicles on distribution networks – a review. *Journal of Power Sources*, 277:205–214, Mar 2015. doi: 10.1016/j.jpowsour.2014.12.020.

[233] K.M. Tan, V.K. Ramachandaramurthy, and J.Y. Yong. Integration of electric vehicles in smart grid: A review on vehicle to grid technologies and optimization techniques. *Renewable and Sustainable Energy Reviews*, 53:720–732, Jan 2016. doi: 10.1016/j.rser.2015.09.012.

[234] A. Aljanad, A. Mohamed, and H. Shareef. Impact study of plug-in electric vehicles on electric power distribution system. In *Student Conference on Research and Development (SCOReD)*, pages 339–344. Institute of Electrical and Electronics Engineers (IEEE), Dec 2015. doi: 10.1109/scored.2015.7449352.

[235] A. Bosovic, M. Music, and S. Sadovic. Analysis of the impacts of plug-in electric vehicle charging on the part of a real medium voltage distribution network. In *PES Innovative Smart Grid Technologies, Europe*, pages 1–7. Institute of Electrical and Electronics Engineers (IEEE), Oct 2014. doi: 10.1109/isgteurope.2014.7028830.

[236] A. Bouallaga, A. Davigny, V. Courtecuisse, and B. Robyns. Methodology for technical and economic assessment of electric vehicles integration in distribution grid. *Mathematics and Computers in Simulation*, 131:172–189, Jan 2017. doi: 10.1016/j.matcom.2016.05.003.

[237] I. Drovtar, A. Rosin, M. Landsberg, and J. Kilter. Large scale electric vehicle integration and its impact on the Estonian power system. In *PowerTech*, pages 1–6, Grenoble, France, Jun 2013. Institute of Electrical and Electronics Engineers (IEEE). doi: 10.1109/ptc.2013.6652181.

[238] M.D. Galus, R.A. Waraich, F. Noembrini, K. Steurs, G. Georges, K. Boulouchos, K.W. Axhausen, and G. Andersson. Integrating power systems, transport systems and vehicle technology for electric mobility impact assessment and efficient control. *IEEE Transactions on Smart Grid*, 3(2):934–949, Jun 2012. doi: 10.1109/tsg.2012.2190628.

[239] J. Glueck and H.T. Le. Impacts of plug-in electric vehicles on local distribution feeders. In *Power & Energy Society General Meeting*, pages 1–5. Institute of Electrical and Electronics Engineers (IEEE), Jul 2015. doi: 10.1109/pesgm.2015.7286348.

[240] G. Hoogsteen, A. Molderink, J.L. Hurink, G.J.M. Smit, F. Schuring, and B.K. Liandon. Impact of peak electricity demand in distribution grids: A stress test. In *PowerTech*, pages 1–6, Eindhoven, Jun 2015. Institute of Electrical and Electronics Engineers (IEEE). doi: 10.1109/ptc.2015.7232412.

[241] M. Huber, A. Trippe, P. Kuhn, and T. Hamacher. Effects of large scale EV and PV integration on power supply systems in the context of Singapore. In *3rd PES Innovative Smart Grid Technologies Europe (ISGT Europe)*, pages 1–8. Institute of Electrical and Electronics Engineers (IEEE), Oct 2012. doi: 10.1109/isgteurope.2012.6465831.

[242] P. Jain and T. Jain. Assessment of electric vehicle charging load and its impact on electricity market price. In *International Conference on Connected Vehicles and Expo (ICCVE)*, pages 74–79. Institute of Electrical and Electronics Engineers (IEEE), Nov 2014. doi: 10.1109/iccve.2014.7297648.

[243] I. Karakitsios, E. Karfopoulos, and N. Hatziargyriou. Impact of dynamic and static fast inductive charging of electric vehicles on the distribution network. *Electric Power Systems Research*, 140:107–115, Nov 2016. doi: 10.1016/j.epsr.2016.06.034.

[244] W. Khamphanchai, M. Pipattanasomporn, S. Rahman, and A.T. Al-Awami. Impact of electric vehicles on household voltage profiles and possible mitigation approach. In *PES Innovative Smart Grid Technologies, Europe*, pages 1–6. Institute of Electrical and Electronics Engineers (IEEE), Oct 2014. doi: 10.1109/isgteurope.2014.7028988.

[245] E.R. Muñoz, G. Razeghi, L. Zhang, and F. Jabbari. Electric vehicle charging algorithms for coordination of the grid and distribution transformer levels. *Energy*, 113:930–942, Oct 2016. doi: 10.1016/j.energy.2016.07.122.

[246] A.G. Neagoe-Ştefana, A.C. Neagoe, and A.C. Mandiş. Impact of charging electric vehicles in residential grid on the power losses and voltage plan. In *International Symposium on Fundamentals of Electrical Engineering (ISFEE)*, pages 1–4. Institute of Electrical and Electronics Engineers (IEEE), Nov 2014. doi: 10.1109/isfee.2014.7050603.

[247] L. Pinter and C. Farkas. Impacts of electric vehicle chargers on the power grid. In *5th International Youth Conference on Energy (IYCE)*, pages 1–6. Institute of Electrical and Electronics Engineers (IEEE), May 2015. doi: 10.1109/iyce.2015.7180811.

[248] G. Razeghi and S. Samuelsen. Impacts of plug-in electric vehicles in a balancing area. *Applied Energy*, 183:1142–1156, Dec 2016. doi: 10.1016/j.apenergy.2016.09.063.

[249] N.B.M. Shariff, M. Al Essa, and L. Cipcigan. Probabilistic analysis of electric vehicles charging load impact on residential distributions networks. In *International Energy Conference (ENERGYCON)*, pages 1–6. Institute of Electrical and Electronics Engineers (IEEE), Apr 2016. doi: 10.1109/energycon.2016.7513943.

[250] Y. Wang, S. Huang, and D. Infield. Investigation of the potential for electric vehicles to support the domestic peak load. In *International Electric Vehicle Conference (IEVC)*, pages 1–8. Institute of Electrical and Electronics Engineers (IEEE), Dec 2014. doi: 10.1109/ievc.2014.7056124.

[251] R.A. Waraich, G. Georges, M.D. Galus, and K.W. Axhausen. Adding electric vehicle modeling capability to an agent-based transport simulation. In *Data Science and Simulation in Transportation Research*, pages 282–318. IGI Global, 2014. doi: 10.4018/978-1-4666-4920-0.ch014.

[252] J. Xiong, K. Zhang, X. Liu, and W. Su. Investigating the impact of plug-in electric vehicle charging on power distribution systems with the integrated modeling and simulation of transportation network. In *Conference and Expo Transportation Electrification Asia-Pacific (ITEC Asia-Pacific)*, pages 1–5. Institute of Electrical and Electronics Engineers (IEEE), Aug 2014. doi: 10.1109/itec-ap.2014.6940855.

[253] K. Zafred, J. Nieto-Martin, and E. Butans. Electric vehicles - effects on domestic low voltage networks. In *International Energy Conference (ENERGYCON)*, pages 1–6. Institute of Electrical and Electronics Engineers (IEEE), Apr 2016. doi: 10.1109/energycon.2016.7514060.

[254] IEEE. Power systems test case archive. `http://www2.ee.washington.edu/research/pstca/`. Last accessed 19th December 2016.

[255] J. García-Villalobos, I. Zamora, J.I. San Martín, F.J. Asensio, and V. Aperribay. Plug-in electric vehicles in electric distribution networks: A review of smart charging approaches. *Renewable and Sustainable Energy Reviews*, 38:717–731, Oct 2014. doi: 10.1016/j.rser.2014.07.040.

[256] Sydney Coordinated Adaptive Traffic System (SCATS). An introduction to the new generation scats 6. `http://www.scats.com.au/files/an_introduction_to_scats_6.pdf`, 2012. Last accessed 19th December 2016.

[257] D. Deka and S. Vishwanath. Structural vulnerability of power grids to disasters: Bounds and reinforcement measures. In *Power & Energy Society Innovative Smart Grid Technologies Conference (ISGT)*, pages 1–5. Institute of Electrical and Electronics Engineers (IEEE), Feb 2015. doi: 10.1109/isgt.2015.7131820.